Model Nucleobases and their Metal Complexes: Hydrogen Bonding Patterns, Cytosine Deamination, Metal Migration, and Building Blocks for Architectures.

Pablo J. Sanz Miguel

Universität Dortmund

Fachbereich Chemie der Universität Dortmund

Model Nucleobases and their Metal Complexes: Hydrogen Bonding Patterns, Cytosine Deamination, Metal Migration, and Building Blocks for Architectures.

Pablo J. Sanz Miguel

Vom Fachbereich Chemie der Universität Dortmund
zur Erlangung des akademischen Grades eines
Doktors der Naturwissenschaften
genehmigte Dissertation

Referent: Prof. Dr. Bernhard Lippert
Korreferent: P. D. Dr. Andrea Erxleben
Tag der mündlichen Prüfung: 28.06.2005

Die vorliegende Arbeit entstand in der Zeit von März 2001 bis April 2005 am Lehrstuhl für Anorganische Chemie III des Fachbereichs Chemie der Universität Dortmund.

*Mi especial agradecimiento a **Bernhard Lippert**,*
por el trato personal recibido durante estos años, por lo mucho que de él he aprendido.
Por despertar en mí el interés, por la química que me ha enseñado y por toda su ayuda.

Gracias a Burkhard Costisella y Annette Danzmann por el trato familiar durante estos años, por el buen ambiente de trabajo y por las agradables conversaciones.

Gracias a Clodagh Mulcahy, Jens Müller y Gabi Trötscher-Kaus, por la ayuda en las correcciones del manuscrito. Gracias a Andrea Erxleben por hacer de "Korreferent".

Gracias a todos mis compañeros de despacho: Alex Schneider, Barbara Müller, Markus Drumm, Egla Bivián, Eva Freisinger, Gabi Trötscher-Kaus, Gunnar Kampf, Ivana Ascaso, Jens Müller, Lars Holland, Michele Abbate, Montse Vives, Roland Sigel, Simone Goritz, Sultan Cosar, y especialmente a Deepali Gupta, Michael Roitzsch y Patrick Lax por tantas horas inolvidables.

Gracias a Thorsten Berends, Andrea Erxleben, Deepali Gupta, Peter Heines, Marta Morell, Thorsten Oldag, Johannes Preut, Michael Roitzsch, Michael Willermann y Uwe Zachwieja por ayudarme de una u otra forma con la cristalografía; también lo hicieron Burkhard Costisella, Annette Danzmann y Jens Müller con la resonancia magnética; a Patrick Lax y Deepali Gupta por los cálculos DFT, a René Schubert y Thorsten Grund por la ayuda informática, a Markus Hüffner por los análisis elementales y a Karina Andoura por el microscopio electrónico. Gracias a Simone Goritz. Gracias a Dominik Böhme, Dinah Dux, Alex Kaufmann, Dirk Kiesewetter y Lars Wimbert, mis compañeros de prácticas.

Gracias a Michaela Markert, Dinah Dux, Andrea Erxleben, Jola Hermann, Ralf Nowak, Irene Szymanski, Michael Willermann, Mahdi Hadjizadeh-Ziabari, Thorsten Berends, Alex Kaufmann, Frank Neumann, Vero Dodero, Rafa Martín, Davide Crisà, Elisa Barea, Marta Garijo, Myriam Gil, Clodagh Mulcahy, Weizheng Shen, Marta Morell, Jens Müller, Fabian Polonius, Dominik Böhme, Oliver Gerbersmann, Christine Klimek y a los que he olvidado nombrar, por el ambiente en el trabajo.

Gracias a Lars Rohde, Laura Mediavilla, Luis Salazar, Deepali "Ohne" Gupta, Sven Seydler, Matias Bönke, Jana Wriedt, Barbara Schweighöfer, Miguel Sanz, Rike Meyer-Belitz y Luiggi Bueno por su amistad y ayuda en los momentos difíciles. A mis vecinillos Jens Brune, Peter Kommorowski, Roberto Secín, Peter Glösekötter y Henk Muhmann. A mis chicas.

Gracias a Birgit Thormann y Burkhard Wellnitz, por su amistad y toda su ayuda desde el principio.

Gracias a Sebastian, Güncem y a mi familia Campagna por su sincera amistad.

Gracias (y mis disculpas) a mis amigos que quedaron en España, a los que tengo bastante olvidadillos últimamente. Al chicolapiliii.

Gracias también a toda la gente que ha hecho posible que nunca me sintiera extranjero.

A la memoria de mi amigo Santiago "Kenni" Gracia Royo.

Dedicado a mis padres.

Parts of the results reported in this thesis have already been published or are in press:

[1] J. Müller, E. Freisinger, P. J. Sanz Miguel, B. Lippert, *Inorg. Chem.,* 2003, 42, 5117.

[2] P. J. Sanz Miguel, P. Lax, M. Willermann, B. Lippert, *Inorg. Chim. Acta,* 2003, 42, 5117.

[3] J. E. Šponer, P. J. Sanz Miguel, L. Rodriguez-Santiago, A. Erxleben, M. Krumm, M. Sodupe, J. Šponer, B. Lippert, *Angew. Chem., Int. Ed.,* 2004, 43, 5396.

[4] P. J. Sanz Miguel, Bernhard Lippert, *Dalton Trans.,* 2005, 1679.

[5] P. Amo-Ochoa, P. J. Sanz Miguel, P. Lax, I. Alonso, M. Roitzsch, F. Zamora, B. Lippert, *Angew. Chem., in press*.

Desde hace años, llevo una doble vida. Durante el día trabajo, pero por la noche, mi corazón y mi adrenalina se disparan. Al verme, no podrías decir que he dirigido Ejércitos, que he conquistado Mundos... Yo sí puedo decir que he vivido.

Quizá un día juegue por primera vez y descubra la magia de la Play Station.

0.- Summary.

Metal-nucleic acids interactions represent today an important area within the field of Bioinorganic Chemistry. Metal ions are known to play rather diverse roles in the chemistry and biology of nucleic acids, which range from necessity to neutralize the negative charges of the polynucleotide anions, to the stabilization of particular structural elements in DNA (e.g. tetrastranded DNA in telomeres) to distortion of DNA in order to achieve antitumor activity (e.g. Cisplatin), or to catalytic processes involving RNA molecules. Moreover, many (heavy) metal ions are mutagenic, employing different mechanisms to achieve this. Central to the latter aspect is a detailed understanding of the effects of metal coordination to nucleobases on basic features such as chemical reactivity as well as hydrogen bonding behavior. As will be shown in several parts of this thesis, the interplay of hydrogen bonding and metal binding leads to interesting structures, which are fascinating at their own right, and bridge Bioinorganic Chemistry with Supramolecular Chemistry.

The present thesis consists of four main chapters dealing with

(1) a detailed analysis of hydrogen bonding patterns of selected model nucleobases and/or their protonated forms in the solid state,

(2) the role of the exocyclic amino group of the cytosine nucleobase in deamination and metal migration processes,

(3) the potential role of Pt^{II} complexes of 1-methylcytosine as precursors for larger architectures, as well as

(4) the properties of cationic tetrakis(nucleobase) complexes of Pt^{II} with regard to their potential as metalloligands and supramolecular building blocks.

Concerning the five most important results of this thesis, the following points are noteworthy: First, a novel nucleobase tetrad **8**, consisting of two different purine bases, 9-methyladeninium (9-MeAH^+) and 9-methylhypoxanthine (9-MeHxH), has been characterized. It extends the array of nucleobase quartets

presently known, and adds to the discussion of the existence of mixed adenine, guanine tetrads in natural DNA quadruplexes. The stability of these quadruplexes has been demonstrated in similar structures containing metal entities.

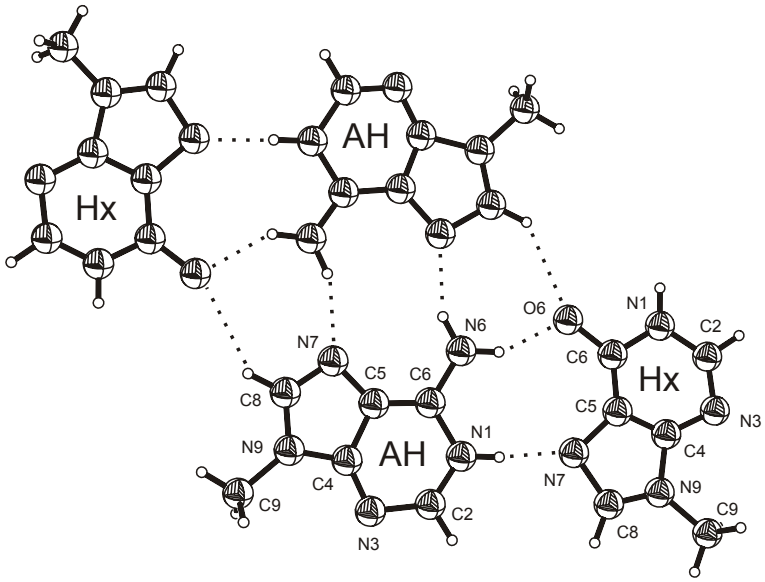

*Novel nucleobase tetrad [{(9-MeAH)(9-MeHxH)}$_2$](ClO$_4$)$_2$ (**8**)*

Second, deamination of cytosine nucleobases is greatly facilitated by metal coordination to the N3 position. This finding appears to be of considerable relevance to the question of the mutagenic potential of 5-methylcytosine bases in DNA, which represent known hotspots for damage in eukaryotic cells. The detailed study of the platinum-assisted deamination of cytosine in some systems reveals that the reaction does not require high temperatures. Rather, after ca. 30 min at the temperature of the human body (37º C) the cytosine is fully converted into uracil.

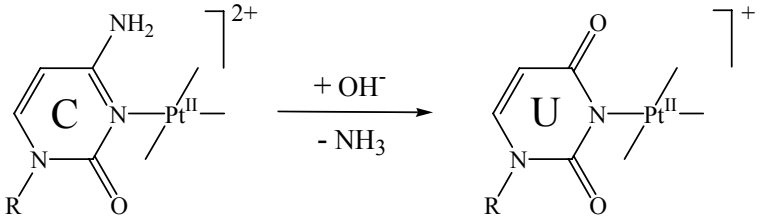

Pt-assisted deamination of Cytosine

Third, conditions leading to the intramolecular migration of (dien)M^{II} (M = Pt or Pd) entities from the N3 position of 1-methylcytosine to the exocyclic N4 position and concomitant transfer of H^+ from N4 to N3 has been studied in detail. This reaction, which competes with cytosine deamination, appears to proceed via a partially (dien) ring-opened intermediate, in which the amino group of the dien ligand functions as a base which abstracts a proton from $N(4)H_2$ of the cytosine. Subsequent nucleophilic attack of the $N(4)^-$ onto Pt generates the N4 bonded complex.

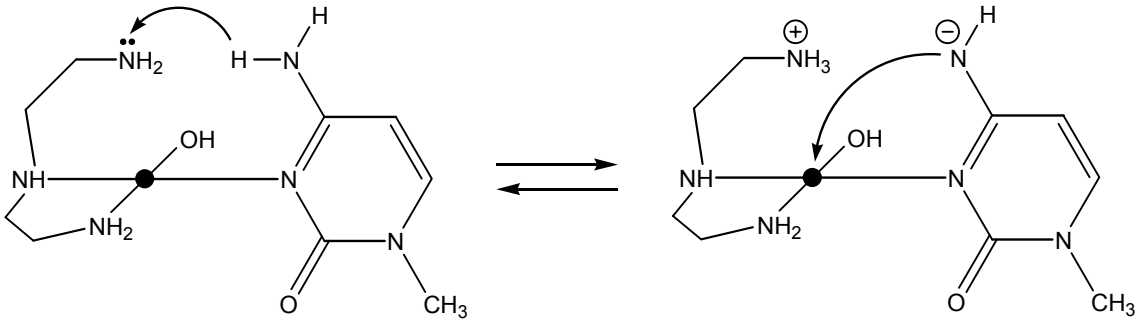

Proton migration and nucleophilic attack by $N(4)^-$ on the platinum atom

Fourth, two complexes of composition *trans*-[Pt(1-MeC-*N3*)(1-MeC-*N4*)X_2] (X_2= Cl_2, I_2; 1-MeC = 1-methylcytosine) have been isolated and structurally characterized, which contain two different tautomers of a nucleobase bound simultaneously to the same metal ion. This is only the second and third example of such a complex containing two different tautomers, the first one being an adenine complex. In nature the two cytosine tautomers exist in a ratio ca. 10000:1!

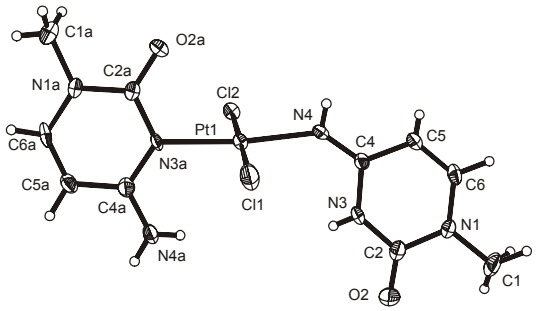

*Two different cytosine tautomers in **24***

Fifth, tetrakis(nucleobase) complexes of Pt^{II} provide adequate properties to be building blocks in Supramolecular Chemistry. They can act as metalloligands for other metal ions (Cu^{II}, Hg^{II}) to produce, as in **32**, a pentanuclear Cu-Pt-Cu-Pt-Cu chain, or even to interact with complementary 1-MeC to give Watson-Crick associates. The capture of additional cations as seen in **32** without undergoing deprotonation at N1 of the purine base, is a potentially biologically relevant feature.

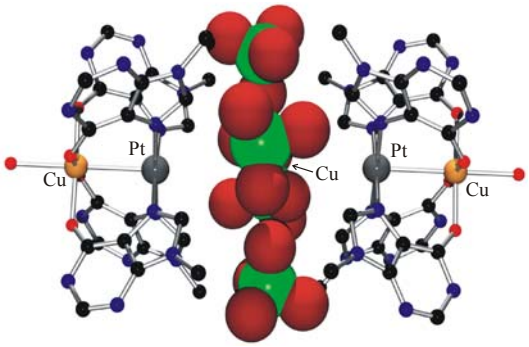

Arrangement of the Cu···Pt···Cu···Pt···Cu array in ***32***

Zusammenfassung.

Wechselwirkungen von Metallen mit Nukleinsäuren stellen heute einen wichtigen Bereich in der Bioanorganischen Chemie dar. Es ist bekannt, dass Metallionen verschiedenartige Rollen in der Chemie und Biologie von Nukleinsäuren spielen, die von der Notwendigkeit zur Kompensation der negativen Ladung der anionischen Polynukleotide über die Stabilisierung bestimmter Strukturelemente der DNA (z.B. viersträngige DNA in Telomeren), dem Abknicken der DNA für Antitumor-Aktivität (z.B. Cisplatin) bis zu katalytischen Prozessen unter Einbezug von RNA-Molekülen reichen. Außerdem sind viele (Schwer)metallionen mutagen, wobei durchaus unterschiedliche Mechanismen hierfür denkbar sind. Im Bezug auf letzteren Aspekt ist ein detailliertes Verständnis der Effekte von Metallkoordination an Nukleobasen im Hinblick auf chemische Reaktivität oder den Einfluss auf Wasserstoffbrücken notwendig. Wie in einigen Teilen dieser Arbeit aufgezeigt wird, führt das Zusammenspiel von Wasserstoffbrücken und Metallkoordination zu interessanten Strukturen, die für sich genommen faszinierend sind und eine Brücke zwischen Bioanorganischer Chemie und Supramolekularer Chemie schlagen.

Die vorliegende Arbeit besteht aus vier Hauptteilen mit folgenden Themen:

(1) Einer detaillierten Analyse von Wasserstoffbrückenbindungs-mustern ausgewählter Modellnukleobasen und/oder ihrer protonierten Formen im festen Zustand.
(2) Der Rolle der exozyklischen Aminogruppe des Cytosins bei Desaminierung und Metallwanderungsprozessen.
(3) Der potenziellen Rolle von Pt^{II}-Komplexen von 1-Methylcytosin-Vorstufen für größere Architekturen.
(4) Den Eigenschaften von kationischen Tetrakis(nukleobase)-Komplexen von Pt^{II} im Hinblick auf ihr Potenzial als Metalloliganden und supramolekulare Bausteine.

Was die fünf wichtigsten Ergebnisse dieser Arbeit betrifft, so sind folgende Punkte heraus zu stellen: Erstens ist ein neues Nukleobasen-Quartett **8** charakterisiert worden, das aus zwei verschiedenen Purinbasen besteht, 9-Methyladeninium (9-MeAH$^+$) und 9-Methylhypoxanthin (9-MeHxH). Es erweitert die bislang bekannten Beispiele für Nukleobasen-Quartette und liefert einen Beitrag zur Diskussion über die Existenz gemischter Adenin-Guanin-Tetraden in natürlichen DNA-Vierstrang-Strukturen. Die Stabilität dieser Quadruplexe ist in ähnlichen Strukturen unter Einbeziehung von Metallionen nachgewiesen worden.

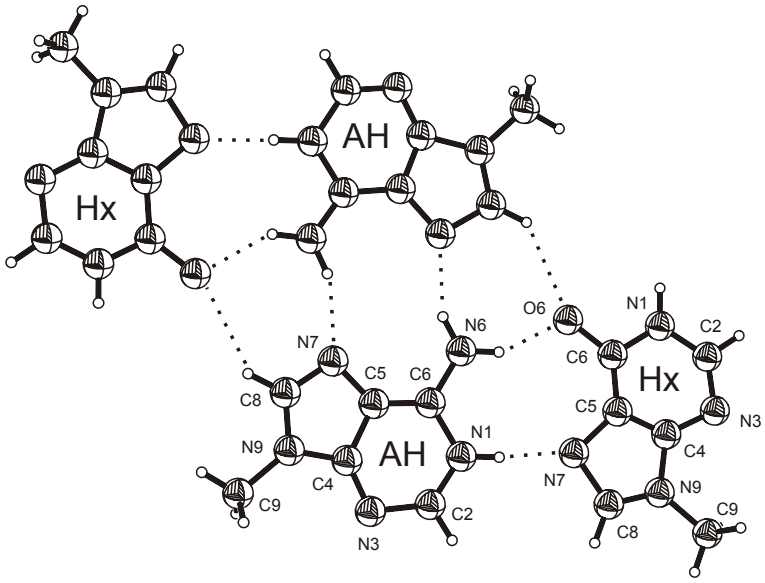

*Neues Nukleobasenquartett [{(9-MeAH)(9-MeHxH)}$_2$](ClO$_4$)$_2$ (**8**)*

Zweitens wird gezeigt, dass die Desaminierung von Cytosin durch Metallkoordination an der N3 Position stark begünstigt wird. Diese Entdeckung scheint von beachtlicher Relevanz hinsichtlich der Frage des mutagenen Potenzials von 5-Methylcytosin-Basen in der DNA zu sein. Diese stellen bekannte Hotspots für Schäden in eukaryontischen Zellen dar. Die mit Hilfe von Platin erreichte Desaminierung von Cytosin in einigen Systemen zeigt, dass die Reaktion keine hohen Temperaturen benötigt. Im günstigsten Fall wird eine vollständige Cytosin-Desaminierung zu Uracil innerhalb von 30 min bei 37ºC beobachtet.

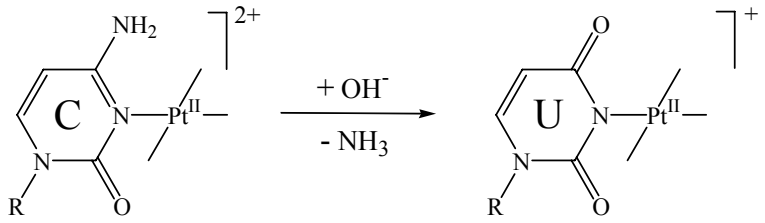

Pt-unterstützte Desaminierung von Cytosin

Drittens wurden die Bedingungen, die zur intramolekularen Wanderung von (dien)M^{II}-Einheiten (M = Pt oder Pd) von der N3 Position von 1-Methylcytosine zur exozyklischen N4-Position bei gleichzeitigem Transfer von H^+ von N4 nach N3 führen, im Detail studiert. Die Reaktion, die mit der Cytosindesaminierung in Konkurrenz steht, scheint über eine Zwischenstufe eines teilweise geöffneten dien-Ringes abzulaufen, in welcher die Aminogruppe des dien-Liganden als Base fungiert und ein Proton von $N(4)H_2$ des Cytosins abspaltet. Der folgende nukleophile Angriff des $N(4)^-$ auf das Pt-Atom generiert den N4 gebundenen Komplex.

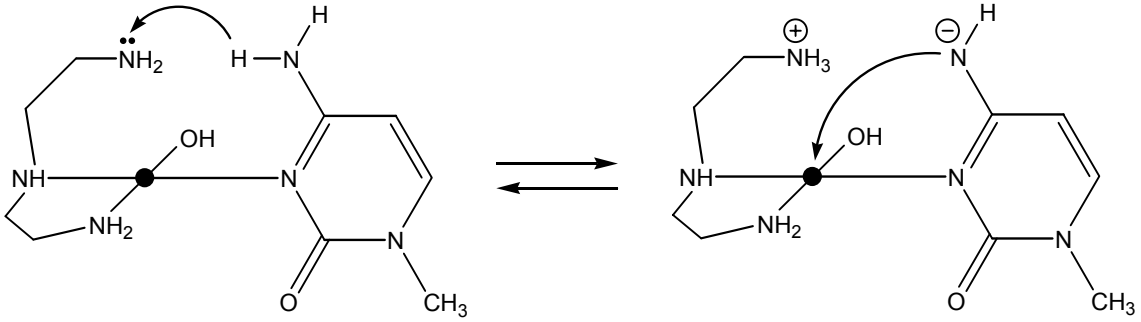

Protonenwanderung und nukleophiler Angriff des $N(4)^-$ auf das Platinatom

Viertens wurden zwei Komplexe, *trans*-[Pt(1-MeC-*N3*)(1-MeC-*N4*)X_2] (X_2= Cl_2, I_2; 1-MeC = 1-Methylcytosin) isoliert und ihre Strukturen charakterisiert, in denen zwei verschiedene Tautomere einer Nukleobase gleichzeitig an dasselbe Metallion gebunden vorliegen. Bisher war nur ein einziges Beispiel eines Metallkomplexes bekannt, in dem zwei unterschiedliche Tautomere einer Nukleobase (Adenin) gleichzeitig als Liganden fungieren. In der Natur liegen beide Cytosin-Tautomere in einen Verhältnis von ca. 10000:1 vor!

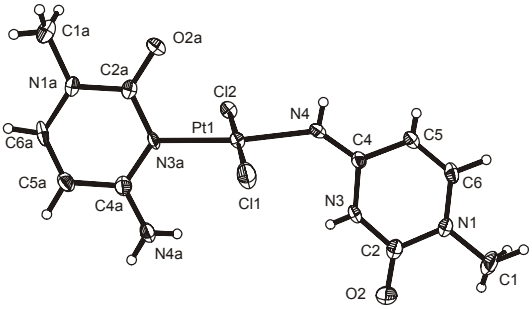

Zwei verschiedene Tautomere des Cytosins in ***24***

Fünftens wurde gezeigt, dass Tetrakis(Purin-Nukleobase)-Komplexe günstige Eigenschaften als Bausteine in der Supramolekularen Chemie aufweisen. Sie können als Metalloliganden für andere Metallionen (Cu^{II}, Hg^{II}) dienen, um –wie in **32** gezeigt– eine pentanukleare Cu-Pt-Cu-Pt-Cu-Kette zu bilden, oder mit komplementärem 1-MeC zu wechselwirken, was zu Watson-Crick-Assoziaten führt. Der Einbau zusätzlicher Kationen ohne Deprotonierung der N1-Position von Guanin ist möglicherweise eine Besonderheit, die auch biologisch relevant sein könnte.

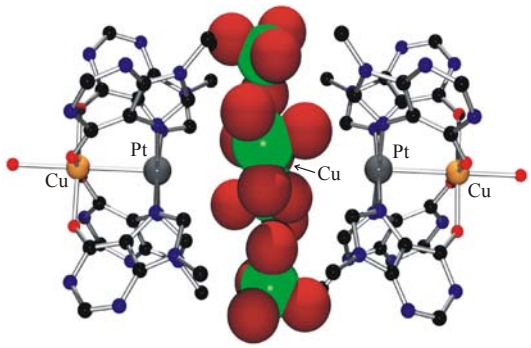

Anordnung der Cu···Pt···Cu···Pt···Cu-Einheit in ***32***

1.- Model Nucleobases: H-Bonding Patterns in Novel Solid State Structures.

Hydrogen bonds between nucleobases are of vital importance in biology and the building of supramolecular structures. The most common base-pairing is the self assembly of complementary nucleobases in nucleic acids. However, base-base recognition is not restricted to the complementary nucleobases. There are many examples of arrangements in which the bases are hydrogen bonded to themselves [6]; for example, cytosine, thymine, adenine and guanine bases have been demonstrated by X-ray crystallography and occasionally by NMR spectroscopy to undergo self-association.

In this chapter, several examples of self-base-pairing complexes are reported, along with other nucleobase salts. In case of the cytosine base, a protonated and an unprotonated cytosine form a triply hydrogen bonded aggregate in a self-recognition base-pairing complex. With the adenine base, three salts of protonated adenine nucleobases have been found to form different self-association homopolymers, and a fourth structure reveals a self-assembled base quartet formed by adenine and hypoxanthine nucleobases. Finally, with the guanine base, two structures with self recognition of guanine bases containing two different water polymers are reported.

With the exception of the adenine, hypoxanthine quartet discussed in 1.4, which was prepared in a planned manner by co-crystallizing the components, all the other compounds reported in this first chapter represent side and/or decomposition products of reactions carried out with the nucleobases and Pt as well as Pt starting compounds. They were frequently isolated in low yield and characterized by X-ray crystallography only. The origin of the various compounds will briefly be outlined at the beginning of each sub-chapter.

Structural and geometrical aspects of the crystals, angles and distances between atoms, orientation of the molecules along the axis of the crystal, and

supramolecular chemistry of the structures including formation of polymers and description of the hydrogen bonding pattern are the most relevant aspects discussed in this chapter.

1.1.- Cytosine derivatives.

1.1.1.- [(1-MeCH)(1-MeC)](I_3) · 2H_2O (1).

Compound **1** was obtained as a side product during the preparation of *trans*-[Pt(1-MeC-*N3*)$_2$$I_2$] (**21**) (chapter 2.5.3). The presence of a triiodide anion in **1** implies formation of elemental iodine at one point, which requires oxidation of I^- either by air or by a Pt^{II} species (which in turn has to undergo reduction to elemental platinum).

$$2\ I^- \xrightarrow{\text{oxid.}} I_2$$

$$I_2 + I^- \longrightarrow I_3^-$$

A second compound, [(1-MeCH)(1-MeC)]I · H_2O, was likewise isolated from preparations containing the Pt complex **21**. As the crystal structure of this compound proved to be identical with that reported already in the literature [7], it will not be further discussed. It is noted, however, that the R_1 factor (R_1= 0.031) of the structure studied here proved better than that of the published structure.

While crystals of [(1-MeCH)(1-MeC)]I · H_2O are colorless, those of the triiodide salt **1** had an intense dark orange coloration. No obvious decomposition in air was observed, unlike in other polyiodide salts [8], which have the tendency to lose elemental iodine. Structural characteristics and comparison with similar 1-methylcytosine structures are discussed below. Details concerning the crystal, X-ray measurement, and the refinement of data are listed in Table A-1 (see Appendix).

The solid state structure of **1** presents the most stable aminooxo tautomer of 1-MeC, accompanied by its protonated form. Both 1-MeC entities are oriented face-to-face, forming H-bonds via the Watson-Crick face. Acting as a counterion, I_3^- has the usual linear geometry [8] found in similar compounds. The molecular geometry in the $[1\text{-MeC}\equiv 1\text{-MeCH}]^+$ complex cation and in the I_3^- anion are displayed in Figure 1.1.

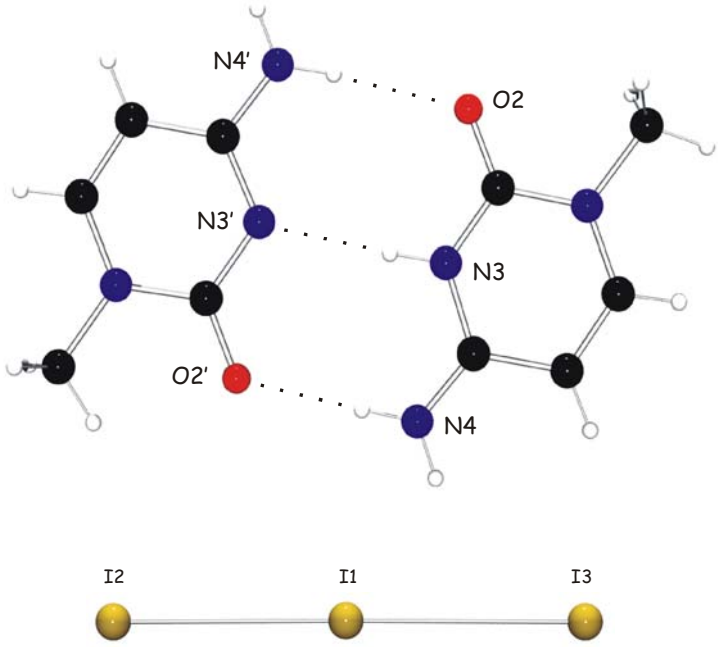

Figure 1.1: *View of the H-bonded cation and view of the anion of **1**.*

Distances and angles in both 1-methylcytosine entities and in the anion are not unusual. The proton between the two 1-methylcytosine rings is not disordered; rather the neutral molecule and the protonated one are readily distinguished on the basis of the largely different internal ring angles C2-N3-C4, which are 125.0(10)º for the cation and 119.0(9)º for the neutral nucleobase. The high electron density of the triiodide anions in the crystal, as compared to the less electron dense atoms of 1-methylcytosine, results in high standard deviation values for atoms of the bases; from 0.009 to 0.013 Å in the case of distances, and from 0.9 to 1.1º in the case of the angles. However, distances and angles related to iodine atoms, present a maximal standard deviation of 0.001 Å and 0.03º, to be considered low values. This effect is observed in other

similar solid state structures having high electron density, with the same counterion, such as [1-MeCH](I_3) [8] or even when the highly electron dense atoms are forming part of the skeleton of a neutral molecule, as for example in the complex *trans*-[Pt(1-MeC-*N3*)(1-MeC-*N4*)I_2] (**23**) [2]. Angles and distances for **1** are summarized in Table 1.2.

Table 1.2: *Distances (Å) and angles (º) for **1**.*

	1-MeC(H)	1-MeC'	O2-C2-N4'	124.3(7)
N1-C2	1.361(12)	1.382(11)	O2'-C2'-N4	124.6(6)
C2-N3	1.337(11)	1.353(12)	N3-N3'	2.891(12)
N3-C4	1.360(12)	1.334(12)	N4-O2'	2.816(10)
C4-C5	1.444(13)	1.420(12)	O2-N4'	2.966(11)
C5-C6	1.341(12)	1.337(13)	O1w-O2(i)	2.789(10)
C6-N1	1.336(11)	1.361(11)	O1w-O2'	2.710(10)
N1-C1	1.468(11)	1.463(11)	O1w-O2w(ii)	2.710(9)
C2-O2	1.225(11)	1.241(11)	O2w-N4	2.960(10)
C4-N4	1.296(11)	1.324(11)	O2w-N4'(iii)	3.051(10)
N1-C2-N3	117.5(10)	120.2(10)	I1-I2	2.887(1)
C2-N3-C4	125.0(10)	119.0(9)	I1-I3	2.970(1)
N3-C4-C5	116.1(10)	122.7(9)	I3-I2(iv)	3.713(1)
C4-C5-C6	117.1(11)	116.3(10)	I2-I1-I3	179.06(3)
C5-C6-N1	123.9(10)	122.2(10)	I1-I3-I2(iv)	167.75(3)
C6-N1-C2	120.3(9)	119.5(9)		
C1-N1-C6	121.4(9)	120.8(9)		
C1-N1-C2	118.0(9)	119.7(9)		
O2-C2-N1	122.3(10)	118.9(10)		
O2-C2-N3	120.2(11)	120.9(10)		
N4-C4-N3	121.1(10)	117.5(9)		
N4-C4-C5	122.7(11)	119.8(10)		

The study of the counterion reveals that the intramolecular I–I distances in I_3^-, 2.887(1) and 2.970(1) Å are different. They are in between 2.715(1) Å of the crystalline I_2 [9], and the distance of 2.92 Å in the free triiodide anion derived

from the relatively non-interacting anion in the tetraphenylarsonium salt [10]. The internal I(3)–I(1)–I(2) angle deviates minimally from linearity, 179.06(3)º. The triiodide anions in the crystalline structure line up in infinite strands, because of short contacts between terminal iodine atoms of consecutive entities, 3.713(1) Å between I(3) and I(2)(-x+2, y+1/2, -z+3/2). Two consecutive triiodide ions display an angle of 167.75(3)º, which can be considered a marked deviation from linearity, and is in strong contrast to the mutually orthogonal disposed I_3^- in the previously mentioned [1-MeCH](I_3).

Protonated and neutral 1-methylcytosine bases, in the given orientation, seem to have a C_2 crystallographic axis in the geometric central point. Though, considering the protons present, geometrical differences (see differences between C2-N3-C4 and C2'-N3'-C4' angles in this chapter), and especially the strength of the hydrogen bonds, it would be a mistake to assign a higher symmetry to the crystal on the basis of statistical reasons. It is clear from the N3···N3' separation of 2.891(12) Å that the central H bond cannot be a symmetrical one. For such a case the separation is much too long. In fact, the asymmetry displayed in the intramolecular hydrogen bonding in the [1-MeC≡1-MeCH]$^+$ complex is consistent with the tendency followed by these complexes in the literature [7,11-14], in which the interaction between the (N4) amino group of the protonated base forms a stronger hydrogen bond to the (O2') carbonyl oxygen of the neutral base than that formed between the (N4') amino group of the neutral base and the (O2) carbonyl oxygen of the protonated base. This phenomenon can be understood considering the stronger acidity of the exocyclic nitrogen atom when the 1-methylcytosine is protonated [15].

Reported DFT calculations in the gas phase of the [1-MeC ≡ 1-MeCH]$^+$ cation predict the presence of an unsymmetrically located proton between both N(3) sites and a typical double minimum potential with a very low activation barrier [16]; in the case of **1**, this proton was not found in the difference Fourier map, probably due to the influence of the high electron density of the counter anion and the temperature of measurement (25º C) of the crystal. A very low temperature measurement seems to be crucial to locate this proton [14],

presenting a temperature dependent change from order to disorder. The rest of the geometrical appreciations of the DFT calculations is in agreement with the experimentally observed results.

With respect to **1**, it is worthwhile to mention that the triple hydrogen bonds between 1-MeC and 1MeCH$^+$ are weaker and have slightly longer distances than in the other published complexes having hemiprotonated 1-MeC base pairs. Namely, the distance O2···N4' is 2.966(11) Å, and N4···O2' 2.816(10) Å (O2, N4 are sites in the protonated 1-MeCH$^+$); to complete the association, the hydrogen donor site N3(H) forms the hydrogen bond with its corresponding site in the neutral 1-MeC, N3···N3' 2.891(12) Å.

The geometrical orientations of the 1-MeC rings and water allow for intermolecular hydrogen bonding between exocyclic groups of the 1-MeC bases and water. Thus, the three hydrogen bonds between the bases are reinforced by five additional hydrogen bonds originating from water molecules to the exocyclic atoms. O1w binds the oxygen of carbonyl sites and O2w the amino groups. Figure 1.2 shows the arrangement. Distance from O1w to O2' is 2.710(10) Å, and to O2 of an adjacent molecule (-x+1, y-1/2, -z+3/2) is 2.789(10) Å. Hydrogen bonds of O2w are with the exocyclic amino group of the protonated 1-methylcytosine (O2w···N4, 2.960(10) Å), and with the amino group of the neutral 1-methylcytosine in the next elemental cell, O2w···N4'(-x+2, y+1/2, -z+3/2), 3.051(10) Å. Likewise two molecules of water are joined to each other, O1w···O2w(-x+1, -y+1, -z+1) 2.710(9) Å. The atoms in each cytosine ring are approximately coplanar with a maximum deviation from the least-squares plane of less than 0.017(7) Å, but the exocyclic C1, O2 and N4 (C1', O2' and N4', respectively) atoms deviate slightly more from the plane, probably because of the active role in the hydrogen bond formation with the opposite 1-MeC, water of crystallization or the I_3^- anion.

The role of the triiodide anion in the hydrogen bonding pattern of the crystal is of least importance. Only a molecule of water (O2w) forms H-bond interactions. Thus, the terminal iodine atom (I3) is in closer proximity to a donor

site: I3···O2w(-x+2, y+1/2, -z+3/2), 3.654(6) Å; at the same time, O2w(-x+2, y+1/2, -z+3/2) interacts with I1 (3.983(6) Å). There are some remarkably short C–H···I contacts (≤ 4.1 Å) with the opposite part of the Watson-Crick edge, especially at the C5 and C6 aromatic sites (see Figure 1.2).

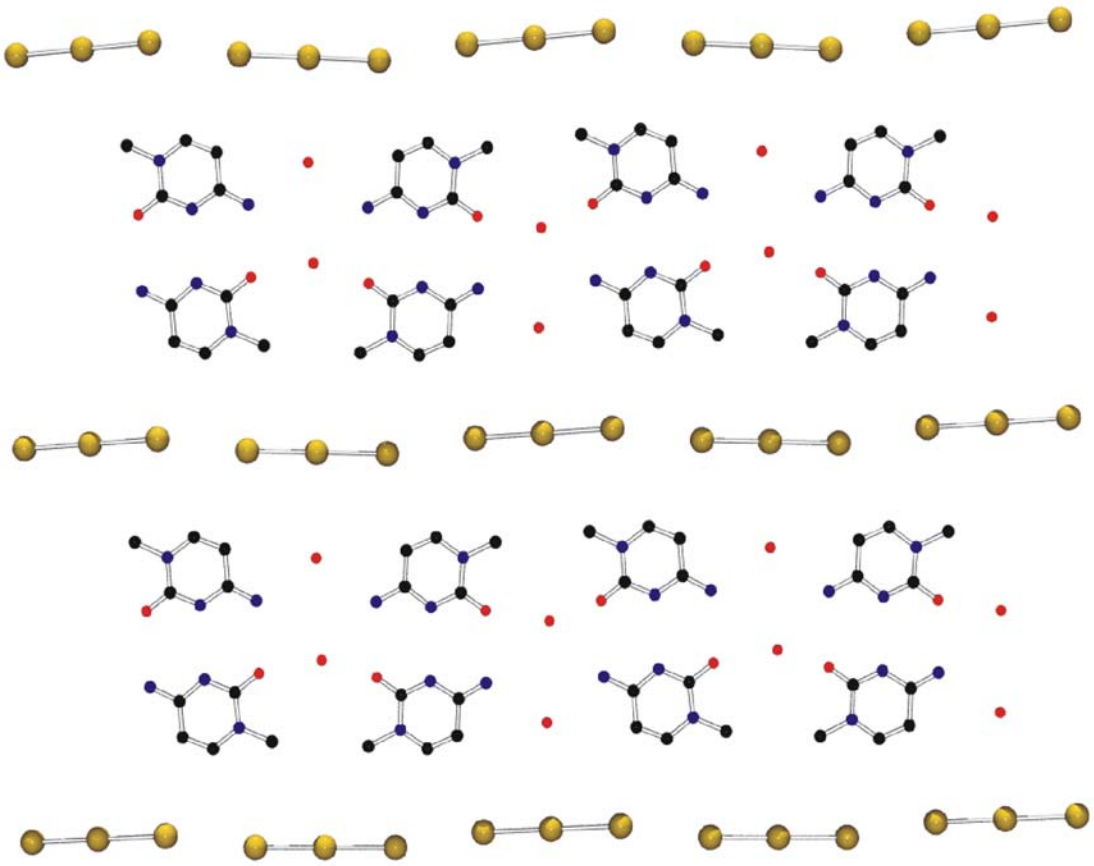

Figure 1.2: *Top view of the layers of **1**.*

The bases along with the water molecules are arranged in infinite ribbons, separated by the unsymmetrical triiodide counteranions and forming supramolecular structures. Figure 1.2 shows a view of the plane. Ribbons and triiodide anions form planes; superposition of planes builds the 3D crystal.

Hydrogen bonding between the 1-MeC bases and water has been discussed previously in the literature; however from the supramolecular point of view, it is interesting to emphasize that H–bonds in the 1-MeC bases are not coplanar with those involving water because water molecules are out of the

plane defined by the nucleobases: O1w, 0.476(14) Å; O2w, 0.379(14) Å. It is also significant that adjacent base pairs (-x+1, y±1/2, -z+3/2) are not coplanar, with a distance between parallel planes of 0.70(4) Å. Hemideprotonated 1-MeC base pairs are sitting above/below in a slight zigzag order. Triiodide anions follow the same zigzag order; terminal iodine atoms of I_3^- are coplanar with the closer pair of 1-methylcytosines, and the central iodine atom remains just in the middle, drawing the diagonal between the high and low extremes of the layer. Figure 1.3 shows the zigzag arrangement in the layers.

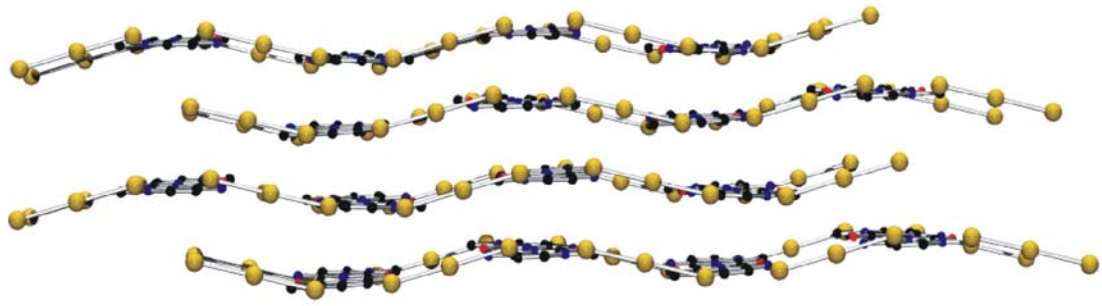

Figure 1.3: *View of the layers. 1-MeC pairs and triiodide counterions are included.*

The arrangement in each layer is identical; superposition of several layers in a similar zigzag arrangement favors the stacking and forms the packing of the crystal. The molecular overlap is always between a protonated 1-methylcytosine base and a neutral one, which are connected by strong π-stacking with a mean distance of 3.33(1) Å.

1.1.2.- [1-MeCH](NO$_3$) (2).

The compound [(dien)Pt(1-MeC-*N3*)](NO$_3$)$_2$ (**9**) was prepared in situ in order to study the different mechanisms of migration and deamination of the metal coordinated cytosine nucleobase, which are reported in the following chapter. Crystals of **2** were obtained from an aged solution of **9**. After several weeks at room temperature, decomposition of the starting compound is evident,

and as a consequence of the progressive increase of acidity, the 1-MeC base in solution is protonated at the N3 position and precipitates as the nitrate salt. The different Pt complexes (see Chapter 3) remain in solution, which acquires a brownish color.

The structure of **2** was determined at room temperature by X-ray crystallographic analysis. It consists of a protonated $[1\text{-MeCH}]^+$ base and nitrate as counter anion. The compound **2** crystallizes in the triclinic space group P-1, hence in very low symmetry in comparison with other reported salts of nucleobases. All the hydrogen atoms were found in the difference Fourier map and refined without restraints. A summary of crystallographic data, data collection parameters and refinement parameters of **2** data is given in Table A-2 (see Appendix).

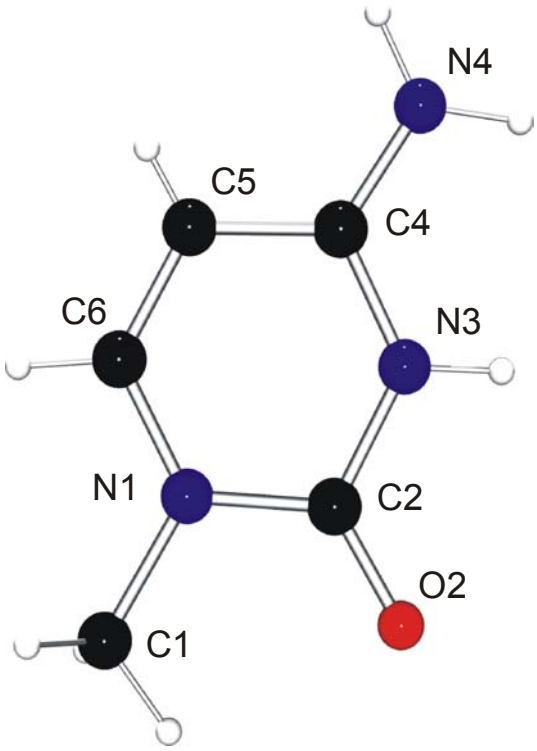

Figure 1.4: *View of 1-MeCH$^+$ (2) with atom labeling scheme.*

Several examples of protonated 1-methylcytosine nucleobase salts are reported, specifically: [1-MeCH](I_3) [8], [1-MeCH](Br) [17], [1-MeCH](Cl) [18] and [1-MeCH](ClO_4) [19]. Other examples of non-coordinated $[1\text{-MeCH}]^+$ are the non-

Watson-Crick base pairs $[1\text{-MeC}\equiv 1\text{-MeCH}]^+$, which are discussed in the previous chapter. This is the first example of an X-ray crystal structure of the nitrate salt of 1-methylcytosinium. Figure 1.4 presents an illustration of $[1\text{-MeCH}]^+$ with the atom numbering scheme.

The geometry of this protonated 1-methylcytosine nucleobase does not differ very much from other reported salts of $[1\text{-MeCH}]^+$. The most important effect is due to the protonation of the N3 site of the ring, which leads to an enlargement of 5.8(3)º of the internal ring angle. Significant differences of the bond distances compared with the unprotonated 1-MeC [20] are a lengthening of the C2–N3 bond (Δ = 0.03 Å), and shortenings of the C4–C5 (Δ = -0.02 Å), C5–C6 (Δ = -0.02 Å), C2–O2 (Δ = -0.04 Å), and C4–N4 (Δ = -0.01 Å) bonds.

Protons are bonded to the corresponding atoms having normal bond distances ranging from 0.79(3) to 1.00(5) Å. The six atoms of the ring in the cytosine nucleobase are almost coplanar, within a maximum deviation from the least-squares plane of less than 0.008 Å; however, the exocyclic N4 nitrogen atom is significantly out of the previously defined plane (0.071 Å). The bond distances and angles of the 1-methylcytosinium cation are compiled in Table 1.2.

The hydrogen bonding pattern is relatively uncomplicated; it is defined exclusively by interactions between the cytosinium cation and the surrounding nitrates. Every 1-MeCH^+ is encircled by four nitrates and two molecules of 1-MeCH^+, which lie in a coplanar layer. There are no inter-pyrimidine hydrogen contacts in the structure with the exception of the only possible interaction between the exocyclic carbonyl group and the proton bonded to the C6 atom of a neighboring cytosinium entity (x+1, y, z). However, the long distance (3.382(4) Å) and the unfavorable angle of the hydrogen bond (C6-H6-O2, 53(1)º) indicate that this C–H···O contact is insignificant in comparison to the other cytosine-nitrate contacts. Table 1.3 presents the shortest distances in the hydrogen bonding pattern of **2**.

Table 1.2: *Distances (Å) and angles (º) for* ***2****.*

	1-MeCH$^+$		1-MeCH$^+$
N1-C2	1.375(3)	N1-C2-N3	114.2(3)
C2-N3	1.388(3)	C2-N3-C4	125.8(3)
N3-C4	1.345(3)	N3-C4-C5	116.8(3)
C4-C5	1.405(4)	C4-C5-C6	118.8(3)
C5-C6	1.329(4)	C5-C6-N1	122.9(3)
C6-N1	1.356(3)	C6-N1-C2	121.4(3)
N1-C1	1.484(4)	C1-N1-C6	121.2(3)
C2-O2	1.211(3)	C1-N1-C2	117.4(3)
C4-N4	1.318(4)	O2-C2-N1	124.4(3)
		O2-C2-N3	121.4(3)
		N4-C4-N3	119.5(3)
		N4-C4-C5	123.7(3)

Table 1.3: *Bond distances (Å) and angles (º) involving the hydrogen atoms for* ***2****.*

D= proton donor atom; A = proton acceptor atom.

D-H	d(D-H)	d(H···A)	<DHA	d(D···A)	A
N4-H42	0.906	2.284	154.45	3.126	O2N (iii)
N4-H42	0.906	2.305	149.16	3.117	O3N (iii)
N4-H42	0.906	2.657	175.82	3.561	N1N (iii)
N3-H3	0.907	1.917	172.50	2.819	O2N (ii)
N4-H41	0.938	1.967	176.15	2.904	O1N (ii)

Symmetry codes: (i) x-1, y, z; (ii) x-1, y-1, z-1; (iii) x, y-1, z-1.

Shorter donor···acceptor interactions in the structure are between the oxygen atoms of the nitrate anions and the protons bonded to the nitrogen atoms of the cytosine base. Thus, the endocyclic N3(H) site has the shortest interaction with O2N(x-1, y-1, z-1) of nitrate, having a distance of 2.819(3) Å. Other relevant interactions are: N4(H)···O1N(x-1, y-1, z-1), 2.904(4) Å; N4(H)···O2N(x, y-1, z-1), 3.126(4) Å; and N4(H)···O3N(x, y-1, z-1), 3.117(4) Å. In the case of the C1(H_3) methyl group, the distances to the closest oxygen atoms of nitrate are 3.167(5) and 3.108(4) Å to O3N and O1N(x-1, y, z), respectively.

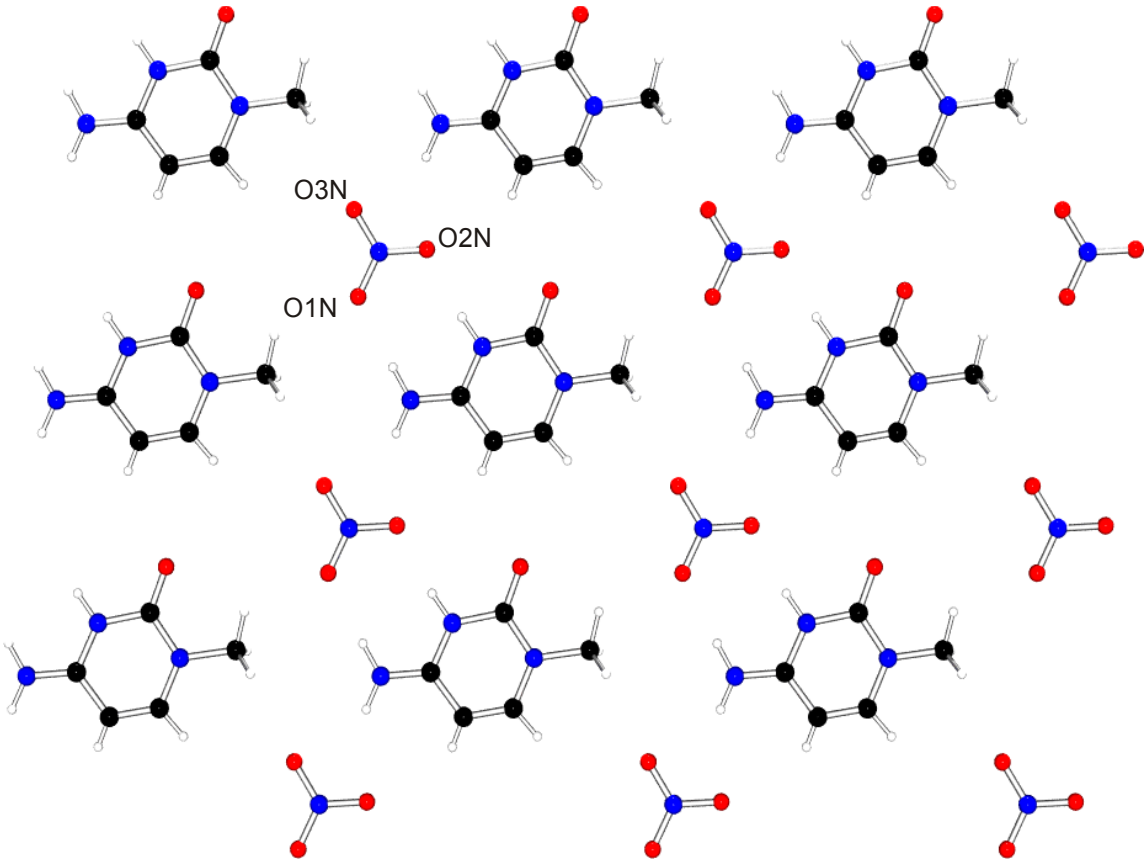

Figure 1.5: *View of a layer of the packing of* ***2****.*

All the hydrogen bonds between the cytosinium nucleobases and the nitrates are extended into infinite layers, which are approximately coplanar. Figure 1.5 gives an overview of the arrangement of cations and anions in the layers of the crystal, in which the unit motifs are repeated in all directions. Packing of the crystal is completed by superposition of layers perpendicularly to the *bc* plane. In this case, the geometrical arrangement of the layers and its superposition avoid the π-stacking overlap between the aromatic rings of the bases, because nitrate anions lie above and below the aromatic rings of the cytosine nucleobases. The separation distance between two consecutive layers is 3.19 Å, significantly shorter than in the other nucleobase salts, in which π-stacking of the aromatic rings of the bases is present. The packing drawing of the structure is given in Figure 1.6.

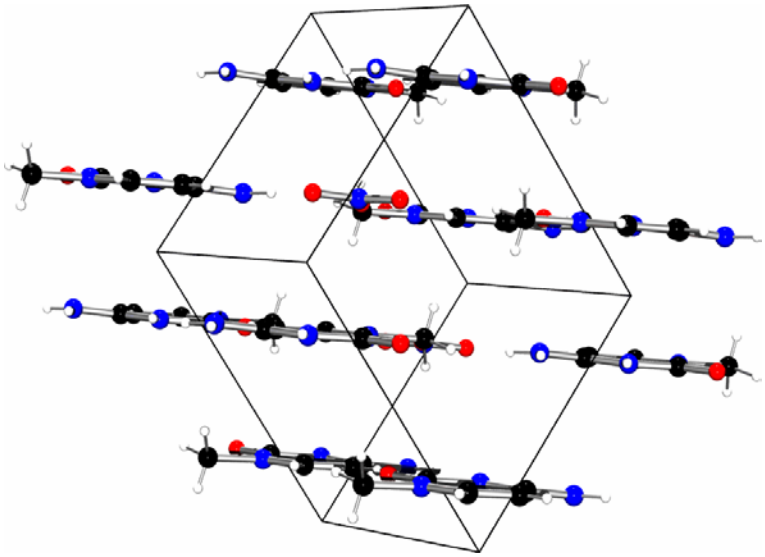

Figure 1.6: *View the unit cell of* ***2****.*

Taking into consideration the low number of hydrogen bonds and the absence of π-stacking in the packing of the crystal, a low crystallization energy value for **2** in comparison to other salts of 1-methylcytosine base is proposed.

1.2.- Adenine derivatives

N(9) substituted adenine nucleobases present a specific pattern of proton donor and acceptor sites, which is of high importance in solid state structures. Packing of the crystal depends on interactions between the nucleobases; these interactions are predominantly hydrogen bonds and π-stacking of the rings. In order to understand the hydrogen bonding, the strength of the donor and acceptor sites can be considered; in π-stacking, distances between the rings are significant. Thus, 9-MeA, for example, uses the endocyclic unprotonated nitrogen atoms as proton acceptor sites, in decreasing strength order: N(1) > N(7) > N(3); on the other hand, the exocyclic N(6) amino group represents the strongest proton donor site unless the N(1) position becomes protonated (see Figure 1.7).

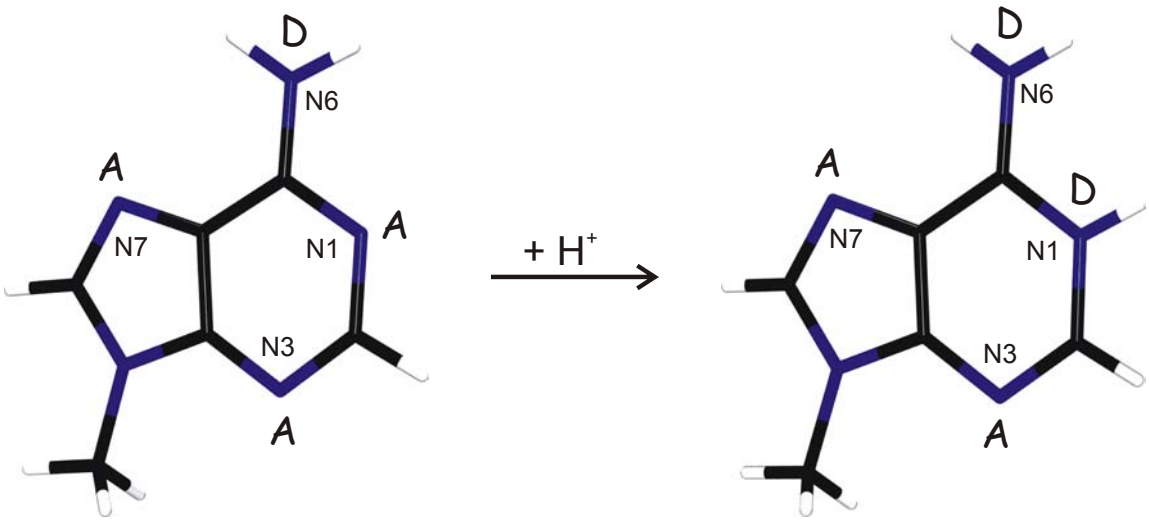

Figure 1.7: *Proton donor and acceptor sites in 9-MeA and 9-MeAH$^+$.*

The solid state structure of the unprotonated 9-MeA nucleobase displays an interesting hydrogen bonding pattern. Three of the four potential donor/acceptor positions are implicated in H-bonding. The shortest hydrogen bonding interaction is between one proton of the N(6) site with the N(1) position of an adjacent molecule. Simultaneously, the second proton of N(6) interacts with the N(7) site of another adjacent base (see H bond interaction "A" in Figure 1.8). Thus, a double (N6(H)···N1' and N6(H)'···N7) hydrogen bond interaction is present between two neighboring adenine nucleobases, with a C_2 axis in the geometrical central point of the internucleobase space. The weakest proton acceptor site N(3) of the 9-MeA nucleobase does not play a relevant role in this H-bond pattern. These interactions are repeated in infinite layers; finally, the crystal is completed by stacking of the layers.

With regard to the hydrogen bonding pattern displayed, protonation of substituted adenine model nucleobase occurs at the strongest proton acceptor site of the ring —the N(1)—, and modifies the pattern of proton donor and acceptor sites of the base. As shown in Figure 1.7, the 9-methyladeninium cation has two proton donor sites (N(1) > N(6)) and two proton acceptor sites (N(7) > N(3)).

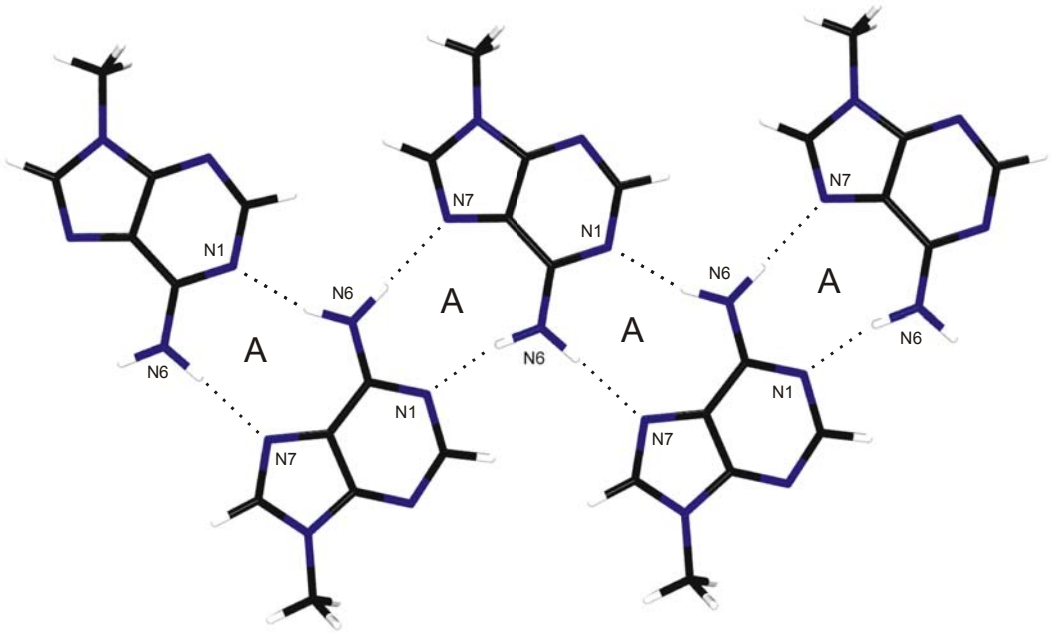

Figure 1.8: *Hydrogen bond pattern of 9-MeA.*

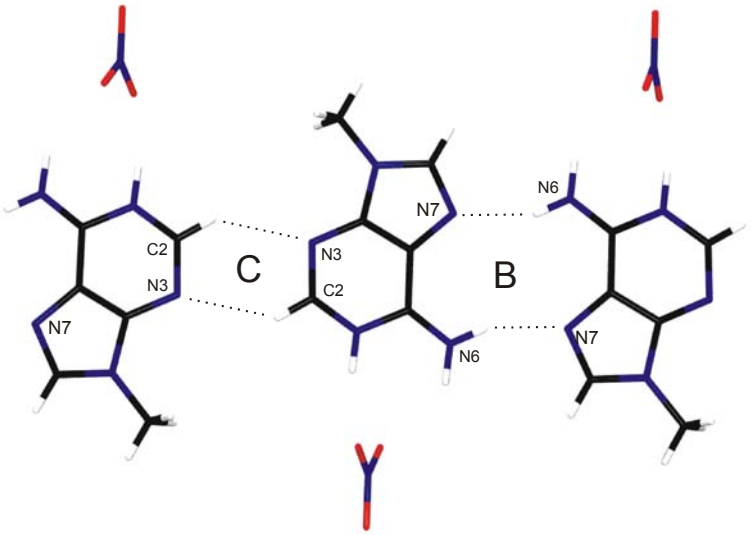

Figure 1.9: *Hydrogen bond pattern of [9-MeAH](NO$_3$).*

The hydrogen bonding patterns displayed in the various substituted adeninium salts are obviously very much influenced by the counter anions. The preferred arrangement of the adeninium cations connects pairs of bases to produce a centrosymmetrical base–pair involving the proton acceptor position N(7) and the proton donor N(6). This type of base pairing is also found in the double stranded homopolymer [polyAH$^+$]$_2$, formed from polyA at pH values under 4. With regard to the model nucleobases, reported 9-methyladeninium

salts of chloride [21] and nitrate (represented in Figure 1.9) [22] display this basic arrangement (interaction "B": N(6)H_2···N(7)' and N(7)···N(6)H_2'), reinforced by an additional double N(3)···HC(2) (interaction C) interaction connecting the base pairs. However, there is an example, [9-MeAH](Br) [17], where no hydrogen bonds are formed between rings; instead, each 9-$MeAH^+$ cation lies surrounded by a three-dimensional network of bromide ions forming hydrogen bonds, and hindering the direct interaction between nucleobases.

In this chapter three novel solid state structures of substituted adeninium salts are presented. The first one, [9-MeAH](PF_6) · H_2O (**3**), is in agreement with the preferred arrangement of the adeninium complexes, presenting a similar inter-nucleobase arrangement as [9-MeAH](NO_3). The second solid state structure, [(9-MeAH)](NO_3) · H_2O (**5**), displays interesting packing modifications due to the presence of a water molecule of crystallization. Finally, [9-EtAH](NO_3) (**4**), has an unusual hydrogen bonding pattern connecting nucleobases. Without doubt and as already mentioned above, counter anions play an important role in the packing of the crystal competing with the nucleobases for the best proton donor sites. A detailed study of the three novel structures is reported in the following.

1.2.1.- [9-MeAH](PF_6) · H_2O (3).

Crystals of [9-MeAH](PF_6) · H_2O (**3**) were obtained from a solution containing 9-methyladenine and 9-methylhypoxanthine bases, to which $NaPF_6$ had been added at acidic pH (HNO_3). It was the aim to investigate the co-crystallization conditions of both nucleobases and to study the hydrogen bonding patterns for comparison with the reported models of putative (AH)G(AH)G nucleobase tetrads (with AH = protonated adenine; G = guanine) [5]. It is noteworthy to point out that hypoxanthine has a proton instead of the exocyclic amino group present in guanine at the 2-position. An objective of the

study was to understand possible structural modifications provoked by the absence of the exocyclic amino group in the guanine base.

Crystals of the title compound were obtained from the solution after several days at room temperature. Composition and structure of **3** were determined by X-ray crystallography. Unexpectedly, no hypoxanthine base was found in the crystal structure. However, a very interesting hydrogen bonding pattern was found in the crystal structure formed by a protonated adenine base, a PF_6^- anion and a water molecule. In the solid state structure of **3**, all the hydrogen atoms, including the ones of the water molecule, were found in the difference Fourier map and refined without restraints. A list of the crystallographic data, data collection parameters and refinement parameters of **3** data is given in Table A-3 (see Appendix).

The 9-methyladeninium cation is practically coplanar; the exocyclic C9 methyl group is slightly out of the plane (0.041(3) Å) defined by the six endocyclic atoms of the ring, with a r.m.s deviation of 0.007 Å. N1 protonation of the nucleobase has the expected effect on the distances and angles between atoms of **3**; thus, its distance and angle values are consistent with other reported protonated adenine nucleobase salts [22]. A list of distances and angles is given in Table 1.4.

The most important intermolecular hydrogen bond interaction occurs via the Hoogsteen edges of the two protonated adenine nucleobases, forming centrosymmetric dimers, similar to the one observed in the double stranded $[polyAH^+]_2$ [23]. This interaction was previously defined in this chapter as “B” type, with pairs of hydrogen bonds between N7 and its symmetry related N6(H) site, separated by a distance of 2.941(3) Å. Consecutive centrosymmetric dimers of nucleobases are H-bonded, forming ribbons in which the observed interaction is of the “C” type (see Figure 1.9). This interaction is less important than the previous one, and consists of a double hydrogen bond contact between N3 and its symmetry generated C2(H), with a distance of 3.241(3) Å. The most important H–bond angles and distances are listed in Table 1.5.

Table 1.4: *Selected distances (Å) and angles (º) for* ***3****.*

N1–C2	1.363(3)	C2–N1–C6	122.9(2)
N1–C6	1.367(3)	N3–C2–N1	126.4(2)
C2–N3	1.289(3)	C2–N3–C4	111.6(2)
N3–C4	1.363(3)	N9–C4–N3	126.8(2)
C4–N9	1.362(3)	N9–C4–C5	106.0(2)
C4–C5	1.377(3)	N3–C4–C5	127.2(2)
C5–N7	1.381(3)	C4–C5–N7	110.8(2)
C5–C6	1.405(3)	C4–C5–C6	118.4(2)
C6–N6	1.310(3)	N7–C5–C6	130.8(2)
N7–C8	1.312(3)	N6–C6–N1	120.6(2)
C8–N9	1.359(3)	N6–C6–C5	125.8(2)
N9–C9	1.471(3)	N1–C6–C5	113.6(2)
		C8–N7–C5	103.2(2)
		N7–C8–N9	114.2(2)
		C8–N9–C4	105.8(2)
		C8–N9–C9	127.5(2)
		C4–N9–C9	126.6(2)

Table 1.5: *Distances (Å) and angles (º) involving the hydrogen atoms of* ***3****.*

D-H	d(D-H)	d(H···A)	<DHA	d(D···A)	A
N1-H1	0.934	1.775	167.18	2.693	O1w
N6-H61	0.854	2.119	161.17	2.941	N7(i)
N6-H62	0.933	2.018	151.50	2.873	F2
N6-H62	0.933	2.344	137.97	3.100	F1
N3-H2	0.906	2.335	102.70	3.241	C2(iii)
O1w-H1w	0.889	1.881	165.59	2.751	F3
O1w-H1w	0.889	2.606	131.24	3.262	F2
O1w-H2w	0.790	1.997	170.46	2.779	F1(ii)

Symmetry codes: (i) -x, -y+1, -z-1; (ii) -x+1, -y, -z; (iii) -x+2, -y, -z-1.

There are additional hydrogen bond interactions involving the nucleobases, the crystallization water molecules and the hexafluorophosphate

anions. As can be observed in Figure 1.10, ribbons formed by the protonated adenine nucleobases are separated by the PF_6^- counter anions and the water molecules. Consecutive ribbons of bases, the central P1 atom of PF_6^- and H_2O are approximately coplanar. The distance from P1 to the plane defined by the adenine rings is 0.098(5) Å (0.02 Å more than C9). The water molecule lies slightly further away, 0.213(4) Å above this plane. In this case, and because the hydrogen atoms of the water molecule were found, it is possible to describe all the hydrogen bonding interactions in the crystal.

The oxygen of the water molecule (O1w) interacts with the protonated N1(H) site of the Watson-Crick edge to produce a hydrogen bond with a relatively short distance (N1(H)···O1w, 2.693(3) Å). The water molecule has a slightly distorted tetrahedral geometry, with the following angles: H1w-O1w-H2w, 104.5º; H1w-O1w···H1, 112.1º; H2w-O1w···H1, 114.3º. The other electron pair is oriented to the 5-membered ring of the base. Protons bonded to the water molecule are oriented towards the fluorine atoms of the counter anion, forming hydrogen bond contacts. Thus, H1w interacts with the F3 atom of PF_6^- (distance O1w···F3, 2.751(3) Å; angle O1w-H1-F3, 165.6º), and a second interaction of minor importance of H1w is observed with the F2 atom (distance O1w···F2, 3.262(3) Å; angle O1w-H1-F2, 131.2º). In the case of H2, the interaction is observed with the F1 atom generated by the -x+2, -y, -z-1 symmetry operation (distance O1w···F1, 2.779(3) Å; angle O1w-H1-F2, 170.5º).

Hexafluorophosphate anions are enclosed by four adenine nucleobases and two water molecules with many hydrogen contacts. The most remarkable interactions are: contacts of F1 and F2 atoms with the H61 proton of the exocyclic amino group (distance N6···F2, 2.873(3) Å; angle N6-H62···F2, 151.5º; distance N6···F1, 3.100(3) Å; angle N6-H62···F1, 138.0º); contact of F3 atom with the H8 proton of the endocyclic C8 (x, y+1, z-1) site (distance C8···F3, 3.127(3) Å; angle C8-H8···F3, 160.5º), and the previously described interactions with the water molecule.

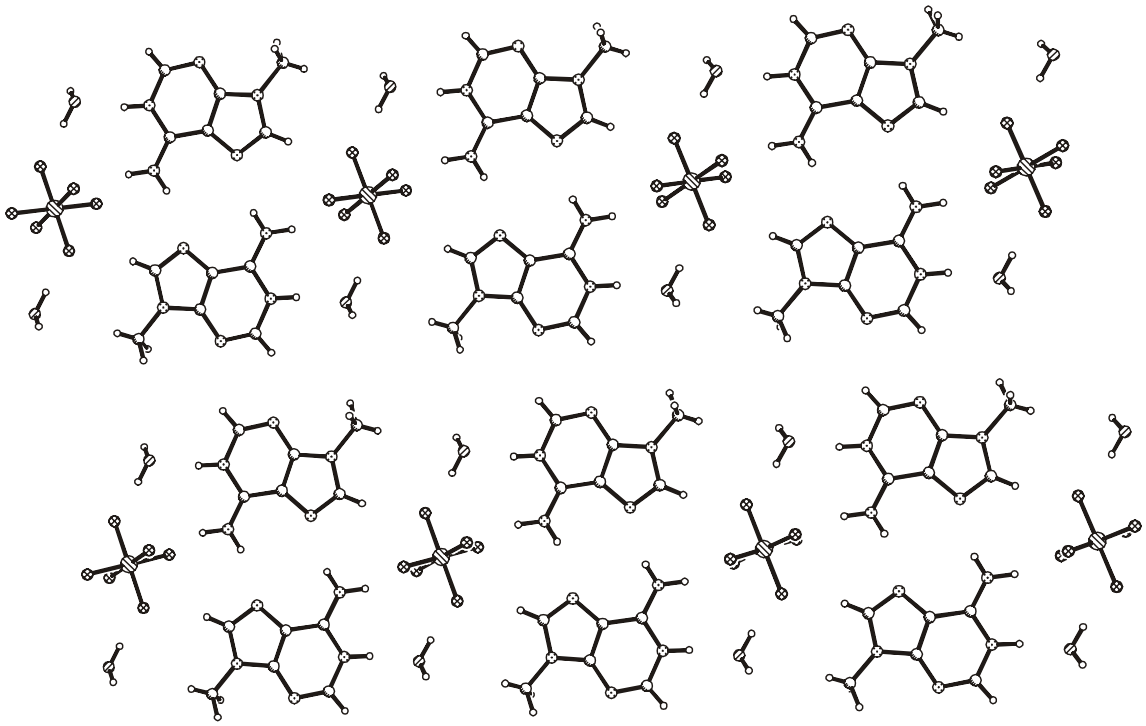

Figure 1.10: *Top view of a layer in the solid state structure of **3**.*

Ribbons of nucleobases, crystallization water and PF_6^- anions are extended, forming infinite layers. The distance between layers is 3.40 Å; protonated adenine nucleobases of two consecutive layers are interconnected by π-stacking. Figure 1.11 shows a crystallographic unit cell, in which each central phosphorous atom (P1) of the PF_6^- counter anion occupies a vertex of the unit cell.

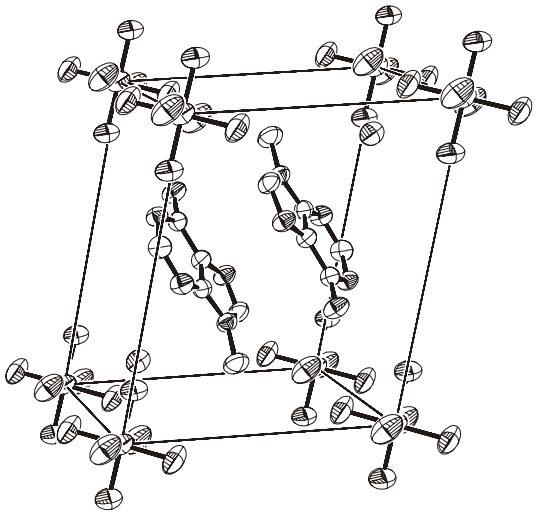

Figure 1.11: *View of a unit cell of the crystal structure of **3**.*

1.2.2.- [9-EtAH](NO_3) (4).

Crystals of the nitrate salt of 9-ethyladeninium were obtained from the mother liquor of a tetrakis(nucleobase) platinum complex which was synthesized by addition of an excess of 9-EtA to K_2PtCl_4 in HNO_3-acidic solution (HNO_3). The solution was allowed to evaporate at room temperature, leading eventually to the precipitation of colorless needles.

The solid-state structure of **4** shows a N(1) protonated 9-ethyladenine and a nitrate counterion. [9-EtAH](NO_3) (**4**) crystallizes in the triclinic crystal system. In the refinement process of the X-ray data, all non-hydrogen atoms were refined anisotropically; the hydrogen atoms were found with difference-Fourier synthesis, and refined isotropically. Details of measurement and refinement of the data are listed in Table A-4.

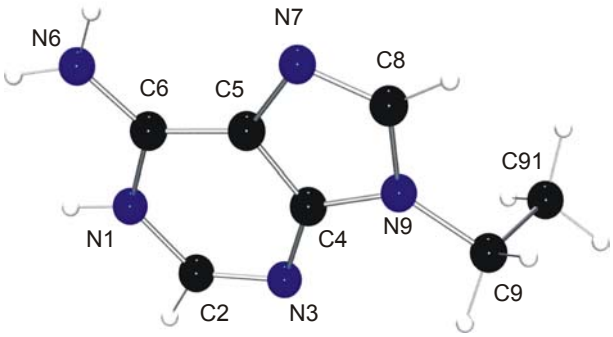

Figure 1.12: *View of the 9-EtAH$^+$ cation of **4**.*

Atoms of the 9-ethyladeninium cation are located in a planar arrangement (with a r.m.s. deviation of ± 0.021 Å), with the exception of the C(91) atom, the terminal CH_3 group of the ethyl substitute. It deviates from the plane of the nucleobase by 1.358(4) Å and forms a dihedral angle (plane of nucleobase rings – plane of ethyl group N9,C9,C91) of 83.5(3)º. Figure 1.12 shows a perspective view of the 9-methyladeninium cation of **4**.

As shown in Table 1.5, the angle and distance values in the 9-ethyladeninium cation are very similar to those of other protonated adeninium

derivatives previously reported [22]. Nevertheless, it is worthy of comment that the protonated N(1) atom has the expected internal ring angle (123.4(2)º) (previously published values between 122º $[(AH)_2](HPO_4) \cdot 2\ H_2O$ [24] and 124.3º of $[AH](Br) \cdot ½\ H_2O$ [25]). As in the case of $[1\text{-MeCH}]^+$, protonation of the endocyclic ring N atom causes the internal ring angle to increase.

Table 1.5: *Selected distances (Å) and angles (º) for non-hydrogen atoms in* ***4****.*

N1-C2	1.366(3)	N1-C2-N3	126.2(2)
C2-N3	1.294(3)	C2-N3-C4	110.9(2)
N3-C4	1.369(3)	N3-C4-C5	127.3(2)
C4-C5	1.377(3)	C4-C5-C6	119.0(2)
C5-C6	1.389(3)	C5-C6-N1	113.2(2)
C6-N1	1.366(3)	C6-N1-C2	123.4(2)
C5-N7	1.385(2)	C5-N7-C8	102.5(2)
N7-C8	1.300(3)	N7-C8-N9	115.3(2)
C8-N9	1.376(3)	C8-N9-C4	104.6(2)
N9-C4	1.354(3)	C4-C5-N7	110.9(2)
C6-N6	1.314(3)	N1-C6-N6	120.2(3)
N9-C9	1.468(3)	N6-C6-C5	126.6(2)
C9-C91	1.509(4)	C8-N9-C9	127.8(2)
		C4-N9-C9	127.7(2)
		C6-C5-N7	130.0(2)
		N3-C4-N9	125.9(2)
		N9-C9-C91	111.9(3)

In the case of **4**, three shared nitrate counterions (two of them belong to adjacent unit cells) are placed around the 9-EtAH^+ cation. Nitrate anions display different orientations in the crystal, with a dihedral angle of 29.5(1)º with the plane of the rings of the base. Figure 1.13 shows interactions of the different nitrates with the nucleobases; it is evident that the most important potential H bonding sites of the 9-ethyladeninium cation are blocked by the three nitrate counterions. Thus it is possible to observe a dense net of hydrogen contacts involving the nitrate groups: HN(1)···O(1), 2.910(3) Å; HN(1)···O(3), 2.937(3) Å;

HC(2)···O(1), 3.211(4) Å; H_{61}N(6)···O(1), 2.908(3) Å; H_{61}N(6)···O(2), 3.256(3) Å; H_{62}N(6)···O(2) 2.961(3) Å.

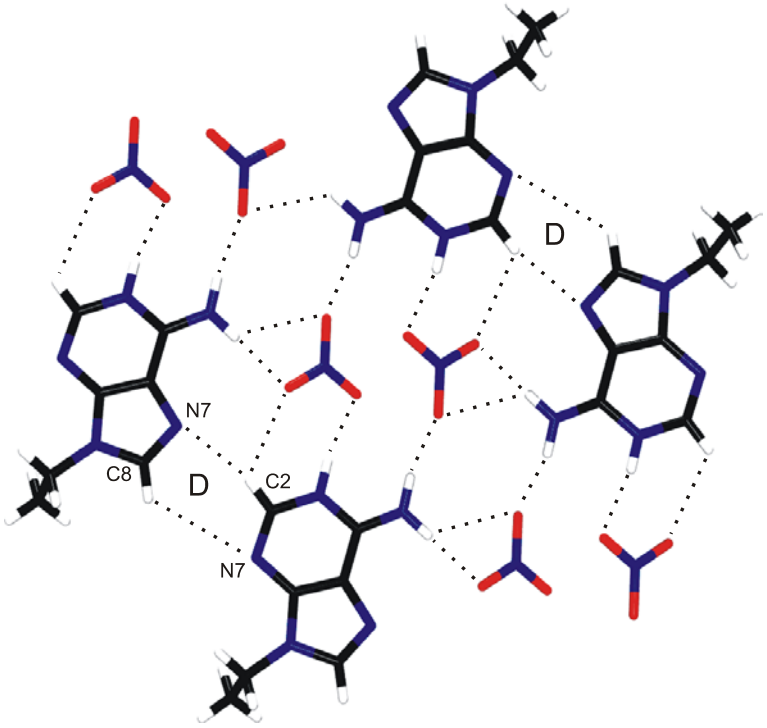

Figure 1.13: *View of the hydrogen bond pattern of* ***4****.*

A possible intermolecular twofold hydrogen contact could also be considered between N(7) and HC(2) of an adjacent molecule (x+1, y, z) with a distance of 3.393(3) Å and a second one, involving HC(8) and N(7) sites of the same two molecules. In principle, this second interaction seems to be unfavorable for a hydrogen bridge; but probably contributes to the stability of the crystal, reinforcing the N(7)···HC(2) contact. In order to assign a nomenclature to this interaction according to the previous criterion, we name this interaction as "D". Nucleobases connected by this "D" intermolecular interaction are coplanar. Bases of adjacent cells are in a slightly displaced plane (0.69 Å). On the other side, the edge containing the N(3) site and the ethyl group does not interact with neighbor molecules; however the ethyl groups are orientated towards the N(3) site of opposite cations. Orientation of the nucleobases in the successive planes along b axis is in opposite direction. There are π-stacking interaction between

rings which are separated by a distance of 3.41 Å. Figure 1.14 shows a better perspective of the planes along the b axis.

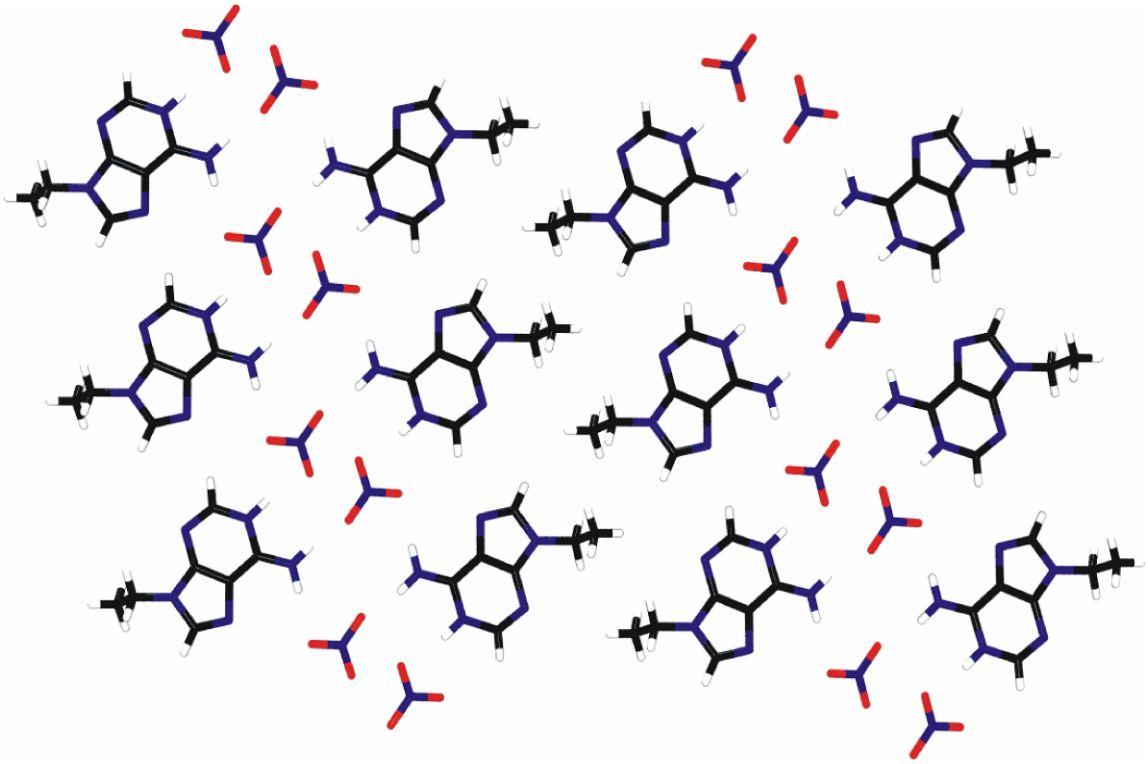

Figure 1.14: *Top view of a layer in the crystal packing of **4**.*

1.2.3.- [9-MeAH](NO$_3$) · H$_2$O (5).

Crystals of [9-MeAH](NO$_3$) · H$_2$O (**5**) were obtained as a byproduct of the reaction of *cis*-[Pt(9-EtGH-*N7*)$_2$(OH$_2$)$_2$]$^{2+}$ with an excess of 9-methyladenine under acidic conditions (HNO$_3$). After a couple of days, colorless crystals were isolated and their composition determined. In the X-ray crystallograpic determination of the structure, all the hydrogen atoms were found in the difference Fourier map and refined without restraints. A list of the crystallographic data, data collection parameters and refinement parameters of **5** is given in Table A-5 (see Appendix).

The 9-methyladeninium cation can be considered planar, presenting a relatively high r.m.s deviation (0.013 Å). However, a meticulous observation of the nucleobase reveals that the two halves of the purine ring are slightly bent across the C4–C5 bond. In other words, the six-atom aromatic ring N1-C2-N3-C4-C5-C6 (r.m.s. deviation: 0.005 Å) forms a dihedral angle of 1.74(9)º with the five-atom aromatic ring C4-C5-N7-C8-N9, which presents a r.m.s. deviation of only 0.0015 Å. Exocyclic atoms are not out of the plane defined by the endocyclic atoms. Except of this small deviation, all the distances and angles in the protonated 9-methyladenine base are not unusual [22]. Distances and angles between the principal atoms in **5** are given in Table 1.6.

Table 1.6: *Distances (Å) and angles (º) for* ***5****.*

N1–C2	1.364(2)	C2–N1–C6	123.6(1)
N1–C6	1.369(2)	N3–C2–N1	125.6(2)
C2–N3	1.301(2)	C2–N3–C4	111.9(1)
N3–C4	1.361(2)	N9–C4–N3	126.7(1)
C4–N9	1.362(2)	N9–C4–C5	106.1(1)
C4–C5	1.384(2)	N3–C4–C5	127.25(1)
C5–N7	1.380(2)	C4–C5–N7	110.7(1)
C5–C6	1.409(2)	C4–C5–C6	118.3(1)
C6–N6	1.301(2)	N7–C5–C6	131.0(1)
N7–C8	1.318(2)	N6–C6–N1	121.6(2)
C8–N9	1.361(2)	N6–C6–C5	125.1(1)
N9–C9	1.462(2)	N1–C6–C5	113.4(1)
		C8–N7–C5	103.3(1)
		N7–C8–N9	114.1(1)
		C8–N9–C4	105.9(1)
		C8–N9–C9	127.3(1)
		C4–N9–C9	126.9(1)

The crystal packing of **5** is governed by hydrogen bonding. The 9-methyladeninium cations form centrosymmetric dimers via the Hoogsteen edges, as seen in the previously reported hexafluorophosphate salt. This type

"B" interaction between N(7) and its symmetry generated (-x, -y+1, -z) N(6)H site displays a distance of 2.980(2) Å. In this case, the adenine bases of the dimers are not coplanar; the distance between the planes of the nucleobases is 0.41 Å. Figure 1.15 shows a stick diagram of the cations, in which the non-planarity of the adjacent cations and the small deviation (1.74(9)º) of the planarity of the nucleobase rings can be recognized.

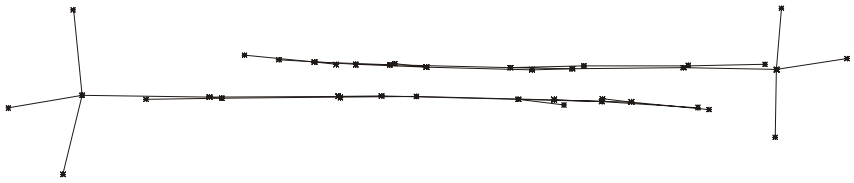

Figure 1.15: *Side view of the bases of **5**. Non-planarity of the rings and distance between the twofold hydrogen bond are observed.*

Proton donor sites of 9-methyladeninium are blocked by H bonds extending from oxygen atoms, either from the crystallization water or from nitrate counter anions, thereby hindering further internucleobase hydrogen bonding interactions. Figure 1.16 shows hydrogen bonding interactions of the centrosymmetric dimer to oxygen atoms of neighboring H bond partners. Mean angles and bond distances involving H bond contacts in the crystal are listed in Table 1.7.

Table 1.7: *Bond distances (Å) and angles (º) involving the hydrogen atoms of **5**.*

D-H	d(D-H)	d(H···A)	<DHA	d(D···A)	A
N6-H61	0.808	2.200	162.13	2.980	N7(i)
N6-H62	0.816	2.069	163.08	2.860	O1w(i)
N1-H1	0.944	1.799	172.25	2.737	O3(ii)
N1-H1	0.944	2.564	126.57	3.217	O1(ii)

Symmetry codes: (i) -x, -y+1, -z; (ii) x-1/2, -y+3/2, z-1/2.

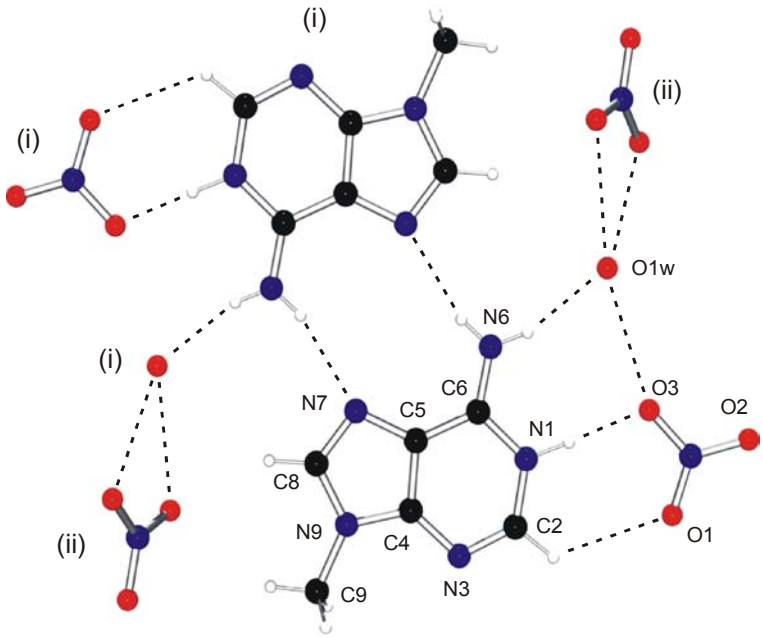

Figure 1.16: *Hydrogen bonding pattern in **5**. 9-MeAH$^+$, nitrate and crystallization water are related by the symmetry operators: (i) -x, -y+1, -z, (ii) x-1/2, -y+3/2, z-1/2.*

Hydrogen bonding between water molecules (O1w) of crystallization leads to the formation of infinite chains. In addition to the principal H-bond interaction of water to the proton of the exocyclic N(6) site of adenine, there are some other hydrogen bond interactions which are involved in assembling the chain. O1w displays sp^3 hybridization, forming a tetrahedron with the following heavy atoms placed in its vertex: N6 (2.860(2) Å), O2 (nitrate, 2.887(2) Å) and two water molecules O1w(-x+1/2, y+1/2, -z+1/2) and O1w(x+1/2, y-1/2, -z+1/2), both at a distance of 2.963(2) Å. Formally, water molecule interactions in this crystal, can be considered a one-dimensional polymer chain with a zigzag arrangement. The distances and angles between water molecules are 2.963(2) Å and 80.82(8)º respectively.

Protons bonded to the carbon atoms in the molecule do not show significant contacts. The distance between the C8(H) atom and the O2 atom of nitrate is 3.299(2) Å, but the angle between H8 and both atoms is very unfavorable 114.0(1)º. C(2)H is perhaps of more interest, but distances are quite long and also display unfavorable angles with the oxygen atoms (most favorable distance is 3.35 Å and the most favorable angle, 122.8º). However, long inter-

nucleobase hydrogen bond contacts between dimers of $[9\text{-MeAH}]^+$ and neighbor dimers involve this proton. Thus, 3.453(2) Å is the distance C2(H)···N3(-x+1/2, y+1/2, -z-1/2) to the previous unit cell, and also the distance N3···(H)C2(-x+1/2, y-1/2, -z-1/2) to the next unit cell. Figure 1.7 shows a detailed view of these hydrogen bond contacts via the sugar edges of the nucleobases.

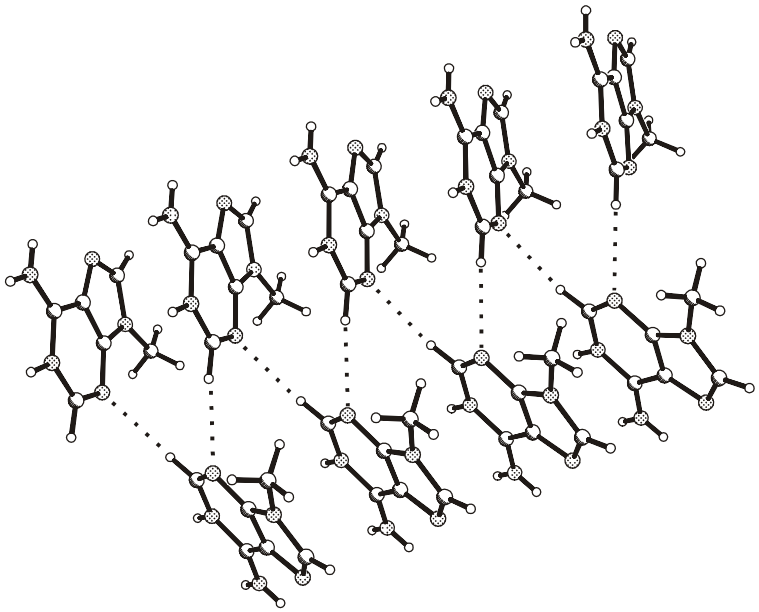

Figure 1.17: *View of the intermolecular H-bond interactions of* ***5****.*

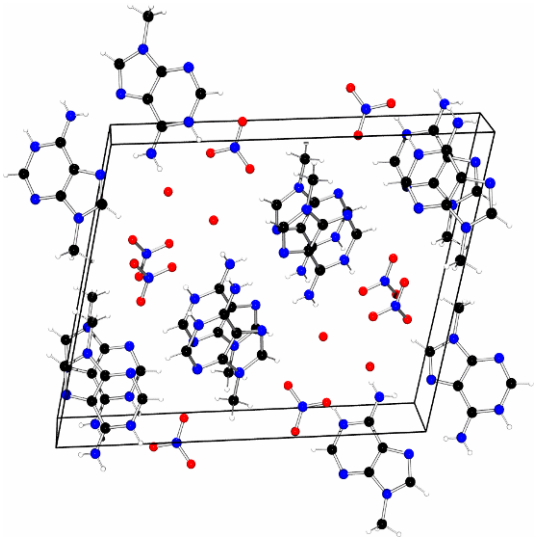

Figure 1.18: *View of a unit cell of the crystal structure of* ***5****.*

Unlike in the structures described above, where the nucleobases are arranged in planes, in **5** the nucleobases do not form infinite planes. Dimers of

9-methyladeninium are piled in blocks bordered by nitrate counter anions and water molecules as previously described. Interactions of a π-stacking nature are observed between rings of 9-MeAH$^+$ separated by a distance of 3.37 Å. Figure 1.18 displays the unit cell of the crystal.

1.3.- Guanine derivatives

Crystals of [(9-EtGH)$_2$] · xH_2O were obtained as a by-product of the tetrakis nucleobase compound [Pt(9-EtGH)$_4$](NO_3)$_2$ (**30**). In the synthesis of the latter an excess of six equivalents of 9-EtGH was added to the solution per equivalent of K_2PtCl_4. Several X-ray crystallography measurements of different crystals isolated from of the remaining solutions were carried out. Consistently only two types of crystals with two types of unit cells were found, which contained 4 and 7 water molecules, respectively. In the following pages, the crystal structures of both complexes, [(9-EtGH)$_2$] · 4H_2O (**6**) and [(9-EtGH)$_2$] · 7H_2O (**7**), are reported.

1.3.1.- [(9-EtGH)$_2$] · 4H_2O (6).

The structure of [(9-EtGH)$_2$] · 4H_2O (**6**) was determined by means of X-ray crystallography and was found to consist of a neutral 9-EtGH dimer accompanied by four molecules of water of crystallization. Due to the very high quality of the measured crystal it was possible to study the internal interactions of it in detail. Compound **6** crystallizes in the triclinic crystal system. In the refinement process, all the hydrogen atoms, including the ones of the four water molecules, were found in the difference Fourier map and refined without restraints. Crystallographic data, data collection parameters and refinement parameters of **6** data are listed in Table A-6 (see Appendix).

In contrast to the other nucleobase crystal structures reported in this chapter, the nucleobase present in **6** (and **7**) is not protonated. Thus, no counteranions were found in the crystal structure. However, the presence of the crystallization water and its interactions provides a very rich hydrogen bonding pattern. In this case, the localization of the protons of the water of crystallization was fundamental to the accurate description of the hydrogen bonds, including interactions between the 9-ethylguanine nucleobases, and interactions between different water molecules of crystallization.

The crystal structure of **6** contains two molecules of the 9-EtGH nucleobase forming a dimer. Non-hydrogen atoms of each 9-EtGH are situated in a planar arrangement, including the exocyclic ethyl groups; the r.m.s. deviations are 0.015 Å and 0.041 Å, respectively. Deviations from planarity are largest for the exocyclic groups, with a major effect in the ethyl groups; the carbon atom of the terminal CH_3 group (C92A) displays the longest distance to the nucleobase plane, 0.096(2) Å. Other atoms also show minor deviations, which are not very remarkable, however. Distances and angles between atoms of the 9-EtGH bases are not unusual in comparison to other reported guanine bases [26-29]. With the only exception of the ethyl group of the nucleobases, which are not identically located in the two nucleobases, the remaining distances and angles between atoms of the bases are equivalent. Bond distances and angles between atoms of 9-EtGH bases are listed in Table 1.8.

Both 9-ethylguanine entities are oriented in such a way to form a double intermolecular hydrogen bond in which the Watson Crick edge of one guanine nucleobase is located in front of the Hoogsteen edge of the second base. Both nucleobases display parallel orientation but are not coplanar; $(9\text{-EtGH})_b$ lies 0.19 Å above the plane defined by the first nucleobase. Distances of the hydrogen bonds are: O6···N2A, 2.886(3) Å; N7···N1A, 2.869(3) Å. A third hydrogen bond contact (C8···O6A, 3.593(3)) is observed; this last interaction is much longer than the other two hydrogen bonds, but probably also contributes to the stability of the crystal. Figure 1.19 shows the 9-EtGH dimer and its orientation.

Table 1.8: Selected distances (Å) and angles (º) for **6**.

	9-EtGH	9-EtGH$_a$		9-EtGH	9-EtGH$_a$
N1–C2	1.361(3)	1.377(3)	C2-N1-C6	125.1(2)	124.0(2)
N1–C6	1.399(3)	1.400(2)	N3-C2-N2	119.3(3)	119.4(2)
C2–N3	1.331(3)	1.330(3)	N3-C2-N1	124.7(2)	124.9(2)
C2–N2	1.349(3)	1.347(3)	N2-C2-N1	116.0(2)	115.7(2)
N3–C4	1.364(2)	1.365(2)	C2-N3-C4	111.0(2)	110.9(2)
C4–N9	1.367(3)	1.371(2)	N3-C4-N9	124.7(2)	124.6(2)
C4–C5	1.368(3)	1.372(3)	N3-C4-C5	128.5(2)	128.6(2)
C5–N7	1.403(2)	1.402(2)	N9-C4-C5	106.9(2)	106.9(2)
C5–C6	1.418(3)	1.404(3)	C4-C5-N7	110.4(2)	110.0(2)
C6–O6	1.249(3)	1.240(2)	C4-C5-C6	119.7(2)	119.6(2)
N7–C8	1.311(3)	1.320(3)	N7-C5-C6	129.9(2)	130.3(2)
C8–N9	1.380(3)	1.374(3)	O6-C6-N1	119.8(2)	120.0(2)
N9–C91	1.465(3)	1.470(3)	O6-C6-C5	129.2(2)	128.1(2)
C91–C92	1.493(4)	1.517(3)	N1-C6-C5	111.0(2)	111.9(2)
			C8-N7-C5	103.5(2)	103.9(2)
			N7-C8-N9	113.7(2)	113.3(2)
			C4-N9-C8	105.5(2)	105.9(2)
			C4-N9-C91	123.7(2)	124.8(2)
			C8-N9-C91	130.6(2)	129.4(2)
			N9-C91-C92	114.1(3)	111.8(2)

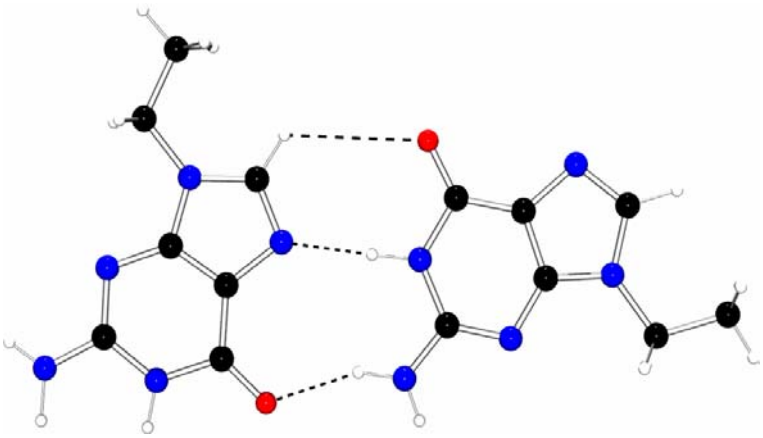

Figure 1.19: *View of the double H-bond between the two 9-EtGH bases in* ***6****. A third, long hydrogen bond interaction reinforcing the double H-bond is also observed.*

The crystal is dominated by this type of self-assembly of guanine nucleobases; consecutive 9-ethylguanine bases are arranged according to these hydrogen bond interactions in which each nucleobase has its Watson-Crick and Hoogsteen edges implicated in hydrogen bond formation. Thus, infinite chains are formed in which both edges of the bases are involved in forming hydrogen bonds in a zig zag fashion. N1(H)···N7A and N2(H_2)···O6A form cyclic hydrogen bonds, in which the secondary interactions (crossed, N2(H_2)···N7A and N1(H)···O6A) are favorable [30,31]. Secondary interactions are defined positive if the crossed interactions are between a proton acceptor site and a H bonded to a proton donor site (A···H-D); in the other cases (A···A, or D-H···H-D), the secondary interaction is defined negative. Figure 1.20 shows a H-bonded 9-EtGH chain and its orientation along the b axis.

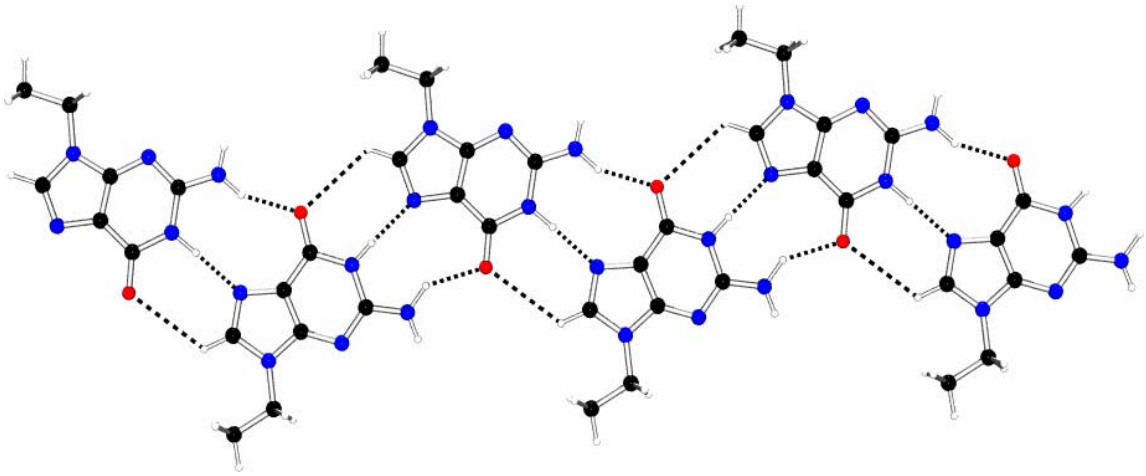

Figure 1.20: *View of the 9-EtGH base chain along the b axis in* ***6****.*

Infinite ribbons are π-stacked with a separation distance of 3.40 Å between parallel nucleobases. Ribbons of guanine nucleobases form layers with other parallel ribbons lying in the same plane. The water molecules of crystallization are placed in the hollows generated between adjacent ribbons, forming the particular polymeric structure described below.

Several examples of self-association of guanosine derivatives have been reported previously. Three different polymeric structures are described, two of which relate to polymeric ribbon formation [32], and the third one to G_4 tetrad

formation [33,34]. In the first type, to which **6** belongs, N1(H)···N7' and N2(H_2)···O6' interactions are observed, and obviously, the secondary interactions are defined positive. The second type of polymer displays guanine derivatives connected by twofold hydrogen bonds; the Watson Crick edge of a guanine base is H-bonded to the Watson Crick edge of the next base N1(H)···O6' and O6···(H)N1'. On the other side sugar edges of the guanine nucleobases are also connected with a double N2(H_2)···N3 hydrogen bond. In this case both secondary interactions, N1(H)···(H)N1 and O6···O6 in the Watson Crick edges and N2(H_2)···(H_2)N2 and N3···N3 of the sugar edges are negative defined. The third type of self association patterns of G pairs refers to the formation of a G_4 tetrad; in this quartet each guanine nucleobase displays two double hydrogen bonds to neighbor bases: N2(H_2)···N7' and N1(H)···O6' (and vice versa). In this pattern the secondary interactions are likewise positive.

There are no other twofold bond interactions between guanine bases possible that could be involved in the formation of polymers from a geometrical point of view (as N1(H)···N3, N2(H_2)···O6; N1(H)···N3, N2(H_2)···N7; or N1(H)···N7, N2(H_2)···N3). In Figure 1.21, the three possible types of self-assembly guanine base are depicted: on top, the N1(H)···N7' and N2(H_2)···O6' interaction; in the middle, N1(H)···O6' and N2(H_2)···N3 double hydrogen bond; and on the bottom the tetrad structure, with the double N2(H_2)···N7' and N1(H)···O6' hydrogen bond.

To continue the description of the H-bond pattern displayed in **6**, Table 1.9 lists the most important hydrogen bond interactions between possible proton donor and acceptor sites of the guanine bases and water. A brief glance at the table reveals the rich H-bond pattern of the structure. In addition to the intermolecular 9-EtGH interactions, multiple water molecules of crystallization are interacting either with the guanine base ribbons or with other water molecules.

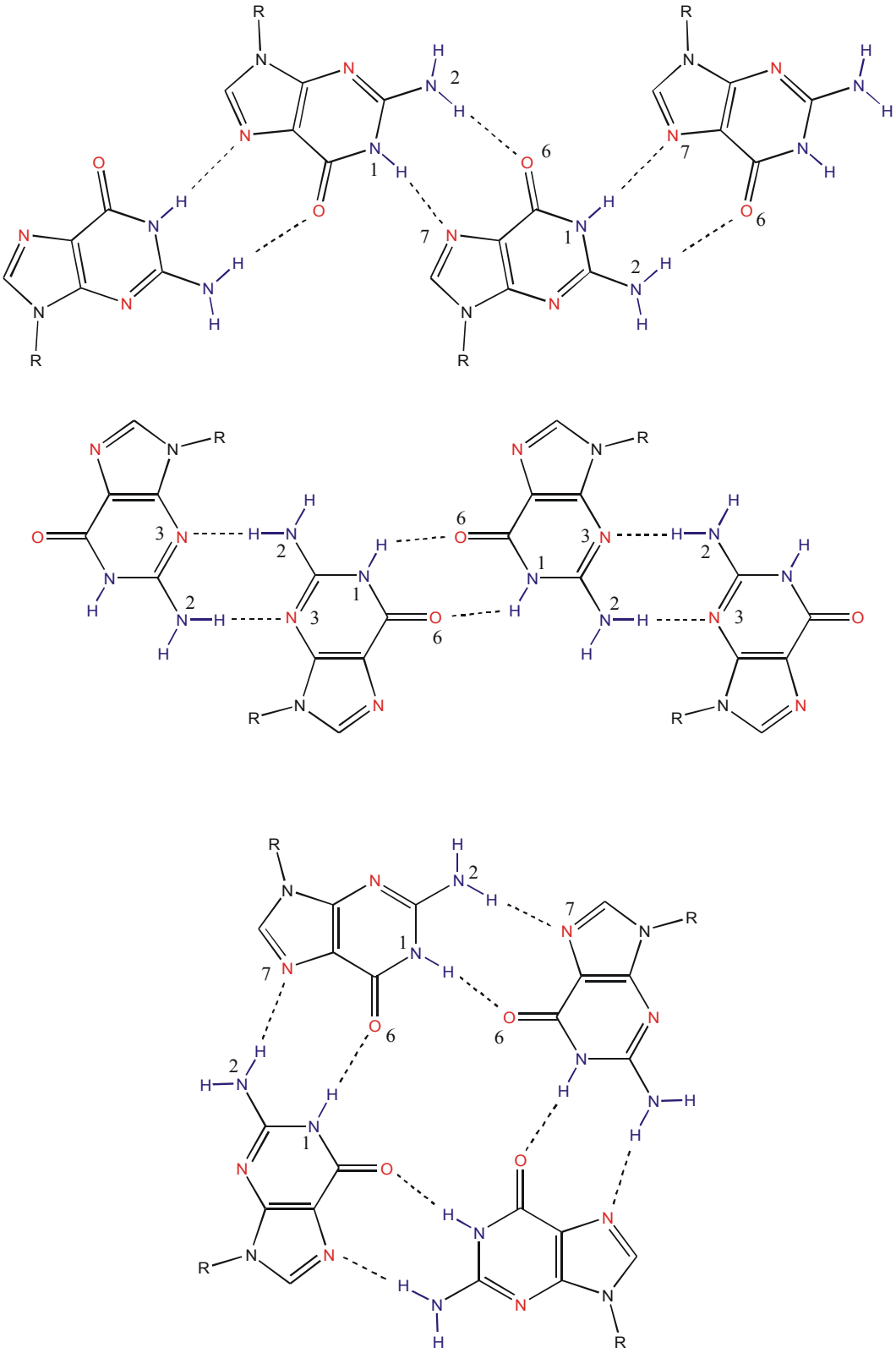

Figure 1.21: *Possible self-association patterns of guanosine. Twofold H-bond interactions are: (i) N2(H)···O6 and N1(H)···N7, with positive secondary interactions; (ii) double N2(H)···N3 and double N1(H)···O6, with negative secondary interactions in both cases; (iii) N1(H)···O6 and N2(H)···N7, with positive secondary interactions.*

Table 1.9: *Bond distances (Å) and angles (º) involving the hydrogen atoms of* ***6****.*

D-H	d(D-H)	d(H···A)	<DHA	d(D···A)	A
N1-H1	0.923	1.896	176.93	2.818	N7A(i)
N2-H21	1.007	2.019	142.59	2.884	O6A(i)
N2-H21	1.007	2.616	135.19	3.4051	N7A(i)
N2-H22	0.881	2.433	138.45	3.147	O3w(ii)
N1A-H1A	0.992	1.880	174.23	2.869	N7
N2A-H21A	0.958	1.986	155.73	2.886	O6
N2A-H22A	0.864	2.222	149.18	2.997	O2w
O1w-H11w	0.781	2.065	166.76	2.831	O2w
O1w-H12w	1.141	1.736	161.04	2.839	O6A(iii)
O2w-H21w	0.843	1.940	177.33	2.782	O4w
O2w-H22w	1.012	1.771	176.65	2.782	O3w
O3w-H31w	0.915	1.843	165.40	2.739	O1w(iv)
O3w-H32w	0.844	1.944	165.87	2.770	O6
O4w-H41w	1.053	1.781	169.42	2.822	N3(v)
O4w-H42w	0.862	2.125	172.49	2.982	O3w(vi)

Symmetry codes: (i) x, y-1, z; (ii) -x-3, -y-3, -z-1; (iii) -x-2, -y-2, -z-1; (iv) x-1, y, z; (v) x, y, z-1; (vi) -x-3, -y-3, -z-2.

Three of the water molecules of crystallization and their symmetry-related partners (-x-3, -y-3, -z-2) adopt a very interesting cyclic hexamer structure in the crystal. A relatively high stability of the water hexamer structure can be anticipated because the protons between oxygen atoms of the water molecules were detected in the X-ray crystallographic measurements. Vertices of the hexamer are the atoms O2w, O3w, O4w and its symmetry related atoms O2w', O3w', O4w' (symmetry operator: -x-3, -y-3, -z-2). Distances O2w···O3w and O2w···O4w are exactly the same, 2.782(3) Å. However, the distance between O4w···O3w' is slightly longer (2.982(3) Å). The angles between oxygen atoms of the hexamer are: O3w-O2w-O4w, 109.80(9)º; O2w-O4w-O3w', 129.8(1)º, O2w-O3w-O4w', 114.11(9)º. The distances and angles in **6** are in agreement with reported examples that include this type of water cyclic architectures [35-38].

Figure 1.22 shows top and side views of the hexameric arrangement including the protons and hydrogen bonding pattern.

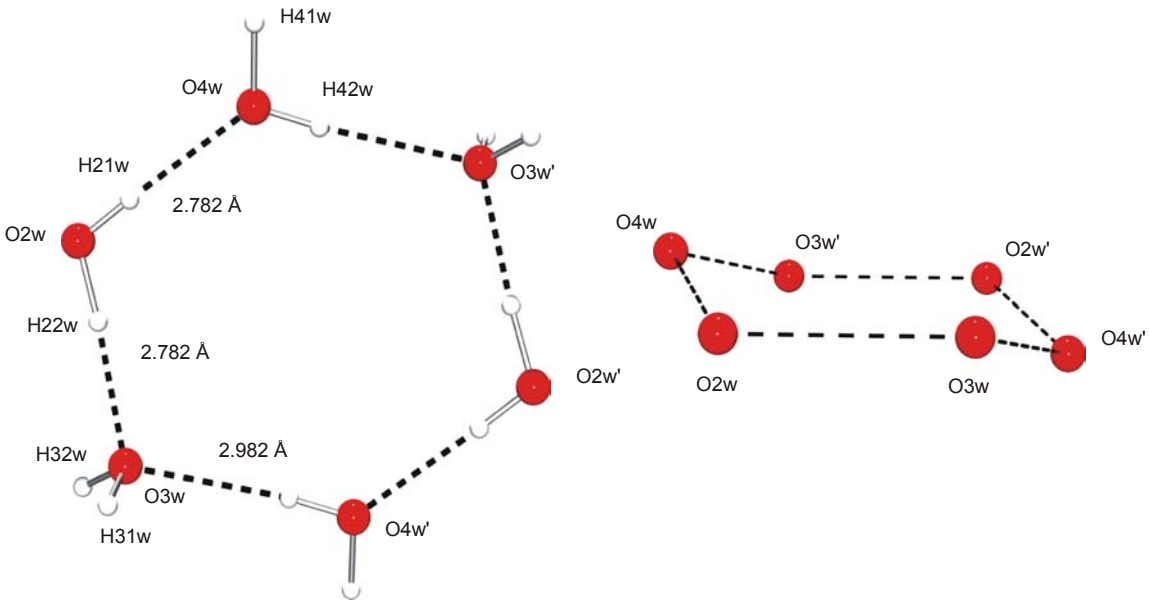

Figure 1.22: *Top view of the cyclic water hexamer structure in* ***6*** *(left). Side view of the cyclic water hexamer structure showing its chair conformation (right).*

Atoms in the hexamer adopt a slight chair conformation. The value of the sum of the internal angles of the ring is 707.4º; this value is much closer to 720º (planar structure) than to 657º (perfect chair conformation). The atoms O4w and symmetrical related atom O4w' lie 0.60 Å out (above and below, respectively) of the plane defined by the other four water molecules (O2w, O3w, O2w', O3w').

Parallel hexamers are connected to each other by means of a water molecule of crystallization, O1w (see Figure 1.23). Thus, O1w is H-bonded to O2w and O3w(x+1, y, z) of different hexamers displaying distances of 2.831(2) and 2.739(3) Å, respectively. As a result of these interactions, a new geometrical structure can be envisaged, namely an octamer formed by O2w'-O4w-O2w-O1w-O3w''-O4w''-O3w'''. Figure 1.23 shows a view of the polymeric structure of water formed by superposition of hexamers (black lines) and octamers (dashed-continuous lines). Due to the dense net of hydrogen bonds displayed by these water molecules, H-bond distances and stability, the structure must be

considered as an infinite non-covalent polymeric nanostructure of water in the solid state, achieved by co-crystallization with a guanine nucleobase.

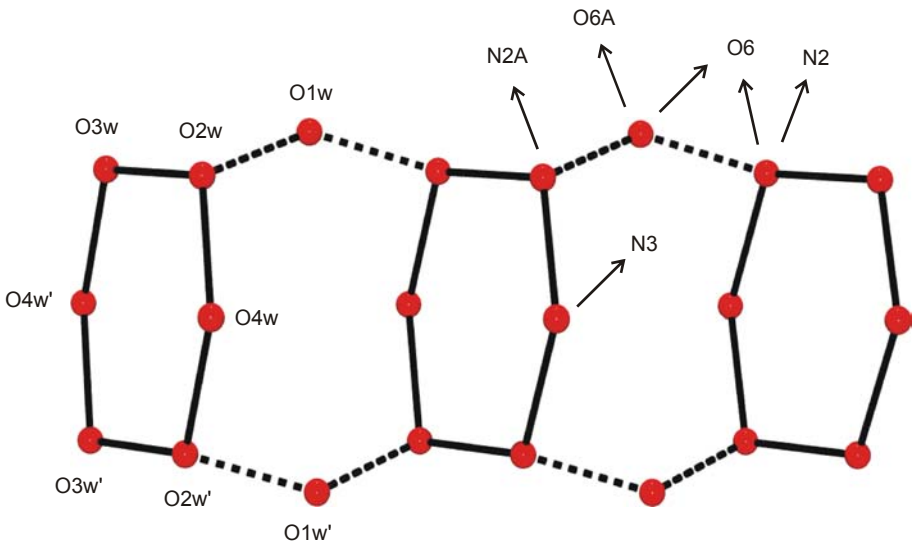

Figure 1.23: *View of the polymeric structure of crystallization water in* ***6****. Hydrogen atoms are omitted for clarity.*

Both types of polymers in the crystal are connected to each other via additional hydrogen bonds. Water molecules of crystallization take part in the water polymer formation and also form hydrogen bonds to the 9-ethylguanine polymeric system. Thus, O1w interacts with the carbonyl group of both guanine bases, in addition to the O2w and O3w atoms of the water polymer: O1w···O6, 3.296(3) Å; O1w···O6A(-x-2, -y-2, -z-1), 2.839(3) Å. Water molecule O2w interacts with the other three water molecules of the guanine polymer and also with the exocyclic N2A(H22A) position; O2w···N2A, 2.997(4) Å. O3w has interactions with O1w, O2w, O4w water molecules and with the O6 and N2 atoms of the exocyclic groups of the guanine: O3w···O6, 2.770(3) Å; O3w···N2(-x-3, -y-3, -z-1), 3.147(3) Å. The last water molecule, O4w, forms a hydrogen bond of 2.822(3) Å to the endocyclic unprotonated N3 site, O4w···N3(x, y, z-1), in addition to the bonds to O2w and O2w'.

The relevance of water clusters in biological systems and chemical processes has been intensively studied in recent years [36,39-44]. The H bonded water molecules of the clusters can display different geometries. Some

examples of tetramers [45,46], pentamers [47], hexamers [48-51], octamers [52,53], decamers [54], have been reported. These water rings as basic units can be considered as building blocks for the formation of supramolecular entities. There are many examples of 1D (see **5** in 1.2.3) [37,55-57], 2D [58-61], and 3D polymers [38].

1.3.2.- $[(9\text{-EtGH})_2] \cdot 7H_2O$ (7).

$[(9\text{-EtGH})_2] \cdot 7H_2O$ (**7**) was the second type of crystal obtained under conditions of formation of **6**. There are two remarkable differences between both solid state structures, however. The first difference is related to the number of water molecules of crystallization; four water molecules were found in **6**, instead of the seven molecules found in **7**. The second one is a small structural difference: The terminal atoms of the ethyl groups (C91 and C92A) of the guanine bases in **7** are not coplanar with the rest of their respective nucleobases.

In contrast to **6**, which crystallizes in the triclinic space group, **7** crystallizes in the monoclinic crystal system. Unfortunately the quality of the measured crystals was not as high as with **6**. Nevertheless the quality was good enough to allow the study of the hydrogen bonding pattern, but not for an accurate localization of the protons. Crystallographic data, data collection parameters and refinement parameters of **7** data are given in Table A-7.

As in **6**, the crystal structure of **7** contains two molecules of 9-EtGH nucleobase forming an asymmetric dimer. Water molecules of crystallization acquire a significant importance here, representing 35.2% of the molecular mass of the crystal. In is probably this feature and the resulting higher vibrational freedom of the oxygen atoms of the water molecules in comparison to the bound atoms of the guanine bases, which is responsible for the lower accuracy of the crystal structure determination.

Table 1.10: *Selected distances (Å) and angles (º) for 7.*

	9-EtGH	9-EtGH$_a$		9-EtGH	9-EtGH$_a$
N1–C2	1.371(7)	1.378(8)	C2-N1-C6	125.8(7)	122.5(7)
N1–C6	1.408(7)	1.409(7)	N3-C2-N2	119.8(8)	118.7(8)
C2–N3	1.326(7)	1.321(7)	N3-C2-N1	124.2(7)	114.7(8)
C2–N2	1.357(7)	1.329(7)	N2-C2-N1	115.9(8)	126.6(7)
N3–C4	1.335(8)	1.363(7)	C2-N3-C4	111.3(7)	110.1(7)
C4–N9	1.378(7)	1.365(7)	N3-C4-N9	126.8(8)	126.0(8)
C4–C5	1.407(8)	1.369(7)	N3-C4-C5	128.7(7)	128.8(8)
C5–N7	1.392(7)	1.386(7)	N9-C4-C5	104.5(7)	105.2(7)
C5–C6	1.396(8)	1.408(8)	C4-C5-N7	129.3(8)	112.2(7)
C6–O6	1.231(7)	1.249(6)	C4-C5-C6	110.9(7)	119.9(8)
N7–C8	1.293(7)	1.322(7)	N7-C5-C6	119.8(7)	127.9(9)
C8–N9	1.388(7)	1.378(7)	O6-C6-N1	129.5(8)	129.5(8)
N9–C9	1.489(6)	1.456(6)	O6-C6-C5	120.3(8)	118.3(8)
C9–C91	1.408(7)	1.484(7)	N1-C6-C5	110.2(6)	112.1(7)
			C8-N7-C5	104.3(6)	103.0(6)
			N7-C8-N9	114.0(6)	112.9(7)
			C4-N9-C8	106.4(6)	106.7(6)
			C4-N9-C9	125.5(7)	127.4(7)
			C8-N9-C9	128.2(7)	125.8(7)
			N9-C9-C91	114.1(6)	112.8(6)

All the non-hydrogen atoms of the 9-EtGH bases are in a plane, except the terminal atoms (C91 and C92A) of the exocyclic ethyl groups of both bases. The r.m.s. deviations of the endocyclic atoms of the guanine bases are 0.019 and 0.0099 respectively, which cannot be considered a low value, in comparison to other free nucleobases. The C91 atom is located 0.98(1) Å above the plane defined by the guanine aromatic rings; the plane defined by N9-C9-C91 forms a dihedral angle of 55.3(8) Å with the plane of the ring. In the case of (9-EtGH)$_a$, the distance from C91A to the nucleobase plane is much longer (1.383(9) Å). As evidenced by this value, the respective dihedral angle has to be much closer to a right angle, 83.8(7)º. Distances and angles within the 9-EtGH entities are not

unusual in comparison to other reported guanine bases [26,29], and are very similar in the two nucleobases of **7**. Bond distances and internal angles for the two 9-EtGH bases in the unit cell are given in Table 1.10.

Pairs of guanine bases in **7** are connected by hydrogen bonds following the same molecular arrangement as in **6**, namely: O6···N2A, N7···N1A, and C8···O6A (see Figure 1.21). Bases within the dimer in **7** are not coplanar, however, with a distance of 0.36 Å between both nucleobase planes. This contrasts with the distance of only 0.19 Å displayed in **6**. The distance of the twofold hydrogen bonds in **7** is similar to the one displayed in **6**, O6···N2A (2.923(7) Å), N7···N1A (2.786(7) Å). In this case, it is noteworthy that the distance of the first hydrogen bond O6···N2A is considerably longer than the corresponding distance in **6** (2.923(7) vs. 2.886(3) Å), opening the angle between the nucleobases. It allows realization of the third hydrogen bond interaction C8···O6A, 3.379(9) Å. The corresponding hydrogen bond contact in **6** has a distance of 3.593(3) Å. Ribbons of guanine bases are assembled with π-stacking between the rings of 3.38 Å.

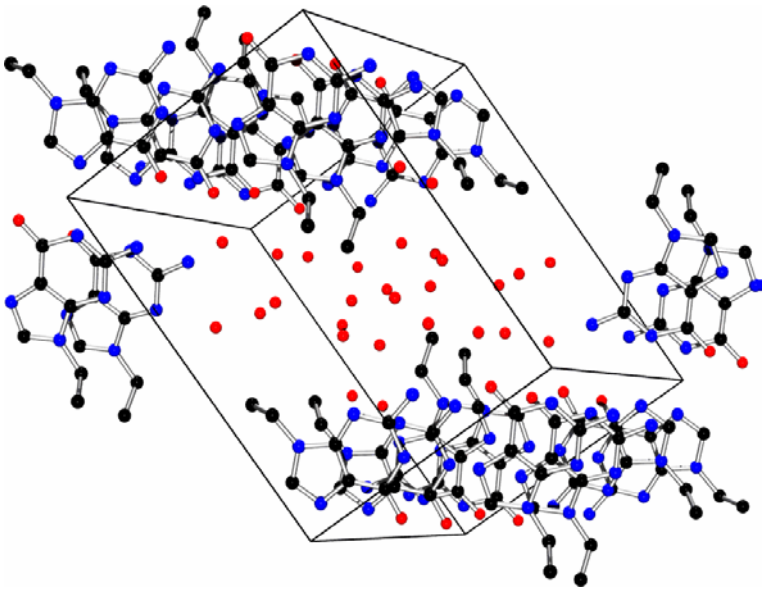

Figure 1.24: *View of the unit cell of 7.*
The water of crystallization is located between the base ribbons.

As shown in Figure 1.24, molecules of water of crystallization are placed between ribbons of guanine bases. A study of the hydrogen bonding pattern shows the formation of a dense water polymer. There are two types of hydrogen bonds involving water molecules: the first one, between water molecules interacting only with other water molecules (formation of the water polymer); and the second one, between water molecules of the water polymer interacting with the guanine polymer.

In order to simplify the description of these interactions, the symmetry operators are omitted in the next lines. Oxygen atoms of the water molecules that are involved in hydrogen bond formation exclusively between water molecules are: O2w (H-bonds with O1w, O4w, O6w and O7w), O6w (H bonds with O2w and two symmetrical O3w) and O7w (H bonds with O1w, O2w and O5w). Oxygen atoms of the water molecules of the water polymer which also join the nucleobase polymer are: O1w (H-bonds with N3, O2w, O3w and O7w), O3w (H-bonds with N3A, O1w, two symmetrical O6w), O4w (H-bonds with N2A, O6A, O2w and O5w), and O5w (H-bonds with O6, O4w and O7w). A detailed list of the interactions including symmetry operators is given in Table 1.11.

Table 1.11: *Hydrogen bond distances (Å) involving the water of crystallization in* ***7****.*

O1w···O2w	2.782(8)	O1w···N3(i)	2.826(7)
O1w···O3w	2.804(8)	O3w···N3A(i)	2.912(8)
O1w···O7w(i)	2.710(9)	O4w···N2A	3.192(9)
O2w···O4w	2.885(9)	O4w···O6A(iv)	2.851(8)
O2w···O6w	2.778(10)	O5w···O6(v)	2.847(8)
O2w···O7w	2.768(10)		
O3w···O6w(i)	2.889(10)		
O3w···O6w(ii)	2.947(11)		
O4w···O5w(iii)	2.938(11)		
O5w···O7w	2.689(11)		

Symmetry codes: (i) -x+1, y-1/2, -z+1/2; (ii) x, -y+1/2, z-1/2; (iii) x, -y+1/2, z+1/2;(iv) -x, y-1/2, -z+1/2; (v) -x, -y+1, -z.

The principal motif of the water polymer is a cyclic water pentamer, in which the atoms O1w, O3w, O6w, O2w and O7w are joined via hydrogen bonds. Two additional water molecules (O4w and O5w) are joined to the cyclic pentamer (via O2w and O7w, respectively). The atoms of the cyclic water pentamer are arranged in an envelope conformation, in which the O1w atom lies 0.766(12) Å above the plane defined by the remaining four atoms. Distances between atoms of the pentamer are: O1w···O7w, 2.710(9) Å; O7w···O2w, 2.768(10) Å; O2w···O6w, 2.778(10) Å; O6w···O3w, 2.889(10); O3w···O1w, 2.804(8) Å. Internal angles of the pentamer range from 99.4(3)º (O7w···O1w···O3w) to 112.2(3)º (O1w···O7w···O2w). Figure 1.24 shows in detail the distances and angles between atoms of the cyclic pentamer.

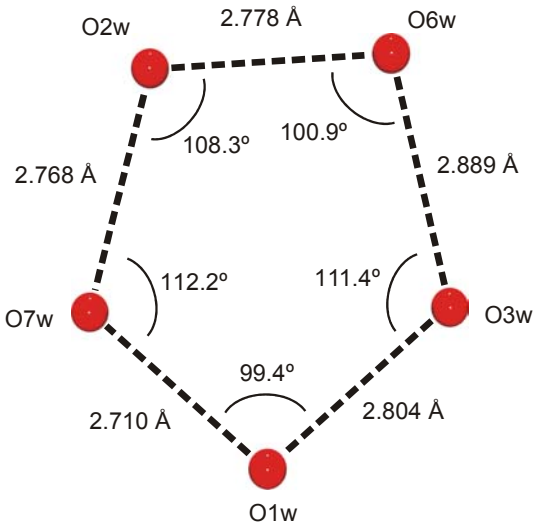

Figure 1.24: *View of the cyclic pentamer present in 7.*

In the 3D building of the polymer, the side defined by the O3w···O6w atoms of two pentamers of adjacent unit cells approach each other very closely. As a consequence of this, a cyclic tetramer can be observed between two pentamers. The tetramer and the pentamer entities share the O3w and O6w oxygen atoms. The tetramer-pentamer basic unity is repeated infinitely in the three dimensional polymer. A perspective of two basic units of the water polymer is depicted in Figure 1.25.

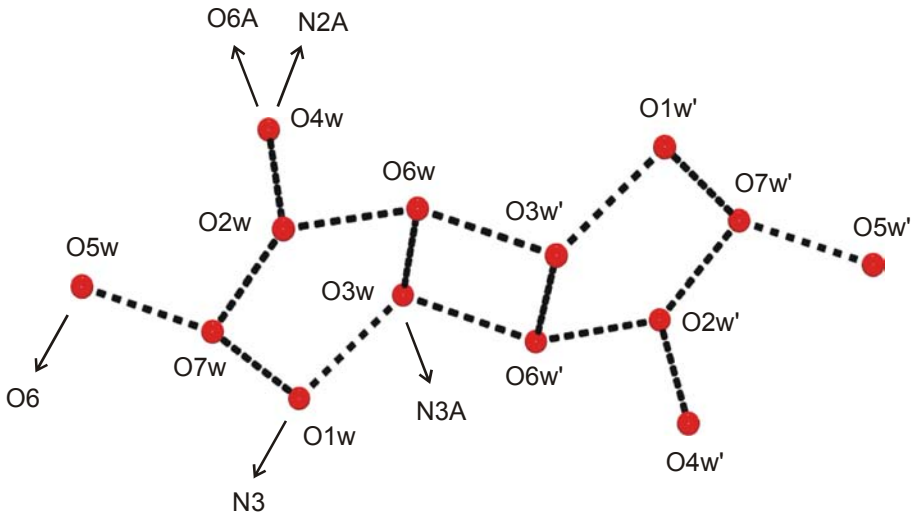

Figure 1.25: *Basic entity of the water polymer in 7. Connections with the nucleobase ribbons are depicted.*

The four oxygen atoms of the cyclic tetramer are coplanar; distances between oxygen atoms of the water molecules are: O3w···O6w(-x+1, y-1/2, -z+1/2), 2.889(10) Å; O3w···O6w(x, -y+1/2, z-1/2), 2.947(11) Å. Internal angles are 105.2(3)º and 74.8(3)º. The shortest distance between opposite vertices of the tetramer, O6w···O6w(-x+1, -y+1, -z+1), is 3.546(14) Å. Figure 1.26 shows the cyclic tetramer in detail.

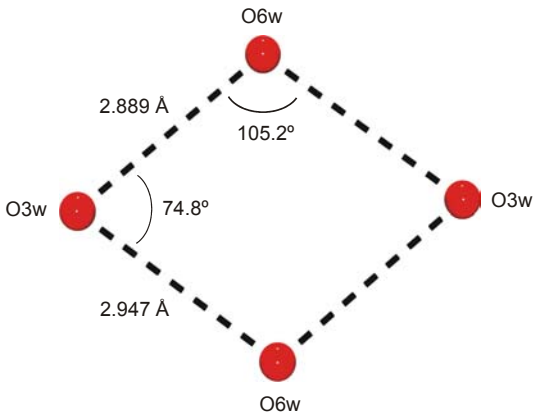

Figure 1.26: *View of the cyclic tetramer displayed in 7.*

1.3.3.- Remarks.

The known stability of the described ribbons of guanine bases allows the capture of a high number of water molecules. In the solid state, these water molecules crystallize together with the nucleobases and form very interesting cycles and polymers of water molecules joined to each other via hydrogen bonds. In the case of the two reported solid state structures, cyclic structures containing 4, 5, 6 and 8 water molecules were identified. Additional water molecules of crystallization are joined to these cycles, building three-dimensional polymers. It is also observed that the number of water molecules enclosed in the structure influences the geometry of the guanine base polymer (see Figure 1.21), varying the angles and distances of the main internucleobase hydrogen bond interactions. There are potential donor and acceptor proton sites of the guanine bases that are not participating directly in the structure of the guanine polymer; however these sites play an important role acting as bridges between the guanine and the water polymers.

1.4.- Adenine – Hypoxanthine Quartet.

The existence of homo(nucleobase) quartets such as those of guanine (G), adenine (A), thymine (T), and uracil (U) in multistranded nucleic acid structures is well established today and their potential relevance in biology and medicine is increasingly recognized [62-65]. The exceptional stability of G quartets (G_4), whether formed through folding of a single-stranded oligonucleotide, via side-by-side alignment of four single-stranded oligonucleotides, two hairpins, or two cyclic oligonucleotides, facilitates formation of the other tetrads through stacking. This applies also to mixed nucleobase tetrads such as CGCG [66], TATA [67], and even GCAT [68]. It is surprising that the existence of AGAG tetrads is still controversial [69-72], considering the variety (four) of possible AG mispairs in nucleic acid structures, and their high stabilities, respectively [73].

1.4.1.- [(9-MeAH)(9-MeHxH)](ClO_4) (8).

Co-crystallization of 9-MeAH$^+$ cations and 9-MeHxH bases was achieved applying different counter ions. Eventually, the solid state structure of [(9-MeAH)(9-MeHxH)](ClO_4) (**9**) was characterized by X-ray crystallography. The complex **9** forms of a tetrad containing two 9-MeAH$^+$ and two 9-MeHxH bases. A comparison of this novel tetrad with another tetrad containing two protonated 9-MeAH$^+$ and two 9-EtGH bases is likewise made here. In the crystallographic measurement, all the hydrogen atoms were found in the difference Fourier map and refined without restraints. Crystallographic details of **8** and refinement parameters are listed in Table A-8 (see Appendix).

From the geometrical point of view, the nucleobases are not unusual in comparison to other 9-MeAH$^+$ [22] cations and 9-MeHxH [74] bases. Distances and angles of 9-methyladeninium and 9-methylhypoxanthine bases are listed in Table 1.12. The 9-MeAH$^+$ cation shown in Figure 1.27 is almost coplanar, with an r.m.s. deviation of 0.011 Å. The exocyclic atoms (N6a and C9a) have the largest deviation from the plane defined by the purine skeleton (0.015(4) Å and 0.021(7) Å), respectively).

The internal ring angle at the site of protonation (N1) (C6-N1-C2, 121.8(5)º) has a trend toward slightly smaller values compared to 9-methyladeninium salts (see part 1.2 of this chapter). Without doubt this effect is due to the proximity of the 9-MeHxH nucleobase in the crystal and as a consequence of hydrogen bond formation between the N7h position of 9-MeHxH and the N1a(H) site of 9-MeAH$^+$ (2.833(4) Å). Thus, the proton corresponding to this N1a site is probably further away from the adenine base and closer to the hypoxanthine base, decreasing the effect in the protonated site angle. The 9-MeHxH nucleobase is also almost coplanar; the r.m.s. is 0.0102 Å.

Table 1.12: *Distances (Å) and angles (º) for* ***8****.*

N1h–C2h	1.366(7)	N1a–C2a	1.347(7)
N1h–C6h	1.379(6)	N1a–C6a	1.374(6)
C2h–N3h	1.310(6)	C2a–N3a	1.296(6)
N3h–C4h	1.341(6)	N3a–C4a	1.378(6)
C4h–C5h	1.359(7)	C4a–C5a	1.353(6)
C4h–N9h	1.389(6)	C4a–N9a	1.368(6)
C5h–N7h	1.388(6)	C5a–N7a	1.397(6)
C5h–C6h	1.412(7)	C5a–C6a	1.407(6)
O6h–C6h	1.239(5)	C6a–N6a	1.303(6)
N7h–C8h	1.323(6)	N7a–C8a	1.315(6)
C8h–N9h	1.342(6)	C8a–N9a	1.360(6)
N9h–C9h	1.479(8)	N9a–C9a	1.460(7)
C2h-N1h-C6h	125.5(6)	C2a-N1a-C6a	121.8(5)
N3h-C2h-N1h	124.4(6)	N3a-C2a-N1a	129.2(6)
C2h-N3h-C4h	110.8(5)	C2a-N3a-C4a	108.9(5)
N3h-C4h-C5h	129.6(6)	C5a-C4a-N9a	106.7(5)
N3h-C4h-N9h	125.6(6)	C5a-C4a-N3a	127.8(5)
C5h-C4h-N9h	104.8(5)	N9a-C4a-N3a	125.5(5)
C4h-C5h-N7h	111.8(5)	C4a-C5a-N7a	111.3(5)
C4h-C5h-C6h	119.1(6)	C4a-C5a-C6a	119.5(6)
N7h-C5h-C6h	129.1(6)	N7a-C5a-C6a	129.2(6)
O6h-C6h-N1h	119.6(5)	N6a-C6a-N1a	121.3(5)
O6h-C6h-C5h	129.8(6)	N6a-C6a-C5a	126.0(6)
N1h-C6h-C5h	110.6(5)	N1a-C6a-C5a	112.7(5)
C8h-N7h-C5h	103.1(5)	C8a-N7a-C5a	102.2(5)
N7h-C8h-N9h	113.5(6)	N7a-C8a-N9a	114.7(5)
C8h-N9h-C4h	106.8(5)	C8a-N9a-C4a	105.1(5)
C8h-N9h-C9h	127.3(7)	C8a-N9a-C9a	128.2(6)
C4h-N9h-C9h	125.9(6)	C4a-N9a-C9a	126.6(6)

The two nucleobases are connected by additional hydrogen bonds and form a quartet with another symmetry generated pair. The quartet consists of a

central centrosymmetric 9-methyladeninium pair, with hydrogen bonds between the N(7) and N(6)H_2 sites, to which the 9-methylhypoxanthine bases are hydrogen bonded via N(1)H and N(6)H_2 of adeninium as well as N(7) and O(6) of the 9-methylhypoxanthine (see Figure 1.27).

In addition, the H(8) proton of the 9-methyladeninium base is involved in weak hydrogen bonds to the O(6) atom of the 9-methylhypoxanthine base. Distances of the more important hydrogen bonds involving the nitrogen atoms of the nucleobases are listed in Table 1.13 (the O3 and O4 atoms of the Table belong to the perchlorate counter anion). Other hydrogen bond contacts involving protons bonded to carbon atoms are: C8a(H)···O6a, 3.318(8) Å; C2h(H)···N3h, 3.284(9) Å.

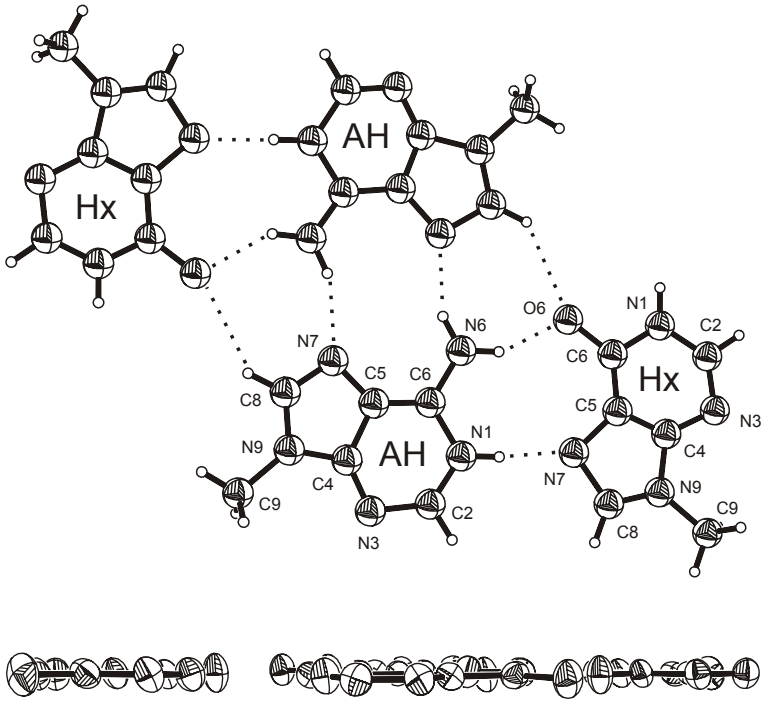

Figure 1.27: *View of base quartet [{(9-MeAH)(9-MeHxH)}$_2$](ClO$_4$)$_2$ (**8**) with anions deleted. The four bases are coplanar.*

The quartet formed by the nucleobase is virtually completely flat (maximum deviation of atoms from best plane ≤ 0.03 Å). The base tetrads are linked via pairs of hydrogen bonds involving the sugar edges of the 9-MeHxH

base, namely N(3) and C(2)H of the 9-methylhypoxanthine into infinite tapes (see Figure 1.28).

Table 1.13: *Bond distances (Å) and angles (º) of the hydrogen bonding scheme in* ***8****.*

D-H	d(D-H)	d(H···A)	<DHA	d(D···A)	A
N1h-H1h	0.964	2.076	173.13	3.036	O3(i)
N1h-H1h	0.964	2.519	129.06	3.215	O4(i)
N6a-H61	1.146	1.747	157.68	2.841	N7a(ii)
N6a-H62	1.000	1.789	156.80	2.739	O6h(iii)
N1a-H1a	1.040	1.859	155.08	2.837	N7h(iii)

Symmetry codes: (i) x, -y+1/2, z-1/2; (ii) -x+1, -y, -z; (iii) x+1, y, z.

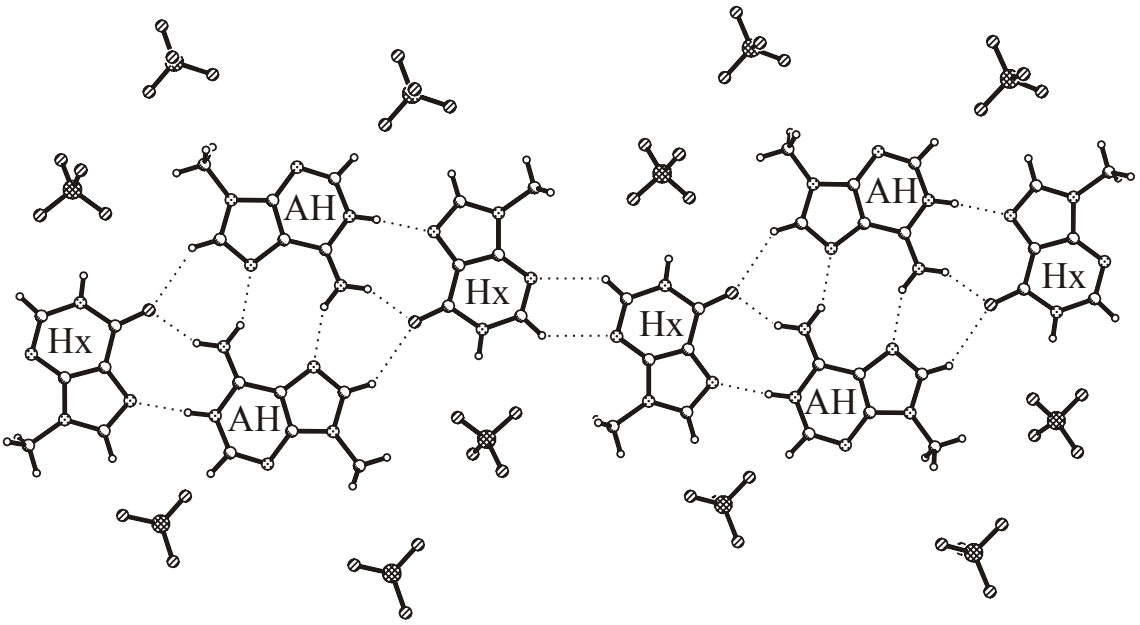

Figure 1.28: *Association pattern of base quartet* ***8*** *leading to an infinite tape structure. Abbreviations used: AH = 9-MeAH$^+$, Hx = 9-MeHxH. Perchlorate anions connect adjacent tapes of base quartets.*

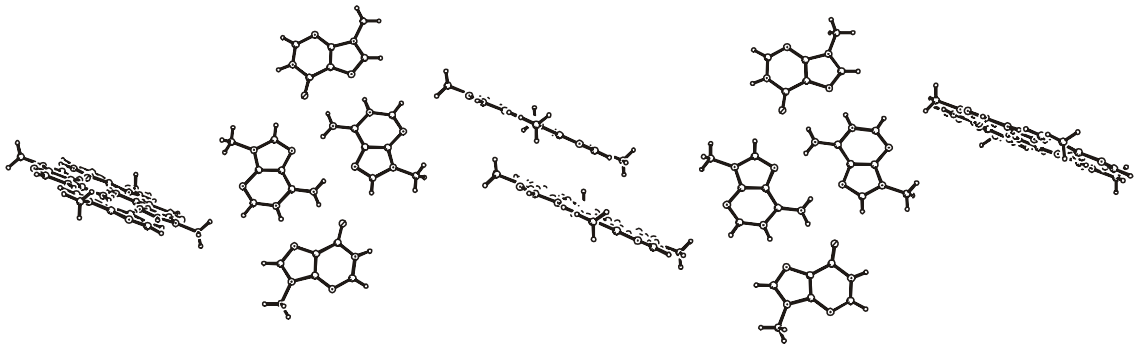

Figure 1.29: *Detail of packing pattern of **8**. ClO_4^- anions are omitted.*

The tapes are stacked on top of each other at a distance of ca. 3.42 Å, to produce piles. The piles are slightly inclined (77º) and separated by the tetrahedral counter ions (ClO_4^-). However, the piles are not oriented in a parallel fashion as in the case of [{(9-MeAH)(9-EtGH)}$_2$](BF_4)$_2$ (analogous tetrad containing 9-EtGH instead of 9-MeHxH as 6-oxopurine) [5]; in **8** only every second pile is parallel, while adjacent piles form angles of 65º with the former; Figure 1.29 shows the disposition of the piles, perchlorate counter anions are omitted for a better view.

Table 1.14: *Distances (Å) between ClO_4^- anions and nucleobase H donor sites in **8**.*

Cl-O1···C(9)a	3.440(8) Å
Cl-O1···C(2)a (x-1, y+½,-z+½)	3.203(9) Å
Cl-O2···C(2)a (-x+1, y+½,-z+½)	3.215(7) Å
Cl-O3···N(1)h (x, -y+½, z+½)	3.043(7) Å
Cl-O4···N(1)h (x, -y+½, z+½)	3.215(6) Å
Cl-O4···C(9)h (-x+1, y+½,-z+½)	3.393(8) Å
Cl-O4···C(2)a (-x+1, y-½,-z+½)	3.261(8) Å

In **8**, an analysis of the H bonding interactions reveals that with exception of the H8 proton of 9-MeHxH, all the remaining protons of the two nucleobases not already engaged in base-base H bond formation, are involved in H bonds between the quartet and the perchlorate anions. Specifically, N(1)H and C(9)CH_3 of 9-MeHxH, as well as C(2)H and C(9)CH_3 of 9-MeA form such contacts, ranging from ca 3.0 to 3.4 Å (see Table 1.14).

1.4.2.- Remarks.

Excluding the long hydrogen bonding contacts between the C(8)H of 9-MeAH$^+$ and O(6) of the 6-oxopurines, the intermolecular separations via N3 and C(2)H in **8** are clearly longer than the other intramolecular ones, thus supporting the notion of **8** being base tetrad. Similar hydrogen bonding patterns involving the sugar edges are also observed in Pt^{II} complexes of adenine, guanine and hypoxanthine nucleobases [75,76].

Synthesis of the corresponding guanine base quartet compound, $[\{(9\text{-MeAH})(9\text{-EtGH})\}_2](BF_4)_2$ [5], was achieved using similar conditions. The compound was prepared by P. Amo-Ochoa and is also reported in [5]. It displays a rather similar hydrogen bond patterns as seen in **8**. This guanine base quartet presents slight arrangement variations due to the presence of the exocyclic ethyl and amino groups of the guanine and also due to the counteranion. Nevertheless, both structures can be considered similar. Formation of these base tetrads can be envisaged as an association of two $AH^+_{anti} \cdot G/HxH_{syn}$ mispairs [77]. There are two principal ways of dimerization, which are interrelated by a simple sliding motion of the two mispairs. In both cases H-bonding interactions between donor and acceptor sites can form, which give rise to favorable secondary electrostatic interactions [30,31]. Geometry-optimized structures of the tetrads were calculated by P. Lax in our group [5].

2.- Aspects of the Chemistry of the Exocyclic Amino Group in 1-MeC.

The kinetically preferred binding site of N1-blocked cytosine nucleobase for soft metal ions such as Pt^{II} or Pd^{II} is the N3 position [78]. This is also true for the monofunctional [(dien)Pt^{II}] moiety, as will be shown in this chapter. The exocyclic amino group, whose lone pair is delocalized into the π-system of the pyrimidine ring, is no donor site for metal ions unless it becomes deprotonated. There are indeed occasional reports in the literature on twofold metal binding to N3 and the deprotonated N4 position, and even fewer cases of exclusive metal binding to N4 [78]. The latter situation is considered to represent the thermodynamically favored binding pattern. Concerning pathways leading to dinuclear, N3,N4 bridged cytosine complexes, nothing is known. As to formation of N4 platinated cytosine, a redox assisted pathway involving a Pt^{IV} intermediate, has been revealed [79]. Direct migration of a Pt^{II} species has not been observed before. In the course of the studies described below, it was found that such a possibility exists indeed. At the same time it was found, that at high pH, this metal migration process competes with a change in nucleobase composition. It is the result of a hydrolytic deamination of the cytosine nucleobase in the presence of a N3 coordinated Pt^{II} entity.

2.1.- Metal Mediated Deamination of 1-MeC.

Deamination is the removal of an amino group from a molecule. Deamination in organisms is a common process; degradation of amino acids involves deamination as the first step of its catabolism. Cytidine deaminase catalyzes the hydrolytic deamination of cytidine to uridine in a thermodynamically favorable reaction (see Figure 2.1). The product, uridine, can undergo phosphorolysis to yield pentose derivatives. However, when a

spontaneous deamination occurs in DNA, a mutation as a consequence of pairing with adenine is possible, in principle (see below).

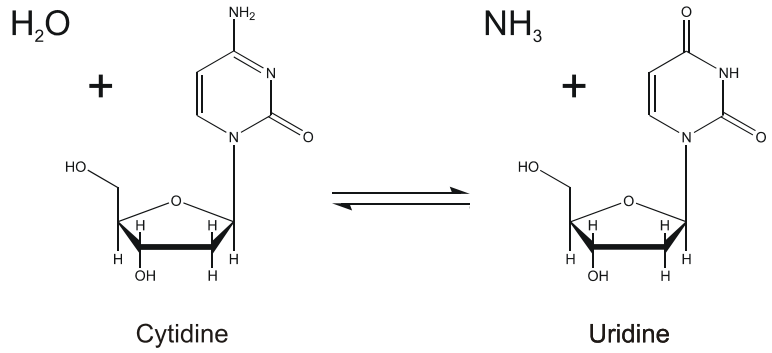

Figure 2.1: *Schematic interrelationship between Cytidine and its deamination product Uridine.*

It has been estimated that within 1 day, DNA in every cell will be spontaneously damaged more than 10000 times. Deamination of cytosine to uracil represents a major source of DNA damage in eukaryotic cells [80]. If not repaired, these processes give rise to mutations. While uracil, the deamination product of cytosine, is rapidly excised from replicating DNA by the enzyme uracil-DNA glycosylase, 5-methylcytosine, which is involved in the regulation of gene expression, is converted to thymine upon deamination. The rate of the latter reaction is 3-4 times faster than that of cytosine [81]. Thymine is not excised, yet the GT mispair is subject to mismatch repair, which is, however, considerably slower than excision of uracil. As a consequence, 5-methylcytosine residues represent hotspots for spontaneous transition mutations [82-83]. It has been estimated that ^{m}CpG sequences are preferred targets for spontaneous point mutations (GC $\rightarrow$ AT transition) which could account for as much as one-third of single–site mutations found in inherited human diseases [84]. In non-dividing cells RNA polymerases are not arrested by uracil in the DNA and consequently produce mutant transcripts with high efficiency [85]. Spontaneous hydrolytic deamination of cytosine and 5-methylcytosine appears to occur without any particular sequence specificity, but single-stranded DNA is considerably more susceptible to this reaction [80].

Regarding 5-methylcytosine, two aspects are of interest. First, 5-methylcytosine can be a regular base in (resting, transcriptionally inactive) DNA, with an enzyme called DNA methyltransferase available for C5-methylation of cytosine. Second, deamination of cytosine (or 5-methylcytosine) generates NH_3 which is toxic to cells. Its accumulation in the organism would rapidly have lethal consequences. Usually, ammonia is eliminated by the liver by means of the urea cycle. Although the organism can not tolerate high concentrations of urea, it is much less poisonous than ammonia, and can be removed through the kidneys.

Cationic complexes of Pt^{II} containing the model nucleobase 1-MeC and 1,5-dimethylcytosine (1,5-DimeC) undergo unexpectedly facile cytosine deamination at basic pH with formation of the corresponding complexes of 1-methyluracilate (1-MeU) or 1-methylthyminate (1-MeT) [5]. It is remarkable that the free bases, 1-MeC and 1,5-DiMeC show no sign of deamination under comparable conditions for months and that even deamination of deoxycytidine [86] or cytosine in single- or double-stranded DNA [87-88] likewise requires unphysiologically high pH values. This seemingly paradoxical situation in fact calls for catalytic acceleration of this reaction which could be through a metal ion, and also may occur in vivo.

Interestingly, bacteria and fungi contain cytosine deaminases (CDases) for pyrimidine salvage [89]. These enzymes contain either Zn^{2+} or Fe^{2+} at the active site, these metal ions are thought to add an OH^- nucleophile to the C4 position of the cytosine.

Deamination reactions of N3 platinated cytosine nucleobases were first discovered in our group when treating compounds of composition *trans*-[a_2Pt(1-MeC-*N3*)$_2$]$(NO_3)_2$ (with a = NH_3, CH_3NH_2) and *trans*-[a_2Pt(1,5-DimeC-*N3*)$_2$]$(NO_3)_2$ with base (KOH, NaOH) at pH ≥ 12.5. Formation of *trans*-[a_2PtL_2] (L = 1-methyluracilate, or 1-methylthyminate) compounds was recognized because of the poor solubility of the complexes, which permitted easy characterization and comparison with authentic samples. In the case of *trans*-[$(NH_3)_2$Pt(1,5-DimeC-*N3*)$_2$]$^{2+}$, precipitation of the 1-MeT complex started virtually

instantaneously on addition of base. Very recently, Arpalahti and Klika reported on similar deamination reactions observed with 9-methyladenine complexes of Pt^{II} [90,91]. In this chapter, the deamination reaction of two monofunctional platinum complexes of 1-methylcytosine, $[(dien)Pt(1\text{-}MeC\text{-}N3)]^{2+}$ and $[(NH_3)_3Pt(1\text{-}MeC\text{-}N3)]^{2+}$ will be discussed.

2.1.1.- $[(dien)Pt(1\text{-}MeC\text{-}N3)]^{2+}$ (9) as Starting Compound.

In order to study the cytosine deamination reactions, it was decided to simplify the system by having only a single cytosine base present. The starting compound $[(dien)Pt(1\text{-}MeC\text{-}N3)]^{2+}$ (with dien = diethylenetriamine) was prepared by reaction of $[(dien)Pt(H_2O)_2]^{2+}$ and 1-MeC. As counterions nitrate and perchlorate were used with identical results. An important property of the complex is its stability at high temperature, which proved advantageous in some of the experiments. A sample of $[(dien)Pt(1\text{-}MeC\text{-}N3)]^{2+}$ kept for several hours in water at 90º C and at neutral pH, does not decompose. Variations of pH of the solution modify this behavior; if the solution is very alkaline or acidic, $[(dien)Pt(1\text{-}MeC\text{-}N3)]^{2+}$ is no more stable: at acidic pH values (HNO_3) it decomposes over time to give $[(dien)Pt(H_2O)]^{2+}$ and the nitrate salt of protonated 1-methylcytosine. Its solid state structure is described in the previous chapter. At basic pH the reaction proceeds into two different pathways as described below.

2.1.1.1.- Crystal Structure.

Crystals of $[(dien)Pt(1\text{-}MeC\text{-}N3)](ClO_4)_2$ (**9**) were isolated from an aqueous solution and characterized by X-ray crystallography. An analogous Pd^{II} complex, $[(dien)Pd(1\text{-}MeC\text{-}N3)](ClO_4)_2$ (**14**), with a similar structure having a palladium atom as the metallic centre is discussed later in this chapter. The complex **9** crystallizes in the orthorhombic crystal system. In the refinement

process of the X-ray data, all non–hydrogen atoms of the crystal were refined anisotropically. The hydrogen atoms were placed at geometrical idealized positions and refined isotropically. Crystal data, data collection and refinement parameters for **9** are summarized in Table A-9 (see Appendix).

The solid state structure of **9** consists of a platinum atom coordinated to the three nitrogen atoms of the dien ligand and to the N(3) atom of the 1-methylcytosine in a square-planar coordination geometry, with distinct distortions. A view of the cation [(dien)Pt(1-MeC-*N3*)]$^{2+}$ with a labeling scheme is shown in Figure 2.2.

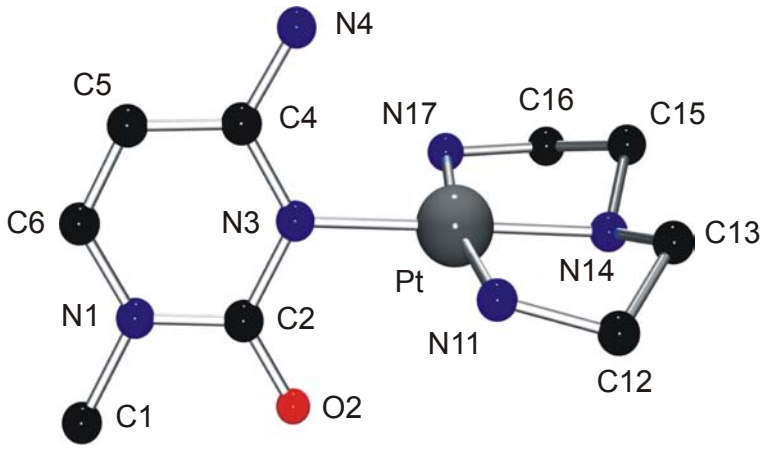

Figure 2.2: *View of the cation [(dien)Pt(1-MeC-N3)](ClO$_4$)$_2$ (**9**) with a labeling scheme.*

Firstly, the distortion of the square-planar coordination of the platinum atom consists of a marked deviation from linearity of the angle between the platinum atom and the two coordination sites of the dien ligand *cis* positioned to the cytosine nucleobase: N11-Pt-N17, 168.9(3)º. This contrasts with the almost linear orientation of N3-Pt1-N14, 179.3(3)º. Thus the Pt1, N3, N14 atoms are situated below (-0.024(3), -0.030(3) and -0.039(4) Å, respectively) and the N11 and N17 atoms above (0.046(4) and 0.047(4) Å, respectively) the platinum coordination plane, with a r.m.s. deviation of 0.038. Secondly, there are distortions of angles in the respective *cis* positioned atoms to the Pt. Thus, the angles between the platinum atom, the N(3) atom of the cytosine base and the N11 and N17 nitrogen atoms of the dien group are about 10º larger (95.0(3) and 95.4(3)º, respectively) than those complementary angles N11-Pt1-N14, 85.2(3),

and N14-Pt1-N17, 84.4(3)º. Pt-N distances about the Pt center range from 2.019(8) to 2.046(7) Å. A list of selected distances and angles involving the Pt atom of **9** is given in Table 2.1.

Table 2.1: *Selected distances (Å) and angles (º) for non-hydrogen atoms in* ***9.***

N3-Pt1-N11	95.0(3)	Pt1-N3	2.046(6)
N11-Pt1-N14	85.2(3)	Pt1-N11	2.046(7)
N14-Pt1-N17	84.4(3)	Pt1-N14	2.019(8)
N17-Pt1-N3	95.4(3)	Pt1-N17	2.030(7)
N3-Pt1-N14	179.3(3)		
N11-Pt1-N17	168.9(3)		

The coordination sphere of platinum is completed by weak interactions with two O1a oxygen atoms of the perchlorate counter anions. Distances between Pt and O1a atoms are: Pt–O1a(x, y-1, z), 3.422(7); and Pt–O1a(-x+1/2, y-1/2, z), 3.466(7) Å. Thus, the platinum atom is present in a distorted octahedral environment, in which the oxygen atoms occupy the apical positions, forming angles of 90.6(3) and 88.3(3)º with the platinum and the N11 site. This situation is shown in Figure 2.3.

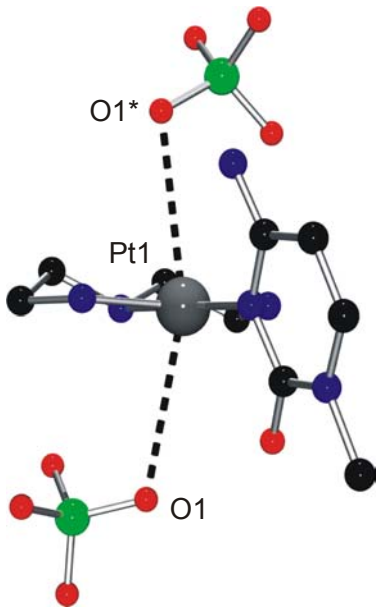

Figure 2.3: *Square-planar coordination of Pt with two oxygen atoms in the apical positions (cation* ***9****).*

The cytosine ligand in **9** has normal distances and angles between atoms. The two external Pt-N-C angles are clearly different: the Pt-N3-C2 angle is 115.5(5)º and the Pt1-N3-C4 angle is larger, 122.7(5)º. This is a common feature of many 1-MeC compounds of Pt [92]. The atoms of the 1-methylcytosine base are coplanar, with a r.m.s. deviation of 0.027. The dihedral angle between the cytosine ring and the platinum coordination plane is 77.2(2)º (see Figure 2.4). As a consequence of this large angle, no intramolecular hydrogen bonds are observed in the cationic entity.

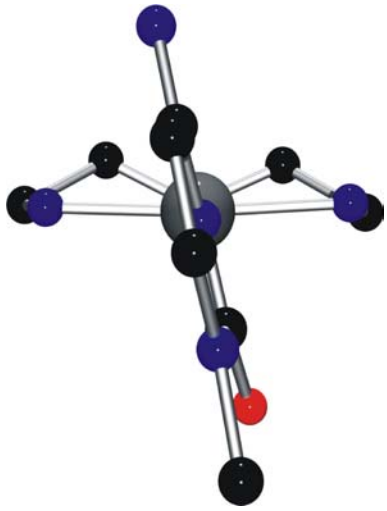

Figure 2.4: *View of the angle between the cytosine ring and the platinum coordination plane in the cation [(dien)Pt(1-MeC-N3)]$(ClO_4)_2$ (**9**).*

The nitrogen atoms of the dien ligand coordinated to the platinum metal are practically coplanar with the C12 and C16 atoms (r.m.s. deviation, 0.039). The other two atoms of the dien group, C13 and C15, are located out of this plane, by 0.595(14) and 0.646(13) Å, respectively. Distances between atoms of the dien group range from 1.462(11) to 1.526(13) Å. Angles are in agreement with the sp^3 hybridization of the atoms, displaying angles from 107.6(6) to 109.6(5), with one exception, that of the C13-N14-C15 angle, 121.0(8)º.

The crystal packing of **9** is based on interactions between the $[(dien)Pt(1\text{-}MeC\text{-}N3)]^{2+}$ cation and the perchlorate counter anions. As shown in Figure 2.5, the O1a atom in the crystal structure is shared by two platinum atoms and forms chains. The arrangement of the cations and anions in the

crystal does not allow π-stacking between the aromatic rings of the cytosines. The other oxygen atoms of the perchlorates are involved in hydrogen bonding with the protons of the cation; no intermolecular nucleobase interactions were observed. The protons of the exocyclic amino group form hydrogen bonds with the oxygen atoms of ClO_4^-: N4(H4a)···O1(x, y-1, z), 3.100(11) Å; N4(H4b)···O1(-x+1/2, y-1/2, z), 3.018(10) Å. The protons of the dien ligand are also involved in some hydrogen bonds, the shortest one is N14(H14a)···O2A(-x+1/2, y-1/2, z), 3.123(10) Å. The only intermolecular hydrogen bond found in the structure is between the N17(H17b) proton and the exocyclic O2 of two neighboring cations, N17(H17b)···O2(-x+1/2, y-1/2, z), 2.926(10) Å.

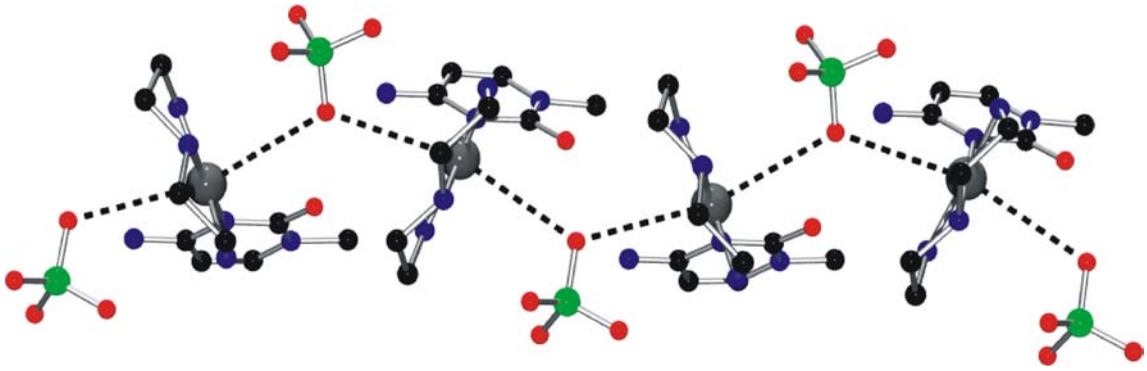

Figure 2.5: *View of the chains in the packing of* ***9****.*

2.1.1.2.- NMR spectroscopy.

The first characterization of **9** prepared in situ was done by means of NMR spectroscopy. The ^{1}H NMR spectrum of a solution containing the cationic $[(dien)Pt(1\text{-}MeC\text{-}N3)]^{2+}$ entity displays two sets of doublets in a 1:1 ratio in the aromatic region corresponding to the H6 and H5 protons of the 1-methylcytosine base, a singlet corresponding to the methyl group of 1-MeC and the CH_2 resonances of the dien ligand. When the solution is in a broad pH range close to neutral, the signals corresponding to the H6 and H5 doublets as well as the CH_3 singlet of 1-MeC have chemical shifts of δ = 7.62, 6.03 and 3.41 ppm, respectively; signals associated with the dien ligand range from 2.7 to 3.3 ppm.

As shown in detail in Figure 2.6, ^{195}Pt satellites of 15.0 Hz of the H5 doublet (^{3}J = 7.4 Hz) are observed, confirming coordination of 1-MeC through N3.

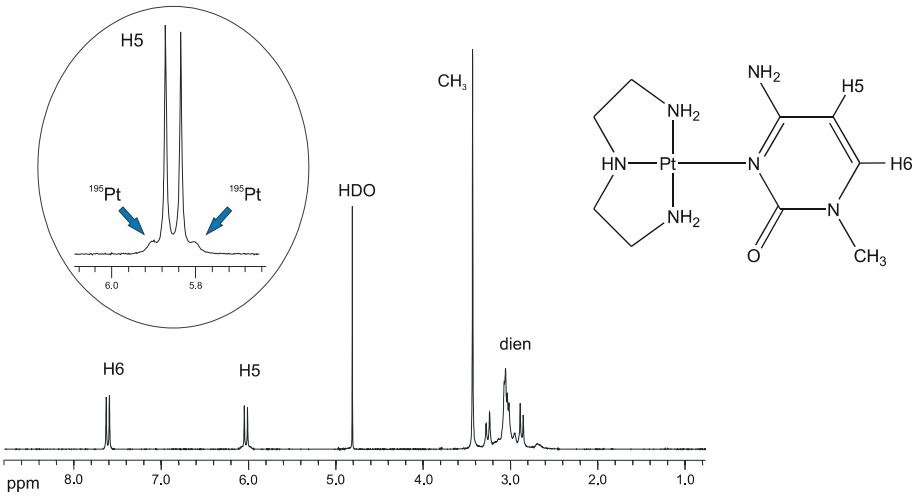

Figure 2.6: *^{1}H NMR spectrum in D_2O (pD 4.5 of the starting compound, $[(dien)Pt(1\text{-}MeC\text{-}N3)]^{2+}$. The spectrum displays two sets of doublets (H6, H5 of 1-MeC), one singlet (CH_3 of 1-MeC), and the CH_2 resonances of dien, and it is also possible to recognize ^{195}Pt satellites for H5.*

The spectrum is consistent with a complex containing N3 coordinated 1-MeC and tri-coordinated diethylenetriamine. In the ^{195}Pt NMR spectrum of $[(dien)Pt(1\text{-}MeC\text{-}N3)]^{2+}$ two resonances at -2906 and -2924 ppm are displayed, as is frequently found in dien complexes [93]. It is possible to explain this effect with two different arguments. The first argument proposes slow movement of the atoms of the dien group in solution, allowing two different conformers, with the C13 and C15 atoms (see the previous crystallographical study of **9**) facing the N4 and the O2 side of 1-MeC, respectively. The second argument provokes the same final conformers; in this case, it is attributed to the rotation of the 1-MeC about the Pt-N3 bond. Rotation about this bond is possible but sterically hindered due to the proximity of the exocyclic amino group of the cytosine base to the N11 and N17 sites of the dien ligand. Thus, there are only two possible final conformers. It is not clear if the conversion of one to the other conformer is due to the rotation of the cytosine base or due to internal movement of the dien group, or both. Anyway, the two signals of the ^{195}Pt NMR spectrum correspond to the presence of both conformers in solution.

A ^{195}Pt NMR temperature dependence study was performed, in which a sample containing [(dien)Pt(1-MeC-*N3*)]$^{2+}$ was measured at 23, 40, 60, 80 and 90º C. Between the spectrum recorded at 23ºC (two signals) and the spectrum recorded at 90ºC (only one signal) the resonances gradually merge with no typical coalescence behavior observed. In other words, the conversion between the two conformers becomes more favorable at high temperatures.

Later in this chapter, the ^{195}Pt NMR spectrum corresponding to [(dien)Pt(1-MeU-*N3*)]$^{+}$ is discussed. This complex presents only a single signal at -2844 ppm in the ^{195}Pt NMR spectrum. It implies that the two possible conformers are equivalent, at least referring to the environment of the platinum atom. Probably in this case, due to the formal "substitution" of the exocyclic amino group by a carbonyl group, rotation about the Pt-N3 bond is more favorable, because there are fewer steric restrictions. As additional information, a ^{195}Pt NMR spectrum of [(dien)Pt(D_2O)]$^{2+}$ was measured, displaying also a single signal at -2547 ppm, in the region of a typical Pt(II) coordinated to three nitrogen atoms and one oxygen atom.

2.1.1.3.- pH dependence.

The chemical shifts of [(dien)Pt(1-MeC-*N3*)]$^{2+}$ were independent of pH over a large range. After measurement of the chemical shifts of the aromatic protons at different pD values, it can be concluded that under strongly basic conditions [(dien)Pt(1-MeC-*N3*)]$^{2+}$ becomes deprotonated at the exocyclic amino group. The pK_a (N4) of [(dien)Pt(1-MeC-*N3*)]$^{2+}$ was determined to be approximately ca. 13.5 in D_2O, corresponding to ca. 13 in water [94].

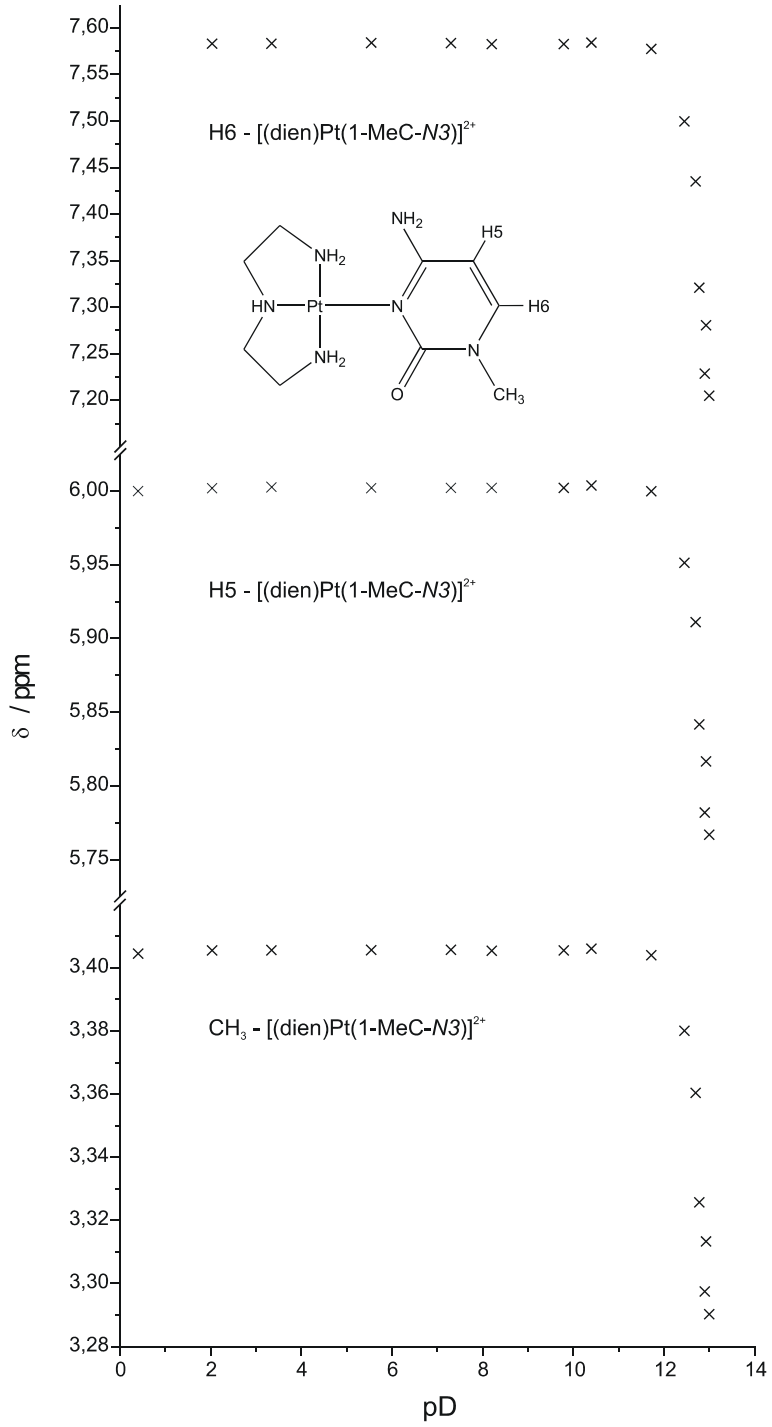

Figure 2.7: *^{1}H NMR pD-dependence (δ, ppm) of H6, H5 and CH_3 resonances in D_2O of the cation $[(dien)Pt(1\text{-}MeC\text{-}N3)]^{2+}$ (**9**).*

The graphical representation of the pD-dependence is depicted in Figure 2.7. A significant upfield shift of the signals at basic pH values can be observed, due to the N4 deprotonation of the cation. This effect is more pronounced in the H6 aromatic proton, with a $\Delta\delta$ of approximately 0.40 ppm; $\Delta\delta$ of the H5 proton is

about 0.25 ppm; and 0.12 ppm in the case of the methyl group. Measurement of the pD dependence was carried out using identical samples, in which the pD of the solutions was modified in small increments by addition of small amounts of DNO_3 and NaOD. NMR spectra of the samples were recorded immediately after modification of pD, with the aim to avoid the migration and deamination reactions which occur spontaneously under basic conditions (see below).

The estimated pK_a value (~13) of the N4 exocyclic amino group of **9** is markedly decreased in comparison with the pK_a value (~16.7) [95] of the free nucleobase. The presence of a platinum atom coordinated to the endocyclic N3 position thus influences the acid-base properties of the neighboring N4 amino group. This acidification of the amino group is frequently observed in other metal complexes of cytosine and also in many metal-modified or alkyl-modified nucleobases [5,96].

2.1.2.- Deamination and Migration.

After preliminary studies of the reaction leading to deamination of [(dien)Pt(1-MeC-*N3*)]$^{2+}$, it became evident that this reaction occurs simultaneously with a parallel reaction; namely the migration of the [(dien)Pt^{II}] group from the initial N3 position to the exocyclic N4 site of cytosine. As a result of the reaction studied, [(dien)Pt(1-MeU-*N3*)]$^{+}$ (**10**) is obtained, together with ammonia, as deamination products, and [(dien)Pt(1-MeC^{-}-*N4*)]$^{+}$ (**11**) as migration product. After the N3→N4 migration of the [(dien)Pt^{II}] group, the N3 site of 1-MeC remains unprotonated because of the high pH. A ^{1}H NMR study of the latter complex reveals that it adopts two different geometries. These are assigned to *syn*-[(dien)Pt(1-MeC^{-}-*N4*)]$^{+}$ (**11a**) and *anti*-[(dien)Pt(1-MeC^{-}-*N4*)]$^{+}$ (**11b**). Details of the ^{1}H NMR study are given in section 2.1.5 of this chapter. Scheme 2.1 shows the different pathways of metal migration and ligand deamination.

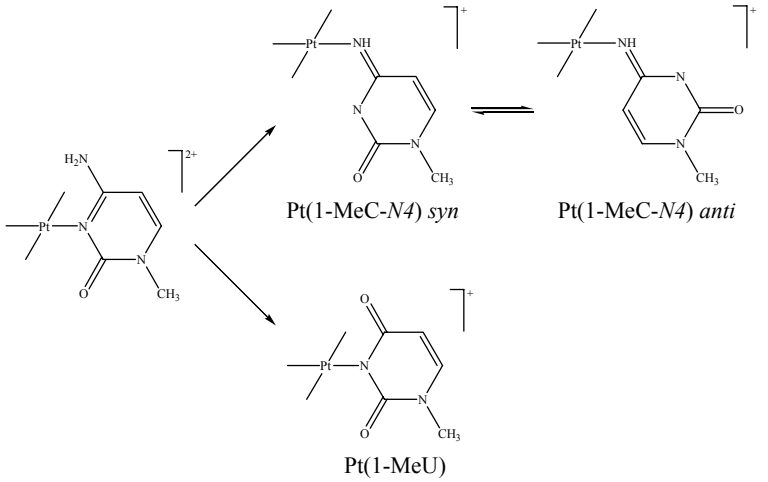

Figure 2.7: *Deamination of the cytosine nucleobase in [(dien)Pt(1-MeC-N3)]$^{2+}$ and competing migration of the Pt^{II} center to N4.*

Variations in the conditions of the reaction can significantly modify the yield of the products. In the studies carried out, it is evident that a high concentration of the starting compound does not have any pronunced effect on the course of the reaction, but have a negative effect in the quality of the ^{1}H NMR spectrum. External variation of pH does not modify the yields of the products. However, as the reaction proceeds, the pH changes. This variation comes as a consequence of the migration pathway, wherein the exocyclic amino group of cytosine loses a proton, causing a progressive acidification of the solution. The reaction sets on when pH is higher than 12.7. Vice versa, the reaction stops when the pH is below this value. A further increase in pH does not accelerate the reaction. The most remarkable effect is played by temperature. Increasing the temperature significantly changes the yields of the individual products. The higher the temperature of the reaction, the higher the amount of migration product. For example, at room temperature (23ºC), when the starting compound is used up, yields are about 73% for the deamination product and 27% for the migration products; these yields are approximately 50% each at 60ºC. The rate of both reactions increases considerably at higher temperatures. However, additional signals associated with di-metallic cytosine complexes are observed if the temperature of the reaction is too high (see part 2.4 of this chapter). Migration and deamination processes are, of course, irreversible.

In this way, it was not possible to separate the deamination and migration pathways using (dien)Pt^{II}. The aim of this study was to understand the conditions for spontaneous deamination of cytosine mediated by a metal entity. Both the chemical transformation of [(dien)Pt(1-MeC-*N3*)]$^{2+}$ to [(dien)Pt(1-MeU-*N3*)]$^{2+}$ (**10**), which was also achieved by means of sodium nitrite ($NaNO_2$) resulting exclusively in the deamination product, and the direct synthesis of **10** provide useful information for the characterization of the deamination products.

2.1.2.1.- Conditions and NMR study.

Samples of **9** were dissolved in D_2O, the pD was adjusted to 12.7 by addition of NaOD, and the reaction was followed at ambient temperature (23º C) with time. These reaction conditions appear to be ideal for the principal investigation of deamination pathways and kinetic profiles: this is the lower pH value at which the reaction proceeds; at higher temperatures the reaction is too fast to estimate the rate constants. The resulting ^{1}H NMR spectra are shown in Figure 2.8, recorded after different reaction times. The first aspect relates to the spectrum at the bottom; it was recorded at the beginning of the reaction, after 10 minutes at room temperature and pD 12.7. Signals of the starting compound (A) display the expected high field shift (c.f. Figure 2.7), hence δ = 7.17 for H(6) and δ = 5.74 for H(5). The effect of the pH on the complex is evident; a proton of the exocyclic N4 amino group can be lost at strong alkaline conditions. The second aspect refers to the previously described deamination and migration products. With time, it is progressively easier to distinguish the different species coexisting in the solution. A detailed spectrum is shown in Figure 2.9.

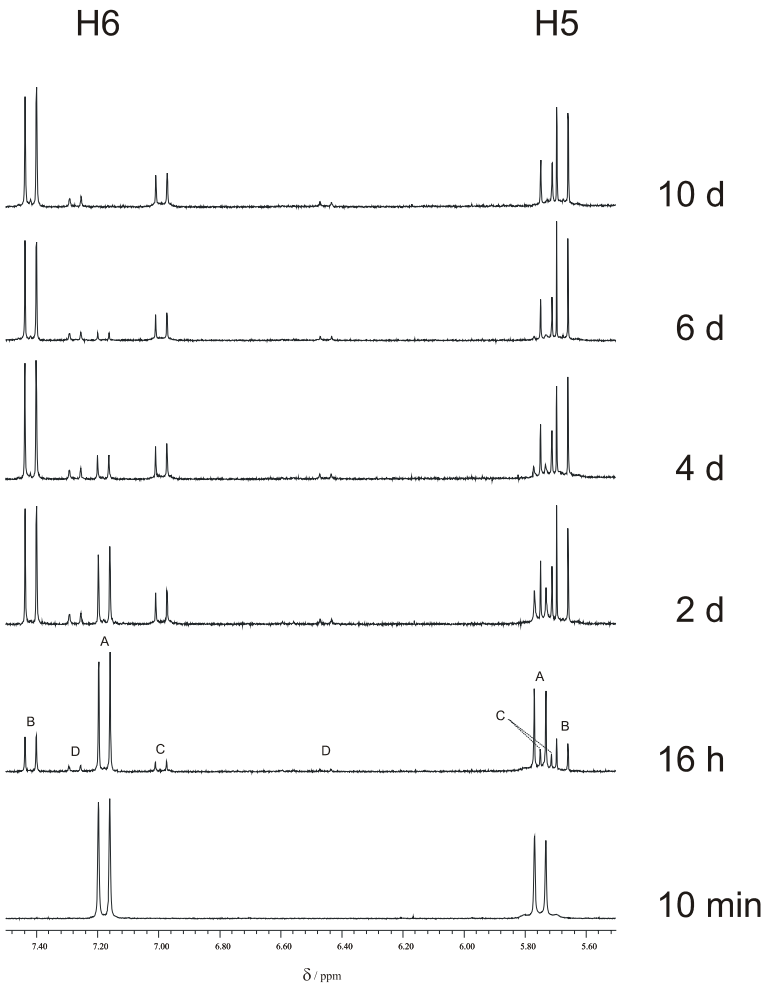

Figure 2.8: *Lowfield sections of ^{1}H NMR spectra of [(dien)Pt(1-MeC-N3)]$^{2+}$ (D_2O, pD 12.7, room temperature) at different reaction times (from bottom to top): 10 min, 16 h, 2 d, 4 d, 6 d, 8 d, 10 d. A= [(dien)Pt(1-MeC-N3)]$^{2+}$, B= [(dien)Pt(1-MeU-N3)]$^{+}$, C= syn-[(dien)Pt(1-MeC-N4)]$^{+}$, D= anti-[(dien)Pt(1-MeC-N3)]$^{+}$.*

The spectrum shown in Figure 2.9 was recorded after 4 days of reaction. As can be observed in this spectrum, resonances due to the starting compound [(dien)Pt(1-MeC-*N3*)]$(ClO_4)_2$ (A) have almost disappeared, while the new sets B, C, and D have grown in. Signal set B can readily be assigned to the deamination product, [(dien)Pt(1-MeU-*N3*)]$^{+}$ from comparison with a sample obtained from [(dien)Pt^{II}] and 1-MeU. The two other sets are identified, on the basis of 2D NMR spectroscopy as well as their pD dependence (see part 2.1.5 of this chapter), as being due to two rotamers (C, *syn*; D, *anti*) of the cytosine-N4 linkage isomer [(dien)Pt(1-MeC^{-}-*N4*)]$^{+}$. It is thus evident that in strongly alkaline medium,

deamination of the cytosine nucleobase in **9** competes with metal migration from N3 to N4.

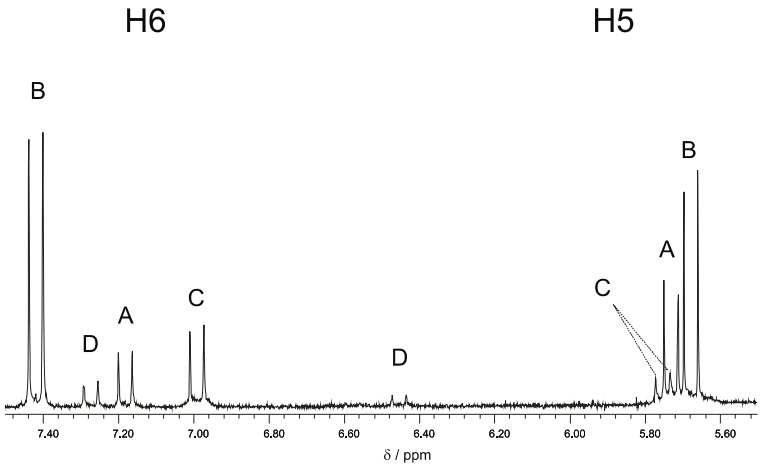

Figure 2.9: *Lowfield section of ^{1}H NMR spectrum of [(dien)Pt(1-MeC-N3)](ClO$_4$)$_2$ at room temperature after 4 days. A= **9**, B= **10**, C= **11a**, D= **11b**.*

The reaction is 100% complete in 10 days; the kinetics of the reaction are analyzed in part 2.1.4 of this chapter. Over this time, the proportion of deamination–migration yields is approximately constant at 1:4; this implies that the migration pathway, of lesser yield, has necessarily a higher rate constant to reach this radio at the early stage of the reaction. This fact is confirmed in the kinetic studies of the reaction.

With regard to the migration products, **11a** and **11b** have also a constant ratio (3:1) with respect to each other in solution, the *syn* rotamer being the major product. This ratio displays no variation with time or pH. The signals are clearly distinguished in an ^{1}H NMR spectrum. As the NMR technique is slow, it means that the rotation to convert *syn* into *anti* or vice versa is very slow. As it was mentioned, at acidic pH the ratio also remains constant; this observation probably eliminates the argument of possible internal interactions of the protons of NH_2 of the dien group with the free N3 site of the cytosine base to explain the non-rotational behavior. In the case of the *anti* rotamer, the H5 doublet appears furthest downfield due to the proximity of the platinum atom in this arrangement (see Scheme 2.2).

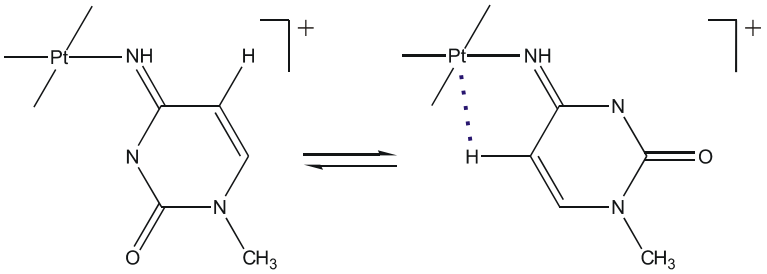

Pt(1-MeC$^-$-N4) *syn* Pt(1-MeC$^-$-N4) *anti*

Scheme 2.2: *Syn and anti linkage isomers. The proximity of the platinum atom to the H(5) proton is realized in the anti geometry.*

The pD dependence of the H5 and H6 resonances of *syn* and *anti* rotamers was determined (see part 2.1.1 of this chapter); pK_a values (H_2O) are 7.4 and 7.7, respectively.

In order to identify the described species present in alkaline solution, a variety of parallel reactions were successfully performed. In some cases these were useful to compare results, like in the case of the deamination product; and in other cases were useful to eliminate the existence of other feasible species or intermediates in the solution.

One of the most interesting supplementary studies was performed in order to identify released ammonia (second product of deamination) in the solution. Identification of NH_4^+ was successful in other cases, for example in our work with the aqua species of *trans*-[Pt(1-MeC-N3)$_2$I$_2$] (**21**) [1]. The typical 1:1:1 triplet corresponding to the free NH_4^+ ion was observed in a ^{1}H NMR spectrum of a deuterated DMSO solution. In the present case, our effort was aimed at finding the signals of the ammonium ion in deuterated water. For this purpose a saturated solution of ammonium chloride in water was prepared, the pH was adjusted to 1.4 with addition of acid (HCl), and 400 µL of D_2O were added to the solution. A ^{1}H NMR spectrum of the fresh sample was measured immediately.

Figure 2.10 shows the spectrum obtained, which displays a 1:1:1 triplet in the aromatic region (peaks are centered around 7.14 ppm with ^1J = 52.0 Hz.), assigned to the ammonium species (protonated due to the low pH; NH_4^+).

Ammonia species in water usually undergo fast isotopic exchange (proton – deuteron) with the medium. Because of this, after only a few minutes ND_4^+ is the only existing species in the solution, evidently not measurable by ^1H NMR spectroscopy. This effect is also observable when NH_3 is coordinated to a metal center or even in amines ($–NH_3$, $–NH_2$, –NH).

With regard to the nitrogen atom, ^{14}N (99.6% of isotopic natural abundance) has a spin state of 1. In this case, the high quadrupolar moment in a high symmetry environment (tetrahedral NH_4^+) allows to observe three lines of equal intensity (I = 1 has 3 orientations in a magnetic field). The coupling constant $J(^{15}N\text{-}^1H)$, with I = ½, is 73,3 Hz. The theoretical formula $J(^{15}N\text{-}^1H) = -1{,}4027\ J(^{14}N\text{-}^1H)$ [97] relates coupling constants between both isotopes. Thus, we can estimate theoretically the coupling constant of ^{14}N: $J(^{14}N\text{-}^1H)$ = 52,3 Hz. This value is consistent with the coupling constant observed in this experiment: $J(^{14}N\text{-}^1H)$ = 52,2 Hz.

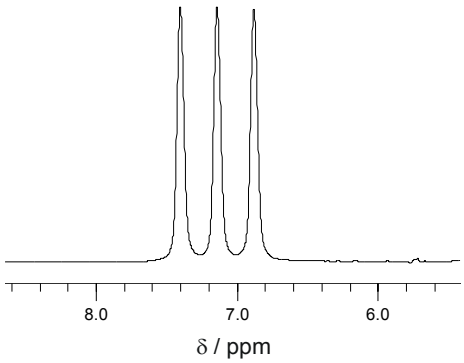

Figure 2.10: *^1H NMR spectrum of NH_4^+ in water.*

2.1.3.- Reaction Mechanisms.

The two parallel reactions that $[(dien)Pt(1\text{-}MeC\text{-}N3)]^{2+}$ undergoes in alkaline conditions can be, in principle, studied individually; in other words, deamination and migration processes are competitive, and do not influence each other. The veracity of this argument is discussed in point 2.3 of this

chapter. In the following paragraph, mechanistic explanations for the deamination and migration reactions are given and analyzed.

2.1.3.1.- Deamination.

Deamination is a known process in organic chemistry, it can be defined as a hydrolytic reaction in which an amino group is removed as ammonia from the molecule and is formally replaced by a hydroxo or keto group. There are many examples of deamination of amino acids in the organisms; NH_3 is the product, which is removed by the urea cycle. Deamination processes are also taking place as part of the degradation of the purine bases guanine and adenine to xanthine.

In the case of spontaneous deamination under extreme alkaline conditions as in the reaction studied here, the deamination mechanism of the reaction involving the metal-modified 1-MeC base in $[(dien)Pt(1\text{-}MeC\text{-}N3)]^{2+}$ is facilitated by a Lewis acid activation in combination with hydroxide activation, in other words, nucleophilic attack by external OH^-. It is noteworthy that the deamination only occurs when the solution containing $[(dien)Pt(1\text{-}MeC\text{-}N3)]^{2+}$ has a pH of 12.7 or higher.

The mechanism of deamination can be considered a process comprised of two steps (see scheme 2.3). The first step consists of a nucleophilic attack by OH^- from the solution (pH > 12.7) at the C4 site of the cytosine and the subsequent addition of the hydroxo group. The second step, in which the elimination of the exocyclic N4 amino group takes place, completes the deamination process. This last step requires the formation of a C=O double bond and the transfer of a proton from the hydroxyl to the amino group.

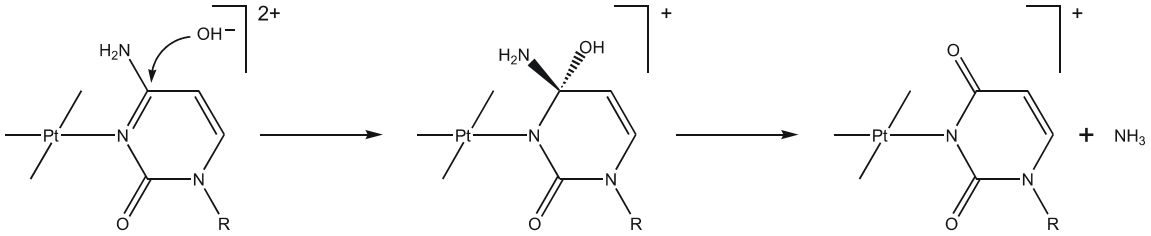

Scheme 2.3: *Deamination mechanism. Nucleophilic attack of OH^- at the C(4) site and elimination of the N(4) amino group.*

This mechanism is in full agreement with the proposed mechanism of spontaneous deamination as deduced from theoretical calculations of the gas-phase optimized structures as well as activation energies [5].

2.1.3.2.- Migration.

In order to elucidate the migration mechanism undergone by **9** under alkaline conditions, some possibilities were considered and evaluated with different cytosine complexes. The investigations suggest, that N(3)→N(4) migration under alkaline conditions is a process, which involves the co-ligands bound to the platinum ion. The first indication for this hypothesis was the observation, that $[(NH_3)_3Pt(1\text{-MeC-}N3)]^{2+}$ (**12**) does not display the phenomenon of migration (see part 2.2.1 of this chapter), contrary to $[(dien)Pt(1\text{-MeC-}N3)]^{2+}$, where the $[(dien)Pt^{II}]$ entity moves from N(3) to N(4) under otherwise identical conditions. The different behavior is remarkable, since there is only little difference between both platinum entities; the three ammine ligands can formally be derived from the dien ligand by substitution of the ethylene groups by protons. Taking this situation into account, a proposed migration mechanism has to explain the different behavior of both compounds; thus the role played by the dien ligand seems to be fundamental.

In general, metal-ion binding to the exocyclic amino group of the cytosine entity requires proton abstraction from the NH_2 group. As was pointed out previously in this chapter, a metal coordinated at the N3 site facilitates this

proton abstraction, because of the acidification suffered by the exocyclic amino group. The pK_a for deprotonation of [(dien)Pt(1-MeC-*N3*)]$^{2+}$, as estimated by pD dependent ^{1}H NMR spectroscopy, was found to be ca. 13. It suggests that [(dien)Pt^{II}] migration is preceded by deprotonation of the exocyclic amino group of cytosine. The linkage isomerization process thus resembles that in the [$(NH_3)_5Ru^{III}$(1-MeC)] system [98] and likewise that of various adenine complexes of Pt^{II} [99-101]. It is different from that of a redox-assisted pathway of linkage isomerization which was discovered previously [102-104]. A mechanism involving two steps is proposed to explain the migration process in agreement with these premises.

The first step of the migration process is a substitution reaction in the coordination sphere of the platinum ion following an associative mechanism: it concludes with the opening of the dien ligand. This reaction is initiated by the nucleophilic attack of a hydroxide anion from the surrounding medium; this attack extends the square planar coordination of the platinum atom leading to a 5-coordinate transition state, which displays a pyramidal arrangement of the cytosine base, the three donor sites of the dien ligand and the incoming hydroxo group (Scheme 2.4).

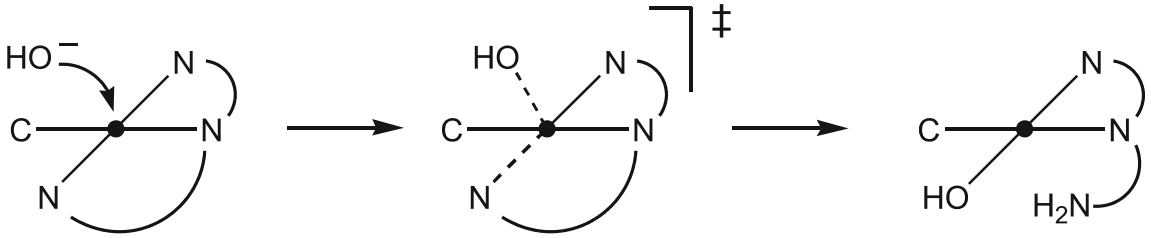

Scheme 2.4: *Nucleophilic attack by OH^- at the platinum atom and formation of the 5-coordinate transition state.*

Eventually, the amino group is displaced from the coordination sphere of platinum, and the hydroxo group occupies the former position of NH_2 in the square planar coordination. In summary, a hydroxo group displaces a part of the dien group, without other geometrical changes, forming the intermediate product

of the migration. This associative mechanism of substitution (via 5–coordinate intermediate) is the most frequent one in platinum chemistry.

In principle, such an intermediate displays in solution fixed and flexible parts in its geometrical arrangement. The fixed part of the complex includes the atoms implicated in the square planar coordination, viz.: the platinum atom, N(3) atom of the cytosine nucleobase and two amino groups of the dien ligand. Parts in the complex with flexibility to be considered are the cytosine ring (through rotation about the Pt-N(3) bond) and the ethylene group placed between the two fixed amino groups of dien forming a 5-membered ring with Pt. However, the uncoordinated dien-arm ($–CH_2–CH_2–NH_2$) has the highest flexibility.

Aliphatic amines of the type $R–NH_3^+$ have pK_a values between 10 and 11. Under the alkaline conditions of the reaction (pD > 12), complete deprotonation of the terminal amino group can be expected ($R–NH_2$). Thus, the terminal nitrogen of the dien-arm is unprotonated and has a free electron pair, allowing it to act as a proton acceptor. The mobility of the dien-arm (proton acceptor site) and the proximity of the exocyclic amino group of the cytosine ring (proton donor site), are the perfect scenario for a hydrogen bond, which connects the dien-arm with the N(4) site.

Theoretically, it is reasonable to expect in solution a dynamic process, in which the *syn* oriented (with respect to the platinum atom) proton moves from the N(4) site to the proton acceptor site (NH_2 of dien-arm). This migration is facilitated once the proposed hydrogen bonding is formed (Figure 2.11). The geometry of the structure of the ring-opened intermediate [(η^2-dien)Pt(OH)(1-MeC-*N3*)]$^+$ (I) was optimized by P. Lax in the gas phase with the Gaussian98 suite of programs. The optimized geometrical arrangement of the intermediate (I) is shown in Figure 2.11.

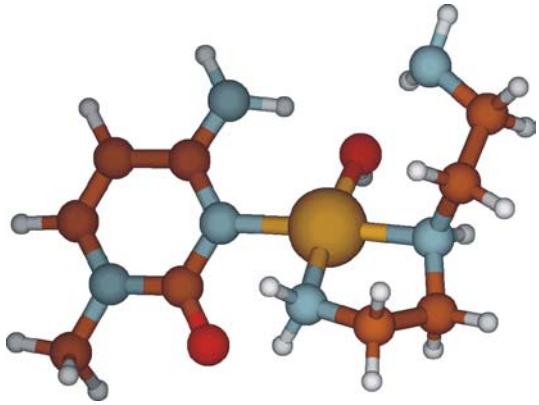

(I)

Figure 2.11: *Optimized structure of [(η^2-dien)Pt(OH)(1-MeC-N3)]$^+$ (I).*

The platinum atom resides in the center of the cation and is coordinated in a square planar fashion by hydroxide, N(3) of 1-MeC and two amino sites of the dien ligand. The uncoordinated part of the dien ligand ("dien-arm") is out of the coordination plane of platinum.

In the calculated structure of (I) the cytosine base is inclined by 38.9° towards the PtN_3O coordination plane, as a consequence of OH^- acting as an intramolecular H bond acceptor for both $N(4)H_2$ of 1-MeC (O···N, 2.668 Å; N(4)-H···O, 154.35°) and for the dangling NH_2 group of the dien ligand (O···N, 2.920 Å; N-H···O, 149.63°). A second structure, which is a tautomer of I, [(η^2-dienH)Pt(1-MeC$^-$-*N3*)(OH)]$^+$ was then computed (see Figure 2.12). In (II) a proton of the $N(4)H_2$ group of 1-MeC has been transformed to the dangling amino group of dien to produce a zwitter ionic form. (II) was found to be only 66 kJmol^{-1} less stable than (I). In (II) the 1-MeC plane forms an angle of 61.9° with the PtN_3O plane, the Pt-OH bong length is 2.052 Å, and the dien-NH_3^+ acts as a H donor for N^4H^- (2.869 Å, N-H···O, 144.01°) and for OH^- (2.486 Å; N-H···O, 158,52°). The distance between N^4 of mcyt and Pt in (II) is 3.298 Å, which compares with 2.668 Å in (I).

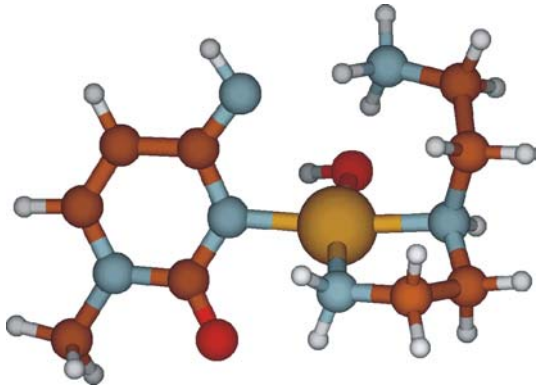

(II)

Figure 2.12: *Optimized structure of [(η^2-dienH)Pt(OH)(1-MeC$^-$-N3)]$^+$ (II).*

Concerning the proton transfer mechanism from (I) to (II), two scenarios are feasible: (i) H^+ transfer through space. For this purpose, one of the two protons of cytosine NH_2 was moved progressively toward the dien-NH_2 group. This process passes over a high energy barrier of ca. 480 kJ/mol, before approaching a local minimum with the dipolar structure II' (430 kJ/mol above I). Optimization of II' leads to structure II, which is only 66 kJ/mol higher in energy than I (see above). (ii) The proton is initially transferred to the OH ligand and subsequently handed over to the dien-NH_2. The energy and optimized structure of this species is still being calculated.

Conclusions drawn from the theoretical studies can be summarized in two principal ideas: a) Opening of the dien group allows its uncoordinated amino-arm to form a hydrogen bond with the N(4) site of 1-MeC; b) proton migration along the hydrogen bond has to exceed low energy barriers in both directions.

On the basis of these two conclusions, a third one can be drawn: proton migration in the hydrogen bond provokes an additional stabilization of the anion $N(4)H^-$ of 1-MeC. Thus, the pK_a value of this site is lowered under these conditions; in other words, stabilization of $N(4)H^-$ by $R–NH_3^+$ provokes an additional acidification of the exocyclic amino group of cytosine.

Therefore, the metal migration process in the [(dien)Pt^{II}] system seems to be clarified. So, it is possible to propose the second step of the metal migration mechanism with a similar scheme as the first migration step: a nucleophilic attack followed by a substitution. As shown in scheme 2.5, proton migration is achieved and the $N(4)H^-$ of cytosine is able to attack the platinum atom following also an associative substitution mechanism as described previously. The 5-coordinate transition state includes at the same time N(3) and N(4) sites of cytosine. Migration is completed with the cleavage of the Pt-N(3) bond.

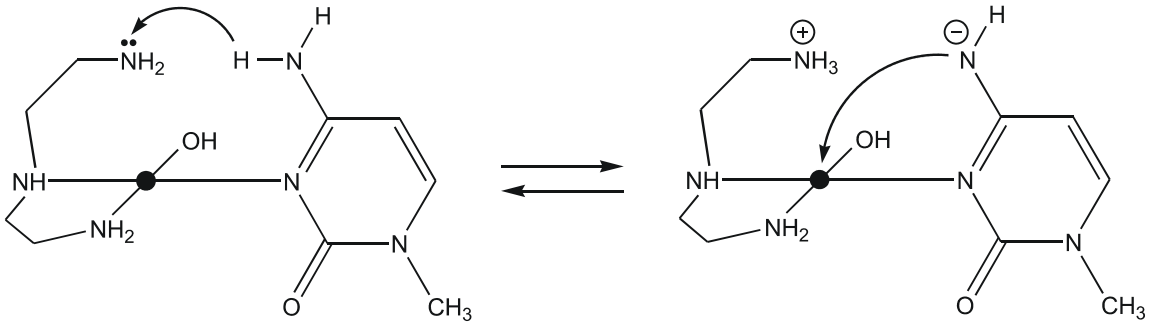

Scheme 2.5: *Proton migration and nucleophilic attack by $N(4)^-$ at the platinum atom.*

Some additional considerations are resumed in this paragraph: A possible attack of the amino group of the dien-arm at the platinum atom occurring before proton migration produces again the starting compound **9**. If the attack takes place after metal migration, migration product **11** is produced. As it is pointed out in the experimental part, a rise in temperature during the process increases also the yield of the migration product at the expense of the deamination product (the attacks are faster). Low pH, on the other hand, hinders the reaction (amino sites are protonated). Both situations are in agreement with the proposed mechanism.

The described mechanism most likely is also valid for other migration processes of [(dien)Pt^{II}] along nucleobases such as the previously mentioned migration involving the adenine nucleobase N(1)→N(6) [99]. There are, however, also migration processes on the adenine nucleobase of *trans*-[$(NH_3)Pt^{II}$] (N7→N6) [100], which can not be rationalized by the above scenario because of lack of a dien ligand. If however, for whatever reason, the exocyclic amino group

is sufficiently acidified, nucleophilic attack on the Pt center and eventual metal migration is possible.

2.1.4.- Kinetics.

The rate profile of the metal migration and deamination reactions is studied assuming that both reactions are different and competitive. In the case of the N3→N4 platinum migration, an intramolecular process takes place; the mechanism of the reaction is described in section 2.1.3.2. It can be considered a first order reaction. In the case of the deamination reaction, the strongly alkaline medium (pH ~ 12.7) of the solution implies a high concentration of hydroxide, which acts as a reactant in the reaction ($[(dien)Pt(1\text{-}MeC\text{-}N3)]^{2+} + OH^- \rightarrow [(dien)Pt(1\text{-}MeU\text{-}N3)]^{+} + NH_3$). Generally, in second order reactions, if the concentration of one reactant is in great excess in comparison with the other one, it can be considered constant with time. Therefore, the rate equation of the second order reaction ($v = -k [A] [B]$) can be approximated, resulting in a pseudo-first order reaction ($v = -k' [A]$). Thus, the kinetics of the migration and deamination reactions can be analyzed assuming first-order conditions. In the case of competitive reactions, disappearance of the starting compound and formation of the products is proportional to the amount of starting compound present. The standard integrated rate expressions are: $[A] = [A]_0 e^{-kt}$, for the formation of the products, and $[A] = [A]_0 (1- e^{-kt})$ for the disappearance of the starting compound.

The slow rate of the reaction in the optimized conditions (23ºC, pH 12.7) permits it to be studied conveniently by ^1H NMR spectroscopy. Different reactions were carried out with consistent results. A graphical profile of the course of these reactions at different reaction times is depicted in Figure 2.13, in which the concentration of the migration product is the addition of its two rotamers (*syn* and *anti*). As expected, in the first steps of the reaction, the reaction rate is faster than when the reaction is partially completed.

Disappearance of the starting compound can be formally considered as the result of the addition of the individual reactions of deamination and migration. In order to estimate quantitatively the presence of the complexes **10**, **11** and **9** in solution, the NMR peaks were integrated. Then, the resulting values were approximated to the first order rate equations considering also the percentage of the different yields obtained by the products. Thus, the formation of the deamination product has a yield of 73%, $t_{½}$ = 1.43 d as half-life and k = 0.49 d^{-1} as rate constant; the formation of the migration products has a yield of 27%, $t_{½}$ = 0.69 d and k = 1.00 d^{-1}; the disappearance of the starting compound has consequently a half-life of 1.40 d. According to the suggested rate profile, the next expressions govern the reactions:

$$[\mathbf{10}] = 73\ [\mathbf{9}]_0\ (1 - e^{-0.49t})$$

$$[\mathbf{11}] = 27\ [\mathbf{9}]_0\ (1 - e^{-0.69t})$$

$$[\mathbf{9}] = 100 - (73\ [\mathbf{9}]_0\ (1 - e^{-0.49t}) - (27\ [\mathbf{9}]_0\ (1 - e^{-0.69t})).$$

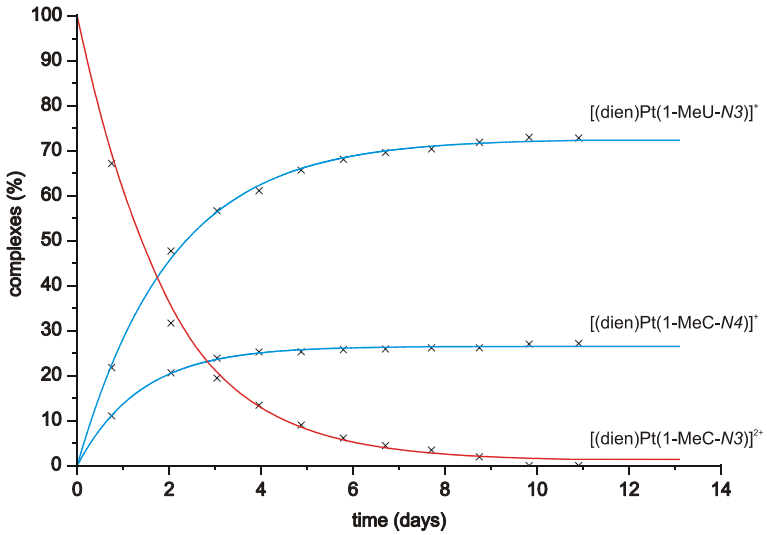

Figure 2.13: *Graphical representation of the course of the deamination and migration reactions of **9** at different reaction times.*

Integration of the rate equation of a first order reaction ($d[A] / dt = -k' [A]$) results in a linear dependence ($ln[A] = -kt + ln[A]_0$), with $-k$ being the slope of the curve and $ln[A]_0$ the value of the ordinate axis at the origin. As shown in Figure 2.14, the graphical representation of the logarithm of the concentration of the

starting compound *vs.* time gives as a result a straight line. In other words, the assumption of first order reactions is consistent with the experimental results.

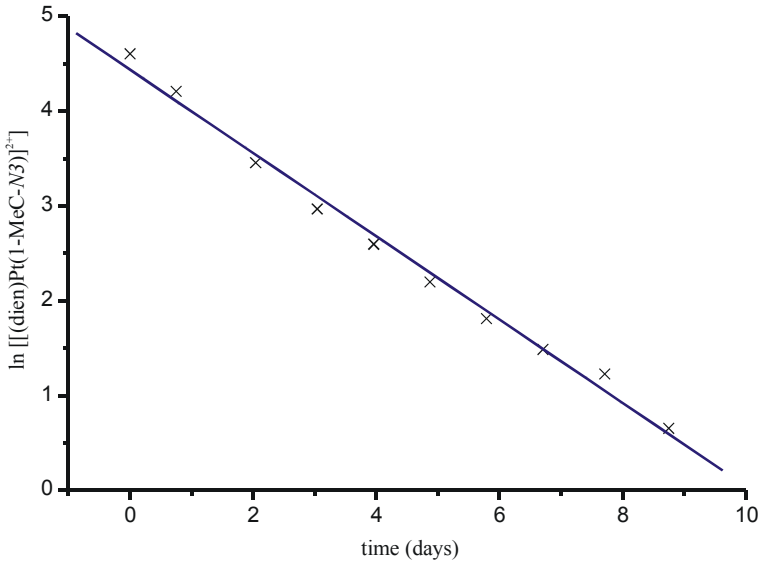

Figure 2.14: *Graphical representation of ln[[(dien)Pt(1-MeC-N3)]$^{2+}$] vs. time.*

The reaction was also carried out at higher temperatures. As expected, not only the yield of the final products (as it was reported in this chapter), but also the rate constants changed. The rates of the reactions increased considerably at elevated temperatures, especially the migration reaction. It increases the yield of the Pt-N4 coordinated resulting product notably. Whereas the reaction at room temperature (23º C) is completed in 10 days, at 40º C 2 hours are required, and only 30 min at 60º C. These short times of reaction prevented the adequate study of the reaction using the NMR spectroscopy.

2.1.5.- Deamination and Migration Products.

Characterization of the deamination and migration products was carried out applying ^{1}H and ^{195}Pt NMR spectroscopy. pH dependences were measured in order to determine the acid–base properties along the pH scale of the

deamination product and the two migration products. The gas-phase idealized structures of the cations were calculated for comparative purposes.

2.1.5.1.- Deamination Product: [(dien)Pt(1-MeU-*N3*)]$^+$ (10).

Metal binding at the N3 site of the uracil nucleobase influences the acid-base properties of the exocyclic oxygen atoms. In general, the influence in the exocyclic amino group of a metallic atom coordinated to an endocyclic nitrogen atom of a nucleobase is smaller than that of a proton [105,106]. Thus, protonation at one of the two exocyclic oxygen atoms occurs at higher pH values when a metal is coordinated to an endocyclic nitrogen atom. Therefore, the rare tautomer of the uracil base in which the O4 atom is protonated (2-oxo-4-hydroxo) is markedly stabilized by the presence of a metal at N3. There are some reported examples in the literature of the stabilization of this 2-oxo-4-hydroxo rare tautomer of the uracil base with a N3 coordinated platinum atom, as in the case of *cis*-[$(NH_3)_2$Pt(1-MeU-*N3*)(1-MeUH)](NO_3) · $2H_2O$ or *cis*-[$(NH_3)_2$Pt(1-MeUH-*N3*)$_2$](NO_3)$_2$ · $3H_2O$ [107].

2.1.5.1.1.- NMR Spectroscopy and pH Dependence of 10.

The NMR spectroscopic study of the deamination product carried out reveals that over a large range pH range (pD values > 2), the signals of the aromatic H6 and H5 protons (doublets) and the CH_3 methyl group (singlet) of **10** in the ^{1}H NMR spectrum are constant and appear at 7.41, 5.68 and 3.33 ppm, respectively. However, at strongly acidic conditions, **10** can be protonated at the carbonyl groups. The spectrum is very similar to the one of the starting compound, with different chemical shifts, however. As in the case of **9**, and under the same conditions, a pD dependence of the cation was measured. The pK_a value of **10** was determined to be 0.09(3) in water. The graphical

representation of the pD-dependence is depicted in Figure 2.15. The dashed blue line of the Figure corresponds to the pK_a value and the red line is the fitted curve after refinement of the chemical shifts.

Several ^{195}Pt NMR spectra of **10** were measured. Throughout the reaction, the chemical shift of the platinum atom in the spectrum appears at -2844 ppm and does not change; the signal remains also invariable with pH. The signal consists of a singlet only; therefore **10** does not have the doubling effect as seen with **9**.

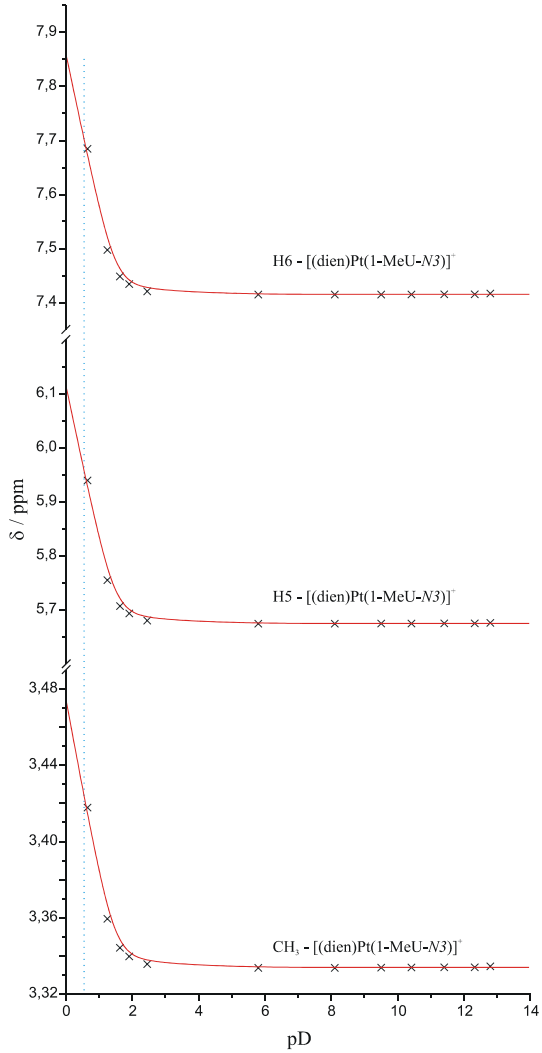

Figure 2.15: *^{1}H NMR pD-dependence (δ, ppm) of H6, H5 and CH_3 resonances in D_2O of the compound [(dien)Pt(1-MeU-N3)]$^+$.*

2.1.5.2.- Migration Product: [(dien)Pt(1-MeC^{-}-*N4*)]$^{+}$ (11).

As reported for **9** and **10**, the presence of a metal entity bonded to a nucleobase influences the acid-base properties of the possible proton donor / acceptor atoms of the base. In this case, the platinum entity is bonded to the N4 exocyclic amino group, and the influence on the endocyclic N3 site is clearly observable. However, the proton bonded to the N4 site is also influenced by the platinum atom; unfortunately, this effect is not measurable in aqueous solution by means of NMR spectroscopy. The pK_a value for the protonation of the N3 site in the free 1-methylcytosine was found to be 4.3. Upon Pt binding to N4, this site undergoes a basification as will be shown below.

2.1.5.2.1.- NMR Spectroscopy and pH Dependence of 11.

The two conformers of the migration product (*syn*-[(dien)Pt(1-MeC^{-}-*N4*)]$^{+}$ and *anti*-[(dien)Pt(1-MeC^{-}-*N4*)]$^{+}$) were identified in solution by ^{1}H NMR spectroscopy. Recognition of the signals was previously reported in section 2.1.2 of this chapter. The chemical shifts of the *anti* conformer range from 7.44 to 7.27 ppm in the case of the H6 proton, and from 6.58 to 6.45 ppm in the case of the H5 proton. The H5 proton signal of this conformer is markedly downfield shifted in comparison with the signal of the *syn* conformer due to the proximity of the platinum atom and H5 in this geometry. The chemical shifts of the *syn* conformer range from 7.09 from 6.99 ppm (H6), and from 5.92 to 5.73 (H5). It can be seen that the variation of the chemical shifts in dependence of pH is not very pronounced; the minimal and maximal variations are those of the H6 ($\Delta\delta$ = 0.10 ppm) and H5 ($\Delta\delta$ = 0.19 ppm) protons of the *syn* conformer. In spite of these small increments of the chemical shifts, accurate values for the pK_a were calculated from the pH dependencies. However, the $\Delta\delta$ of the CH_3 methyl group was not sufficiently sensitive to obtain satisfactory results. A graphical representation of the H6 and H5 protons in the pH dependence is depicted in Figure 2.16. The dashed blue lines in the Figure correspond to the pK_a values of

the conformers and the red lines are the fitted curves after refinement of the chemical shifts.

The pK_a values of both conformers were found to be similar, yet not equal. They were determined to be 7.7 for the *anti* conformer and 7.5 for the *syn* conformer in water. This small difference is supposed to be related to the effect of the NH_2 group of the dien ligand on the N3 position. In the case of the *syn* conformer, the possibility of the [(dien)Pt^{II}] group to form a H bond with the endocyclic N3 site of the cytosine base stabilizes the deprotonated cytosine base and consequently reduces the pK_a of the N3 protonated species, hence of the neutral iminooxo tautomer.

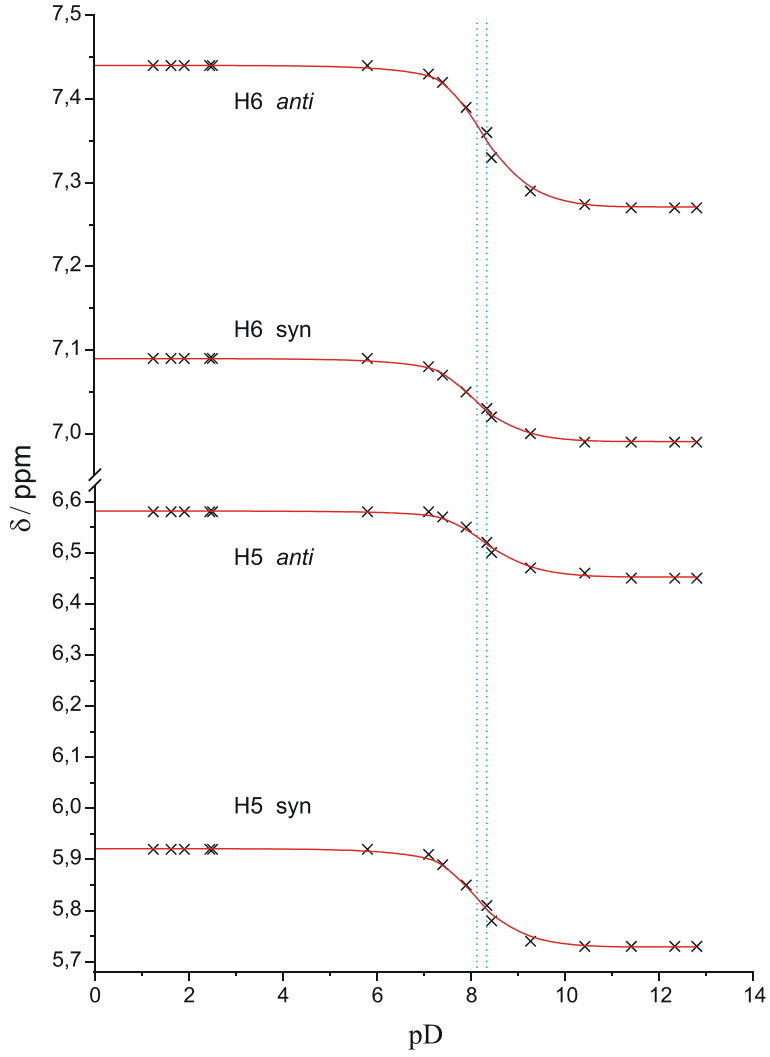

Figure 2.16: *^{1}H NMR pD-dependence (δ, ppm) of H6 and H5 resonances in D_2O of the compound [(dien)Pt(1-MeC$^-$-N4)]$^+$.*

No signals corresponding to the migration products were identified in the ^{195}Pt NMR spectra. Probably the ^{195}Pt signals in the spectrum are superimposed by the intense signal of the deamination product at –2844 ppm, present in the solution at a concentration approximately three times higher. Similar Pt-N4 coordinated cytosine complexes have been shown to display their ^{195}Pt signals in this region of the spectrum [108].

2.1.6.- Remarks.

Hydrolytic deamination of cytosine, a major mutagenic event in DNA, is facilitated by metal coordination to N3 as demonstrated in the studied model system and rationalized by DFT calculations. The effect of a metal atom (platinum) coordinated to an endocyclic nitrogen atom of a nucleobase (1-MeC) is generally smaller than that of a proton. Here it is demonstrated that the N4 site of the cytosine nucleobase is acidified, from 17 (free base) to 13 (Pt-*N3*); in the case of Pt bonded to the N3 site of uracil base the pK_a value of the carbonyl groups are likewise influenced (pK_a increases relative to free uracil); for the migration product, the Pt-N4 coordination influences the pK_a value of the N3 site. In the latter case, the pK_a for the different conformers is also slightly influenced (ΔpK_a = 0.2) by intramolecular H bonding.

2.2.- Deamination of 1-MeC excluding Migration.

The deamination and migration processes undergone by **9** were discussed in section 2.1 of this chapter. The mechanism of the migration process was attributed to an active participation of the dien ligand. Without the presence of the dien group in a N3-platinated 1-methylcytosine base, deamination of the cytosine base should occur under the same conditions, yet without metal migration. The expected deamination of the platinated cytosine base is depicted

in the scheme 2.6. With this aim, $[(NH_3)_3Pt(1\text{-}MeC\text{-}N3)]^{2+}$ was synthesized in order to study its behavior.

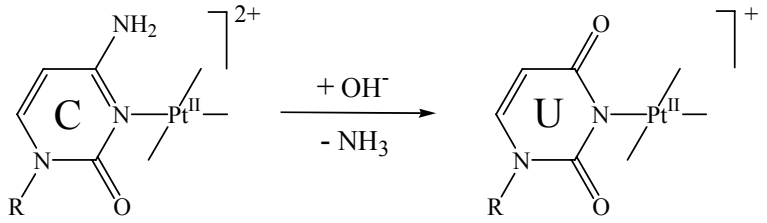

Scheme 2.6: *Pt-assisted deamination of 1-MeC without metal migration.*

2.2.1.- $[(NH_3)_3Pt(1\text{-}MeC\text{-}N3)]^{2+}$ (12) as Starting Compound.

2.2.1.1.- Crystal Structure.

The title compound was obtained from the direct reaction of 1-MeC with a mono-functional platinum complex, $[(NH)_3Pt(H_2O)]^{2+}$, and subsequent addition of perchlorate to the solution. The complex containing $[(NH)_3Pt(1\text{-}MeC\text{-}N3)]^{2+}$ crystallizes in the monoclinic C2/c space group. A half equivalent of potassium perchlorate co-crystallizes with it, completing the unit cell. Data collection for $[(NH)_3Pt(1\text{-}MeC\text{-}N3)](ClO_4)_2 \cdot ½\ KClO_4$ (**12**) was at room temperature. Crystal data, data collection and refinement parameters for **12** are summarized in Table A-12 (see Appendix).

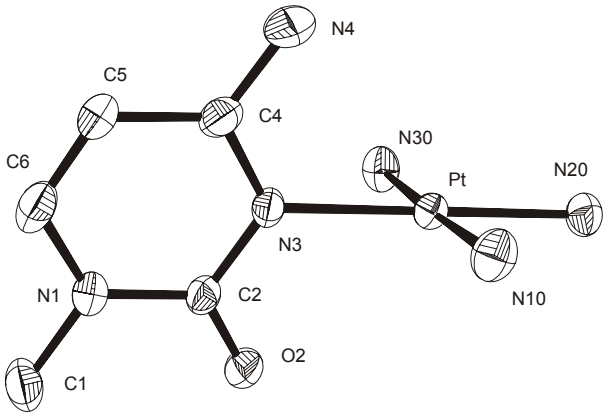

Figure 2.17: *View of the cation $[(NH)_3Pt(1\text{-}MeC\text{-}N3)]^{2+}$ (**12**) (50% probably thermal ellipsoids).*

A view of the $[(NH)_3Pt(1\text{-}MeC\text{-}N3)]^{2+}$ cation is depicted in Figure 2.17. Bond lengths and angles of the structure are listed in Table 2.2. In the square-planar coordination of the central platinum atom, the N3 atom of 1-MeC and the three nitrogen atoms of the ammine ligands are located in the Pt coordination plane with minimal deviations, as evidenced by the values of the N-Pt-N angles: the angles between Pt and two *cis* positioned nitrogen atoms range from 89.3(2)º to 90.9(2)º, and between Pt and the two trans positioned N atoms angles are 179.63(19)º and 177.6(2)º. The platinum ion is coplanar with the four donors that deviate by ± 0.026(3) Å from the mean plane. Pt-N distances are also very similar, ranging from 2.042(5) to 2.056(5) Å.

Table 2.2: *Distances (Å) and angles (º) for* ***12****.*

Pt-N3	2.043(5)	N3-Pt-N10	90.9(2)
Pt-N10	2.056(5)	N10-Pt-N20	89.3(2)
Pt-N20	2.042(5)	N20-Pt-N30	90.1(2)
Pt-N30	2.048(5)	N30-Pt-N3	89.7(2)
C2-Pt-N3	117.5(4)	N3-Pt-N20	179.63(19)
Pt-N3-C4	121.6(4)	N10-Pt-N30	177.6(2)
PtN_4 / 1-MeC	75.6(2)		

The two external C-N-Pt angles are slightly different. The angle on the side of the amino group (Pt-N3-C4, 121.6(4)º) is larger than the one on the side of the carbonyl group (C2-Pt-N3, 117.5(4)º). Similar situations have been observed in many other 1-MeC compounds of Pt [92]. The atoms in the cytosine ring are almost coplanar within ± 0.018(4) Å. The metal coordination plane and the cytosine ring form a dihedral angle of 75.6(2)º. This inclination of the cytosine ring favors a weak internal hydrogen bond contact between O2 atom of the carbonyl group and protons of an ammine ligand (distance O2···N30 is 3.391(7) Å). Other intermolecular hydrogen bond contacts are: O2···N30 (x, y+1, z), 3.358(7) Å; O2···N30 (-x+3/2, y+1/2, -z+3/2), 2.955(6)Å; O2···N20 (-x+3/2, y+1/2, -z+3/2), 3.249(7) Å; N4···O14 (perchlorate), 2.989 (8); N4···O12 (-x+2, -y+1, -z+2) 2.918(8) Å.

Packing of **12** does not allow strong interactions between cations, as evidenced by the previously mentioned H-bond contacts. The main motif of the structure are the potassium atoms in a linear arrangement with the perchlorate counter ions acting as bridges (see Figure 2.18). The potassium cation has six perchlorate anions in its sphere of coordination; four of the chlorine atoms are coplanar with K^+ and two additional apical perchlorates complete the potassium interactions (see Figure 2.19). The cationic entities $[(NH)_3Pt(1\text{-}MeC\text{-}N3)]^{2+}$ are located in the empty holes between the lines drawn by the potassium atoms (see Figure 2.20). No π-stacking interactions are observed between the cytosine rings.

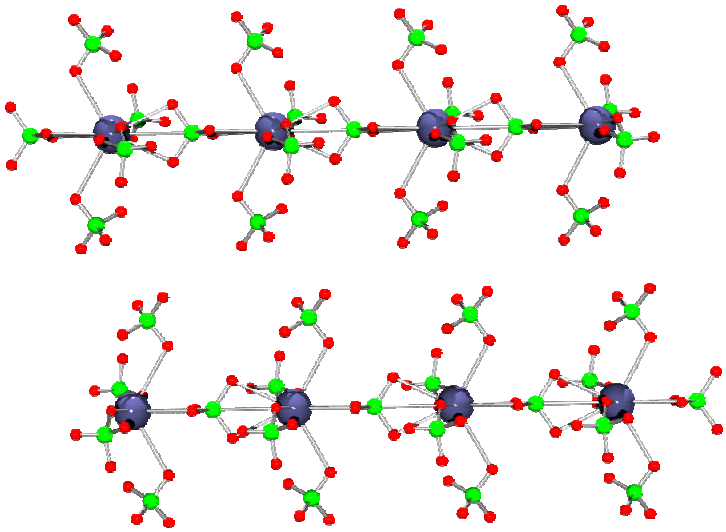

Figure 2.18: *View of the linear arrangement of the potassium cations and the perchlorate anions acting as bridges.*

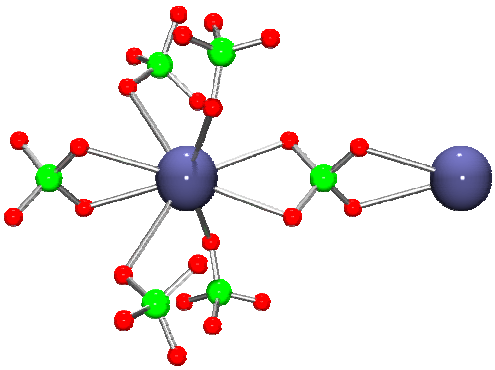

Figure 2.19: *Coordination sphere of the potassium atoms, filled by six shared perchlorate anions.*

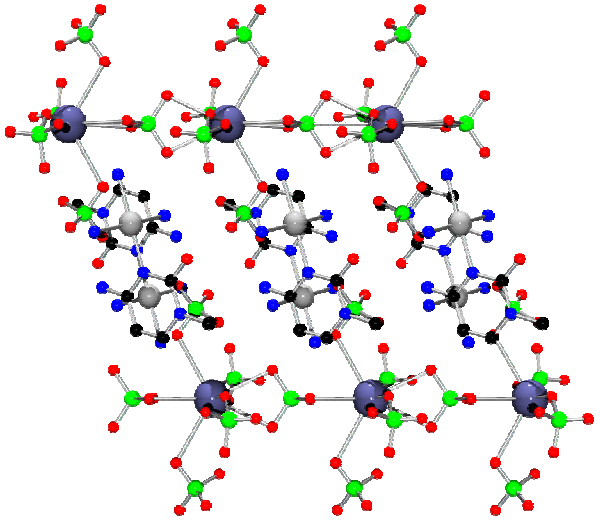

Figure 2.20: *View of the location of the $[(NH)_3Pt(1\text{-}MeC\text{-}N3)]^{2+}$ cations between the potassium–perchlorate lines in* ***12****.*

2.2.1.2.- NMR spectroscopy and pH dependence.

^{1}H NMR spectra of **12** were recorded. In aqueous solution, the spectrum displays two sets of doublets in a 1:1 ratio in the aromatic region (H6 and H5 protons of 1-MeC) as well as a singlet corresponding to the methyl group of 1-MeC. In addition, when a spectrum was recorded immediately after dissolution of crystals of **12** in D_2O, a broad signal associated with the amino groups was observed. Chemical shifts of the signals are at 7.62 ppm (H6), 6.04 ppm (H5) and 3.43 ppm (CH_3) over a wide pH range. Due to the coordination of the platinum atom to the N3 site of 1-MeC, the ^{195}Pt satellites of 14.9 Hz of the H5 doublet are observed as in the case of the homologous dien complex. A ^{195}Pt NMR spectrum was recorded displaying a single signal at –2601 ppm; this is consistent with the argument that the signal doubling seen in the spectrum of $[(dien)Pt(1\text{-}MeC\text{-}N3)]^{2+}$ is due to two conformers. Figure 2.21 shows a detailed view of the downfield section of the spectrum in which, the ^{195}Pt satellites are clearly observed.

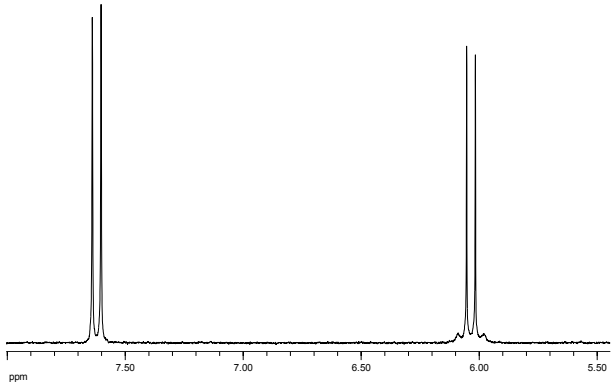

Figure 2.21: *Downfield section of the ^{1}H NMR spectrum of $[(NH_3)_3Pt(1\text{-}MeC\text{-}N3)]^{2+}$ in D_2O in which it is possible to recognize ^{195}Pt satellites for H5.*

As expected after the study of the deamination of **9**, the deprotonation of the exocyclic amino group of $[(NH_3)_3Pt(1\text{-}MeC\text{-}\textit{N3})]^{2+}$ is observed and produces upfield shifts of the proton signals at strongly basic pH values. The pK_a of **12** (N4) was determined to be 13.47(6) in D_2O, corresponding to 12.83(6) in water. A graphical representation of the pH dependence is depicted in Figure 2.22.

Due to the N4 deprotonation of the cation, the signals of the protons are shifted upfield at basic pH values. As in the case of **9**, the effect is more pronounced for H6 ($\Delta\delta$ = 0.39 ppm) than for H5 ($\Delta\delta$ = 0.23 ppm) or CH_3 ($\Delta\delta$ = 0.12 ppm). During the pD dependence measurement no spontaneous deamination was observed. The determined pK_a value (12.83(6)) of **12** is similar to the pK_a value of **9** (~13). Due to the limitations of the AgCl glass electrode used in the pH measurements, it was not possible to get reliable values at around pH 14. Thus, the resulting pH dependence curve was fitted with calculated values (see Figure 2.23).

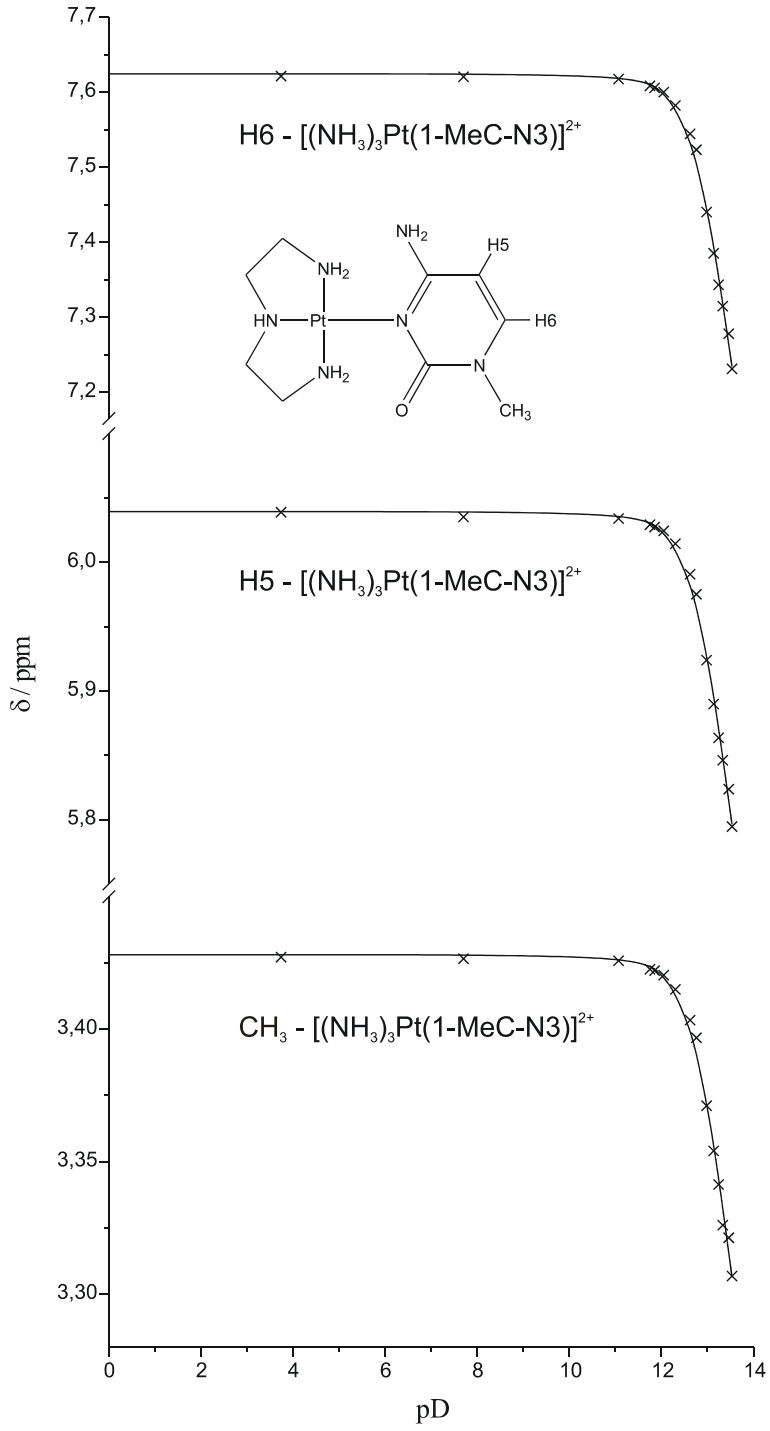

Figure 2.22: *^{1}H NMR pD-dependence (δ, ppm) of H6, H5 and CH_3 resonances in D_2O of the compound $[(NH_3)_3Pt(1\text{-}MeC\text{-}N3)]^{2+}$ (**12**).*

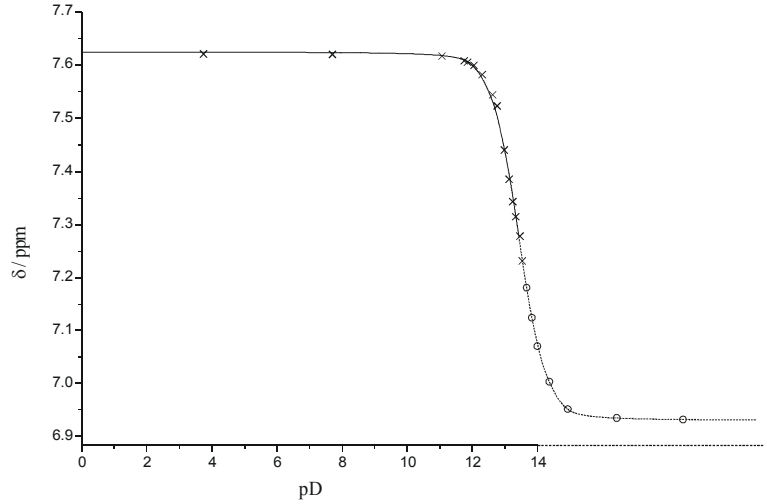

Figure 2.23: *pH dependence curve of H(6).*

Experimental values (x); calculated values (o) based on fitting of pD dependence below.

2.2.1.3.- Conditions and NMR study.

12 was dissolved in D_2O, the pH was adjusted to 12.7 by addition of NaOD, and the reaction was followed at ambient temperature (23º C) with time. A stack plot of the resulting ^1H NMR spectra recorded at different reaction times is depicted in Figure 2.24.

The first spectrum at the bottom corresponds to the first step of the reaction, hence after addition of NaOD (pD 12.7). Due to the deprotonation of the exocyclic N4 amino group, the signals of **12** are strongly shifted upfield. The reaction is complete within 10 days; aspects of the reaction kinetics are analyzed in the next part of this chapter.

The deamination product $[(NH_3)_3Pt(1\text{-MeU-}N3)]^+$ (**13**) displays also two sets of doublets, assigned to the H6 (δ = 7.44 ppm) and H5 (δ = 5.70 ppm) protons, and a singlet (δ = 3.35 ppm) assigned to the methyl group of the 1-methyluracil base.

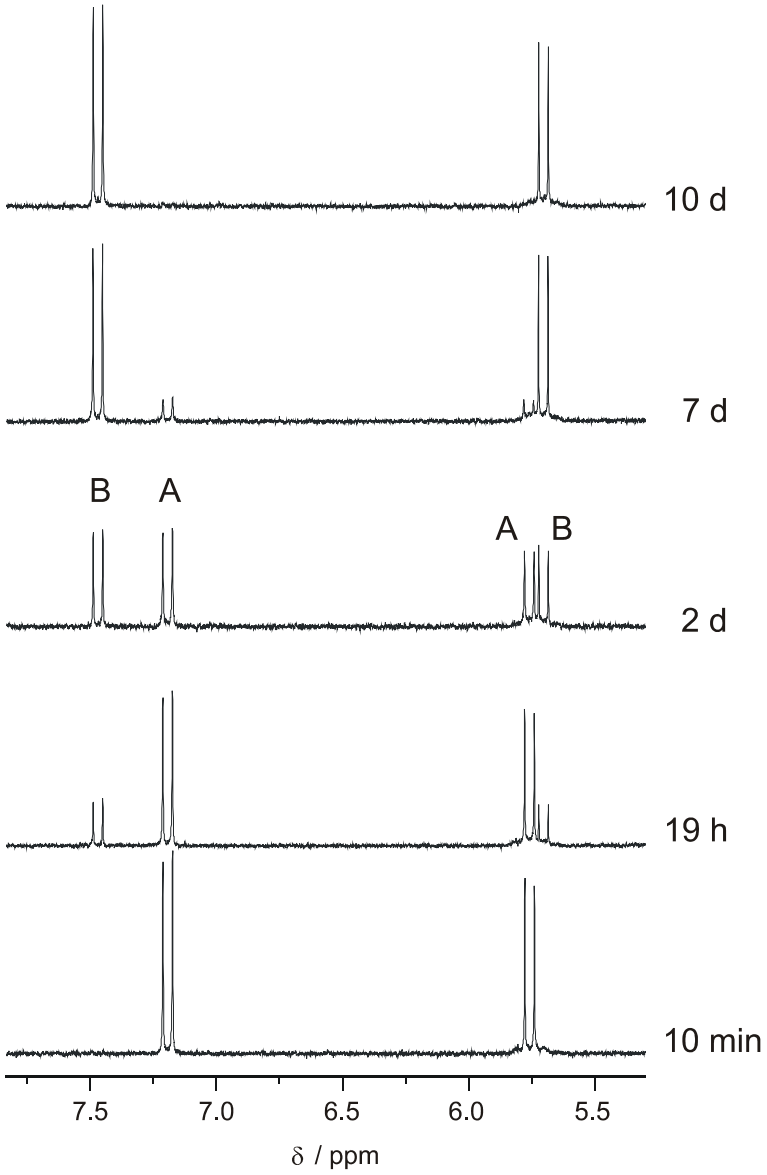

Figure 2.24: *Lowfield sections of ^{1}H NMR spectra of $[(NH_3)_3Pt(1\text{-}MeC\text{-}N3)]^{2+}$ (D_2O, pD 12.7, room temperature) at different reaction times (from bottom to top): 10 min, 19 h, 2 d, 7 d, 10 d. A = **12**, B = **13**.*

2.2.2.- Reaction Mechanism.

The mechanism proposed for the deamination reaction is the same as reported in the section 2.1.3 of this chapter for $[(dien)Pt(1\text{-}MeC\text{-}N3)]^{2+}$, in which the first step consists of a nucleophilic attack by OH^- from the solution (pH >

12.7) at the C4 site of cytosine and the subsequent addition of the hydroxo group. The second step, in which the elimination of the exocyclic N4 amino group takes place, completes the deamination process. This last step requires the formation of a C=O double bond and the simultaneous transfer of a proton from the hydroxyl to the amino group. In this case, the corresponding deamination product is $[(NH_3)_3Pt(1\text{-MeU-}N3)]^+$ (**13**).

2.2.3.- Kinetics.

The reaction was carried out under similar strongly alkaline conditions (pH > 12.7) as the deamination of $[(dien)Pt(1\text{-MeC-}N3)]^{2+}$; thus the expected rate profile should be similar. In this case the approximation to pseudo-first order reaction is also valid (see part 2.1.4 of this chapter) due to the high concentration of hydroxide in the solution. The reaction carried out is: $[(NH_3)_3Pt(1\text{-MeC-}N3)]^{2+} + OH^- \rightarrow [(NH_3)_3Pt(1\text{-MeU-}N3)]^+ + NH_3$. The rate formula for the pseudo first order reaction is: v = -k [A]. The standard integrated rate expressions are: $[A] = [A]_0\ e^{-kt}$ for the formation of the deamination product, and $[A] = [A]_0\ (1- e^{-kt})$ for the disappearance of the starting compound. The rate of the reaction was followed by ^1H NMR spectroscopy at 23ºC and pD 12.7. A graphical profile of the course of the reaction at different reaction times is depicted in Figure 2.25.

The percentage of complexes present in the solution at different reaction times was determined by integration of the proton intensities of its ^1H NMR spectra and then used to fit the first order rate equations. From the experimental data, the formation of the deamination product was found to have a half-life ($t_{½}$) of 2.06 d and a rate constant (k) of 0.337 d^{-1}. These values are also applicable to the disappearance of the starting compound. According to the suggested rate profile, the following expressions are valid:

$[\mathbf{13}] = [\mathbf{12}]_0\ (e^{-0.34t})$

$[\mathbf{12}] = [\mathbf{12}]_0\ (1 - e^{-0.34t})$

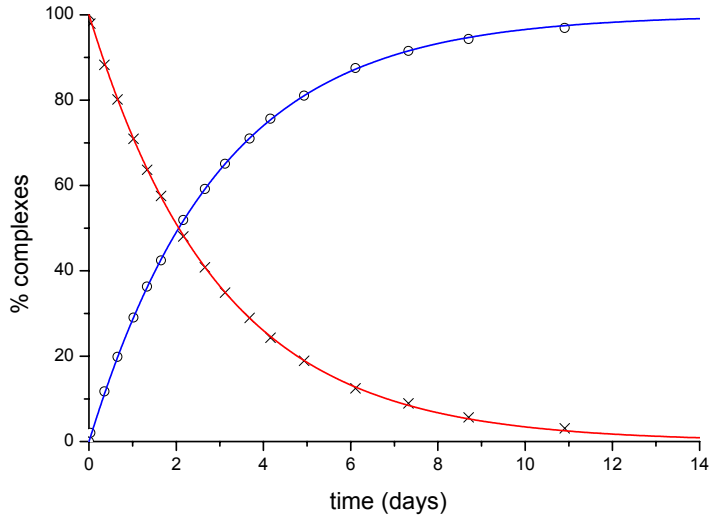

Figure 2.25: *Graphical representation of the course of the deamination at different reaction times (x= $[(NH_3)_3Pt(1\text{-}MeC\text{-}N3)]^{2+}$; o = $[(NH_3)_3Pt(1\text{-}MeU\text{-}N3)]^{+}$).*

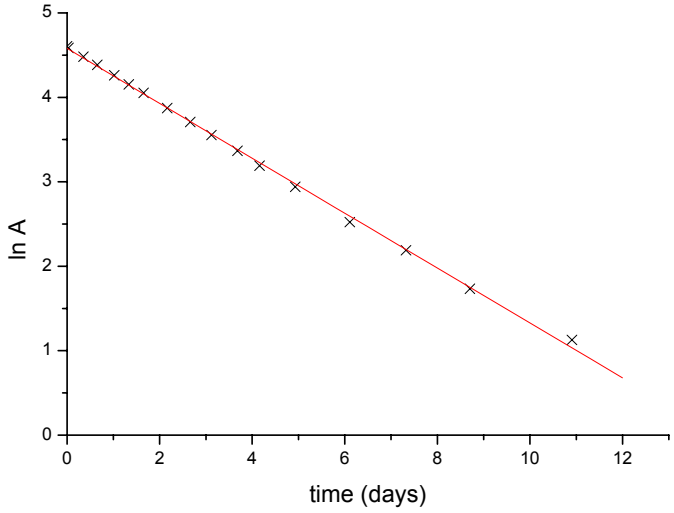

Figure 2.26: *Graphical representation of ln$[[(NH_3)_3Pt(1\text{-}MeC\text{-}N3)]^{2+}]$ vs. time.*

Integration of the rate formula of a first order reaction (d[**12**] / dt = -k' [**12**]) results in a linear dependence (ln[**12**] = -kt + ln[**12**]$_0$). As shown in Figure 2.26, the graphical representation of the logarithm of the concentration of the starting compound vs. time gives as a result a straight line; it is consistent with a pseudo first order reaction.

Higher temperatures during the reaction increase the rate (and the kinetic constant) of the reaction. Signals corresponding to other products are not observed.

2.2.4.- Remarks.

The similar rate constants observed for [(dien)Pt(1-MeC-*N3*)]$^{2+}$ and [$(NH)_3$Pt(1-MeC-*N3*)]$^{2+}$ is evidence that the migration process occurring in parallel with the deamination in [(dien)Pt(1-MeC-*N3*)]$^{2+}$ does not influence the deamination, and vice versa. As it was supposed in section 2.1.4 of this chapter, the reactions are exclusively competitive. Both **9** and **12** present similar acidification of the N4 exocyclic amino group due to the presence of a metal coordinated at the N3 site of 1-MeC. The experimental kinetic and pK_a values for complexes involved in deamination and migration reactions are listed in Table 2.3.

Table 2.3: *Experimental kinetic and pK_a values for complexes involved in deamination and migration reactions.*

	pK_a	k (d^{-1})	$t_{½}$ (d)
[(dien)Pt(1-MeC-*N3*)]$^{2+}$	~13	- -	1.40
[(dien)Pt(1-MeUH-*N3*)]$^{2+}$	0.1	0.49	1.43
syn-[(dien)Pt(1-MeC-*N4*)]$^{2+}$	7.5	0.69	1.00
anti-[(dien)Pt(1-MeC-*N4*)]$^{2+}$	7.7	0.69	1.00
[$(NH)_3$Pt(1-MeC-*N3*)]$^{2+}$	12.8	0.34	2.06

2.3.- Migration in 1-MeC excluding Deamination.

One of the objectives defined in this work was to find the deamination and migration reactions separately in complexes containing 1-MeC. The deamination reaction was reported earlier in this chapter. A reaction involving only migration

of the metal atom was found with a palladium ion as metal in the analogous dine complex, [(dien)Pd(1-MeC-*N3*)]$^{2+}$. After a detailed study of the reaction conditions and products, it was found to be consistent with the reported study of Ménard et al. [109], in which the N3→N4 migration of the palladium entity takes place simultaneously with a parallel dissociation reaction, attributed to the thermodynamic stability of the [(dien)Pd(OH)]$^{+}$ species. In order to complete the study of Ménard et al., some additional information is reported in this chapter. It refers to a minor detail of this study following the induced migration and dissociation at high pH of the starting compound. According to these authors formation of the [(dien)Pd(C-*N4*)]$^{+}$ (with C = cytidine) species is observed at pD 13.4; with signals of the aromatic protons of this product assingned at 7.18 ppm (H6) and 5.80 ppm (H5). Additional unknown signals at 7.50 and 6.55 ppm are reported. In all the cases, the standard (δ = 0) of the solution was DSS (TSP = DSS – 0.294). By comparison with our results, the first signals are consistent with the assigned migration product, but more accurately can be assigned to the anti conformer, *anti*–[(dien)Pd(C^{-}-*N4*)]$^{+}$. The unassigned signals in the article are to be assigned to the *syn*–[(dien)Pd(C^{-}-*N4*)]$^{+}$ conformer. Moreover, the solid state structure of [(dien)Pd(1-MeC-*N3*)](ClO$_4$)$_2$, is reported here. It behaves analogously to the cytidine complex of Ménard et al.. [(dien)Pd(1-MeC-*N3*)](ClO$_4$)$_2$ (**14**) was the complex of our study; it was not possible to measure a pH dependence due to the instability of the complex at extreme pH values. The solid state structure of **14** was determined by X-ray crystallography and is described below.

2.3.1.- Crystal Structure of [(dien)Pd(1-MeC-*N3*)](ClO$_4$)$_2$ (14).

Crystals of [(dien)Pd(1-MeC-*N3*)](ClO$_4$)$_2$ (**14**) were isolated from the solution and characterized by X-ray crystallography. The complex [(dien)Pd(1-MeC-*N3*)](ClO$_4$)$_2$ crystallizes in the orthorhombic crystal system. Crystal data, data collection and refinement parameters for **14** are summarized in Table A-14 (see Appendix). The solid state structure of **14** is similar to the platinum

analogous complex **9**; both complexes crystallize in the same space group (Pbca), and have similar cell constants (a = 15.186(3), b = 12.235(2), c = 19.697(4) for **14** vs. a = 15.088(3), b = 12.195(2), c =19.506(4) for **9**). The only difference are the metallic atom and the distances between atoms in the unit cell.

The solid state structures of **14** and **9** can be considered identical (for comparison, see part 3.1.1.1 of this chapter). Significant angles and distances of **14** are listed in Table 2.4. In this case, the Pd1, N3, N14 atoms are situated below (-0.028(1), -0.032(2) and -0.043(2) Å, respectively) and the N11 and N17 atoms above (0.051(2) and 0.052(2) Å, respectively) the palladium coordination plane, with a r.m.s. deviation of 0.042. A view of the cation [(dien)Pd(1-MeC-*N3*)]$^{2+}$ with a labeling scheme is shown in Figure 2.27.

Table 2.4: *Distances (Å) and angles (º) involving the Pd atom in **14**.*

Pd1–N3	2.039(3)	N3-Pd1-N11	95.55(12)
Pd1–N11	2.051(3)	N11-Pd1-N14	84.44(13)
Pd1–N14	2.011(3)	N14-Pd1-N17	84.17(12)
Pd1–N17	2.045(3)	N17-Pd1-N3	95.88(12)
		N3-Pd1-N14	179.42(14)
		N11-Pd1-N17	167.75(13)

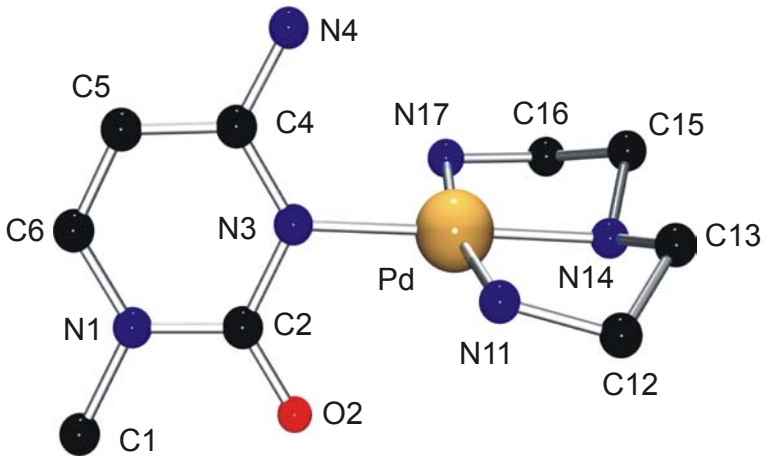

Figure 2.27: *View of the cation [(dien)Pd(1-MeC-N3)]$^{2+}$ **(14)** with atom labeling scheme.*

Interactions in the coordination sphere of palladium are: Pd–O3a(x, -y+3/2, z+1/2), 3.365(3) Å and Pd–O3a(-x+1/2, -y+1, z+1/2), 3.496(3) Å. These distances are shorter that those of analogous **14** containing a platinum atom: 3.422(7) and 3.466(7) Å, respectively. The palladium atom is likewise adopts a distorted octahedral environment; in which the oxygen atoms occupy the apical positions, forming angles of 85.9(1)º with the palladium and the N11 site. This situation is shown in the Figure 2.28.

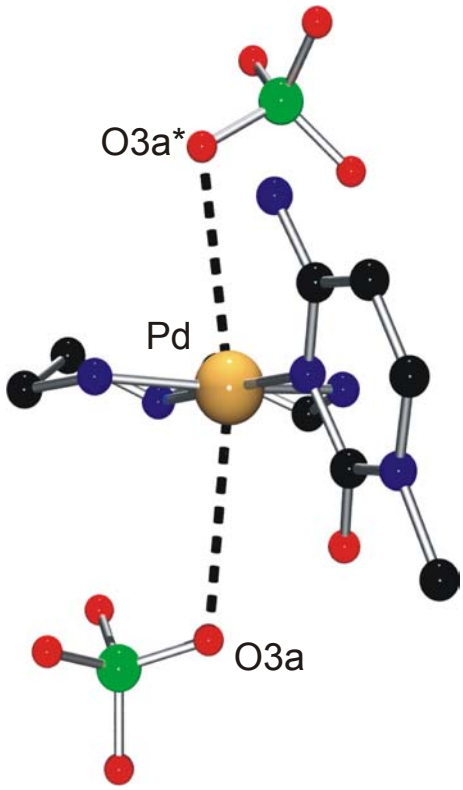

Figure 2.28: *Square planar coordination of Pd in **14** with two oxygen atoms in the apical positions.*

The dihedral angle between the cytosine ring and the palladium coordination plane is 76.23(8)º. No intramolecular hydrogen bonds are observed in the cationic entity. The atoms of the dien ligand coordinated to the palladium metal are practically coplanar with the C12 and C16 atoms (r.m.s. deviation, 0.038). The other two atoms of the dien group, C13 and C15, are located out of this plane by 0.621(6) and 0.666(6) Å respectively.

The hydrogen bonds formed by the exocyclic amino group are: N4(H4a)···O3a(x, -y+3/2, z+1/2), 3.061(5) Å; N4(H4b)···O1(x, y+1, z), 3.197(5) Å. In this case, the shortest hydrogen bond with protons of the dien ligand is N14(H14a)···O2A(-x+1/2, -y+1, z+1/2), 3.127(5) Å. The intermolecular hydrogen bond found in the structure is N17(H17b)···O2(-x+1/2, y-1/2, z), 2.918(4) Å.

2.4.- Poly-metallic Complexes of 1-MeC.

The acidification of the exocyclic amino group of the metal-modified cytosine base and the metal migration observed make the formation of poly-metallic cytosine complexes more favorable. The possible loss of a proton of the amino group and subsequent attack of this site by a metal seems to be viable under strong alkaline conditions. The feasible mechanisms of coordination of a second or third metallic entity to the cytosine base are our main interest. Formation of poly-metallic cytosine complexes was observed in the course of the OH^- induced deamination and migration reactions at high temperatures. There new ^1H NMR signals emerged which were tentatively associated with a di-metallic cytosine complex. Syntheses of some poly-metallic cytosine complexes (containing two or three coordinated metals) as well as their mechanisms of formation are reported in this chapter.

2.4.1.- Di-metallic 1-MeC complexes.

2.4.1.1.- M_2(1-MeC-*N3,N4*) Complexes.

Two di-nuclear complexes of [(dien)M^{II}] (M = Pt, Pd) and 1-methylcytosine base were synthesized and studied by NMR spectroscopy. The reactions were carried out by addition of the [(dien)M^{II}] entity to the mononuclear [(dien)M^{II}(1-

MeC-*N3*)]$(ClO_4)_2$ complex in alkaline solution. In both cases the basic pH of the solution plays a relevant role and has to be meticulously controlled.

Reactions leading to the formation of dinuclear complexes may follow two possible pathways: the first one implies the direct coordination of the metal to the exocyclic N4 amino group associated with deprotonation of this group. The second pathway requires an initial migration of the [(dien)M^{II}] residue from N3 to N4 and subsequent coordination of a second [(dien)M^{II}] metalloligand at the N3 site of 1-MeC. Both pathways are shown in Scheme 2.7. Details of the reaction studies with Pt and Pd as metals are reported below.

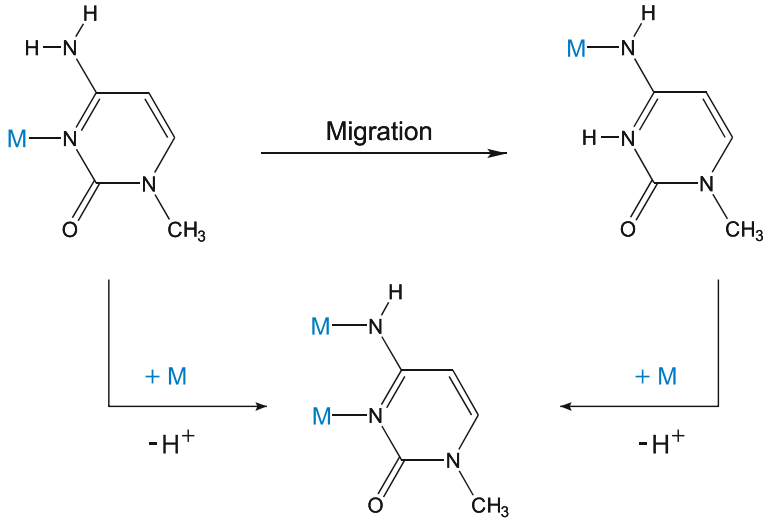

Scheme 2.7: *Two possible pathways leading to the formation of a di-metallic cytosine complex.*

2.4.1.1.1.- [(dien)Pt(*N3*-1-MeC-*N4*)Pt(dien)]$^{3+}$ (15).

In the case of M = Pt, the synthesis of the di-nuclear complex was carried out by addition of one equivalent of [(dien)Pt^{II}] to an aqueous solution containing [(dien)Pt(1-MeC-*N3*)]$^{2+}$. No reaction was observed at neutral or acidic pH. The first changes are observed at basic pH. The reaction begins when the solution is

adjusted to pH 12.7 and heated to 40º C. Under these conditions the formation of the di-nuclear complex is detected by ^{1}H NMR spectroscopy.

When the reaction starts, the pH of the solution decreases gradually due to the loss of a proton from the exocyclic amino group, which is formally substituted by a [(dien)Pt^{II}] entity. Thus, small amounts of NaOD have to be added to the solution in order to keep the reaction going. Within several hours of reaction, the pH of the solution has decreased to ca. 9 and then the reaction stops. A ^{1}H NMR spectrum of the reaction at this point is displayed in Figure 2.29.

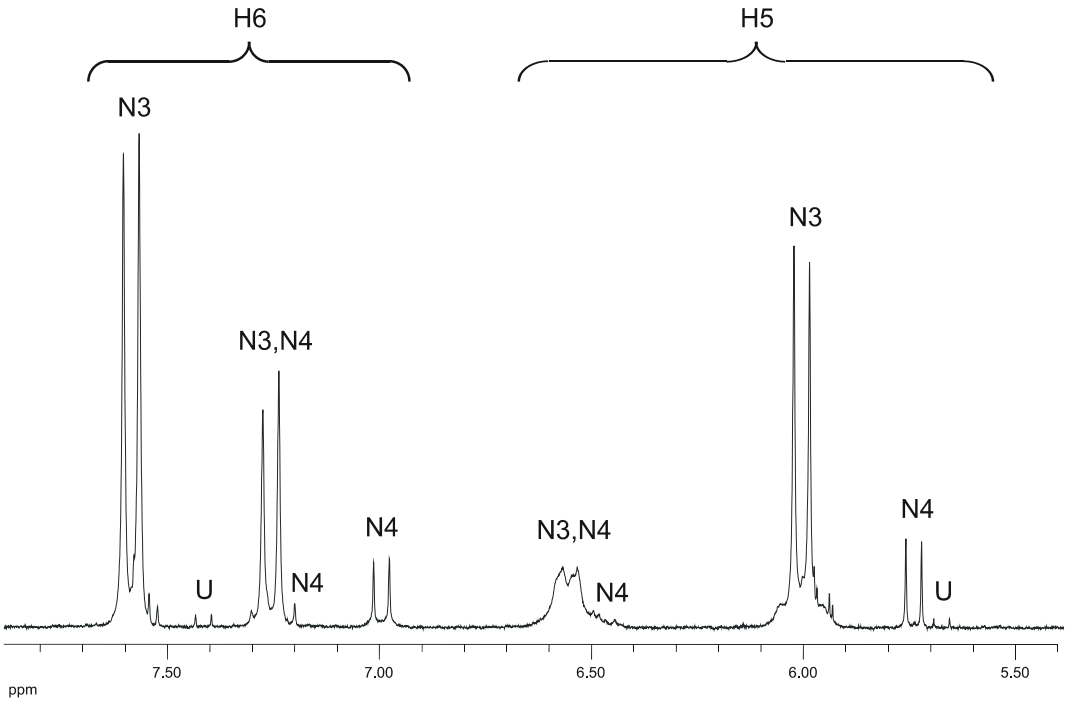

Figure 2.29: *Lowfield section of ^{1}H NMR spectrum (D_2O, pD 9) of a reaction mixture containing the di-metallic [(dien)Pt(N3-1-MeC-N4)Pt(dien)]$^{3+}$ complex (N3,N4). Signals assigned to the starting compound [(dien)Pt(1-MeC-N3)]$^{2+}$ (N3), to the migration products (N4), as well as to the deamination product (U) are also observed.*

As can be observed in Figure 2.29, the deamination reaction of the starting compound is suppressed under these conditions; only signals of low intensity assigned to the deamination product (U) are observed. In addition to the signals assigned to the starting (N3) and the di-nuclear (N3,N4) complexes

in the spectrum as well as the signals assigned to the *anti* and *syn* (N4) migration products are also observable. The latter species are present in relatively small amounts. This fact indicates that the pathway of the reaction mechanism in which migration precedes coordination of the second metal to the N3 site is at least feasible. Both *anti* and *syn* migration products can be considered intermediates of the reaction. This conclusion does not exclude the possible direct coordination of the [(dien)Pt^{II}] metalloligand to the N4 site, however. In solution, as evidenced by the H6 signals (δ = 7.26 ppm) and the high downfield shift of the H5 signals (δ = 6.55 - 6.54 ppm) of the di-nuclear complex, the mutually positioned platinum atoms are *anti* oriented. The signal associated with H5 displays two sets of doublets; this is attributed to the two possible orientations of the dien group.

An interesting point in the chemistry of this di-nuclear complex is its acid-base properties. In a pH dependence study of this complex up to pH 14, no variation of the chemical shifts assigned to the protons of 1-MeC was observed. In other words, the pK_a of the remaining proton at the exocyclic amino group is higher than 14. It was previously discussed that the effect of a Pt bonded to the endocyclic N3 site is smaller than the effect of a proton bonded to this site; this effect is observable in the acidification of N4 (pK_a ~13; ΔpK_a ~ 4). Unexpectedly, coordination of a second platinum atom to the exocyclic amino group has the contrary effect on the remaining proton (pK_a > 14).

2.4.1.1.2.- $[(NH_3)_3Pt(N3\text{-}1\text{-}MeC\text{-}N4)Pt(dien)]^{3+}$ (16).

For the di-nuclear complex **15** discussed above it was concluded that a reaction pathway in which initial metal migration is followed by a direct coordination of the second metal to the N3 site could not be excluded. In order to determine if the direct coordination of the platinum metal to the N4 exocyclic amino group is feasible, the following experiment was conducted.

As outlined in this chapter, the deamination of $[(NH_3)_3Pt(1\text{-}MeC\text{-}N3)]^+$ in alkaline solution is an exclusive process with no parallel migration occurring in tandem with it. Thus, a possible di-nuclear complex formed from $[(dien)Pt^{II}]$ and $[(NH_3)_3Pt(1\text{-}MeC\text{-}N3)]^+$ at basic pH implies direct coordination of the $[(dien)Pt^{II}]$ entity at the N4 exocyclic amino group. This experiment was carried out and followed by ^1H NMR spectroscopy. In this case, the deamination reaction was not hindered by the presence of $(dien)Pt^{II}$, and its yield was higher than expected; however signals associated with the di-nuclear complex were found in the ^1H NMR spectrum (see Figure 2.30).

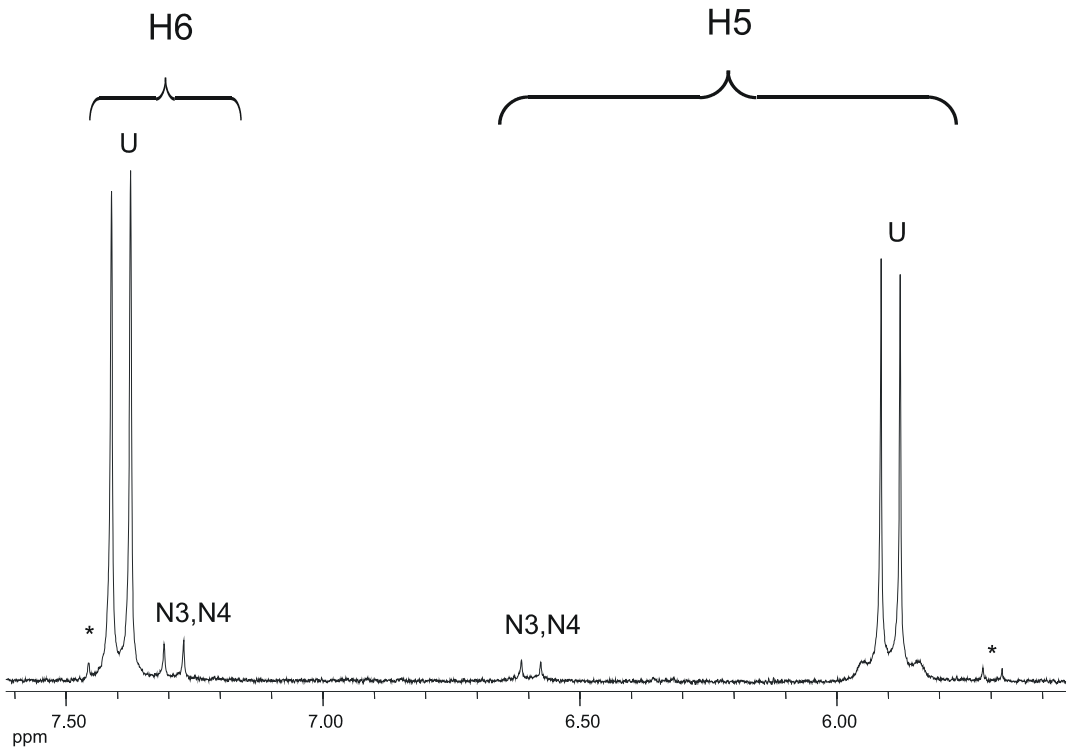

Figure 2.30: *Lowfield section of ^1H NMR spectrum of a mixture of $[(NH_3)_3Pt(1\text{-}MeC\text{-}N3)]^{2+}$ and $[(dien)Pt^{II}]$ at pD 12.7 after 1h at 60ºC. Signals assigned to the deamination product $[(NH_3)_3Pt(1\text{-}MeU\text{-}N3)]^+$ (U) dominate the spectrum. Minor resonances are due to the di-metallic complex $[(NH_3)_3Pt(N3\text{-}1\text{-}MeC\text{-}N4)Pt(dien)]^{3+}$ (N3,N4) and to free 1-MeC (*).*

This experiment proves that direct coordination of a metal at the N4 exocyclic amino group is feasible. Thus, both pathways of the proposed mechanism scheme appear to be possible. However, strictly speaking, the

pathway involving the initial migration from N3 to N4 is not proven beyond doubt. What would be necessary is a [(dien)Pt(1-MeC^{-}-*N4*)]$^{+}$ starting compound and a kinetic study of its reaction with additional M (see 2.4.1.2).

2.4.1.1.3.- [(dien)Pd(*N3*-1-MeC-*N4*)Pd(dien)]$^{3+}$ (17).

The synthesis strategy for the di-nuclear complex containing Pd is somewhat different from that of the reaction of the analogous platinum complex. The migration and dissociation reactions at strong alkaline pH (see point 2.1.2 of this chapter) were the basis of the strategy to obtain **17**. One equivalent of [(dien)Pd^{II}] was added to a solution containing [(dien)Pd(1-MeC-*N3*)]$^{2+}$ and the mixture was brought to pH 13. Under these conditions, as was previously reported, migration and dissociation reactions take place, with [(dien)Pd(1-MeC-*N4*)]$^{+}$, [(dien)Pd(OH)]$^{+}$ and free 1-MeC remaining in the solution. The rate of the reaction is very fast; it can be considered spontaneous.

The second step of the synthesis strategy is a slow acidification of the solution by addition of 1N DNO_3 until neutral pH is reached. Once again, the fast rate of the reaction allows instantaneous coordination of Pd either at the N3 site of the free 1-MeC or at the N3 site of [(dien)Pd(1-MeC-*N4*)]$^{+}$. In the latter case, the di-nuclear complex is obtained. Successive steps of acidification–basification of the solution increase the yield of [(dien)Pd(*N3*-1-MeC-*N4*)Pd(dien)]$^{3+}$, which is stable in solution at neutral pH. The reaction was followed by ^{1}H NMR spectroscopy. Unfortunately, attempts to crystallize this complex were not successful. In all cases, the di-nuclear complex decomposed; only the mono-nuclear complex, as well as some salts containing the [(dien)Pd^{II}] entity were isolated. A ^{1}H NMR spectrum of **17** is depicted in Figure 2.31, in which signals associated with the protons (H6, δ = 7.27; H5, δ = 6.48) of the di-nuclear complex (N3,N4) and of the mono-nuclear complex (N3) can be observed. The [(dien)Pd^{II}] units are, as in the case of the di-platinum complex, mutually *anti* orientated.

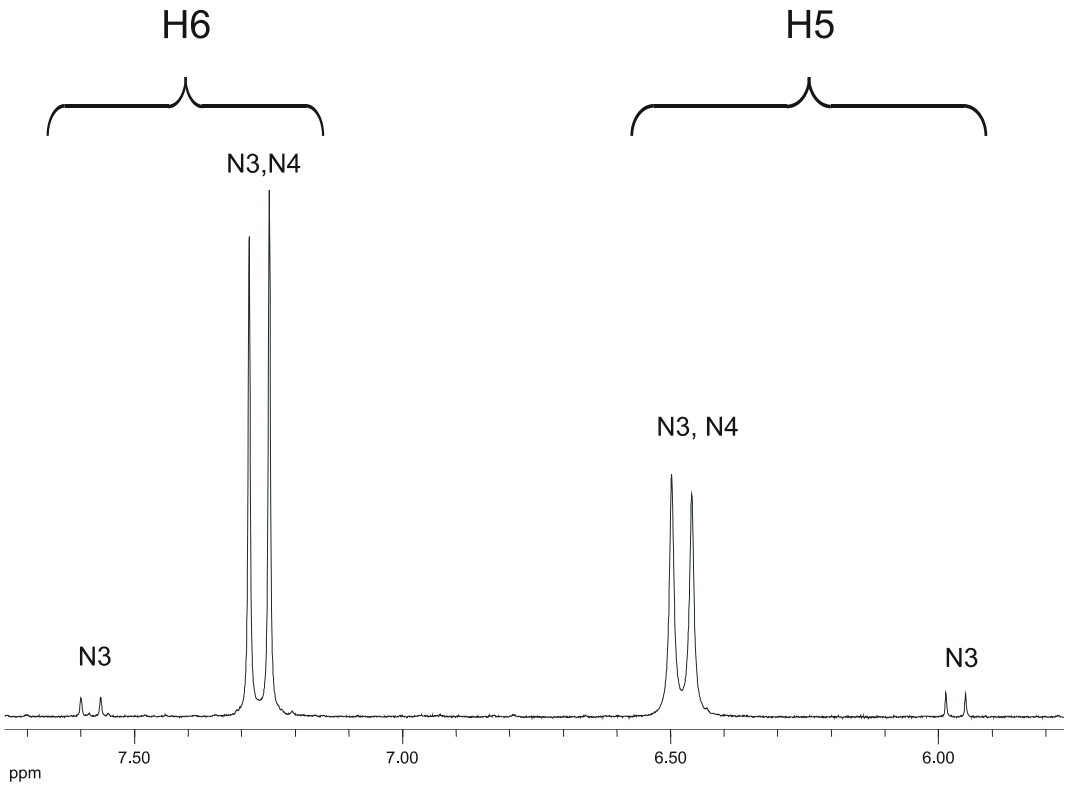

Figure 2.31: *Lowfield section of ^{1}H NMR spectrum of the di-metallic complex [(dien)Pd(N3-1-MeC-N4)Pd(dien)]$^{3+}$ (N3,N4). Signals assigned to the starting compound [(dien)Pd(1-MeC-N3)]$^{2+}$ (N1) are also observed in low intensity.*

2.4.1.2.- M,M'(1-MeC-*N3,N4*) Complexes (18).

Synthesis of hetero di-nuclear M,M'(1-MeC-*N3,N4*) complexes (M = Pt, M' = Pd) was achieved using the two different metal entities [(dien)Pt^{II}] and [(dien)Pd^{II}]. As in the previous case of homo di-nuclear complexes, two possible mechanisms pathways are feasible: The first one involves metal migration of M to the N4 site, followed by coordination of the second metal M' to the N3 site. According to the second pathway, the second metal M' directly coordinates to the N4 site. However in this case, the resulting products are not identical as before (c.f. Scheme 2.7), metals are differently positioned at the N3 and N4 sites depending on which pathway occurs (see Scheme 2.8).

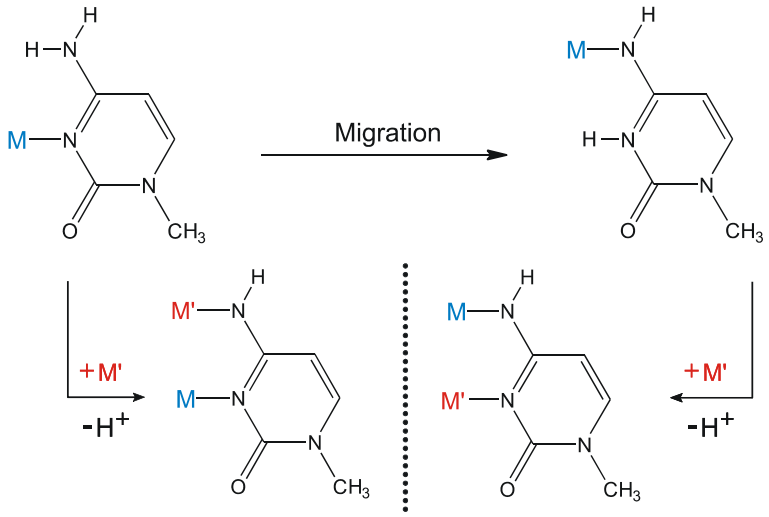

Scheme 2.8: *Possible pathways in the formation of isomeric M,M' di-metallic cytosine complexes.*

The first pathway was followed by addition of [(dien)Pd^{II}] to [(dien)Pt(1-MeC^{-}-*N4*)]$^{+}$. The latter compound had not been isolated but rather a reaction mixture from a deamination/metal migration experiment of [(dien)Pt(1-MeC-*N3*)]$^{2+}$ had been used. The reaction works well and signals associated with [(dien)Pd(*N3*-1-MeC-*N4*)Pt(dien)]$^{3+}$ (**18**) emerge immediately after addition of (dien)Pd^{II}.

As can be observed in Figure 2.32, the spectrum at the bottom contains the signals of the *syn* and *anti* conformers of [(dien)Pt(1-MeC-*N4*)]$^{+}$ (**11a** and **11b**) in addition to the deamination product **10**. The spectrum on the top was measured immediately after addition of [(dien)Pd^{II}]: Signals associated with the aromatic protons of [(dien)Pd(*N3*-1-MeC-*N4*)Pt(dien)]$^{3+}$ (**18**) appear at 7.25 (H6) and 6.49 (H5) ppm, which suggest that the Pd and Pt metals of this complex are *anti* orientated. As can be seen, the reaction leading to the mixed Pt,Pd compound is completed within minutes.

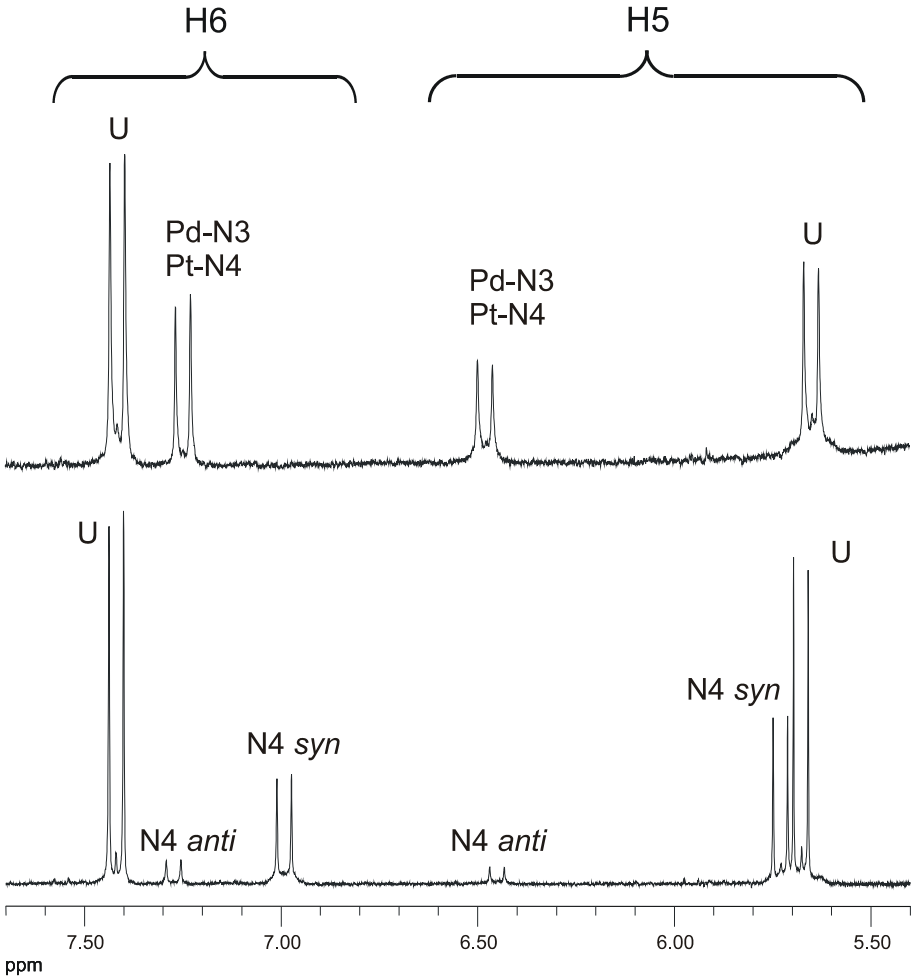

Figure 2.32: *^{1}H NMR lowfield sections of ^{1}H NMR spectra. Bottom: [(dien)Pt(1-MeU-N3)]$^{2+}$ (U) and [(dien)Pt(1-MeC-N4)]$^{2+}$ (N4 syn; N4 anti). Top: after addition of [(dien)Pd^{II} with, signals of [(dien)Pd(N3-1-MeC-N4)Pt(dien)]$^{3+}$ (Pt-N4/Pd-N3) are immediately observed.*

Unfortunately, attempts to obtain the isomeric complex [(dien)Pt(*N3*-1-MeC-*N4*)Pd(dien)]$^{3+}$ were not successful. The strategy was to initiate a N3→N4 metal migration of [(dien)Pd(1-MeC-*N3*)]$^{2+}$ in an alkaline solution containing also [(dien)Pt(H_2O)]$^{2+}$. The anticipated migration (plus dissociation) was successful. If, however, at this point the pH of the solution was kept basic or strongly basic, no reaction took place. If the pH was lowered, the Pt and Pd entities in solution can coordinate to the N3 sites of free 1-MeC and [(dien)Pd(1-MeC^{-}-*N4*)]$^{+}$ without selectivity. A differentiation of the two isomeric hetero di-nuclear M,M'(1-MeC-*N3,N4*) complexes by means of ^{1}H NMR spectroscopy seems to be very difficult due to the similar chemical shifts of both

products. In the case of the homo di-nuclear complexes, (Pt-N3,Pt-N4) and (Pd-N3,Pd-N4) a $\Delta\delta$ for the aromatic H6 and H5 of only 0.01 and 0.06 ppm, respectively, is found. It is assumed there may be even smaller differences in chemical shifts of the hetero di-nuclear (Pt-N3,Pd-N4) and (Pd-N3,Pt-N4) complexes.

2.4.2.- Tri-metallic 1-MeC complex (19).

The addition of a third [(dien)Pt^{II}] to [(dien)Pt(*N3*-1-MeC-*N4*)Pt(dien)]$^{3+}$ leads to the formation of a tri-nuclear platinum complex of 1-methylcytosine: {[(dien)Pt]$_3$(1-MeC-*N3,N4,N4*)}$^{4+}$ (**19**). This reaction requires a long time, high pH and high temperatures. The synthesis strategy was similar to those of the di-nuclear complexes; in this case one equivalent of the [(dien)Pt^{II}] species was added to a solution containing the di-nuclear complex. Formation of the Pt_3 compound may also follow two different pathways (see Scheme 2.9). The first pathway involves a N3→N4 migration of the [(dien)Pt^{II}] and subsequent coordination of the third Pt at N3. The second pathway a direct coordination of the third [(dien)Pt^{II}] at N4.

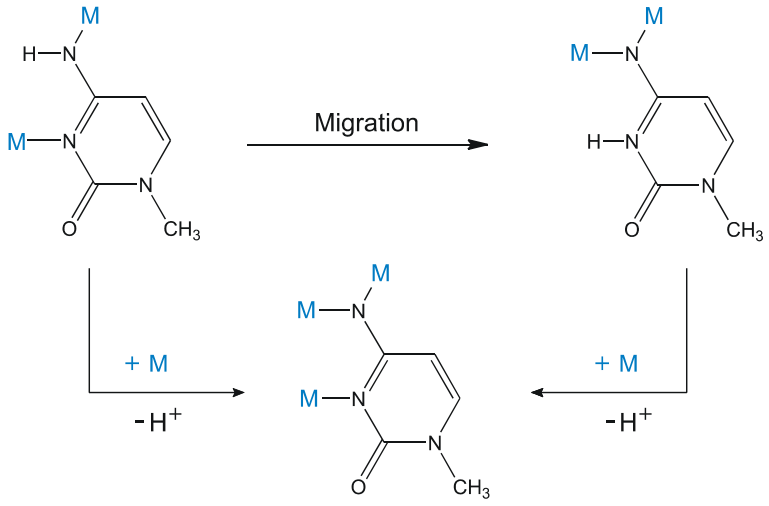

Scheme 2.9: *Possible pathways in the formation of the tri-metallic cytosine complex.*

The reaction requires continuous addition of NaOD due to proton loss of the exocyclic amino group. New signals assigned to the trinuclear complex are observed at 7.18 (H6) and 6.32 ppm (H5). The signals assigned to the H5 proton are doubled in the cases the di- and tri-nuclear complexes, possibly due to different conformations of the dien group. A meticulous study of the reaction reveals the existence of another set of signals which are of vital importance to understand the mechanism.

With the same principle as in the di-nuclear complex, ^{1}H NMR spectra were recorded until the pH had dropped to 9, then the first quantity of NaOD was added. The first ^{1}H NMR spectra were measured at 200 MHz (see Figure 2.33), in which the signals of the expected compounds (mono-, di- and three-nuclear complexes) were found. However, the signals of the anticipated $\{[(dien)Pt]_2(1\text{-}MeC\text{-}\textit{N4,N4})\}^{2+}$ were expected at chemical shifts between those of $\{[(dien)Pt]_2(1\text{-}MeC\text{-}\textit{N3,N4})\}^{2+}$ and the tri-nuclear complex. Therefore two additional ^{1}H NMR spectra were measured at 400 MHz and 600 MHz (see Figure 2.33). In these spectra, especially at 600 MHz, the signals associated with $\{[(dien)Pt]_2(1\text{-}MeC\text{-}\textit{N4,N4})\}^{2+}$ were detected at 7.22 (H6) and 7.51 ppm (H5). This situation is consistent with a pathway in which a second metal migration takes place from N3 to N4 prior to coordination of a third Pt to N3. However, this does not rule out the feasibility of the other pathway, in which direct coordination of a third [(dien)Pt^{II}] at N4 is feasible.

Due to the extreme conditions of the reaction (high temperatures, high pH values and long time), an isotopic exchange (H→D) is observed not only in the aromatic H6 and H5 protons of the uracil base but also in the aromatic H6 and H5 protons of the cytosine base.

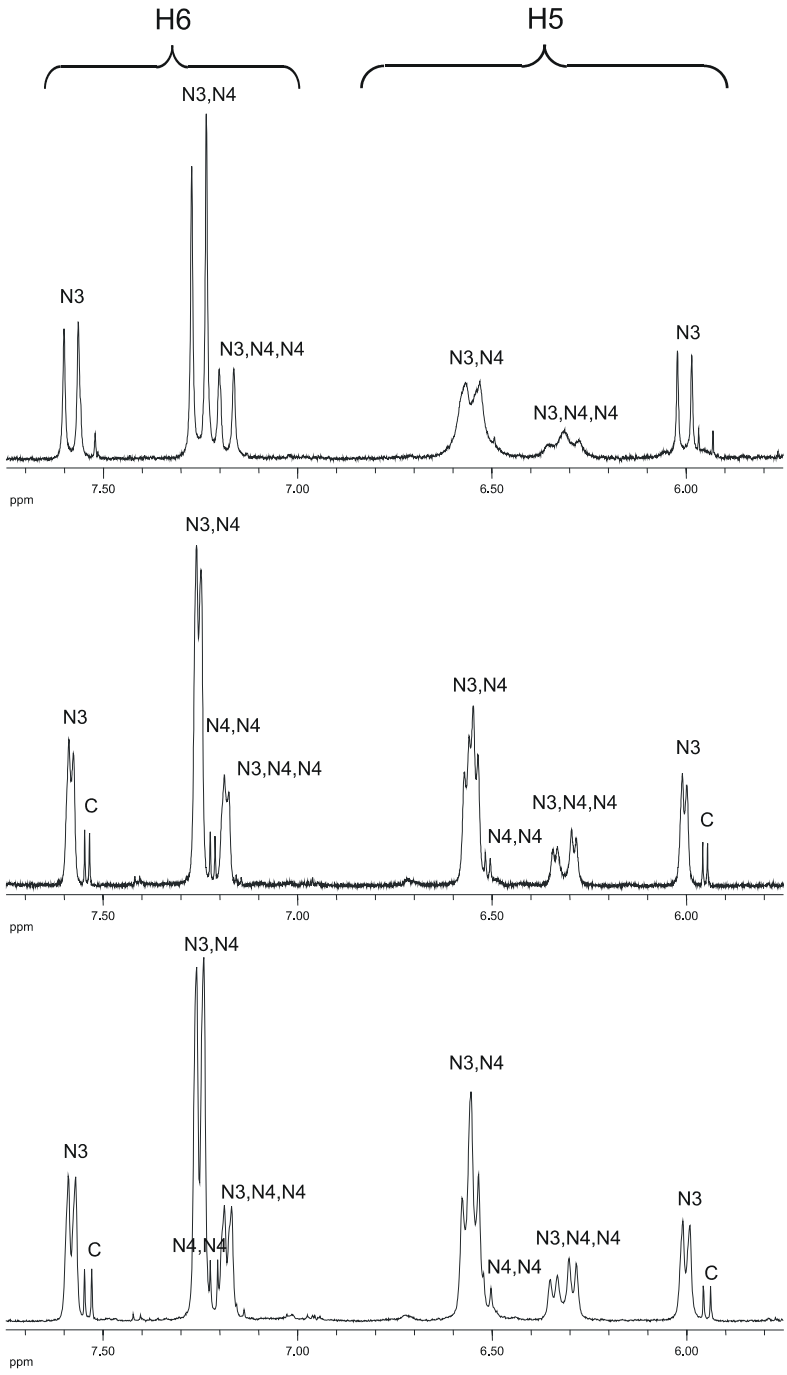

Figure 2.33: *Lowfield sections of ^{1}H NMR spectra (from top to bottom: 200, 400 and 600 MHz) in which signals assigned to 1-MeC (C), $[(dien)Pt(1\text{-}MeC\text{-}N3)]^{2+}$ (N3), $\{[(dien)Pt]_2(1\text{-}MeC\text{-}N4,N4)\}^{2+}$ (N3,N4), $[(dien)Pt(N4\text{-}1\text{-}MeC\text{-}N4)Pt(dien)]^{3+}$ (N4,N4), and $\{[(dien)Pt]_3(1\text{-}MeC\text{-}N3,N4,N4)\}^{4+}$ (N3,N4, N4) are observed.*

2.4.3.- Remarks.

Formation of di- and tri-metallic complexes of 1-MeC follows two pathways. It has been demonstrated that both direct coordination of a second metal entity to the exocyclic amino group of a N3 metalated 1-MeC, and migration of a metal atom to the N4 site, followed by coordination of the second metal entity to the N3 position, are possible. In all the studied cases, the *anti* conformation of the two metals at N3 and N4 is preferred.

If only a single metal is coordinated at the endocyclic N3 site, an acidification of the exocyclic amino group (pK_a = 13; ΔpK_a = 4) is observed. Coordination of a second metal (at the N4 site) has no measurable acidifying effect on the remaining proton (pK_a > 14).

Figure 2.34 shows a graph with the chemical shifts of the most relevant $\{[(dien)M]_x(1\text{-MeC})\}^{n+}$ complexes reported in this chapter.

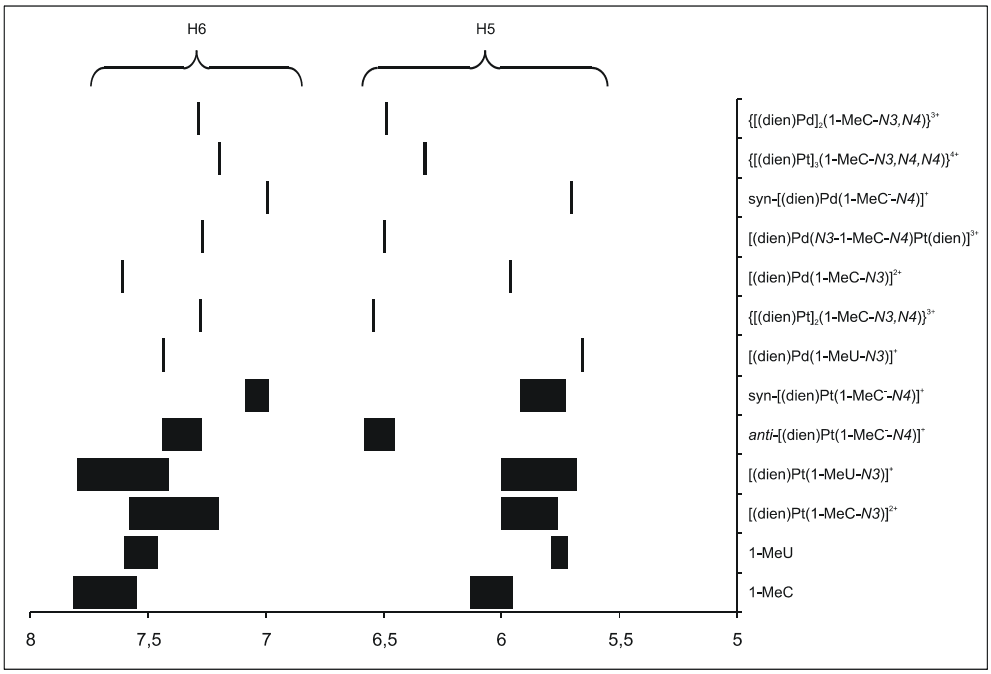

Figure 2.34: *Chemical shift of different $\{[(dien)M]_x(1\text{-MeC})\}^{n+}$ complexes. It shifts are pD dependent, ranges are given.*

2.5.- Metal Migration N3 → N4 at acidic pH.

After this detailed study of deamination and migration processes, it seems obvious that the common condition required for these reactions to take place is high pH. The question at this point is, if it is absolutely necessary to have such high pH values to force a metal migration from the endocyclic N(3) to the exocyclic N(4) site of the cytosine. With this purpose in mind, several experiments were carried out, all of them at moderately acidic pH. As will be shown, metal migration is possible even under these conditions. As a starting compound, the tris(nucleobase) complex [Pt(1-MeC-*N3*)$_3$I]I (**20**) was employed. As products of the reaction, *trans*-[Pt(1-MeC-*N3*)$_2$I$_2$] (**21**) was obtained in high yield as well as *trans*-[Pt(1-MeC-*N3*)(1-MeC-*N4*)I$_2$] · 2H$_2$O (**23**) in low yield. The latter contains both the preferred aminooxo tautomer and the rare iminooxo tautomer of 1-methylcytosine bonded to the heavy metal, via N3 and N4, respectively. A feasible method of formation of **23**, which involves a metal migration process from N3 to N4 occurring at moderately acidic pH, is proposed. It appears to be yet another mechanism of metal migration, different from previously established cases which are redox-assisted and hydroxide-promoted, respectively.

2.5.1.- [Pt(1-MeC-*N3*)$_3$I]I (20) as Starting Compound.

Treatment of [Pt(1-MeC-*N3*)$_3$Cl](NO$_3$)·1.5H$_2$O [110] with a small excess of KI at high temperature and acidic pH, led to **20** in high yield, and eventually to **21** [1]. As **21** is practically insoluble in water, it can be removed by filtration. Slow evaporation of the resulting filtrate provides dark yellow crystals of **23** in low yield. The closely related compounds *trans*-[Pt(1-MeC-*N3*)(1-MeC-*N4*)Cl$_2$] (**24**) and *trans*-[Pt(1-MeC-*N3*)$_2$Cl$_2$] (**22**) were obtained in slightly modified versions of the reaction, and both were isolated as yellow crystals. The ^{1}H NMR spectrum of a solution of **20** displays two sets of resonances in a 2:1 ratio, corresponding to

the two mutually *trans* positioned 1-MeC ligands and the 1-MeC *trans* to the iodo ligand.

2.5.1.1.- Crystal Structure of [Pt(1-MeC-*N3*)$_3$I]I (20).

Crystals of **20** of dark yellow color proved useful for X-ray crystallography. Details concerning the crystal, X-ray measurement, and the refinement of data are listed in Table A-20 (see Appendix). The cation **20** is very similar to that of [Pt(1-MeC-*N3*)$_3$Cl](NO$_3$)·1.5H$_2$O [110] as far as the relative orientation of the three nucleobases (head-tail-head) is concerned. The Pt atom is coordinated to the N3-atoms of the three 1-MeC nucleobases and to the iodo ligand in a square-planar mode.

Table 2.5: *Selected distances (Å) and angles (°) for **20**.*

	I1	1-MeC	1-MeC(a)	1-MeC(b)
Pt1	2.585(1)	2.021(10)	2.012(10)	2.074(10)
I1-Pt1–N3a	90.5(3)		N4–O2b	3.001(14)
I1-Pt1–N3	87.2(3)		N4(i)–O2b	2.966(13)
N3–Pt1–N3b	92.9(4)			
N3a–Pt1–N3b	89.6(4)			
N3–Pt1–N3a	177.2(4)			
I1-Pt1–N3b	177.3(3)			
	1-MeC		1-MeC(a)	1-MeC(b)
PtN4–1-MeC	80.5(3)		81.3(3)	83.9(3)

Symmetry code: (i) -x, -y+2, -z.

The geometrical orientations of the three 1-MeC rings in [Pt(1-MeC-*N3*)$_3$I]I allow for intramolecular hydrogen bonding between exocyclic groups. Thus, O2b forms H bonds with amino groups of the two other bases (O2b···N4, 3.01 Å; O2b···N4a, 3.13 Å) and similarly, N4b is involved in two H bonds, with O2 (2.94 Å) and O2a (3.08 Å). It strikes that the mutually *trans* positioned (1-

MeC) and $(1\text{-MeC})_b$ rings, and in particular the former, display a marked bending, with angles of close to 10° between planes through N3, C2, N4 on one hand and N1, C6, C5 on the other. The packing diagram given in Figure 2.35 strongly suggests that these distortions from nucleobase planarity are caused by the iodo ligand and the ionic iodide, respectively.

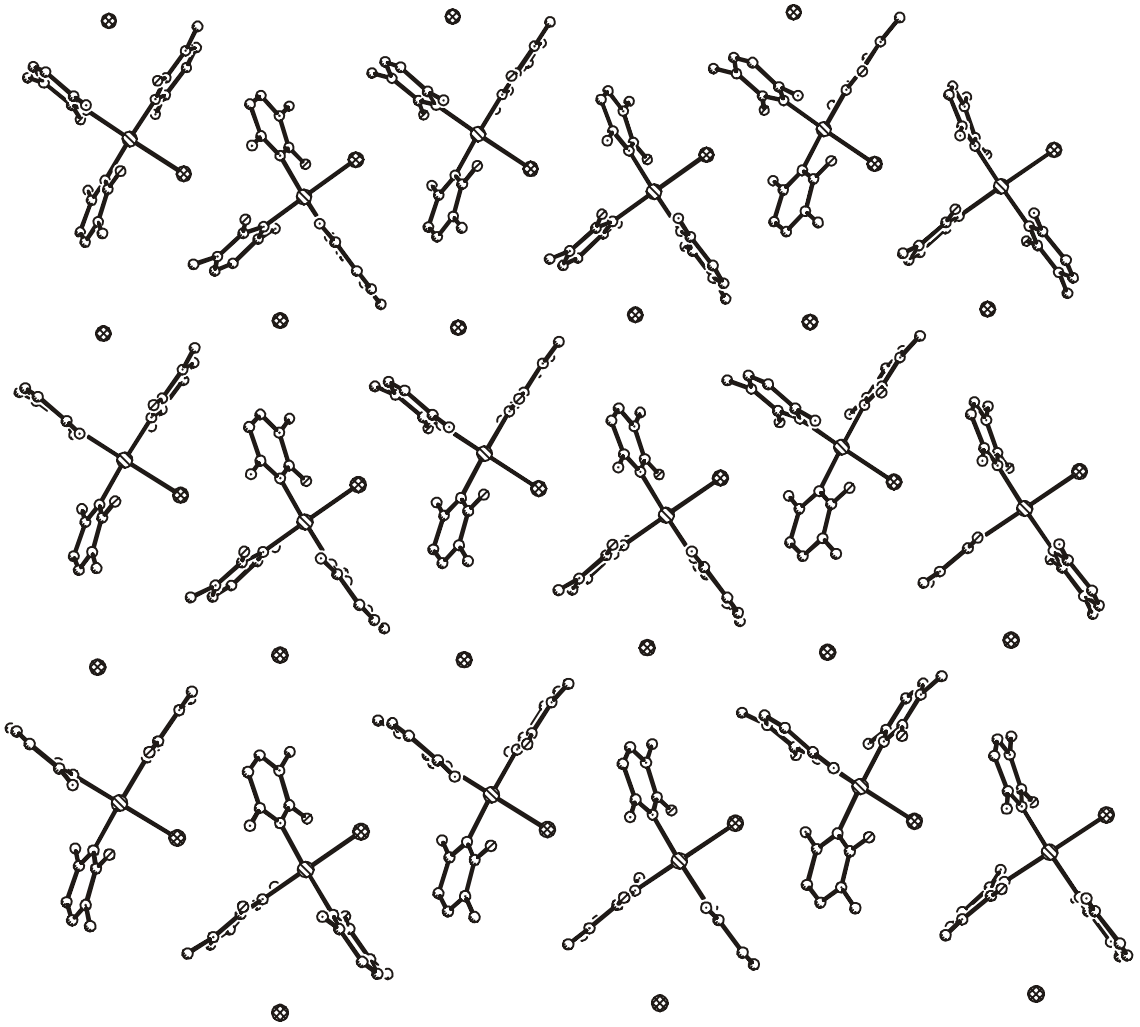

Figure 2.35: *Detail of packing of [Pt(1-MeC-N3)$_3$I]I (**20**).*

Cations of **20** are arranged in layers, separated by the iodide counter ions. These are located between the cytosine rings $(1\text{-MeC})_a$ and $(1\text{-MeC})_b$ by ca. 1.28 Å. The counterion I2 has long contacts to N4a (4.25 Å) and O2b (4.23 Å). Individual layers are connected by intercationic hydrogen bonds (2.98 Å) involving N4 and O2b sites of centrosymmetric pairs (Figure 2.36).

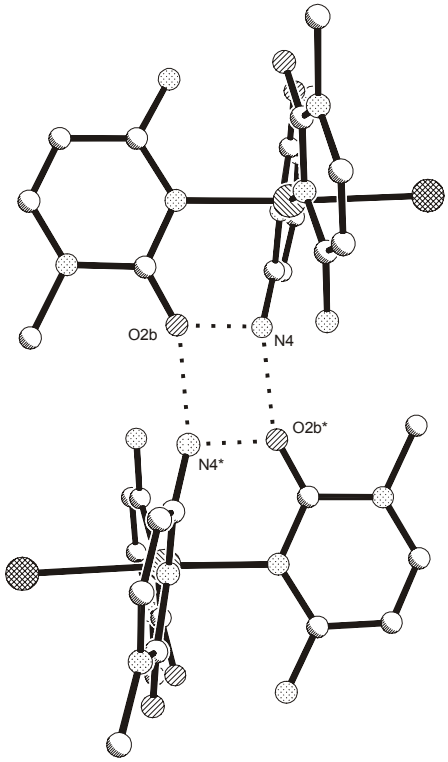

Figure 2.36: *View of the intra (3.01 Å) and intermolecular (2.98 Å) H bonding between symmetry-related pairs of* ***20****.*

2.5.2.- Reaction Conditions and Mechanismus.

The way of formation of *trans*-[Pt(1-MeC-*N3*)(1-MeC-*N4*)I_2] · $2H_2O$ (**23**) and *trans*-[Pt(1-MeC-*N3*)(1-MeC-*N4*)Cl_2] (**24**) from the [Pt(1-MeC-*N3*)$_3$Cl](NO_3) starting material in the presence of excess iodide is not fully clear as yet. At this stage, we can safely exclude the possibility that the starting compound was already contaminated with a trace amount of a species containing 1-MeC-*N4*: The ^{1}H NMR spectrum of [Pt(1-MeC-*N3*)$_3$Cl]$^+$ in D_2O, pD 6.8, does not reveal the existence of such a species. This leaves only the possibility that formation of **23** takes place under the conditions of low pH, excess iodide, and high temperature. Whether it is the consequence of ligand migration (N3 → N4) or inherent coordination of the rare tautomer following initial displacement of the N3 bonded 1-MeC, remains unclear. We tentatively favor the first possibility. Nevertheless, if ligand migration is taking place, then it has to be through a

mechanism different from those previously reported for Pt migration from N3 to N4, which are high pH [5] or H_2O_2 oxidation to Pt^{IV} and subsequent reduction to Pt^{II} [102,103,111].

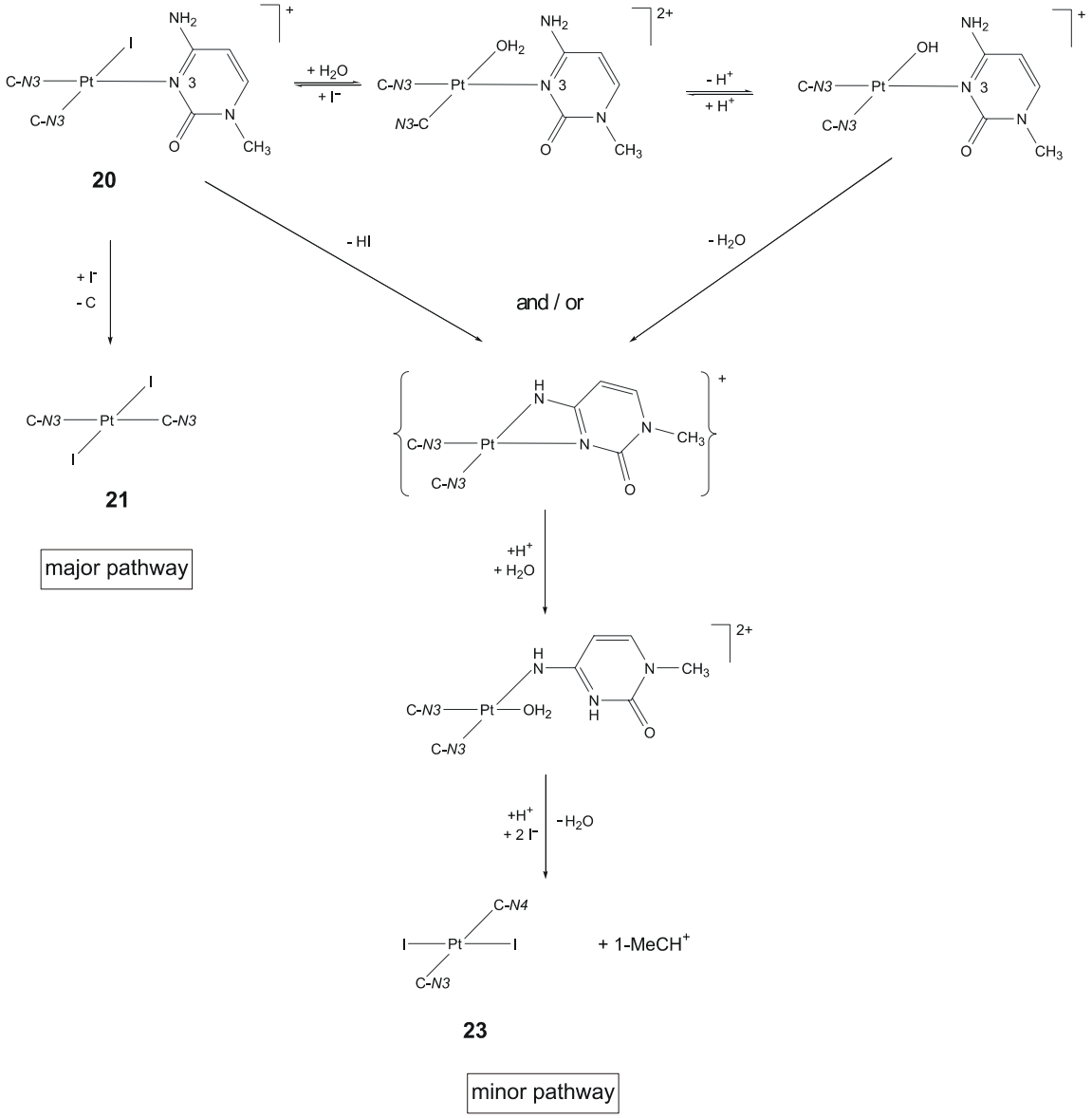

Scheme 2.10: *Different pathways for the formation of **21** and **23**.*

From experience with the solution behavior of the cation *trans*-$[Pt(1\text{-MeC-}N3)_2(H_2O)_2]^{2+}$ in D_2O and its (at least partial) conversion into dinuclear species with a likely N3,N4 bridging mode [1], one can conclude that a hydroxo ligand in a Pt^{II} complex may act as a base in abstracting a proton of the

exocyclic N(4)H_2 group and generating a nucleophile capable of attacking Pt with formation of the Pt-(1-MeC-*N4*) bond (Scheme 2.10). Possibly even the iodo ligand could act as a base. Once deprotonated, the N4(H)$^-$ group could bind to Pt. The resulting N3,N4 chelate, stable in the case of Pt^{IV} [104,112], is expected to be highly unstable with Pt^{II} due to an unfavorably small angle at the metal and to rapidly add H_3O^+ to produce [Pt(1-MeC-*N3*)$_2$(1-MeC-*N4*)(H_2O)]$^{2+}$. The available I^- could then displace the aqua ligand and, as a consequence of its high *trans* effect, displace subsequently 1-MeC-*N3*. If the iodo ligand in **20** does not undergo solvolysis, but rather expels the *trans* positioned 1-MeC, *trans*-[Pt(1-MeC-*N3*)$_2$$I_2$] (**21**) is formed. This reaction is the preferred pathway as judged from the high yield of **21**.

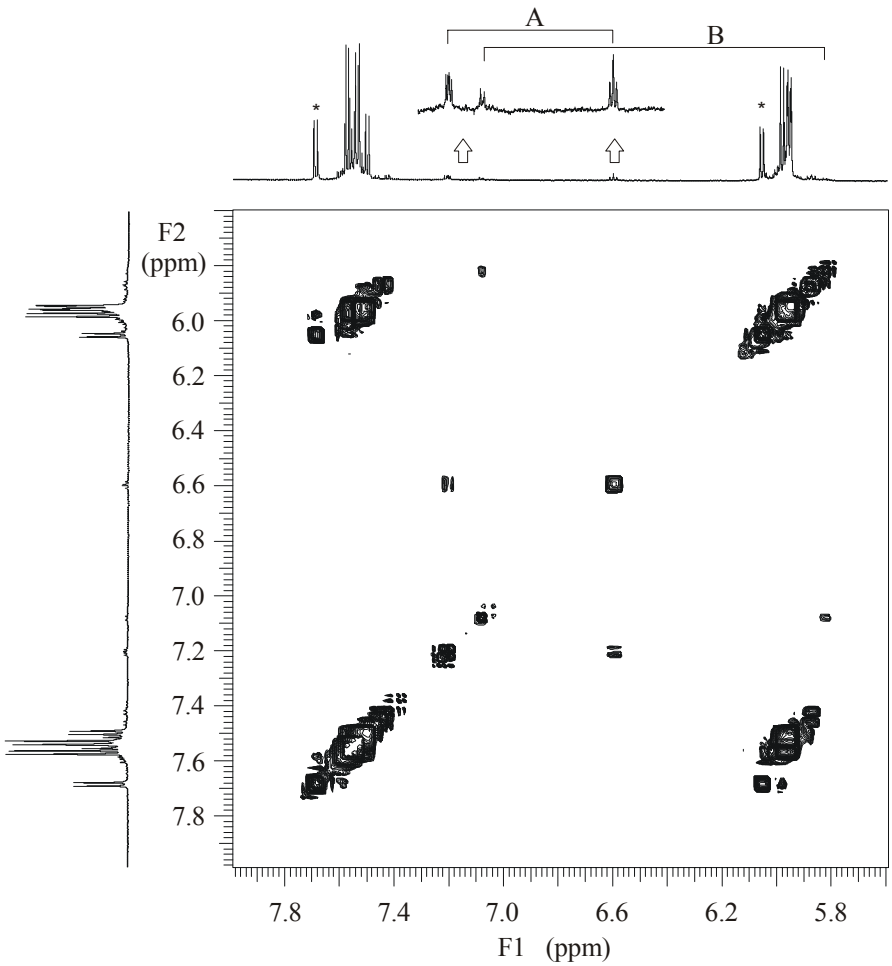

Figure 2.37: *2D $^1H,^1H$-COSY NMR spectrum (lowfield section, 600 MHz) of aged solution (5 days, 60° C) of [Pt(1-MeC-N3)$_3$I]$^+$ (D_2O, pD 4.8). Free 1-MeC/1-MeCH^+ is indicated by an asterisk.*

^{1}H NMR spectroscopy provides unambiguously proof of formation of Pt(1-MeC-*N4*) species when $[Pt(1\text{-MeC-}N3)_3Cl]^+$ is mixed with KI and the aqueous solution kept at 60ºC for a few days. Formation of several new 1-MeC doublets of low intensity is observed. The chemical shifts of some of these doublets unambiguously reveal them as being due to Pt(1-MeC-*N4*) species [102,103,111]. Their appearance is accompanied by a moderate decrease in pD, from ca. 5.6 to ca. 4.8. In addition, the original H5 and H6 doublets of the starting compound [110] become more complex, and doublets for free 1-MeC/1-$MeCH^+$ appear (see Figure 2.37). As revealed by a 2D NMR experiment, the pairs of doublets at ca. 6.6 (H5) and 7.2 ppm (H6) are coupled (A), as are the two doublets at ca. 5.8 (H5) and 7.1 ppm (H6) (B).

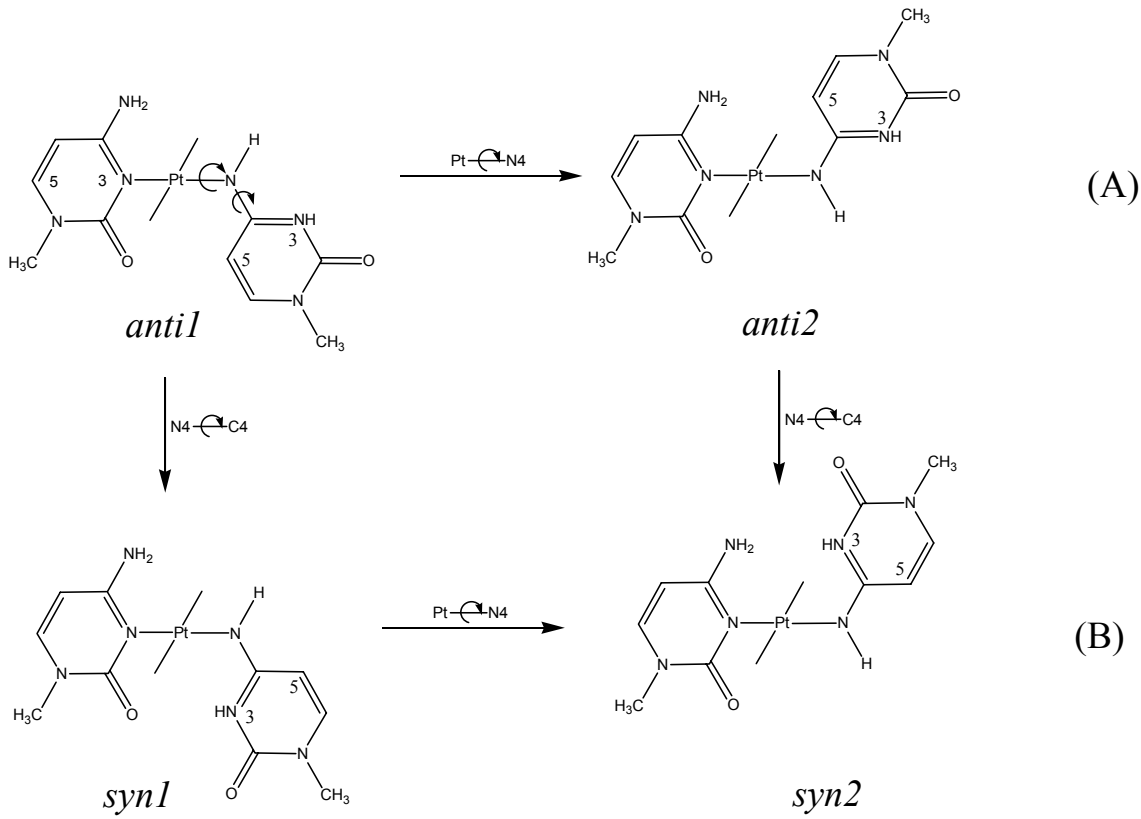

Figure 2.38: *Schematic representation of various rotamers: (a) The 1-MeC-N4 ligand is anti with respect to Pt. Two rotamers are feasible (anti1, anti2). (b) The 1-MeC-N4 ligand is syn with respect to Pt. Again two rotameres are possible (syn1, syn2).*

The strong downfield shift of the H5 doublets of (A) is highly characteristic of an *anti* orientation of the 1-MeC-*N4* ligand, in which the H5 proton is pointing

toward the heavy metal (see Figure 2.38). If slow rotation about the Pt-N4 bond is anticipated, two sets of doublets are expected. In principle, solvolysis of halide ligands could likewise lead to a doubling of resonances. The other doublets (B) are assigned to a species, in which the N4 bonded 1-MeC adopts a *syn* orientation, with H5 far removed from Pt. Species A and B also display H5 and H6 doublets of 1-MeC-*N3*, but these are not assigned. They are observed, as expected, in the region of the major doublets at around 5.9 – 6 and 7.4 – 7.6 ppm.

2.5.3.- Major Product: *trans*-[Pt(1-MeC-*N3*)$_2$I$_2$] (21).

Addition of nucleobases to a $PtCl_4^{2-}$ solution leads to the substitution of the chloro ligands by nucleobases with the following order: $[Pt(nucleobase)Cl_3]^-$, *cis*–$[Pt(nucleobase)_2Cl_2]$, $[Pt(nucleobase)_3Cl]^+$, $[Pt(nucleobase)_4]^{2+}$, when the number of nucleobase equivalents involved in the reaction is 1, 2, 3 and 4 respectively. This behavior is consistent with the *trans* effect concept, and is also applicable to other nucleobases and heterocycles with N donor atoms. In the case of two equivalents of nucleobase, the platinum complex always displays a *cis*- geometry. In order to obtain the *trans* complex, a different strategy needs to be employed. An excess of potassium iodide given to an aqueous solution of [Pt(1-MeC-*N3*)$_3$I]I (**20**) at 80ºC with a pH value of 2, are the best conditions to get **21**. In order to obtain the respective chloro complex, a substitution of the iodo ligands by chloro ligands is required (see Experimental part). As a result of this, *trans*-[Pt(1-MeC-*N3*)$_2$Cl$_2$] (**24**) was obtained.

2.5.3.1.- NMR study of 21.

The behavior of *trans*-[Pt(1-MeC-*N3*)$_2$I$_2$] in water is difficult to determine due to its poor solubility; hence it was not possible to obtain a ^{1}H NMR spectrum

in D_2O. Solubility in other common solvents was checked without positive results, except in the case of DMSO. Probably because of substitution of the iodo ligands by solvent molecules *trans*-[Pt(1-MeC-*N3*)$_2$(DMSO)$_2$]$^{2+}$ is formed which gives a ^{1}H NMR spectrum in deuterated DMSO (Figure 2.40).

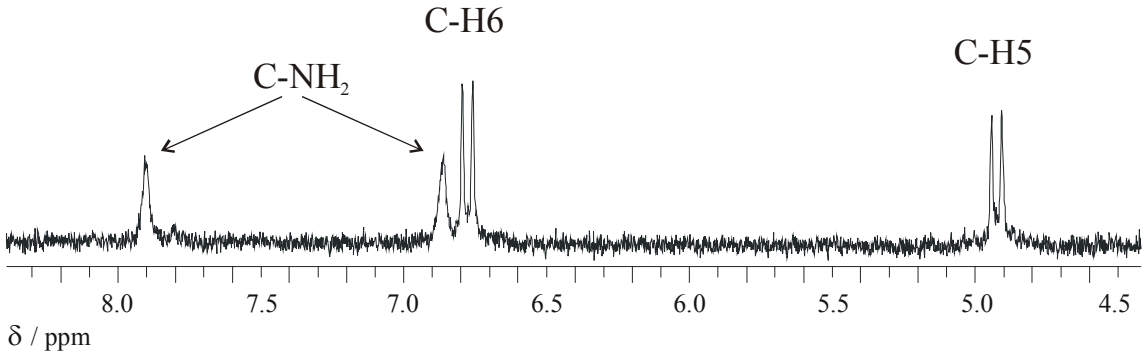

Figure 2.39: *Lowfield section of trans-[Pt(1-MeC-N3)$_2$(DMSO)$_2$]$^{2+}$ in DMSO-d$_6$.*

The spectrum shows signals corresponding to the protons of 1-MeC, including those at the N4 exocyclic amino group. Coupling constants of the aromatic 1-MeC protons of the DMSO species *trans*-[Pt(1-MeC-*N3*)$_2$(DMSO)$_2$]$^{2+}$ are ^3J = 7.15 Hz (H6). The two protons of the NH_2 group have a ^2J value of 207.7 Hz.

2.5.3.2.- Crystal Structure of *trans*-[Pt(1-MeC-*N3*)$_2$Cl$_2$] (22).

Dark-yellow crystals of *trans*-[Pt(1-MeC-*N3*)$_2$I$_2$], although isolated proved not suitable for X-ray diffraction studies and rather showed rapid decomposition. Eventually exchange of I^- by Cl^-, which gave the analogue **22**, provided crystals for a structure determination.

The length of the longest parameter in the unit cell (c = 8.470(2) Å), which is clearly shorter than the size of the molecule in its largest direction (11.564 Å), implies that the molecule belongs to a centrosymmetrical space group. After refinement of the measured crystal data, the molecule was found to be in the *P-1* space group, having the platinum atom located in the inversion centre of the

molecule. In its case, all the hydrogen atoms were found in the Fourier difference and refined isotropically. Details concerning the crystal, X-ray measurement, and the refinement of data are listed in Table A-22 (see Appendix).

The complex **22** consists of symmetrical monomeric molecules. The mirror plane in the complex includes the platinum atom and forms an angle of 45.0º with the Pt-N3 and Pt-Cl1 bonds. The platinum atom is coordinated to the N3 site of 1-MeC and to the chloride ion in a non-distorted square planar coordination. The cytosine ring, and its symmetrically generated (-x+1, -y, -z+1) ring are almost coplanar; exocyclic groups show a maximal deviation of ± 0.073 Å due to hydrogen bonding interactions. As shown in Table 2.6, distances and angles in the complex are not unusual. The Pt-N3 distance is 2.018(12) Å and thus similar to the corresponding distances in the N3 coordinated cytosine ring of **24** (2.055(3) Å), and comparable to other Pt-N3 coordinated 1-MeC bases. Also, the angle between the platinum coordination plane and the cytosine plane is similar to the same angle involving the N3 coordinated cytosine in **24**, 75.6(4)º vs. 75.0(1)º. The two 1-methylcytosine rings are parallel to each other.

Table 2.6: *Selected distances (Å) and angles (º) for **22**.*

Cl1-Pt1-N3	90.0(4)	Pt-Cl1	2.298(4)
N3-Pt1-Cl1(i)	90.0(4)	Pt-N3	2.023(12)
Cl1(i)-Pt1-N3(i)	90.0(4)	Pt-N3-C2	118.1(9)
N3(i)-Pt1-Cl1	90.0(4)	Pt-N3-C4	121.8(11)
N3-Pt1-N3(i)	180.0(0)	PtL_4 / 1-MeC	75.6(4)
Cl1-Pt1-Cl1(i)	180.0(2)		

Symmetry code: (i) -x+1, -y, -z+1.

As shown in Figure 2.40, the two *trans*-positioned cytosines are in a head-tail arrangement. With regard to the intramolecular interactions in *trans*-[Pt(1-MeC-*N3*)$_2$Cl$_2$], the distance between the opposite exocyclic groups N4-O2(-x+1, -y, -z+1) is 4.15(2) Å, which is too long for H-bonding. The distance between the chloro ligand (Cl1) and the nearest exocyclic amino group is

shorter, 3.575(17) Å, but still to be considered a long intermolecular contact [113]. These facts rule out possible intramolecular H-bond interactions. The Pt-H41 distance (2.53 Å) is shorter than the sum of the van der Waals radii of Pt and H (3.5 Å); hence it may reflect a weak platinum-hydrogen interaction [114].

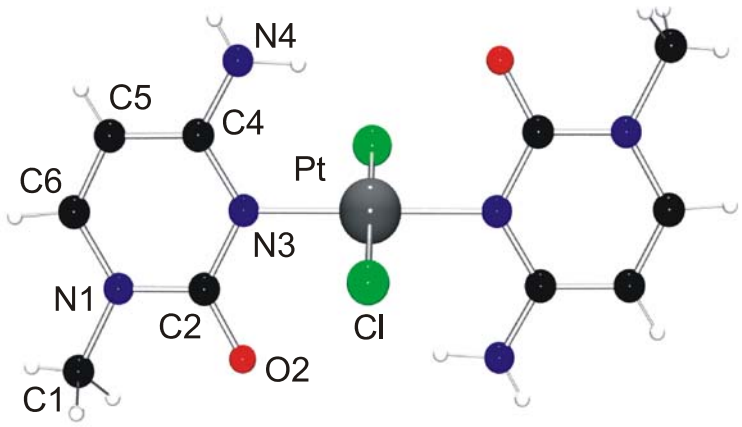

Figure 2.40: *View of the complex trans-[Pt(1-MeC-N3)$_2$Cl$_2$] (**22**) with atom numbering scheme.*

Concerning intermolecular interactions, the packing of the crystal plays an important role. The absence of counter ions allows for a relatively compact packing pattern. However, in contrast to other related structures involving nucleobases, the hydrogen bonding pattern has not a principal role in the packing of the crystal. The closest intermolecular contacts (2.99(2) Å) are between O2 and N4 atoms of adjacent molecules along the *a* axis. Hydrogen atoms bonded to N4 are necessarily coplanar with the cytosine ring, that means that H42 is not located in the straight line defined by N4···O2 (angle N4-H42-O2* is 151.2º). The distance between adjacent planes defined by the cytosine rings is 1.22 Å (see Figure 2.41). The closest intermolecular approach to a hydrogen atom is between O2 and H41(x+1, y, z), which could be considered a weak hydrogen bond contact. The molecules are arranged in infinite chains along the *a* axis via this weak hydrogen bond contact.

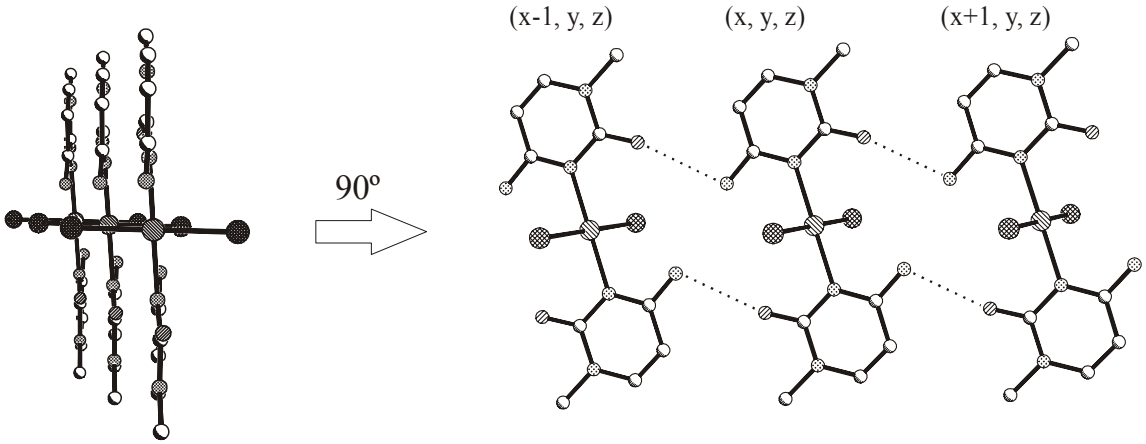

Figure 2.41: *View along the a axis of the packing of **22**. Intermolecular N4(H)···O2 hydrogen bonds are observed.*

A view along the *a* axis, shown in Figure 2.42, reveals that two coplanar molecules on two different sheets are not connected to each other; the distance C6-C6*(-x+1, -y+1, -z-1) is 6.16(3) Å. However, Cl1*(-x+1, -y, -z) is connected to the C6 atoms with a distance of 3.60(2) Å forming weak inter-sheet interactions. Finally, contacts between chains are dominated by π-stacking (3.47 Å) involving the cytosine rings along the *b* axis. The geometry about the heavy metal in **22** is comparable to corresponding ones found in the cationic *trans*-[$(NH_3)_2$Pt(1-MeC-*N3*)$_2$]$^{2+}$ [115,116] and in *trans*-[Pd(1-MeC-*N3*)$_3$Cl$_2$] [117], but with some differences.

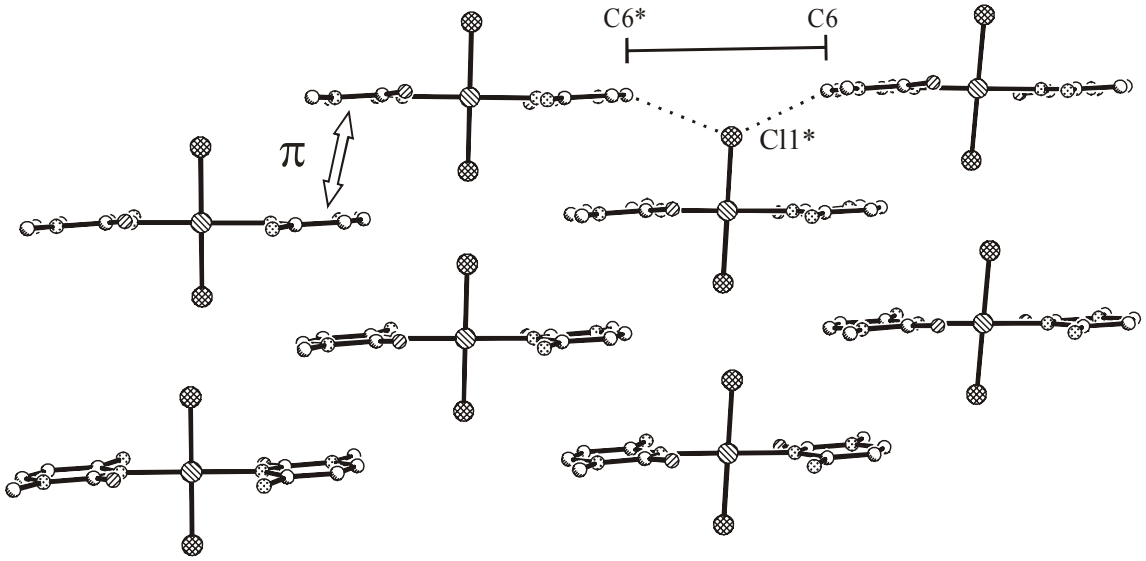

Figure 2.42: *View along the b axis of the packing of **22**. Intermolecular Cl1···C6 hydrogen bonds contact and π-stacking between the bases are observed.*

2.5.4.- Pt Complexes Containing two Different Tautomers.

In the overwhelming majority of reported metal-nucleobase complexes, the predominant tautomer of the nucleobase is found bonded to the metal ion. There are only few examples where rare tautomers are bonded to the metal [78], and in fact only a single example, *trans*-$[(NH_3)_2Pt(9\text{-MeA-}N7)(9\text{-MeA-}N6)]^{2+}$ [100], where two different tautomers of a single nucleobase are simultaneously coordinated to a single metal. Here two more examples, containing two different tautomers of 1-MeC, are described.

2.5.4.1.- *Trans*-[Pt(1-MeC-*N3*)(1-MeC-*N4*)X_2] Complexes (23, 24).

Optimization of the reaction conditions led to an improved yield of *trans*-[Pt(1-MeC-*N3*)(1-MeC-*N4*)I_2]. These modifications can be summarized in four points: a) Increase of pH; b) reduction of the temperature; c) increase of the reaction time; d) reduction in the number of equivalents of iodide added. In order to obtain *trans*-[Pt(1-MeC-*N3*)(1-MeC-*N4*)Cl_2], the excess of iodide in the solution was eliminated by precipitation with Ag^+ and subsequent addition of Cl^-.

2.5.4.1.1.- Crystal Structures.

Crystals of *trans*-[Pt(1-MeC-*N3*)(1-MeC-*N4*)I_2] · $2H_2O$ (**23**) and *trans*-[Pt(1-MeC-*N3*)(1-MeC-*N4*)Cl_2] (**24**), both of yellow color, were collected and proved useful for X-ray crystallography. Details concerning the crystal, X-ray measurement, and the refinement of data are listed in Tables A-23 and A-24 (see Appendix).

Views of **23** (X = I) and **24** (X = Cl) are given in Figure 2.43. In both compounds the two bases are *trans* to each other and bonded to Pt in different

fashions, via N3 and N4, respectively. As the N4 bonded cytosine is protonated at N3 (only in **24** is the expected opening of the internal ring angle C2-N3-C4 clearly seen: 127.8(4)° vs. 120(0)° in neutral 1-MeC [20]), it is present in both **23** and **24** in the rare iminooxo tautomer structure, with the metal attached to the N4 position. The relative orientation of the heavy metal with respect to the proton at N3 is *syn* in both compounds.

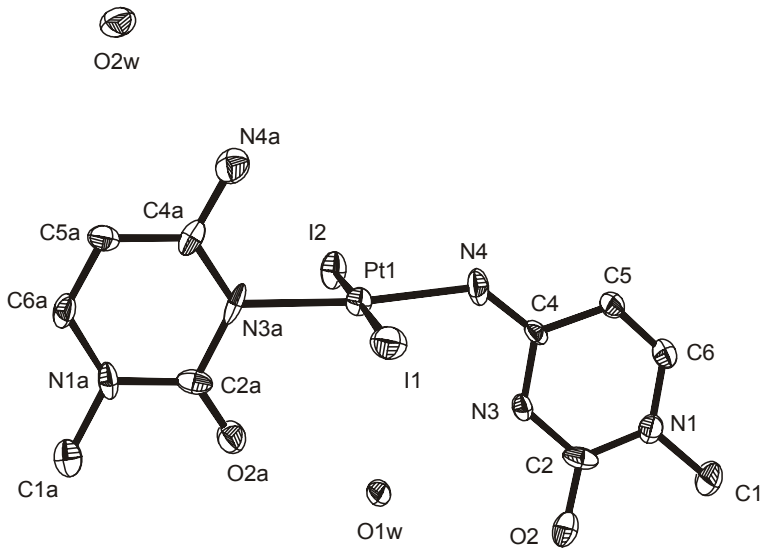

Figure 2.43a: *Top view of **23**.*

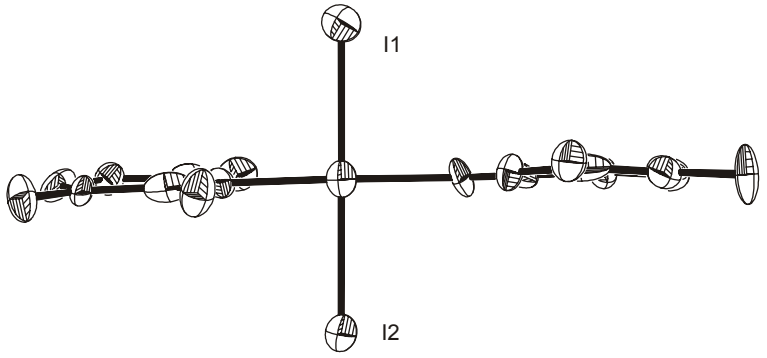

Figure 2.43b: *Side view of **23**.*

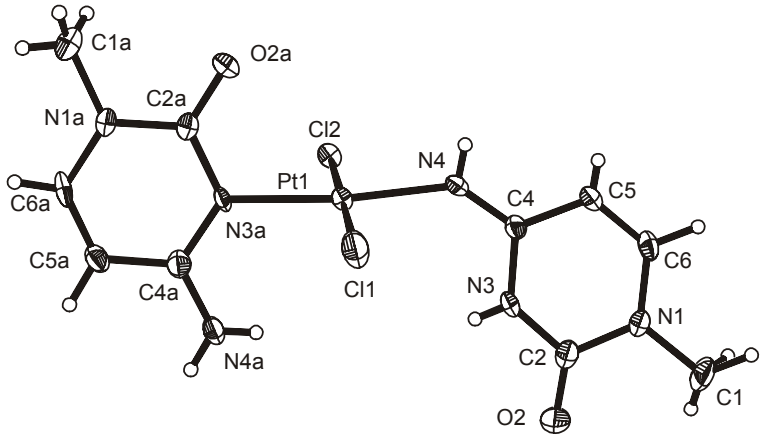

Figure 2.43c: *Top view of **24**.*

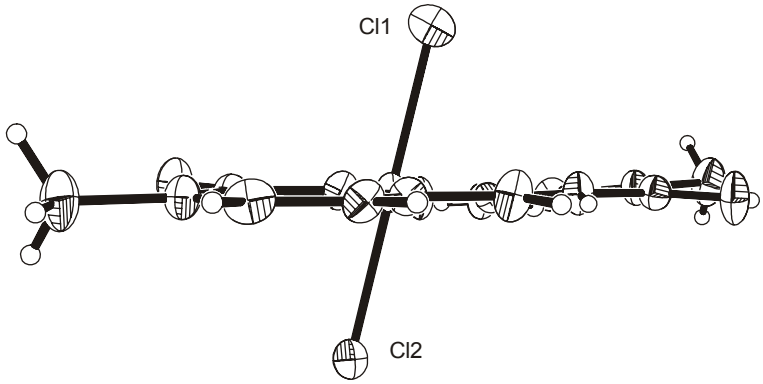

Figure 2.43d: *Side view of **24**.*

The two nucleobases are close to perpendicular to the PtN_2I_2 plane in the case of **23**, but more inclined to the PtN_2Cl_2 plane in the case of **24** (see Table 2.7).

The two nucleobases adopt almost coplanar orientations, despite the fact that the N3 bonded bases display different orientations in **23** and **24**: In **23**, O2a is across N3 (*syn1*), while in **24** it is N4a which is across N3 (*syn2*). Bonding distances and angles about the Pt centers are not unusual, even though the deviation of N3a-Pt-N4 angles from linearity is to be noted (Table 2.7). In the case of **24**, the difference between Pt-N3a and Pt-N4 is significant, with the latter being shorter (2.055 (3) Å vs. 2.015 (4) Å). Geometries of the cytosine ligands compare well with reported ones [102,103,110,111,115,118,119]. C4-N4 distances are slightly shorter than C4a-N4a distances (**23**: 1.29 (1) Å vs. 1.33 (1) Å; **24**: 1.275 (1) Å vs. 1.301 (1) Å), but only in **24** is this difference significant (18.6 σ).

Table 2.7: *Selected distances (Å) and angles (°) for **23** and **24**.*

	23	**24**
Pt1-N3a	2.046 (9)	2.055 (3)
Pt1-N4	2.033 (9)	2.015 (4)
Pt1-X1	2.615 (1) (X1=I)	2.302 (1) (X1=Cl)
Pt1-X2	2.606 (1) (X2=I)	2.306 (1) (X2=Cl)
N3a-Pt1-X1	91.7 (2)	91.37 (9)
N3a-Pt1-X2	88.1 (2)	88.06 (9)
N4-Pt1-X1	89.7 (2)	91.7 (1)
N4-Pt1-X2	90.6 (2)	88.7 (1)
N3a-Pt1-N4	174.1 (6)	173.5 (1)
X-Pt-X	178.75 (7) (X=I)	179.35 (4) (X=Cl)
(1-MeC-*N3*) / Pt	89.2 (2)	75.0 (1)
(1-MeC-*N4*) / Pt	84.4 (2)	77.3 (1)
(1-MeC-*N3*) / (1-MeC-*N4*)	6.7 (2)	2.7 (2)

A major difference between the two complexes **23** and **24** relates to their hydrogen bonding patterns. Figure 2.44 provides a top view of a layer of molecules **23** and Figure 2.45 gives a side view. As can be seen, **23** forms a sheet structure with antiparallel strands of molecules of **23**. Within each strand, the two water molecules accomplish the interactions between molecules: O1w bridges the O2a position of (1-MeC-*N3*) (2.76 Å) with N3 of (1-MeC-*N4*) (2.86 Å), and at the same time bridges to O2w (3.11 Å), which in turn is H bonded to N4a of (1-MeC-*N3*) of an adjacent molecule within the strand (2.88 Å). Iodo ligands of molecules sitting above and below the sheet, respectively, form a zigzag chain.

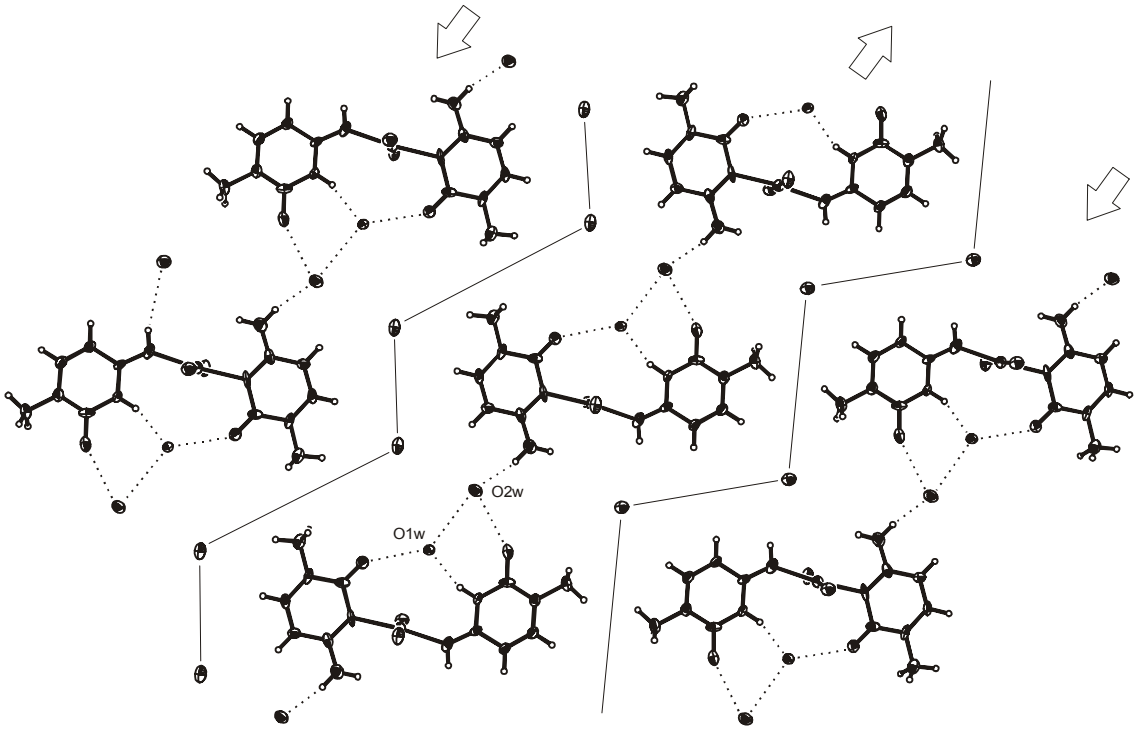

Figure 2.44: *Layer structure of **23** with H bonds involving the water molecules O1w and O2w indicated. The antiparallel strands are separated by iodo ligands, which due to packing of molecules are almost coplanar with the cytosine rings (deviation I1: -0.34 Å, I2: 0.64 Å).*

A sheet structure is also present in the case of **24**, but in contrast to **23**, it forms parallel strands separated by Cl1 atoms of adjacent layers located slightly above (0.88 Å) the nucleobases plane. Arrangement in every sheet is identical. Distances between Cl1 and neighboring protons are ≥ 3.58 Å (minimum distance to C6a). Two direct H bonds are joining adjacent molecules in the strand: N4a with O2a (2.95 Å) and O2 with C5 (3.27 Å). These two hydrogen bonds are reinforced by three additional H bonds originating from Cl2 atoms of molecules in the layer below and the following hydrogen donors: N3H (3.21 Å), to N4H (3.24 Å) and to N4aH(H) (3.19 Å). The Cl2 atoms are 1.22 Å out of the plane of the two nucleobases (see Figure 2.46).

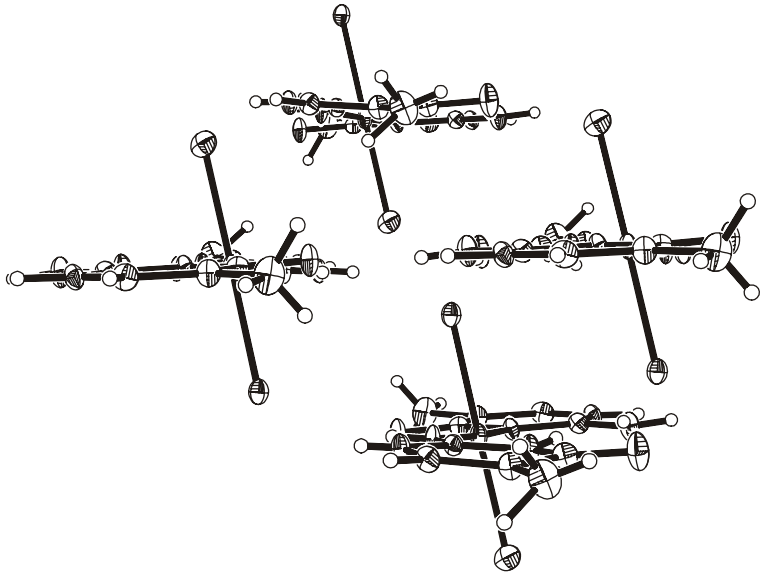

Figure 2.45: *Side view of the parking of **23**.*

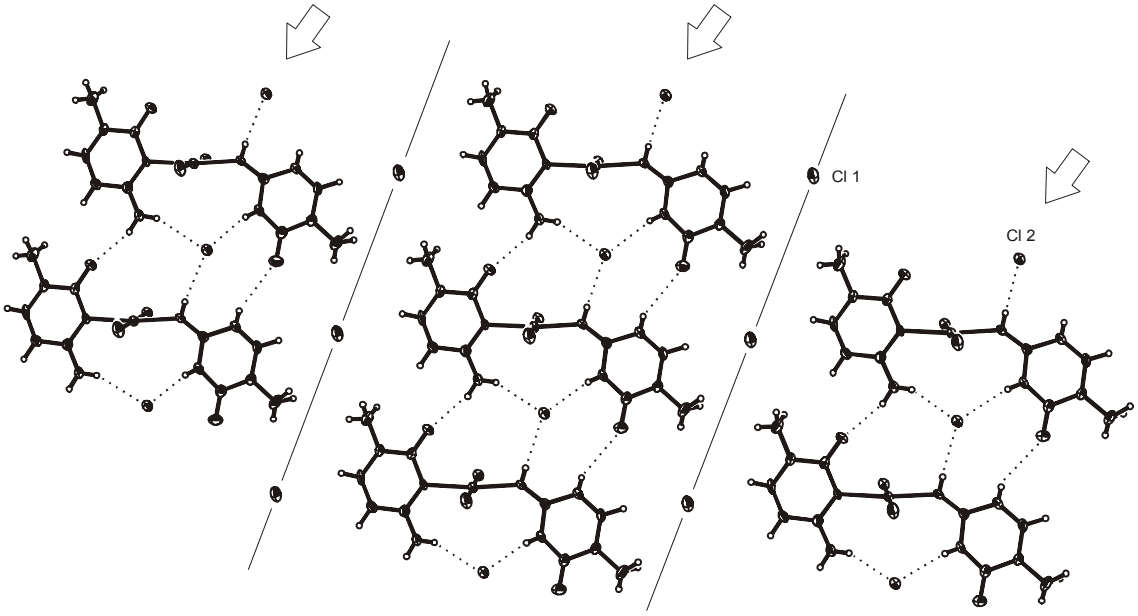

Figure 2.46: *Arrangement of molecules **24** in parallel strands. Cl1 ligands of adjacent layers separate individual stands. Cl2 ligands of molecules in the lower layer are located between pairs of H bonded molecules and form additional three hydrogen bonds with amino protons.*

In order to complete this study, several feasible geometries of rotamers of *trans*-[Pt(1-MeC-*N3*)(1-MeC-*N4*)Cl_2] and *trans*-[Pt(1-MeC-*N3*)(1-MeC-*N4*)I_2] · n H_2O (n = 0, 1, 2, 3) were optimized [2].

2.5.5.- Remarks.

The two complexes described (**23** and **24**) contain simultaneously the major aminooxo and the minor iminooxo tautomer forms of the model nucleobase 1-MeC. Previously established cases of formation of the N4 linkage isomer in Pt or Ru complexes involved redox-assisted pathway. It is interesting to point out here that metal-stabilized rare tautomers could be relevant in metal mutagenesis [102,103,111,120,121]. Formation of **23** and **24** occurs in weakly acidic aqueous solution, most likely by a metal migration process from the endocyclic N3 to the exocyclic N4 position. This demonstrates that the metal migration process along cytosine does not require necessarily strong basic conditions to be achieved.

3.- Platinum-Cytosine Complexes as Potential Building Blocks for 1D-Polymers.

Coordination polymers built up of organic ligands and metal ions represent today an important field within Supramolecular Chemistry [122]. Depending on the geometry of the metal, and the interconnecting and hydrogen bonding properties of the ligands, self-assembled discrete molecular polygons and polymers can frequently be synthesized in a rational way. With nucleobases involved in such systems, the typical forces —H bonding and base stacking— may become important determinants for the resulting structures.

Here some preliminary experiments aimed at obtaining a onedimensional polymer containing platinum and 1-MeC bases as principal components are presented. At the onset of these attempts it was clear that the increasing positive charge in the polymer may represent a problem. Still, the experience with highly charged, discrete cyclic nanostructures [123] suggested that the effort may be worth while. Consequently, some reactions were designed with **20** and **21** as metal building blocks.

The initial idea was to synthesize building blocks in which the entity *trans*-[Pt(1-MeC-*N3*)$_2$]$^{2+}$ is bonded to two linear bidentate ligands; pyrazine and 4,4'-bipyridyl were used in this attempt. Once the building blocks are obtained, these have to be joined to other *trans*-[Pt(1-MeC-*N3*)$_2$]$^{2+}$ entities to form chains containing different number of blocks, depending of the number of equivalents used. This strategy should allow the formation of onedimensional polymers of desired length. In the case of finite 1D-molecules, terminal platinum atoms in the chains could be bonded to three 1-MeC bases, using **20** as final building block. Scheme 3.1 shows the synthesis strategies for the preparations of 1D-polymers.

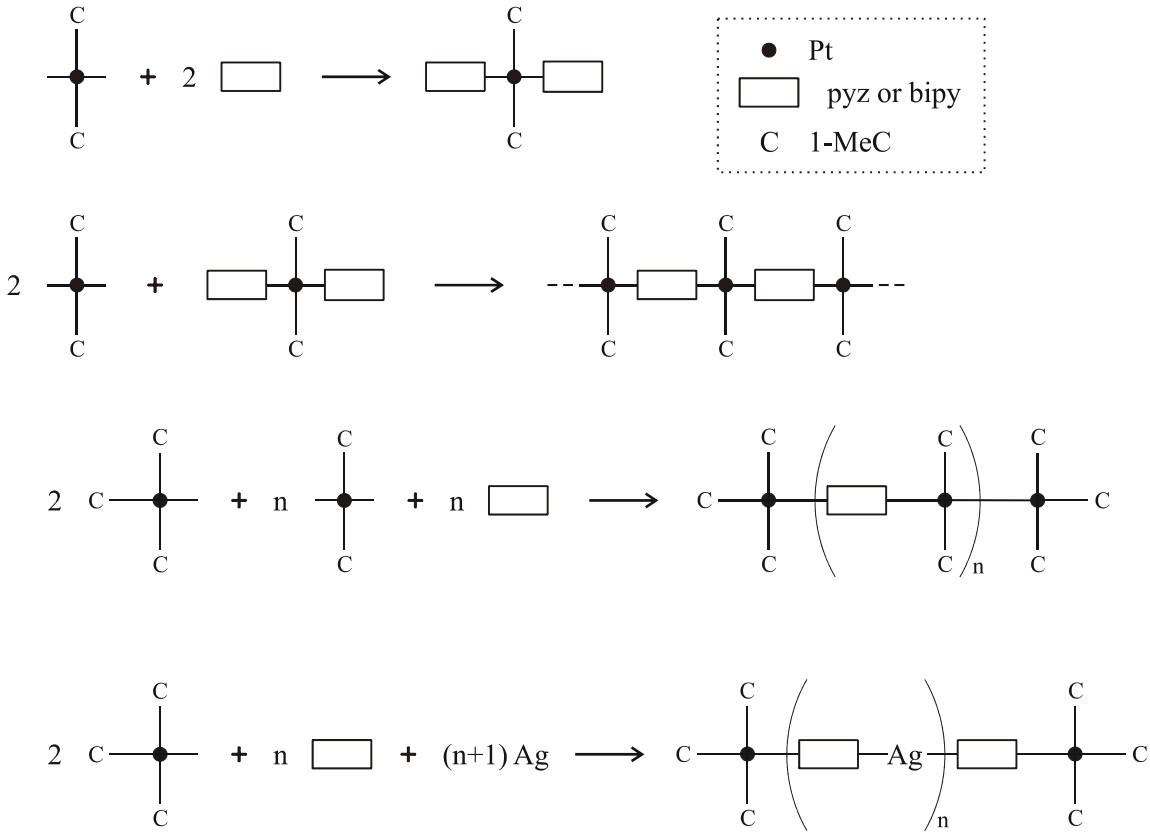

Scheme 3.1: *Different synthetic strategies for the 1D-polymers.*

In the aforementioned strategy, the use of **21** as pre-building block presents some difficulties. Substitution of the *trans* positioned iodo ligands by other ligands requires extended reaction times and relatively high temperatures depending on the nature of other ligands, or addition of other solvents. This is the case with 4,4'-bipyridyl acting as ligand, where the addition of ethanol (1:1) to the water solution is necessary due to the insolubility of 4,4'-bipyridyl in water. Some properties of the starting compound are also worth mentioning; its poor solubility in water and the low pH and instability of the aqua species proved of disadvantage. All these factors made the proposed objective unfeasible, and the reaction conditions led to decomposition of the starting compound and no coordination of the ligands was observed. However, it is worthwhile to characterize two interesting by-products of this project: [(4,4'-bipyridyl)H]I · H_2O, (**25**) and [Ag(pyz)](NO_3) (**26**). The products for terminal positions in the 1D-polymer [Pt(1-MeC)$_3$(pyz)](NO_3)$_2$ · H_2O (**27**) and [Pt(1-MeC)$_3$(pyz)Ag](NO_3)$_3$ (**28**) are discussed later in this chapter.

3.1.- [(4,4'-bipy)H]I · H_2O (25).

Reactions of **21** with varying equivalents of 4,4'-bipyridyl were carried out following addition of two equivalents of $AgNO_3$. Several times, colorless crystal blocks were recovered after slow evaporation of the solvent and separation from a black aggregate. It was possible to identify these black solid particles as elemental platinum by means of EDX analysis, unequivocal evidence that the starting compound had decomposed. Some of the colorless crystals were suitable for analysis by X-ray crystallography.

The solid state structure reveals it to be 4,4'-bipyridinium monohydroiodide monohydrate **(25)**. It crystallizes in the orthorhombic crystal system. Details of measurement and refinement of the data are listed in Table A-25 (see Appendix). Some aspects of the geometrical arrangement, proton bridging and π-stacking interactions are discussed further.

Monoprotonation of the 4,4'-bipyridyl entity is interesting not only because it is the key for the formation of hydrogen bonds but also because from a crystallographic point of view, there is a change of absolute configuration when going from the neutral molecule to the monoprotonated one. Monoprotonated 4,4'-bipyridyl has two chiral isomers, which were identified in the X-ray structure. The presence of the H4 proton does not allow converting one into another by a symmetry operation. The Flack parameter [124] converged to x = 0.56(3), indicating racemic twinning in the crystal; it was taken into account during the final cycles of least-squares refinement.

In the structure determined in the solid state, the 4,4'-bipyridinium entity is present in a non-planar arrangement. The two halves of the cation are at a dihedral angle of 31.0(1)º about the C1-C1' bond (see Figure 3.1). This value is typical for non-planar 4,4'-bipyrimidinium cations, where torsion angles normally range between 17(1) and 38.4(9)º [125-129].

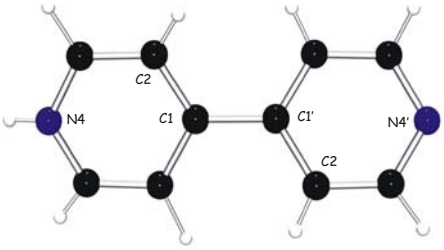

Figure 3.1: *Top view of the cation of **25**. Rods representation of a chiral isomer, with an internal angle of 31.0(1)º. Iodide anion and water are omitted for clarity.*

As shows Table 3.1, bond distances or angles are not unusual. The atoms of the heterocyclic rings are approximately coplanar within ± 0.013(4) Å and ± 0.006(4) Å in the first and in the second ring; sums of the internal angles are 720.0(16)º and 720.0(14)º, respectively.

Table 3.1: *Selected distances (Å) and angles (º) for **25**.*

	ring (H)	ring'
C1-C2	1.393(7)	1.360(6)
C2-C3	1.371(7)	1.373(7)
C3-N4	1.336(7)	1.352(7)
N4-C5	1.317(7)	1.314(7)
C6-C1	1.383(7)	1.393(7)
C1-C1'	1.488(7)	
N4-N4'(i)	2.716(7)	
	ring (H)	ring'
C1-C2-C3	118.9(6)	120.4(6)
C2-C3-N4	120.9(6)	122.2(6)
C3-N4-C5	121.7(6)	117.3(5)
N4-C5-C6	119.7(6)	123.3(6)
C5-C6-C1	121.3(6)	120.1(6)
C6-C1-C2	117.5(6)	116.8(5)
C6-C1-C1*	121.9(5)	121.3(5)
C2-C1-C1*	121.9(5)	121.9(5)
ring-ring'	31.0(1)	

Symmetry code: (i) x, y-1, z.

The aggregation of **25**, as can be seen in Figure 3.2, is structured by infinite strands along the b axis, where the cationic entities **25** are longitudinally connected by hydrogen bonding between the protonated N4 position and the non-protonated N4' site of an adjacent molecule (x, y-1, z). The distance between N4 and N4' of the next molecule in the strand is 2.716 (7) Å; we can consider this a strong H-bond interaction. To complete the arrangement, similar strands are disposed above and below, forming layers. Interactions between strands are defined by π-stacking of both rings of each molecule with neighbor ones. The rings do not lie directly on top of each other, to avoid repulsion of the other rings; rather they are layered in a staggered fashion. Distances between π-stacked rings are 3.57(2) and 3.43(2) Å, respectively (see Figure 3.2). From the chiral point of view, every strand is formed exclusively by one of the enantiomers. The neighboring strands are formed by the other enantiomer. Thus, π-stacking occurs always between a pair of enantiomers.

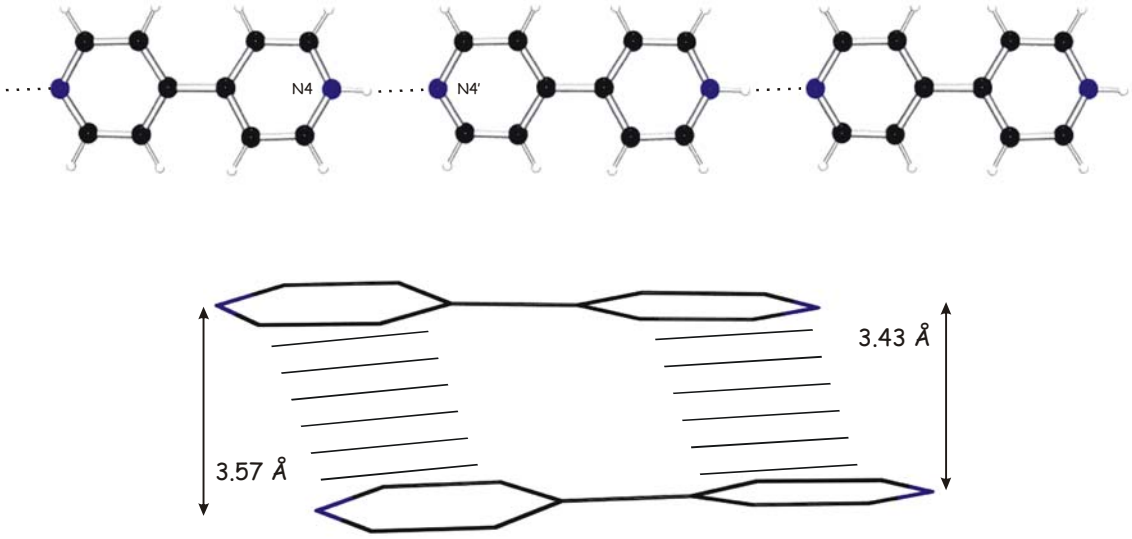

Figure 3.2: *Packing in **25**: 4,4'-Bipyridinium entities forming strands by hydrogen bonds (top), π-stacking with rings of adjacent strands(bottom).*

Iodide counter ions and water of crystallization occupy alternately empty sites between adjacent layers. Distances between iodide anions and atoms of the aromatic rings appear to be relatively long, but considering the size of iodide radii (2.20 Å) [130], we can suggest hydrogen bonding exists. Thus, the estimated

mean distance C···I in a hydrogen bond (iodide anion to aromatic C bonded to N and C in the ring) is 4.00 Å [113]. Precisely, 4.001(6) Å is the distance of the hydrogen bond I1···N4(-x+1/2, -y+1, z-1/2). There are also some short C–H···I contacts, again involving the iodide anion, which are worthy of being mentioned: I1···C3(-x+1/2, -y+1, z-1/2), 3.628(6) Å; I1···C6'(x+1/2, -y+3/2, -z+1), 3.812(6) Å; I1···C5(-x+1, y-1/2, -z+1/2), 3.875(7) Å; I1···C3'(-x+1, y+1/2, -z+1/2), 3.996(7) Å; and I1···C2(x+1/2, -y+3/2, -z+1), 4.035(6) Å. In the case of hydrogen bonding of iodide ion to water, the estimated mean distance is 3.60(1) Å [113]. In agreement with this, we can also consider hydrogen bonding involving iodide and water, the distance from the iodide anion to the water of crystallization is 3.407(4) Å; this distance is 3.643(4) Å if we take the water molecule of a adjacent unit cell (-x+1, y-1/2, -z+1/2). Some distances and angles involving hydrogen bond contacts are listed in Table 3.2.

Table 3.2: *Distances (Å) and angles (º) of the type D–H···A for* ***25****.*

D–H···A	D–H	H···A	D···A	D–H···A
N4–H4···N4'(i)	0.828	1.891	2.716	174.2
O1–H1w···I1	0.920	2.751	3.643	163.8
O1–H2w···I1(ii)	0.909	2.514	3.407	167.7

Symmetry codes: (i) x, y-1, z; (ii) -x+1, y-1/2, -z+1/2.

Some unsubstituted 4,4'-bipyridinium salts have been studied with the principal objective of controlling the relative orientation of the molecular components of the crystal. Reported examples of diprotonated 4,4'-bipyridyl salts contain: bromide [131], chloride [132], hydrogenmaleate [133], iodide [134], nitrate [135], perchlorate [136], and MCl_n^{2-} [137]. This last case with chlorometallate counter anion include $PtCl_4^{2-}$, $PtCl_6^{2-}$ as well other metals —Os, Pt (n = 6); Fe, Sb (n = 5); Pt, Pd, Mn, Cd, Pb, Co, Zn, Hg (n = 4)—, which form one-, two-, and three- dimensional periodic networks in reliable strategies for crystal synthesis by design. In contrast, there are only two reported examples involving monoprotonated 4,4'-bipyridinium. The first example, a derivative of bipyridinium, is the solid state structure of 4,4'-bipyridyl-3,3'-dicarboxylic acid dihydrate [138], a zwitterionic molecule, *viz.* 3'-carboxy-4,4'-bipyridin-4-ium-3-

carboxylate dihydrate. The second published structure, is a 4,4'-bipyridin-1-ium bromide monohydrate, presenting a similar arrangement as **25**, but with bromide as counterion [139]. In this example, distances between π-stacked layers are shorter than in **25**, probably due to the increase of the halide ionic radius from Br^- to I^-, 1.96 and 2.20 Å [130], respectively. A torsional angle between the two rings about the C1–C1' bridging bond is also present, 29.6(4)º.

In the solid state structures of diprotonated 4,4'-bipyridyl containing iodide, perchlorate and in the monoclinic modification of the nitrate [135] the two pyridil moieties are coplanar. On the other hand, in the orthorhombic modification of the nitrate, hydrogenmaleate, chloride and bromide both rings are twisted.

3.2.- [Ag(pyz)](NO_3) (26).

One of the monodimensional polymers described previously is formed by a building block in which Ag^+ is bonded to two pyrazine ligands. The crystal structure of this building block, [Ag(pyz)](NO_3), has been reported [140] in the monoclinic space group. Here is reported a modification of [Ag(pyz)](NO_3) which crystallizes in the triclinic space group. Crystallographic data, data collection parameters and refinement parameters of **26** data are listed in Table A-26 (see Appendix).

The main motif of the structure is an alternating chain consisting of Ag^+ and pyrazine ligands extending along the *c* axis in a slight zig-zag fashion. The angle between Ag^+ and the coordination sites of pyrazine is 157.7(4)º, and the distances Ag–N are: Ag–N1, 2.205(10) Å; Ag–N4, 2.220(10) Å. Dihedral angles between the pyrazine rings are 26.9(6)º. Pyrazine rings have usual distances and angles. Adjacent chains along the *b* axis are coplanar, forming layers. The nitrate counter anions are located between the layers and are not coplanar with

this plane. A view of the layer formed by the silver-pyrazine entities is shown in Figure 3.3.

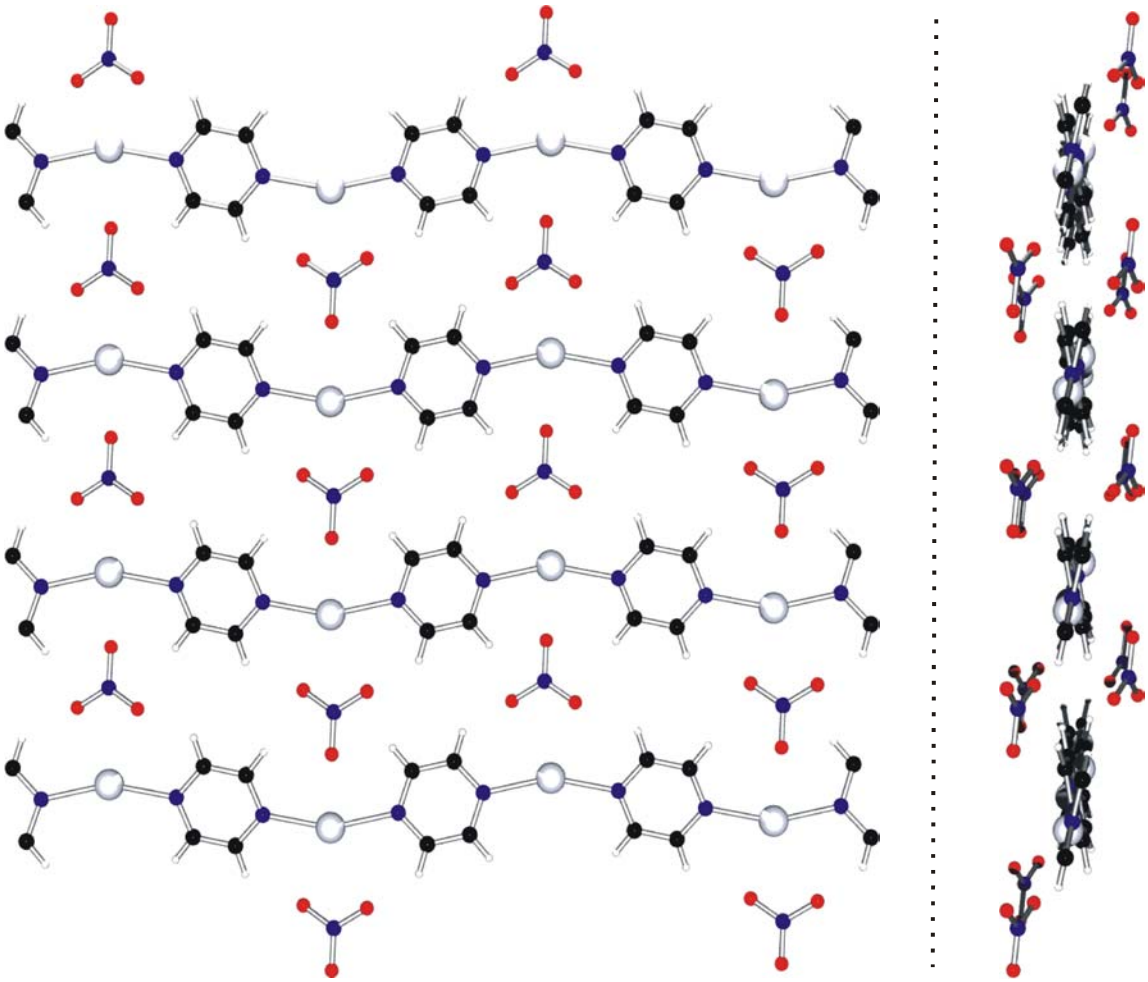

Figure 3.3: *View of the crystal packing of* ***25*** *(bc plane).*
The nitrate counterions are not coplanar with the silver-pyrazine chains.

The Ag-pyz chains π-stack with consecutive chains along the *a* axis. The distance between two stacked pyrazine rings is 3.37 Å. The silver atoms also line up (distance Ag···Ag, 3.4990(7) Å) along the *a* axis, in which a weak interaction between silver cations is observed (see Figure 3.4). Other interactions between Ag and oxygen atoms of the nitrate anions are: Ag···O2, 2.560(9) Å; Ag···O1(x, y-1, z), 2.881(9) Å; Ag···O1(x+1, y-1, z),3.038(9) Å; Ag···O2(x+1, y, z),3.423(10) Å; Ag···O3(x+1, y, z), 2.797(9) Å.

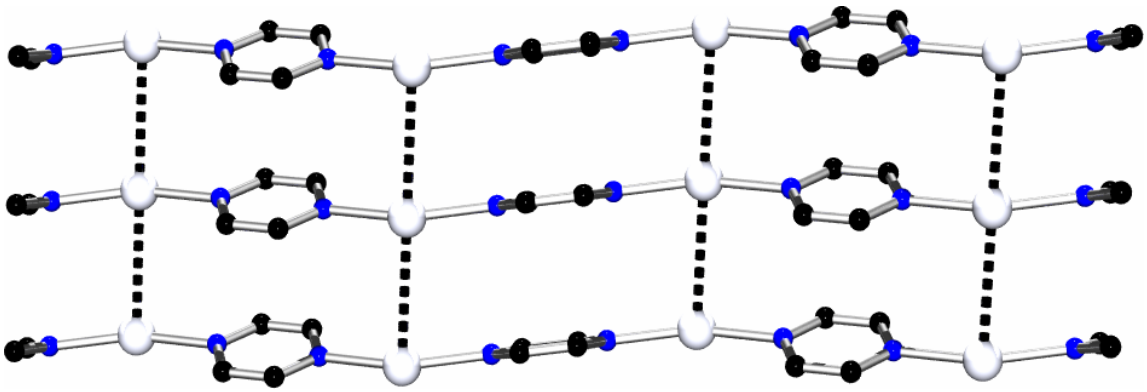

Figure 3.4: *View of* ***25*** *along the b axis, Ag···Ag interactions are observed. The nitrate counterions are omitted for clarity.*

The monoclinic reported structure displays a similar arrangement, without significant differences (maximal differences about 0.04 Å and 2º).

3.3.- [Pt(1-MeC-*N3*)$_3$(pyz)](NO$_3$)$_2$ · H$_2$O (27).

Colorless crystals of **27** were isolated from aqueous solution and were useful for X-ray crystallography. During the refinement of the measured structure, all non-hydrogen atoms in the structure were refined anisotropically except those of the second nitrate counter anion (N2N, O4, O5 and O6), and all hydrogen atoms were included in geometrically calculated positions. Details concerning the crystal, X-ray measurement, and the refinement of data are listed in Table A-27 (see Appendix).

A view of the cation [Pt(1-MeC-*N3*)$_3$(pyz)]$^{2+}$ is depicted in Figure 3.5. The Pt atom is coordinated to the N3-atoms of the three cytosine bases and to the N1 atom of the pyrazine in a square planar mode. The relative orientation of the three nucleobases is head-tail-head.

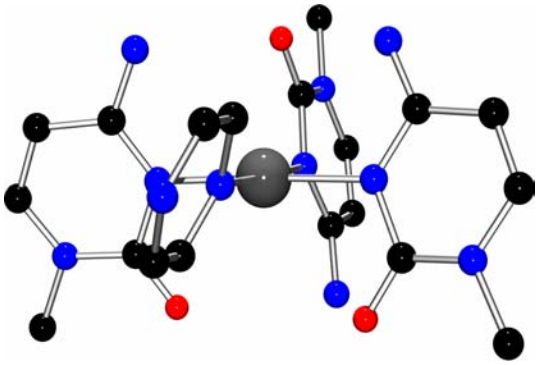

Figure 3.5: *View of the cation $[Pt(1\text{-}MeC\text{-}N3)_3(pyz)]^{2+}$ (**27**).*

The geometry of the square planar coordination of Pt has normal values of angles and distances, with some minor deviations. Angles involving Pt and N1 site of pyrazine are slightly smaller than the other two (89.2(2)º and 88.2(2)º vs. 92.0(2)º and 90.8(2)º); the angles formed by the two trans positioned rings are 176.6(3)º and 177.2(3)º. The Pt-N distances range from 2.019(6) Å (N3B) to 2.061(6) Å (N3C). The distances and angles in the cytosine bases and pyrazine of **27** are not unusual (see Table 3.3).

Table 3.3: *Selected distances (Å) and angles (º) for **27**.*

	$(1\text{-}MeC)_a$	$(1\text{-}MeC)_c$	$(1\text{-}MeC)_b$	(pyz)
Pt1-N	2.037(6)	2.061(6)	2.019(6)	2.030(6)
N3B-Pt1-N1	177.2(3)			
N3B-Pt1-N3A	92.0(2)			
N1-Pt1-N3A	89.2(2)			
N3B-Pt1-N3C	90.8(2)			
N1-Pt1-N3C	88.2(2)			
N3A-Pt1-N3C	176.6(3)			
O2B···N4A	3.099(9)			
O2B···N4C	2.961(10)			
N4B···O2A	3.030(9)			
N4B···O2C	2.921(10)			

The dihedral angles formed by the aromatic rings of the ligands with the coordination plane of the platinum atom are: 75.9(3)º $(1\text{-}MeC)_a$, 79.0(2)º

$(1\text{-MeC})_b$, 76.6(2)º $(1\text{-MeC})_c$, and 65.0(2)º (pyz). This last angle represents a deviation of 25º from the right angle. The dihedral angles formed by the *trans* positioned ligands are 32.1(3)º between the cytosine bases and 36.1(2)º between $(1\text{-MeC})_b$ and (pyz).

Complex **27** displays a poor hydrogen bonding pattern. There are no intermolecular hydrogen bond interactions between ligands of neighboring cations. Thus, the oxygen atoms of the carbonyl groups of the cytosine bases exclusively interact with the exocyclic amino groups of their respective *cis* positioned cytosine bases: O2B···N4A, 3.099(9) Å; O2B···N4C, 2.961(10) Å; N4B···O2A, 3.030(9) Å; N4B···O2C, 2.921(10) Å. There are only two sites involved in intermolecular hydrogen bond contacts. The N4 site of pyrazine forms a hydrogen bond to the water molecule, N4···O1w(x-1/2, -y-7/2, -z+1), 2.891(9) Å. Simultaneously, O1w interacts with the O2N oxygen atom of the nitrate anion: O1w···O2N, 2.800(1) Å. The N4 sites of the nucleobases are also involved in long hydrogen bond contacts with the nitrate anions or with water: N4A···O1N(-x, -y-3, -z+1), 2.820(10) Å; N4A···O1w(-x, -y-3, -z+1), 2.897(9) Å; N4B···O7N(-x+1/2, y+1/2, z), 2.927(10) Å; N4C···O1w(-x, -y-3, -z+1), 3.252(10) Å; N4C···O5N(-x-1/2, y+1/2, z), 3.161(14) Å; N4C···O6N(-x-1/2, y+1/2, z), 3.278(11) Å.

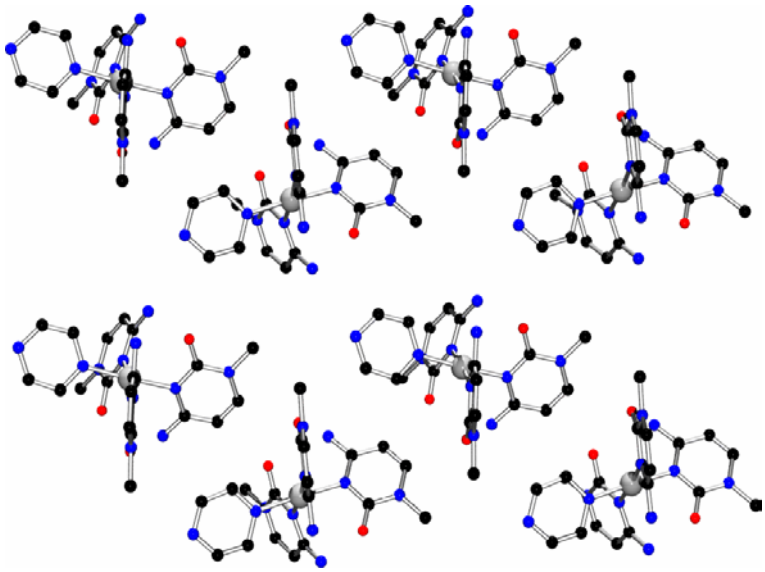

Figure 3.6: *View of the crystal packing of 27.*

The arrangement of the $[Pt(1\text{-}MeC\text{-}N3)_3(pyz)]^{2+}$ cations is shown in Figure 3.6. All the depicted Pt atoms in the figure are coplanar (plane of the page). The orientation of two consecutive cations of the structure is turned by 180º forming strands; layers are formed by strands. Nitrate anions are located between the layers acting as connection. No π-stacking interactions are observed between aromatic rings.

3.4.- $[Pt(1\text{-}MeC)_3(pyz)Ag](NO_3)_3$ (28).

Addition of $AgNO_3$ to a solution containing $[Pt(1\text{-}MeC\text{-}N3)_3(pyz)](NO_3)_2 \cdot H_2O$ (**27**) leads to formation of $[Pt(1\text{-}MeC\text{-}N3)_3(pyz)Ag](NO_3)_3 \cdot H_2O$ (**28**). The colorless crystals of **28** had a rather similar appearance as those of **27**. Details concerning the crystal, X-ray measurement, and the refinement of data are listed in Table A-28 (see Appendix).

The cationic $[Pt(1\text{-}MeC\text{-}N3)_3(pyz)Ag]^{3+}$ entity has a similar arrangement of the ligands as $[Pt(1\text{-}MeC\text{-}N3)_3(pyz)]^{2+}$, with a silver atom coordinated at the N4 position of pyrazine. The Pt atom is bonded to the N3 sites of the three cytosine bases and to the N1 site of the pyrazine in a square planar fashion. A view of the di-metallic cation is shown in Figure 3.7.

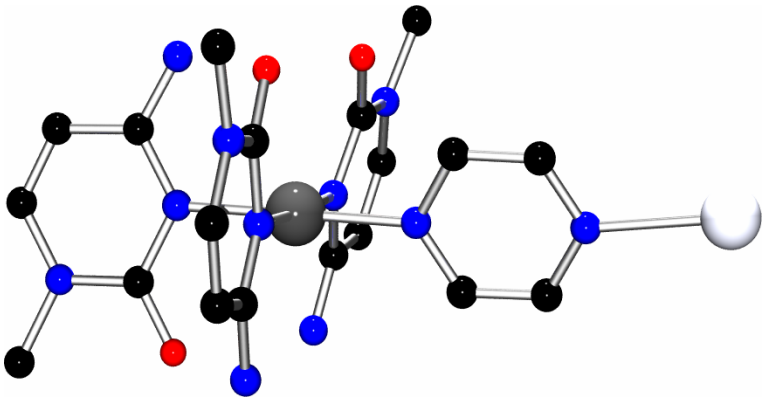

Figure 3.7: *View of the cation $[Pt(1\text{-}MeC\text{-}N3)_3(pyz)Ag]^{3+}$ (**28**).*

The deviations from the square-planar coordination are comparable to those of **27**. Angles N-Pt-N of the *cis* positioned ligands range from 88.0(2)º to 91.1(2)º; and the angles involving the *trans* positioned ligands are 175.5(2)º and 179.0(2)º. As in **27**, the distances and angles of 1-MeC and pyz are normal. Selected distances and angles for **28** are listed in Table 3.4.

Table 3.4: *Selected distances (Å) and angles (º) for **28**.*

	$(1\text{-MeC})_a$	$(1\text{-MeC})_c$	$(1\text{-MeC})_b$	(pyz)
Pt1-N	2.046(5)	2.037(5)	2.042(5)	2.020(5)
Ag1-N4				2.306(7)
N3B-Pt1-N1	179.0(2)			
N3B-Pt1-N3A	90.8(2)			
N1-Pt1-N3A	90.2(2)			
N3B-Pt1-N3C	91.1(2)			
N1-Pt1-N3C	88.0(2)			
N3A-Pt1-N3C	175.5(2)			
O2B···N4A	2.921(7)			
O2B···N4C	2.974(7)			
N4B···O2A	2.936(7)			
N4B···O2C	3.155(7)			

The most significant difference with respect to **27** (in addition to the presence of the silver atom) concerns the dihedral angles between the aromatic rings of the ligands (1-MeC, pyz) and the coordination plane of Pt: 89.5(2)º $(1\text{-MeC})_a$, 86.3(2)º $(1\text{-MeC})_b$, 77.6(1)º $(1\text{-MeC})_c$, and 71.9(2)º (pyz). In this case, only two dihedral angles, those of the pyrazine ring and $(1\text{-MeC})_c$, display a remarkable deviation from 90º. Thus, the dihedral angle between *trans* positioned ligands is 12.2(4)º in the case of the cytosine bases, and 21.9(3)º in the case of the angle between $(1\text{-MeC})_b$ and (pyz).

The $[Pt(1\text{-MeC-}N3)_3(pyz)Ag]^{3+}$ cations are forming dimers in the solid state. Two cationic entities are joined via the Ag atoms, with a inter-metallic distance Ag···Ag(-x, -y+1, -z) of 3.844(2) Å. It could be the consequence of an

"argentophilic" interaction between two silver ions. The angle N4-Ag1-Ag1* is 104.4(2)º. The usual two-fold linear coordination of the Ag^+ cation is not observed in this case; in addition to the N4 nitrogen atom and Ag(-x, -y+1, -z), the sphere of coordination of Ag is completed by some interactions with the oxygen atoms of the nitrate counterions. Thus, the Ag···O distances are: Ag···O11, 2.606(11) Å; Ag···O12, 2.593(10) Å; Ag···O22, 2.417(11) Å; Ag···O21, 2.456(13) Å. A view of this dimer is depicted in Figure 3.8.

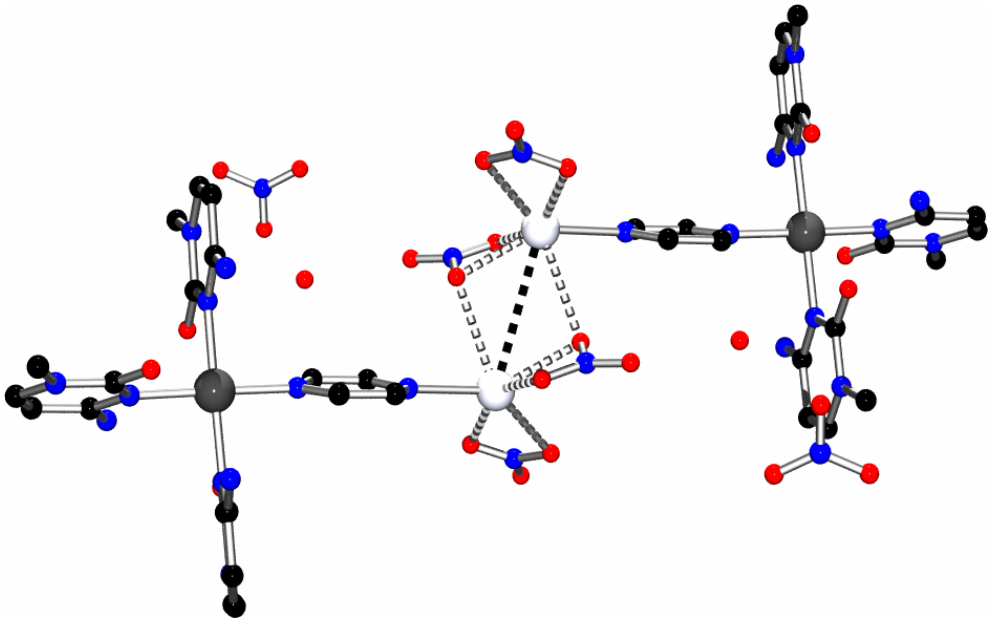

Figure 3.8: *View of two neighboring $[Pt(1\text{-}MeC\text{-}N3)_3(pyz)Ag]^{3+}$ cations. The silver atom is bonded to the pyrazine, and shows an Ag···Ag interaction.*

The geometrical orientations of the three 1-MeC rings in **28** allow for intra- and inter-molecular hydrogen bonding between exocyclic groups. In the case of the intramolecular hydrogen bonding, O2B forms hydrogen bonds with the amino groups of the other two bases: O2B···N4A (2.921(7) Å) and O2B···N4C (2.974(7) Å); on the other site, N4B is also involved in hydrogen bonds: N4B···O2A (2.936(7)Å), and N4B···O2C (3.155(7)Å). In the case of the intermolecular hydrogen bonding, O2B in also involved in a inter molecular hydrogen bond with the N4C amino group of a neighbor unit cell (-x+1, -y, -z), forming a distorted O2B···N4C···O2B···N4C tetrad. The distance between both atoms is 2.827(6) Å (see Figure 3.9).

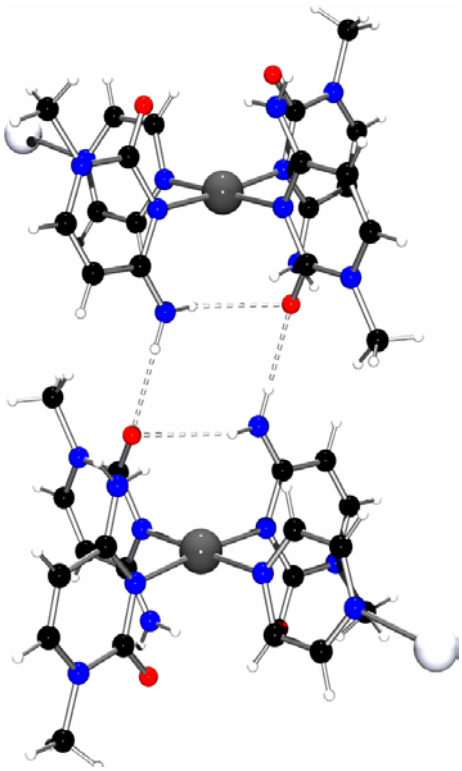

Figure 3.9: *View of intermolecular H bonding between symmetry-related pairs of* ***28****.*

The water molecule of crystallization is placed between the cytosine rings and interacts only with the nitrate anions: O1w···O23(-x, -y+1, -z), 2.717(2) Å; and O1w···O33(x, y, z-1), 3.089(19) Å. The packing of the cationic dimers $[Pt(1\text{-}MeC\text{-}N3)_3(pyz)Ag\cdots Ag(pyz)(1\text{-}MeC\text{-}N3)_3Pt]^{6+}$ is in a zig-zag arrangement; no π-stacking is observed between the aromatic rings.

4.- Cationic Tetrakis(nucleobase) Complexes of Pt^{II} as Metalloligands and Potential Building Blocks for Molecular Architectures.

Complexes of square-planar transition metal ions (M) with four heterocyclic ligands (L) carrying additional functionalities are potential building blocks for supramolecular architectures involving hydrogen bond formation, cation binding, or anion binding (Scheme 4.1).

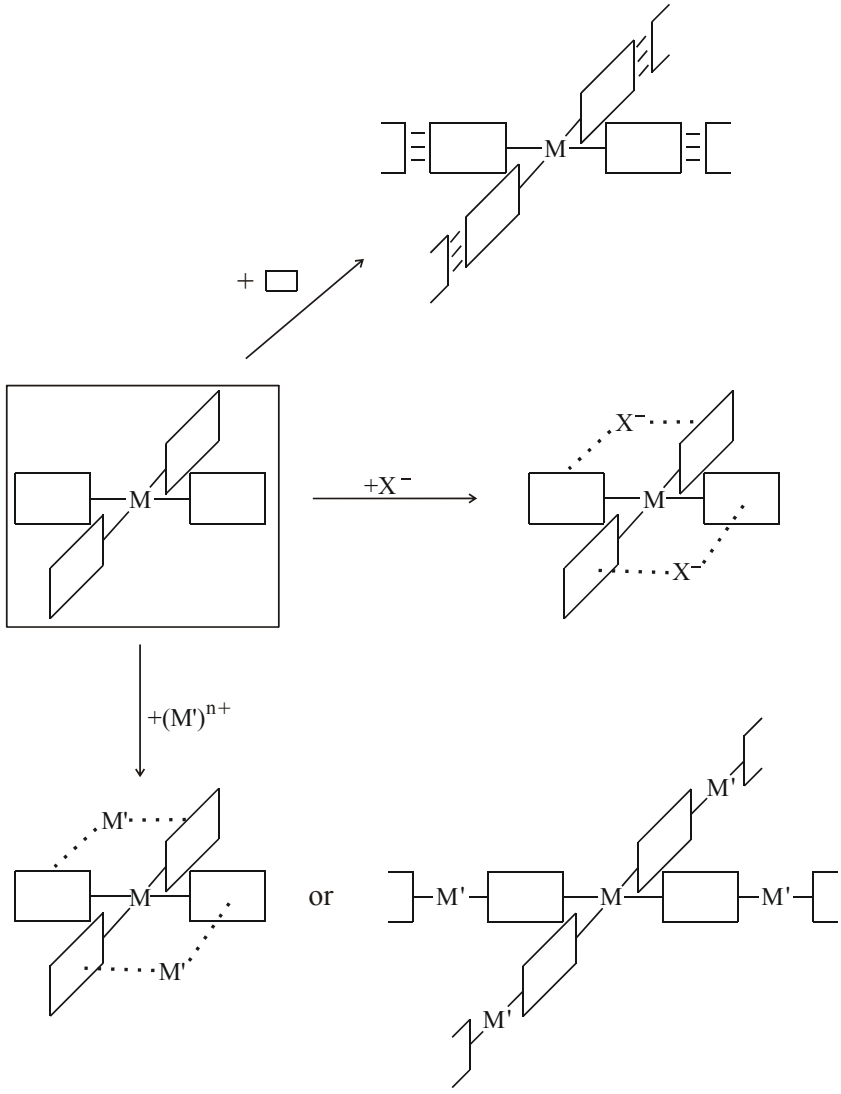

Scheme 4.1: *The tetrakis(nucleobase) M^{II} complex as potential building block in supramolecular chemistry.*

For example, homoleptic [141,142] $[PtL_4]^{2+}$ and dinuclear $[Pd_2L_4]^{2+}$ complexes [143] have been shown to act as anion receptors, and numerous coordination polymers are known which display ML_4 motifs [144-147]. As to homoleptic ML_4 compounds with L being a nucleobase, several examples have been prepared [110,148-150] and characterized by X-ray crystal structure analysis [110,144-150]. These are $[Pt(9\text{-MeGH})_4]Cl(CF_3CO_2)$ [149], $[M(1\text{-MeC})_4]X_2$ (M= Pd^{II}, X=NO_3^- [150]; Pt^{II}, X=NO_3^- and Cl^- [110]; Cu^{II}, X=ClO_4^- [151]), and $M_2[Pd(1\text{-MeU})_4]^{2-}$ (M= Na^+, K^+, Cs^+) [152]. With unsubstituted cytosine, two salts of a Cu^{II} compound have also been reported [153,154]. Of the various possibilities outlined in Scheme 4.1, only heterometal binding has been studied, to anionic $[Pt(1\text{-MeU})_4]^{2-}$ [152] and to $[M(1\text{-MeC})_4]^{2+}$, which in essence results in deprotonation of all four 1-MeC ligands (at the exocyclic N4 position) and hence reveals the likewise anionic $[Pt(1\text{-MeC})_4]^{2-}$ species as the metalloligand [110]. Of the examples described, the trinuclear $Cu^{II}Pt^{II}Cu^{II}$ derivatives are unique in that they are diamagnetic as a result of a strong exchange interactions between the Cu spins over a distance of 5 Å, with Pt^{II} mediating this process [110].

In this chapter it is reported, among others, on a formally pentanuclear Cu-Pt-Cu-Pt-Cu chain compound isolated upon addition of Cu^{II} to the cationic $[Pt(9\text{-MeHxH})_4]^{2+}$ complex. The feature of “complex cation binds cation”, while not unprecedented in metal nucleobase chemistry [155-158], is certainly noteworthy.

Concerning the utilization of guanine containing complexes for self-recognition and complementary hydrogen bonding with cytosine, they add to a group of compounds, for which recently such possibilities have demonstrated, e.g. for compound $[Pt(NH_3)(9\text{-EtGH-}N7)_3]^{2+}$, and which is capable of forming a supramolecular aggregate consisting of two metal ions and ten nucleobases [159].

4.1.- Tetrakis(nucleobase) Complexes of Pt^{II}.

Three cationic tetrakis(nucleobase) complexes of Pt^{II} have been studied: $[Pt(9\text{-MeHxH-}N7)_4](NO_3)_2 \cdot H_2O$ (**29**), $[Pt(9\text{-EtGH-}N7)_4](NO_3)_2 \cdot 2KNO_3 \cdot 5H_2O$ (**30**), and *trans*-$[Pt(1\text{-MeC})_2(9\text{-EtGH-}N7)_2](NO_3)_2$ (**31**). The X-ray crystal structure of (**29**) has been determined. All three cationic compounds rapidly react with Hg^{II}, but gel formation prevented an adequate characterization of the products formed. However, a Cu^{II} adduct of (**29**) was isolated in crystalline form and characterized crystallographically.

The complexes **29** and **30** were obtained through direct reaction of $K_2[PtCl_4]$ and the respective nucleobases, followed by anion replacement by means of $AgNO_3$. **31** was prepared via *trans*-$[Pt(1\text{-MeC-}N3)_2I_2]$ (**21**) [1,2,110] and subsequent reaction with $AgNO_3$ and 9-EtGH.

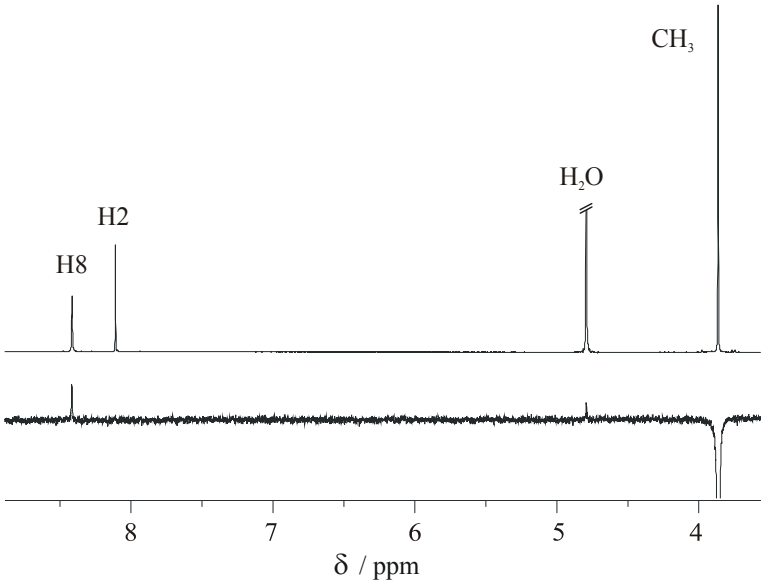

Figure 4.1: *1D-NOE NMR experiment (irradiation at the CH_3 resonance) with aqueous solution of **29** leading to the assignment of H2 and H8 resonances.*

The three compounds were characterized by elemental analysis, ^1H NMR spectroscopy, and in the case of **29** also by X-ray crystallography. The ^1H NMR spectra of the three complexes are consistent with *N7* metal coordination of 9-methylhypoxanthine and 9-ethylguanine as well as binding of Pt to N3 of 1-MeC.

In D_2O, signals due to coordinated 9-MeHxH **29** are singlets for all three observable protons. The differentiation of the two aromatic protons was achieved by a 1D-NOE experiment (Figure 4.1), which is based on the different proximities of the aromatic protons from the methyl group at N9.

Chemical shifts δ of the individual protons in D_2O, pD 4.5 are 8.49 (H8), 8.18 (H2) and 3.79 (CH_3) with NMe_4^+ as standard. The use of TSP as an internal standard gave slightly higher chemical shifts (0.03 - 0.05 ppm), depending on the amount of standard present. In other words, the $Si(CH_3)_3$ resonance of TSP was shifted upfield, indicating that there was some interaction with the cation of **29** and that TSP was no longer useful as a reference. Concomitant with this shift, there was also a definite broadening of this resonance observed, which was not seen with the $N(CH_3)_4^+$ standard. This feature of TSP was previously observed in our group [160]. It also applies to compound **30** and the mixture of **30** and 1-methylcytosine (see below). In DMSO-d_6 the resonances of **29** are observed at δ 12.67 (d, N1(H), ^3J (H-H) 4 Hz), 8.60 (s, H8), 8.16 (d, H2), and 3.73 (t, CH_3). The splitting of both the N1(H) and one of the aromatic protons unambiguously permits a differentiation between the two aromatic protons (See Figure 4.2). Neither in D_2O nor in DMSO-d_6 is coupling of the H8 proton with the ^{195}Pt isotope at N7 observed.

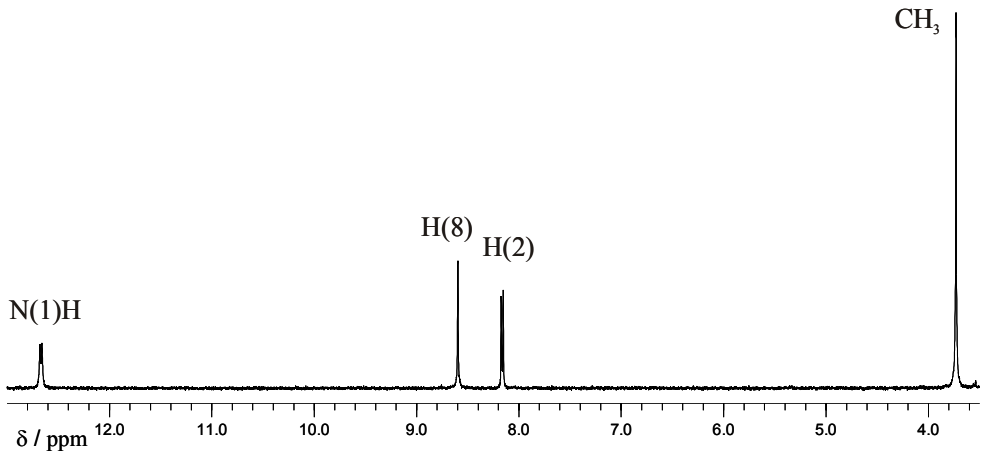

Figure 4.2: *^1H NMR spectrum of **29** (DMSO-d6).*

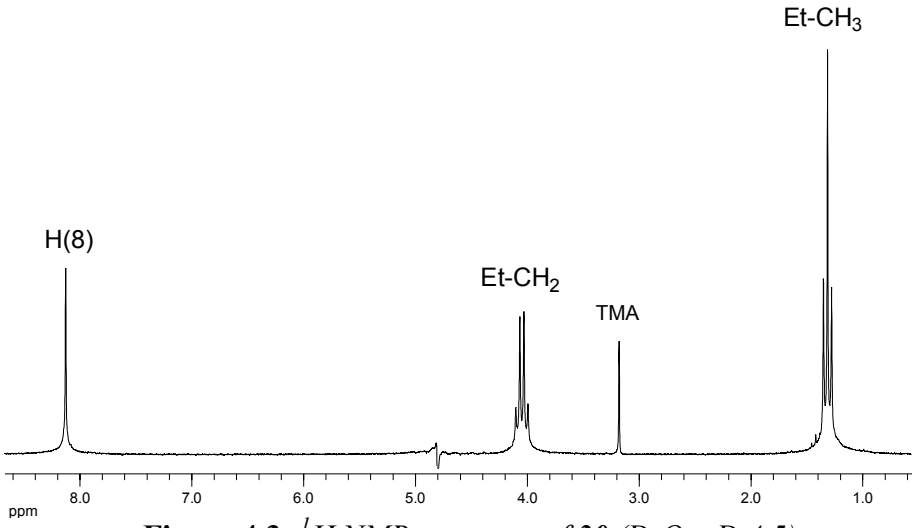

Figure 4.3: *^{1}H NMR spectrum of **30** (D_2O, pD 4.5).*

Compound **30** displays its ^{1}H resonances in D_2O (pD 4.5, NMe_4^+ as internal reference) at δ 8.13 (s, H8), 4.05 (q, CH_2) and 1.32 (t, CH_3). Again, TSP proved not useful as a standard (see Figure 4.3). In DMSO-d_6, the ^{1}H resonances of **30** are observed at δ 10.85 (s, N1(H)), 8.25 (s, H8), 6.69 (s, N2(H_2)), 4.01 (q, CH_2) and 1.27 (t, CH_3).

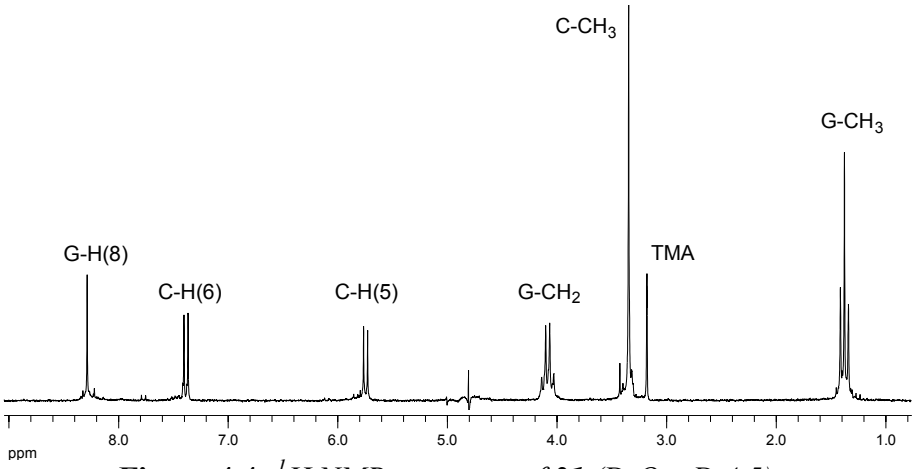

Figure 4.4: *^{1}H NMR spectrum of **31** (D_2O, pD 4.5).*

The ^{1}H NMR spectrum of **31** in D_2O (pD 4.5) has its resonances at δ 8.29 (s, H8 of 9-EtGH), 7.38 (d, ^3J (H-H) 7.4 Hz, H6 of 1-MeC), 5.75 (d, H5 of 1-MeC), 4.09 (q, CH_2 of 9-EtGH), 3.35 (s, CH_3 of 1-MeC), and 1.38 (t, CH_3 of 9-EtGH) with relative intensities as expected (See Figure 4.4). In DMSO-d_6, shifts

are as follows for 9-ethylguanine resonances: δ 11.29 (s, N1(H)), 8.23 (s, H8), 6.95 (s, N2(H_2)), 4.09 (q, CH_2), and 1.28 (t, CH_3). 1-Methylcytosine resonances are observed at δ 9.21 and 8.65 (s each, 1:1, N2(H_2)), 7.59 (d, ^3J (H-H) 7.4 Hz, H6), 5.60 (d, H5), and 3.26 (s, CH_3).

4.1.1.- $[Pt(9\text{-}MeHxH\text{-}N7)_4](NO_3)_2 \cdot H_2O$ (29).

Colorless crystals were picked from a solution containing $[Pt(9\text{-}MeHxH\text{-}N7)_4]^{2+}$. X-ray crystallography in **29** reveals nitrate counterions and a water of crystallization in the structure. Crystal data, data collection and refinement parameters for **29** are summarized in Table A-29 (see Appendix).

The coordination geometry of the Pt atom is square-planar, with a measurable distortion toward tetrahedral. Thus N7-Pt-N7 angles between *trans* positioned bases deviate markedly from linearity and are 173.8(2) and 172.5(2)º, respectively. The tetrahedral distortion is nevertheless not nearly as pronounced as in $[Pt(PEt_3)_4](ClO_4)_2$ [161]. A list of selected distances and angles of **29** is given in Table 4.1.

Table 4.1: *Selected distances (Å) and angles (º) for* ***29****.*

	a	b	c	d
Pt-N7	2.016 (4)	2.000 (4)	2.007(4)	2.004 (4)
C6-O6	1.215 (6)	1.226 (6)	1.212 (6)	1.221 (7)
Pt-N4/9-MeHxH	82.6 (1)	87.2 (1)	86.1 (1)	83.5 (1)
C2-N1-C6	126.2 (5)	124.3 (5)	125.1 (5)	125.3 (6)
C2-N3-C4	111.5 (5)	110.3 (5)	110.9 (5)	111.1 (5)
O6-O1w		2.675(6)		2.895(8)

	ab	bc	cd	da	ac	bd
N7-Pt-N7	91.1 (2)	88.9 (2)	89.4 (2)	91.3 (2)	173.8 (2)	172.5 (2)

As evident from Figure 4.5, the four nucleobases are almost perpendicular to the PtN_4 coordination plane, with dihedral angles ranging from 82.6(1) to 87.2(1)º.

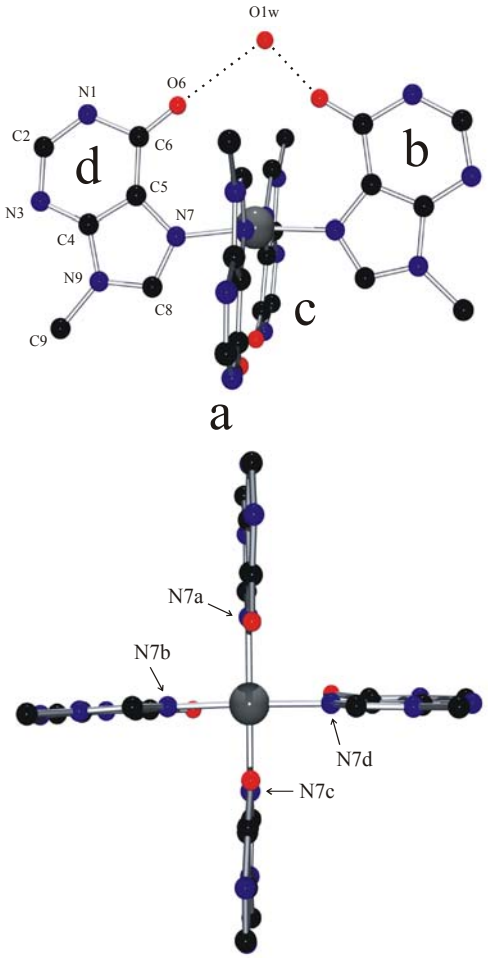

Figure 4.5: *Side view (top) of cation **29** with hydrogen bonded water molecule (O1w), and top view (bottom) with water molecule omitted.*
The orientation of the four purine bases is head-tail-head-tail.

The exocyclic O6 atoms of rings b and d are linked by a water molecule (O1w) with H bonds of 2.675(6) Å and 2.895(8) Å, respectively, leading to a separation of 3.627(6) Å between these two exocyclic groups. In contrast, the O6 atoms of the two other rings (a, b) do not display this pattern and approach each other more closely (O6a···O6b, 3.423(6) Å).

The four 9-methylhypoxanthine ligands are neutral and hence protonated at their N1 positions. All four protons at the N1 sites were found during refinement. Internal ring angles at N1 and N3 positions agree with expectations concerning relative sizes. Thus, whereas the four protonated sites have angles [C6-N1-C2] between 124.3(5) and 126.2(5)º, the four deprotonated N3 sites have smaller angles, ranging from 110.3(5) to 111.5(5)º. The analogous angles in the free base are 124.7(1) and 110.6(1)º, respectively [74].

With regard to supramolecular chemistry, the four bases are in principle capable of engaging in donor-acceptor interactions through N1, O6 and even C2 positions with adjacent molecules. The first base, $(9\text{-MeHxH})_a$, interacts via H bond formation with its symmetrical base of the neighbor entity. On the basis of H bond lengths, H bonding is to be considered moderately strong, displaying distances of 2.711(6) Å between N1a and O6a' as well as O6a and N1a' sites. In the case of the bases $(9\text{-MeHxH})_b$ and $(9\text{-MeHxH})_c$, nitrate counter anions block these positions by H bonding to the nucleobases. Distances between protonated N1b and O1n and O2n of nitrate are 2.820(9) and 3.120(8) Å, respectively. The neighboring C2b has a distance of 3.161(9) Å with O2n of the same nitrate. Corresponding distances in $(9\text{-MeHxH})_c$ are N1c···O5n 2.914(7) Å, N1c···O6n 3.049(8) Å, C2c···O6n 3.048(10) Å. The very short distance of O6b to the water molecule, 2.675(6) Å, should be pointed out. The fourth base $(9\text{-MeHxH})_d$ has only H-bonding interactions with water molecules: N1d···O1w 2.760(8) Å, O6d···O1w' 2.895(8) Å.

4.1.2.- $\{[(H_2O)Cu(9\text{-MeHxH})_4Pt]_2Cu(ClO_4)_4\}(ClO_4)_2(NO_3)_4 \cdot 6H_2O$ (32).

Crystals of $\{[(H_2O)Cu(O6\text{-}9\text{-MeHxH-}N7)_4Pt]_2\ Cu(ClO_4)_4\}\ (ClO_4)_2(NO_3)_4 \cdot 6H_2O$ (**32**) were obtained after addition of $Cu(ClO_4)_2$ to an aqueous solution containing **29**. The originally colorless solution changed to blue and then yellow.

In the X-ray refinement process, all non-hydrogen atoms were refined anisotropically, except Cu2. Crystallographic data and details of refinement of **32** are summarized in Table A-32.

$[\{(H_2O)Cu(9\text{-}MeHxH)_4Pt\}_2Cu(ClO_4)_4](ClO_4)_2(NO_3)_4 \cdot 6H_2O$ (**32**) crystallizes in a centrosymmetric Cu-Pt-Cu-Pt-Cu chain structure with Cu-Pt separations of 2.791(1) Å (outside) and 3.8980(9) Å (inside). Two of the three Cu^{II} ions are bound via exocyclic O6 sites of the Hmhyp nucleobases. At neutral and moderate alkaline pH both **29** and **30** form virtually insoluble precipitates, which redissolve at strongly alkaline pH to give eventually anionic $[Pt(L)_4]^{2-}$ species (L = 9-MeHx, 9-EtG). Finally, **30** interacts with complementary 1-MeC to give Watson-Crick associates, as demonstrated by ^1H NMR spectroscopy in DMSO-d_6.

As we have previously demonstrated in numerous cases, cationic Pt^{II} complexes of nucleobases frequently have the ability to bind additional metal *cations* via exocyclic groups of the bases [155-158,162]. Among others, we found that the dipositive compound *trans*-$[Pt(NH_3)(9\text{-}EtGH\text{-}N7)_2(1\text{-}MeC\text{-}N3)]^{2+}$ binds Na^+ via the exocyclic carbonyl oxygen atoms of the three bases. Here we show that the dipositive cation **29** with its four neutral 6-oxopurine ligands is capable of binding a dipositive Cu^{II} cation to give a heteronuclear $[Pt(N7\text{-}9\text{-}MeHxH\text{-}O6)_4Cu]^{4+}$ cation with a charge of +4. Two of these cations are further weakly connected by a third Cu^{II} ion at midpoint between the two dinuclear entities, thereby generating an array of five metal ions in **32**. The cation is centrosymmetric with Cu(2) in its center. The positive charge of this third Cu^{II} is, of course, more than compensated by the four perchlorate anions bound to it, and consequently this entity may be also considered a tetrakis(perchlorato) cuprate (II) species. Figure 4.6 gives a view of this arrangement. Salient structural features of **32** are provided in Table 4.2.

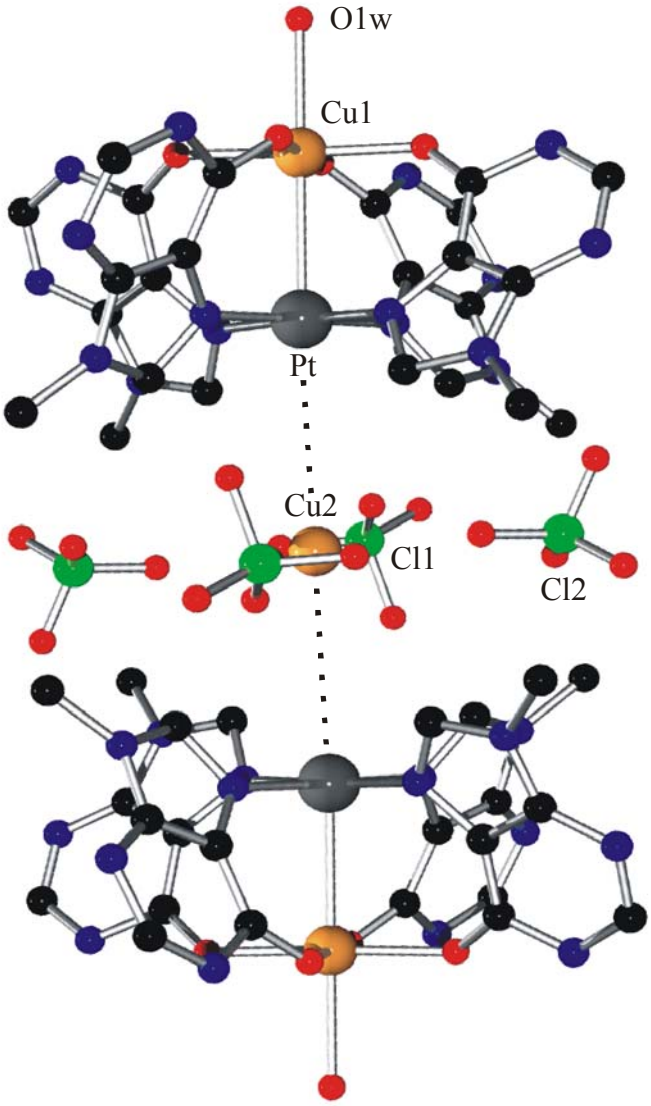

Figure 4.6: *View of Cu···Pt···Cu···Pt···Cu array seen in* ***32****.*
For assignment of atoms of purine bases see Figure 4.7.

Table 4.2: *Selected distances (Å) and angles (°) for* ***32****.*

	a	b	c	d
Pt-N7	2.002(6)	2.010(6)	2.020(6)	2.009(6)
Cu1-O6	1.980(5)	1.960(5)	1.969(5)	1.958(5)
C6-O6	1.269(9)	1.265(9)	1.261(9)	1.280(9)
PtN_4/9-MeHxH[a]	64.5(2)	63.6(2)	61.8(2)	64.5(2)
C2-N1-C6	125.1(8)	124.6(8)	124.6(8)	124.1(7)
C2-N3-C4	111.0(7)	111.4(7)	111.2(7)	110.7(7)
C9-O (ClO_3)	O41 3.21(2)	O22 3.03(1)	O42 2.99(2)	O21 3.11(1)
	O22 3.25(2)	O42 3.24(2)	O43 3.35(2)	O41 3.30(2)
C8-O(ClO_3)	O12 3.11(1)[b]	O44 2.80 (3)	O24 3.06(2)	O41 2.30(2)
	O24 3.28(2)		O11 3.23(1)[b]	O23 3.27(1)

	ab	bc	cd	da	ac	bd
N7-Pt-N7	90.1(3)	89.8(3)	89.9(3)	90.2(2)	178.2(3)	179.2(3)
O6-Cu1-O6	89.6(2)	89.6(2)	90.0(2)	90.7(2)	178.1(2)	177.7(2)

Cu1-O1w	2.291(6)	
Pt-Cu1	2.791(1)	
Pt-Cu2	3.8980(9)	
Pt-Cu1-O1w	175.7(2)	
Cu1-Pt-Cu2	176.4(2)	
Cu2-O(ClO_3)	O24 2.66(2)	O44 2.89(1)
O24-Cu2-O44	82.4 (8)	
O24-Cu2-O44'	97.6(8)	

[a] *Dihedral angle between Pt coordination plane (Pt-N_4) and Hmhyp.*

[b] *Contacts to other ClO_4^- anions (not shown) which are not involved in Cu2 bindings.*

Two views of the dinuclear Pt-Cu(1) entity are depicted in Figure 4.7. In Pt-Cu(1) the four 9-MeHxH ligands adopt *head-head-head-head* orientations (cone conformation) to provide a coordination sphere of four O6 donors for Cu^{II}. Two of the purine bases thus have undergone rotation from their orientation in the starting compound **29**. A water molecule in the apical position completes the coordination sphere of Cu(1). The second apical position is taken by the Pt. The equatorial Cu-O6 distances vary between 1.958(5) and 1.980(5) Å, the distance

to the water ligand is 2.291(6) Å and the distance to Pt is 2.791(1) Å. Angles involving metals in the central part are 175.7(2)º for H_2O-Cu(1)-Pt and 176.4(2)º for Cu(1)-Pt-Cu(2).

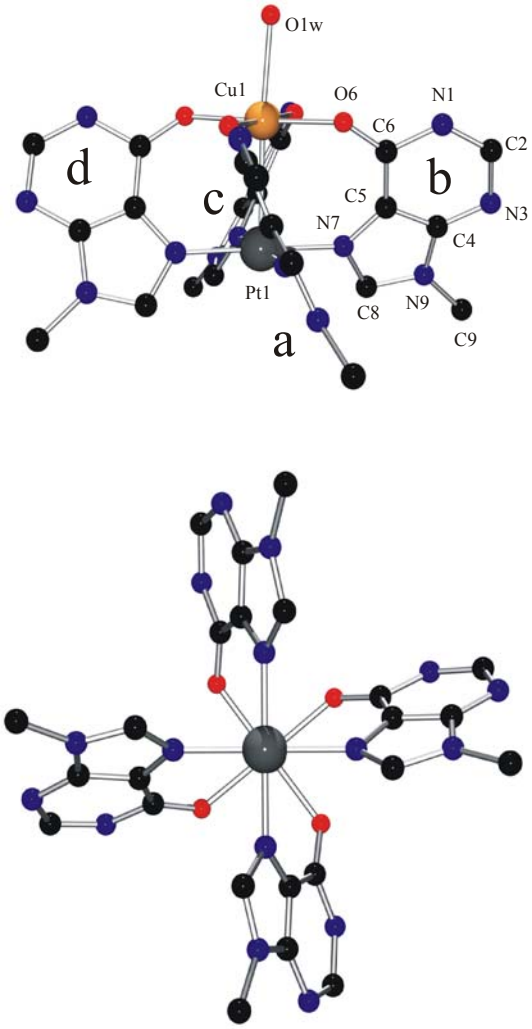

Figure 4.7: *Side view (top) and top view (bottom) of Pt, Cu entity in* ***32****.*

These distances suggest that the coordination geometry of the Cu is to be described as an octahedron with tetragonal distortion, with the unpaired electron of Cu^{II} occupying the $d_{x^2-y^2}$ orbital, pointing toward the four O6 oxygen atoms. The Pt-Cu contact is closely similar to that found in the 1-methyluracilate bridged compound *cis*-$[(NH_3)_2Pt(1\text{-}MeUH)_2Cu(H_2O)_2]SO_4 \cdot 4.5H_2O$ (2.765(3)Å) [163], and Cu-O distances are likewise similar. Although in trinuclear PtCuPt complexes with CuO_4 coordination and Pt···Cu contacts the distances between the metals are somewhat shorter (2.681(1)Å [158] and 2.685(1)Å) [164]), the situation is still

comparable. However, it is in strong contrast to those nucleobase complexes where Pt → Cu dative bond formation is occurring, which results in short Pt-Cu bonds of 2.50 - 2.56 Å [165,166]. The ligating groups of the Cu^{II} entity are likewise different in these cases and include exocyclic amide functions of bridging 1-methylcytosinate residues.

A view along the Cu(1)-Pt axis (see Figure 4.7) reveals that the $PtCu(1)(9\text{-MeHxH})_4$ unit is chiral, with a twist angle of 38.0(2)º about the Pt-Cu(1) vector (N7-Pt-Cu(1)-O6). It is evident that any reduction in this angle toward an eclipsed arrangement as seen in **29** (see Figure 4.5) will lead to a lengthening of the Pt-Cu(1) contact. The dihedral angles between the 9-MeHxH planes and the PtN_4 planes are between 61.8(2) and 64.5(2)° in **32** compared to values of 82.6(1) - 87.2(1)° in **29**.

The introduction of a second transition atom into the coordination sphere of the platinum distorts the geometry of the mononuclear tetrakis(nucleobase) complex. In contrast to the mononuclear complex **29**, in the heteronuclear complex **32** the Pt atom does not display a distortion toward tetrahedral. Rather Pt is located slightly (0.019 Å) out of the plane defined by the four N7 atoms, directed toward the copper atom. Cu is likewise placed below the plane defined by the four O6 atoms (0.032 Å), and again directed toward the platinum atom.

Binding of a Cu^{II} ion to the hypoxanthine nucleobase via O6 has no major structural consequences for the base geometry, except for the C6-O6 entity. Thus, there is a lengthening observed for the C6-O6 distances in **32** (1.261(9) - 1.280(9) Å) as compared to those in **29** (1.212(6) - 1.226(6) Å), accompanied by a trend to modest enlargement of the C5-C6-O6 angles in the coordinated carbonyl group of **32** (128.6(7) – 130.1(7)º) with respect to the free ones in **29** (126.4(6) – 130.1(6)º).

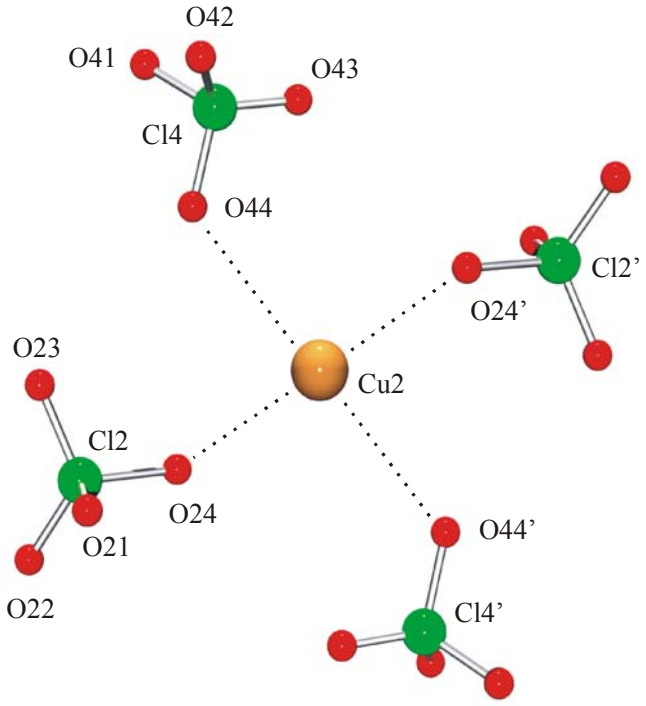

Figure 4.8: *Coordination geometry of central Cu2 in* ***32****.*

The central Cu(2) ion displays a distortred square-planar coordination geometry, with four oxygen atoms from four different ClO_4^- anions representing the donor atoms (Fig. 4.8). The distortion of the Cu(2) coordination sphere is toward a parallelogram.

Angles about Cu(2) are 82.4(8) and 97.6(9)°, and Cu-O distances are 2.66(2) and 2.89(1) Å. As pointed out, the whole entity may also be considered a tetrakis(perchlorato)cuprate(II) anion. It is nestled between the hydrophobic ends (C8-C9-C10) of the two $[PtCu(1)(9\text{-}MeHxH)_4]^{4+}$ cations, as indicated in Figure 4.9.

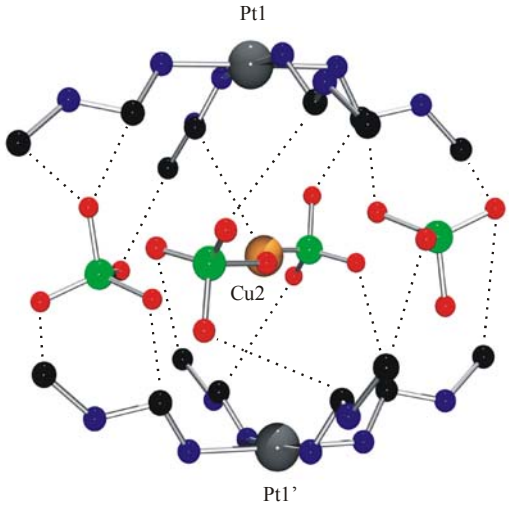

Figure 4.9: *Detail of "capture" of* $[Cu(ClO_4)_4]^{2-}$ *by the two cationic* $[(OH_2)CuPt(9\text{-}MeHxH)_4]^{4+}$ *entities. Only N7-C8-N9-C9 fragments of the eight 9-MeHxH rings are shown.*

Apart from attractive anion-cation interactions between the perchlorate anions and the dinuclear PtCu(1) cations, there are also several hydrogen bonds between H8 protons of the purine bases and perchlorate oxygen atoms. The shortest C8···$OClO_3^-$ distance is 2.80(3)Å. The Pt-Cu(2) separation is expectedly rather long, 3.8980(9) Å.

Pentanuclear cations and anions form layers, which are separated by sheets of water molecules.

4.1.3.- Nucleobase Deprotonation.

Typically, N7 platinum binding to 6-oxopurine bases shifts the pK_a value of the N1 proton to ca. 8 [78,162], and NMR spectroscopy is in general an excellent tool to monitor the nucleobase protonation state. However, attempts to follow deprotonation of 9-methylhypoxanthine and 9-ethylguanine nucleobases in **29** and **30** by pD dependent ^{1}H NMR spectroscopy was not possible in the pD range 7 – 10. In this range **29** and **30** proved virtually insoluble and no ^{1}H NMR spectra could be reported. In the acidic pD range these compounds were well

soluble and nucleobase resonances remained at constant chemical shifts (e.g. δ H8 of 9-EtGH in **30**, 8.13), as was the case at strongly alkaline pD (10.0), with shifts upfield then (H8 of 9-EtGH, 8.01 ppm). It can be anticipated that complexes of composition $[Pt(9\text{-MeHxH})_2(9\text{-MeHx})_2]$ (**29'**) and $[Pt(9\text{-EtGH})_2(9\text{-EtG})_2]$ (**30'**) are of low solubility due to their neutrality, whereas anionic species of composition $[PtL_3(LH)]^-$ and $[PtL_4]^{2-}$ (with L = 9-MeHx or 9-EtG) become soluble again. However, the fact that virtual insolubility of **29** and **30** was already observed at pD values (e.g. 7), where at most partial deprotonation of 9-MeHxH and 9-EtGH could have been expected, calls for additional explanations. It feet that, at least in the case of the 9-EtGH complex **30**, the possibility of formation of hydrogen bonded intermolecular aggregates should be considered, as it could contribute to the poor solubility of this compound at neutral and moderately acidic pH. Neutral 9-EtGH and anionic 9-EtG are complementary as far as hydrogen bonding between their Watson-Crick faces is concerned (Scheme 4.2) and consequently can engage in multiple pairing patterns [159,167].

As schematically outlined in Scheme 4.2, oligomers can form even at stoichiometries of **30**: $OH^- \leq 1$. After addition of one equivalent of base per **30** formation of a H-bonded polymer can be envisaged, as is the case upon addition of two more equivalents of base. The presence of added 1-MeC (see part 4.1.5 of this chapter) had no effect whatsoever on this behavior. In fact, as confirmed by integration of 1-MeC and reference signals, the precipitate did not contain any of the 1-MeC added.

One of the objectives of this work at its onset was to try to generate supramolecular aggregates of tetrakis(nucleobase) complexes of Pt^{II} by means of cross-linking via linear metal entities such as Hg^{II}, for example. On the basis of our earlier observations [35,168,169] that M-N vectors in N7,N1 dimetalated purines are frequently perpendicular to each other, and our findings with the *head-tail-head-tail* orientation of the purines in **29**, we reasoned that it might be possible to obtain strings of mixed Pt, Hg complexes (Scheme 4.3). Unfortunately all our attempts have failed thus far, due to poor solubility of the products and the formation of gels.

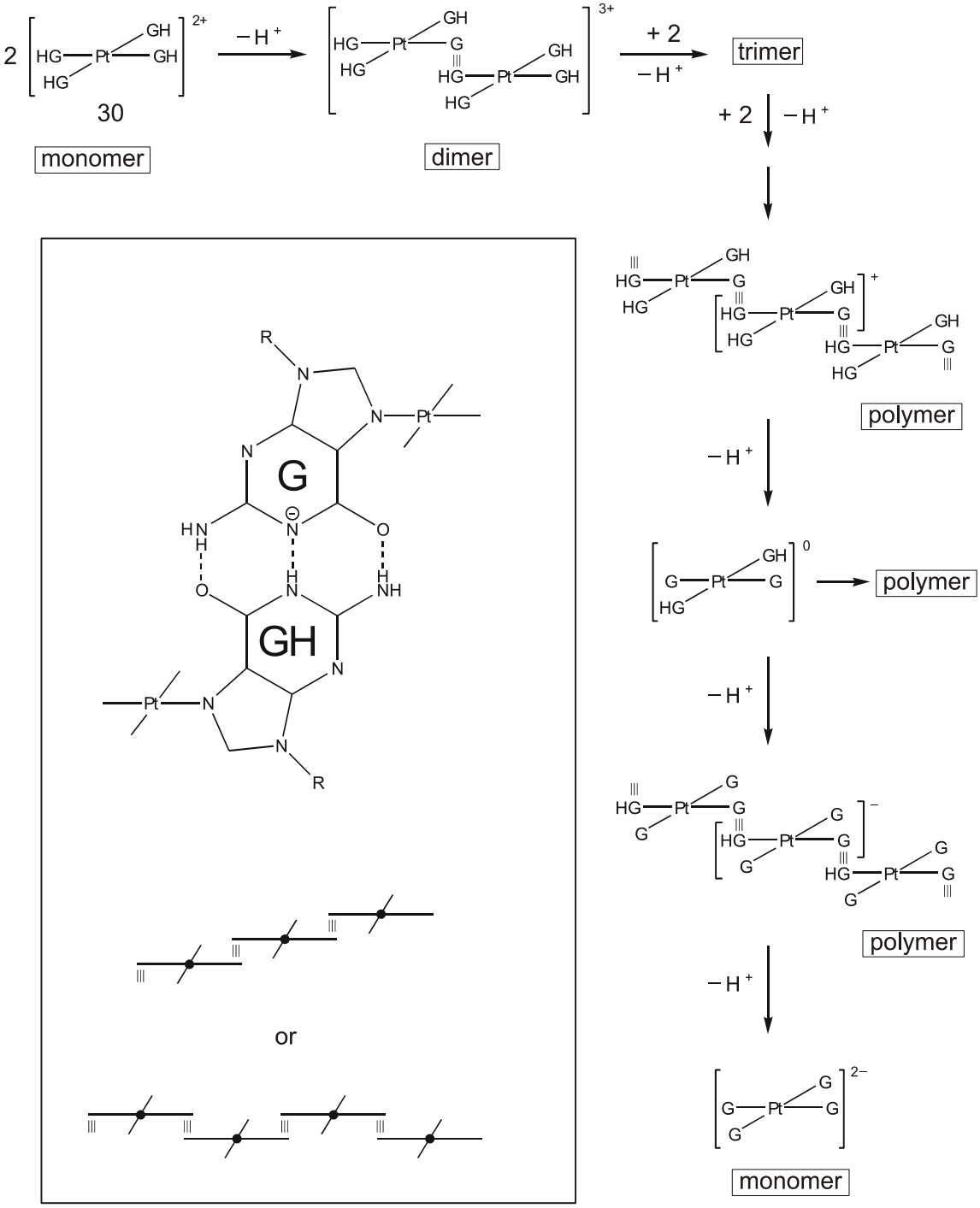

Scheme 4.2: *Association of PtG_4 complexes via H-bonding.*

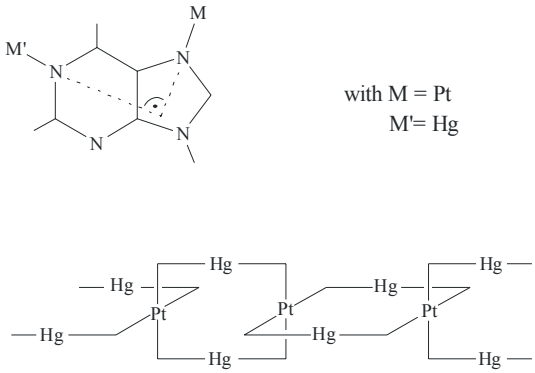

***Scheme 4.3**: Mutually orthogonal arrangement of purine bases with metal binding via N1 and N7.*

4.1.4.- Interactions of 29-31 with $Hg(CH_3COO)_2$.

It was only possible to follow the reaction of **29**-**31** with $Hg(CH_3COO)_2$ by ^1H NMR spectroscopy during the first minutes after mixing. Then precipitation took place with no resonances detectable any more. Both with **29** and **30**, addition of 0.5 equiv of the Hg^{II} salt resulted in formation of a new compound with its aromatic protons (H2 and H8 of 9-MeHxH in **29**, H8 of 9-EtGH in **30**) shifted upfield relative to those of **29** and **30** by 0.12 - 0.15 ppm. The splitting (ca. 1:2) of the shifted aromatic protons of **29** could indicate the presence of different rotamers. The methyl (**29**) and ethyl resonances (**30**) were hardly affected ($\Delta\delta \leq 0.02$ pmm). The latter findings definitely rule out any metal binding to N3 of these nucleobases, because such a binding pattern should have caused dramatic downfield shifts of the alkyl resonances [170,171]. The observed upfield shifts support the view that nucleobase deprotonation has occurred, with Hg^{II} binding most likely via N1 sites.

A different situation was envisaged when $Hg(CH_3COO)_2$ (0.5 equiv) was added to a solution of **31** (see Figure 4.10). In the new compound formed, H5 of 1-MeC was affected most strongly and was downfield shifted by 0.24 ppm, whereas H6 of this ligand was shifted upfield by 0.1 ppm. H8 of guanine was least influenced and underwent a very minor upfield shift of 0.03 ppm only.

These findings tentatively suggest that Hg^{2+} interacts, at as least initially, with the cytosine nucleobase of **31** at the exocyclic amino group and/or the exocyclic carbonyl group. However, the simplicity of the new set of resonances rules against a mixed N4,O2 pattern in a hypothetical dinuclear PtHg complex. It is also noted that the shift pattern is not identical with that of *trans*-$[(MeNH_2)_2Pt(1\text{-}MeC)_2Hg]^{2+}$, where deprotonation of the exocyclic amino group of 1-methylcytosine and subsequent Hg^{II} cross-linking causes upfield shifts of both H5 (0.18 ppm) and H6 (0.3 ppm) [172].

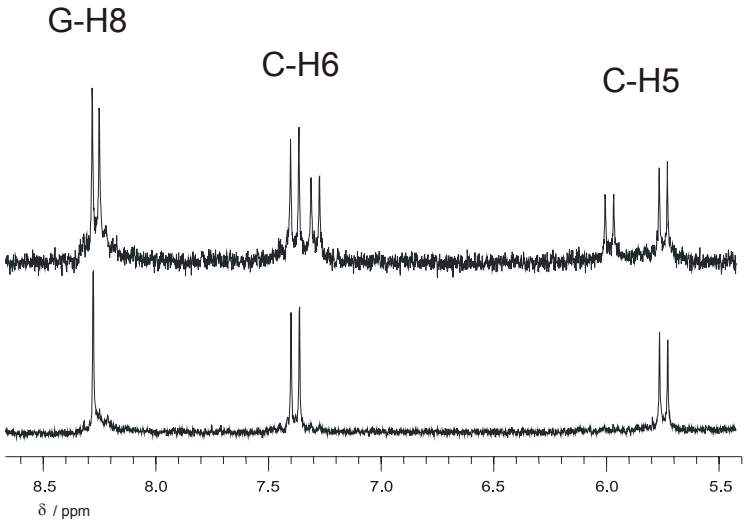

Figure 4.10: *Lowfield ^1H NMR spectra of trans-$[Pt(9\text{-}EtGH)_2(1\text{-}MeC)_2]^{2+}$ (bottom) and immediately after addition of 0.5 eq of $Hg(CH_3COO)_2$ (top). Precipitation starts rapidly after recording the spectrum in the presence of the Hg^{II} salt.*

4.1.5.- Hydrogen Bonding Interactions of 29 with 1-MeC.

We have previously demonstrated that N7 platination of guanine does not prevent Watson-Crick pairing with cytosine [159,173-175]. In fact, the association constant is even increasing as a consequence of metal binding [173-175]. Here solutions of **30** with variable amounts of free 1-MeC in DMSO-d_6 have been prepared and ^1H NMR spectra were recorded. Quite clearly, the 1-MeC interacts with the guanine ligands of **30** in Watson-Crick fashion. This is evident from the

increasing downfield shifts of the N1(H) and the N2(H_2) resonances of the 9-EtGH resonances with increasing amounts of 1-MeC added. The shift of the N1 proton is roughly twice that of the N2 protons, as expected. With a large excess of 1-MeC (18 equiv per **30**), these shifts are 0.37 and 0.20 ppm, respectively, at a concentration of ca. 4 mM of **30**. Similarly, the N4(H_2) resonance of 1-MeC is shifted downfield upon addition of increasing amounts of **30**. Due to the presence of a large excess of 1-MeC (see above), the downfield shift (0.09 ppm) is smaller than that of the guanine amino group. The C-H protons of both nucleobases are practically not affected.

A concentration dependence of ^{1}H NMR chemical shifts to estimate association constants was not performed because of the complexity of treating four successive equilibria. Moreover, the DMSO-d_6 was wet due to the presence of water of crystallization in **30**, which would have led to an underestimation of actual constants anyway. However, qualitatively there can be no doubt that PtG_4·C, PtG_4·2C, PtG_4·3C, and PtG_4·4C species are formed in DMSO (Scheme 4.4).

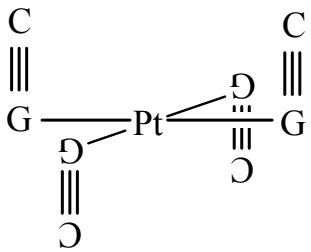

Scheme 4.4*: Schematic representation of adduct of* ***30*** *with four Cytosine bases.*

As expected, H bonding between **30** and 1-MeC is not evident from spectra recorded in D_2O. As pointed out above, TSP likewise proved unreliable in this case.

4.2.- Remarks.

In continuation of previous work on the properties of tetrakis(nucleobase) complexes of Pt^{II} [165], three purine containing representatives **29**-**32** have been prepared and their usefulness as metalloligands for other metal ions (Cu^{II}, Hg^{II}) as well as their ability to engage in intermolecular hydrogen bonding have been examined. Despite certain shortcomings due to insufficient product solubility, the findings confirm the expectations in principle. Thus, the composition of a linear pentanuclear Pt_2Cu_3 complex **32** was X-ray structurally confirmed, and the propensity of N7 platinated guanine bases to form Watson-Crick pairs with free cytosine was confirmed. The heteronuclear compound **32** bears a superficial resemblance with so called “extended metal atom chain” compounds containing five identical metal ions in a row [176-177], even though the metal-metal distances in **32** are probably far too long to expect any communication between the metal centers. From a bioinorganic perspective, the behavior of a N7 platinated 6-oxopurine nucleobase to bind an additional cation, here Cu^{II}, without undergoing deprotonation at N1 [178], is certainly noteworthy. It reiterates earlier findings on Na^+ binding to O6 of N7 platinated guanine [155] as well as observations by Chifotides and Dunbar on the binding of the bis(*μ*-carboxylato)dirhodium(II) fragment to N7 and O6 of isolated guanine bases or G_2 dinucleotides [179-181]. The presence of KNO_3 in **30** most likely also reflects the affinity of O6 to bind additional cations.

5.- Experimental Part.

5.1.- Techniques and Instruments.

5.1.1.- X-Ray Crystallography.

Data collection was performed on an Enraf-Nonius Kappa CCD diffractometer using graphite-monochromated Mo-Kα radiation (λ= 0.71069 Å) [182]. Data reduction and cell refinement were carried out using the programs DENZO and SCALE-PACK [183]. Intensities of reflections were collected at room temperature, 293(2)º. All the structures were solved by standard Patterson methods [184] and refined by full-matrix least-squares methods based on F^2 using the SHELXTL-PLUS [185], SHELXL-97 [186] and WinGX [187] programs. In the refinement process of the X-ray data, if not specified, all non-hydrogen atoms of the crystal were refined anisotropically, and all the hydrogen atoms except those of the water molecules were included in geometrically calculated positions and refined with isotropic displacement parameters according to the riding model. R_1 and wR_2 factors are:

$$R_1 = \Sigma \, ||F_0|-|F_c|| \, / \, \Sigma \, |F_0|$$

$$wR_2 = [\, \Sigma \, w(F_0^2 - F_c^2)^2 \, / \, \Sigma \, w(F_0^2)^2 \,]^{1/2}.$$

5.1.2.- NMR Spectroscopy.

One- and two-dimensional ^{1}H NMR spectra were recorded on a Varian Mercury 200 FT NMR, on a Bruker DRX 300, on a Bruker DRX 400 and on a Varian Inova 600 MHz by or with the collaboration of Burkhard Costisella and Anette Danzmann. TSP (sodium 3-trimethylsilyl-propanesulfonate) (δ = 0 ppm) and/or TMA (tetramethylammonium bromide) (δ = 3.18 ppm) were used as internal standards.

^{195}Pt NMR spectra were recorded on a Bruker DRX 300. Na_2PtCl_6 and/or K_2PtCl_4 were used as external and/or internal standards, respectively. In the case of internal standards for ^{195}Pt NMR (in D_2O), a capillary tube containing a solution of K_2PtCl_4 (or Na_2PtCl_6) in H_2O was introduced in the sample acting as standard. To fill up a capillary tube of glass (∅ = 0.5mm), a tube closed at the bottom was slightly heated and face down introduced in a solution containing the standard. After filling, the tube has to be centrifuged and closed at the top. To measure ^{195}Pt NMR in H_2O, a tube containing enough D_2O (lock signal) is required. The standard Na_2PtCl_6 displays a signal at 0 ppm. However, K_2PtCl_4 displays rapidly two signals after dissolved in water: at -1625 ppm ($[PtCl_4]^{2-}$) and at -1181 ppm ($[PtCl_3(H_2O)]^-$).

The pH (uncorrected pH*) of a D_2O solution was determined by use of a glass electrode on a Metrohm 6321 pH meter. pD values were obtained after addition of 0.4 units to the value displayed on the pH meter [188]. Measurement of the pD dependences were carried out using identical samples, in which the pD of the solutions was modified in small increments by addition of small amounts of DNO_3 and/or NaOD. Due to the limitations of the AgCl glass electrodes, it was not possible to get reliable measurements at pH values close to 14. The pK_a value was obtained after evaluating the chemical shift (δ) data at different pD with a Newton-Gauss non-linear least-squares curve fitting procedure as described in [189]. It was based on Equation 1:

$$\delta = \frac{\delta_1}{\frac{1}{10^{Ka} \times 10^{-pD}} + 1} + \frac{\delta_2}{(10^{Ka} \times 10^{-pD}) + 1}$$

Equation 1: *δ = measured chemical shift; pD = measured pD; K_a = dissociation constant; δ_1 = chemical shift of the protonated form; δ_l = chemical shift of the unprotonated form.*

The pK_a values for D_2O obtained this way were then converted into pK_a values valid for H_2O by use of Equation 2 [94]:

$$pK_a(H_2O) = \frac{pK_a(D_2O) - 0.45}{1.015}$$

Equation 2.

5.1.3.- IR Spectroscopy.

IR spectra were taken on a Perkin-Elmer 580 B FT spectrometer. Measurements (KBr) were performed from 4000 to 250 cm^{-1}.

5.1.4.- Elemental Analyses.

C, H, N analyses were performed on a Carlo-Erba-Strumentazione 1106 Element Analyzer by Markus Hüffner.

5.1.5.- DFT Calculations.

The DFT calculations for the gas-phase optimized structures were performed by Patrick Lax and Deepali Gupta using the computer program Gaussian 98 [190] and its revised version Gaussian 03 [191]. Each optimization was followed by a frequency calculation in order to confirm every structure to be a minimum structure. The built in combination of Becke's three-parameter hybrid function [192] with Lee-Yang-Parr's exchange functional [193] was applied for all structures. Pt, Pd and I atoms were described with the LANL2DZ basis set. For the lighter atoms H, C, N, O and Cl a 6-31G* basis set was used.

5.2.- Preparation of Compounds.

The following compounds were purchased:

- **K_2PtCl_4** (from Heraeus, Hanau, Germany).
- **9-EtGH** (from Chemogen, Konstanz, Germany).

The following starting compounds were synthesized according to published methods:

- **1-MeC**: [7] T. J. Kistenmacher, M. Rossi, J. P. Caradonna, L. G. Marzilli, *Adv. Mol. Relax. Int. Proc.*, 1979, 15, 119.
- **1-MeUH**: [194] W. Micklitz, B. Lippert, H. Schöllhorn, U. Thewalt, *J. Heterocyclic Chem.*, 1989, 26, 1499.
- **9-MeA**: [195] G. Krüger, *Hoppe-Seyler's Z. Physiol. Chem.*, 1894, 18, 434.
- **9-EtA**: [196] J. S. Nowick, J. S. Chem, G. Noronha, *J. Am. Chem. Soc.*, 1993, 115, 7636.
- **9-MeHxH**: [197] E. G. Talman, W. Brüning, J. Reedijk, A. L. Spek, N. Veldman, *Inorg. Chem.*, 1997, 36, 854.
- **$[(NH)_3PtCl]Cl$**: with slight modifications of the method reported in [198] *Inorganic Syntheses, 1983, Volume 22, p. 124*. (Anal. Calc. for $[(NH)_3PtCl]Cl$ ($H_9N_3Cl_2Pt$): H, 2.9; N, 13.3. Found: H, 2.8; N, 13.3 %).
- **[Pt(dien)I]I**: [199] G. W. Watt, W. A. Clude, *Inorg. Chem.*, 1968, 7, 335.
- **[Pd(dien)Br]Br**: [200] D. Gupta, M. Hueselkpf, M. Morell Cerda, Ralf Ludwig, B. Lippert, *Inorg. Chem.*, 2004, 43, 3386.

The preparations of the following nucleobase complexes discussed in this thesis have already been reported in publications from our group:

- **[(dien)Pt(1-MeC-*N3*)]$^{2+}$** (**9**),
  [(dien)Pt(1-MeU-*N3*)]$^{+}$ (**10**),
  ***syn*-[(dien)Pt(1-MeC^{-}-*N4*)]$^{+}$** (**11a**), and
  ***anti*-[(dien)Pt(1-MeC^{-}-*N4*)]$^{+}$** (**11b**): [5]
  J. E. Šponer, P. J. Sanz Miguel, L. Rodriguez-Santiago, A. Erxleben, M. Krumm, M. Sodupe, J. Šponer, B. Lippert, *Angew. Chem., Int. Ed., 2004, 43, 5396*.
- **$[Pt(1\text{-}MeC\text{-}N3)_3I]I$** (**20**),
  ***trans*-$[Pt(1\text{-}MeC\text{-}N3)(1\text{-}MeC\text{-}N4)I_2] \cdot 2H_2O$** (**23**), and
  ***trans*-$[Pt(1\text{-}MeC\text{-}N3)(1\text{-}MeC\text{-}N4)Cl_2]$** (**24**): [2]
  P. J. Sanz Miguel, P. Lax, M. Willermann, B. Lippert, *Inorg. Chimica Acta,* 2003, 42, 5117.

- ***trans*-[Pt(1-MeC-*N3*)$_2$I$_2$]** (**21**): [1]
  J. Müller, E. Freisinger, P. J. Sanz Miguel, B. Lippert, *Inorg. Chem.,* 2003, 42, 5117.
- **[Pt(9-MeHxH-*N7*)$_4$](NO$_3$)$_2$ · H$_2$O** (**29**),
  [Pt(9-EtGH-*N7*)$_4$](NO$_3$)$_2$ · 2KNO$_3$ · 5H$_2$O (**30**),
  ***trans*-[Pt(1-MeC-*N3*)$_2$(9-EtGH-*N7*)$_2$](NO$_3$)$_2$** (**31**), and
  [{(H$_2$O)Cu(9-MeHxH)$_4$Pt}$_2$Cu(ClO$_4$)$_4$](ClO$_4$)$_2$(NO$_3$)$_4$ · 6H$_2$O (**32**): [4]
  P. J. Sanz Miguel, Bernhard Lippert, *Dalton Trans.,* 2005, 1679.
- As mentioned in chapter 1, the nucleobase compounds described there were largely obtained as byproducts of preparations leading to Pt nucleobase complexes, usually in low field only. The procedure leading to **[(9-MeAH)(9-MeHxH)](ClO$_4$)** (**8**) is reported in: [5]
  P. Amo-Ochoa, P. J. Sanz Miguel, P. Lax, I. Alonso, M. Roitzsch, F. Zamora, B. Lippert, *Angew. Chem., in press*.

The following complexes were synthesized as outlined below:

- **[(NH)$_3$Pt(1-MeC-*N3*)](ClO$_4$)$_2$ · ½ KClO$_4$** (**12**):

[(NH)$_3$PtCl]Cl (1 mmol) was reacted with $AgClO_4$ (2 mmol) in 50 ml of water in the dark at 40ºC for 12 h. The precipitated AgCl was removed by filtration and the solution was stirred with 1 mmol of 1-MeC at 40ºC. After 2 days, the volume was reduced to 10 ml. Addition of a saturated solution of $KClO_4$ to the mixture produced within two days colorless cubes which were collected by filtration and characterized by X-ray crystallography. The yield was about 64 %. (*Anal.* Calc. for **12** ($C_5H_{16}N_6O_{11}Cl_{2.5}K_{0.5}Pt$): C, 9.4; H, 2.5; N, 13.1. Found: C, 9.4; H, 2.5; N, 13.4 %).

- **[(dien)Pd(1-MeC-*N3*)](ClO$_4$)$_2$** (**14**):

To a solution of [(dien)PdBr]Br (1 mmol) in 40 ml of water was added $AgClO_4$ (2 mmol) and 1-MeC (1 mmol). The mixture was stirred at 40º C in the dark. After 12 h it was filtered and concentrated by rotary evaporation. The solution was allowed to evaporate. Yellow crystals of **14** were isolated from it and characterized by X-ray crystallography. The yield was 52 %.

- ***trans*-[Pt(1-MeC-*N3*)$_2$Cl$_2$]** (**22**):

A suspension of **21** (0.05 mmol) in D_2O and a solution of $AgNO_3$ (2 eq) were mixed and kept in an ultrasonic bath for five minutes at room temperature. After filtration of the precipitate (containing AgI and undissolved **21**), NaCl was added to the solution. Again, a precipitate was formed and removed by filtration. The remaining filtrate was allowed to crystallize for several days in a NMR tube. Formation of small yellow crystals was observed. After isolation, the crystals were characterized by X-ray crystallography.

- **[Ag(pyz)](NO$_3$)** (**26**):

A solution of $AgNO_3$ in D_2O (0.1 M) was added dropwise to a solution containing pyrazine (0.5 M) to produce immediately a gel. The gel was removed by centrifugation and the remaining solution was allowed to crystallize (4º C). The composition of the crystals was determined by X-ray crystallography.

- **[Pt(1-MeC-*N3*)$_3$(pyz)](NO$_3$)$_2$ · H$_2$O** (**27**):

20 (0.1 mmol) was reacted with $AgNO_3$ (0.2 mmol) in 10 ml of water in the dark at 40ºC for 1 d. The precipitated AgCl was removed by filtration and the solution was stirred with 0.5 mmol of pyrazine at 40ºC. After 2 days, the solution was brought to dryness by rotary evaporation to sublime the excess of pyrazine off. The resulting powder was recrystallized from water to give colorless crystals. Composition of **27** was determined by X-ray crystallography.

- **[Pt(1-MeC-*N3*)$_3$(pyz)Ag](NO$_3$)$_3$ · H$_2$O** (**28**):

To a solution of **27** (0.05 mmol) in water, an excess of $AgNO_3$ (tenfold) was added and the mixture was kept in the dark at 4ºC. After several days, formation of colorless crystals was observed. Composition of a crystal was determined by X-ray crystallography.

5.3.- Crystallographic Tables.

Table A-1: *Crystallographic data for compound **1**.*

Compound	$[(1\text{-MeCH})(1\text{-MeC})]I_3 \cdot 2H_2O$
Formula	$C_{10}\ H_{19}\ N_6\ O_4\ I_3$
Formula weight (g mol^{-1})	668.01
Crystal color and habit	orange blocks
λ (Å)	0.71069
Crystal system	monoclinic
Space group	$P2_1/c$
a (Å)	10.482(2)
b (Å)	18.700(4)
c (Å)	10.315(2)
β (º)	95.11(3)
Z	4
V ($Å^3$)	2013.8(7)
ρ_{calc} (g cm^{-1})	2.203
μ (Mo Kα) (mm^{-1})	4.681
F(000)	1248
θ range (º)	2.87 - 25.95
No. reflections collected	3423
No. reflections observed $I>2\sigma(I)$	1244
No. parameters refined	208
R_1 (obs. data)	0.0458
wR2 (obs. data)	0.0737
Goodness-of-fit, S	0.59
Residual ρ_{max}, ρ_{min} (e $Å^{-3}$)	0.953, -0.799

Table A-2: *Crystallographic data for compound **2**.*

Compound	[1-MeCH](NO_3)
Formula	C_5 H_8 N_4 O_4
Formula weight (g mol^{-1})	188.15
Crystal color and habit	colorless prisms
Crystal system	triclinic
Space group	P $\bar{1}$
a (Å)	6.8730(14)
b (Å)	7.4110(15)
c (Å)	8.2880(17)
α (º)	107.32(3)
β (º)	94.99(3)
γ (º)	92.70(3)
Z	2
V ($Å^3$)	400.32(14)
ρ_{calc} (g cm^{-1})	1.561
μ(Mo Kα) (mm^{-1})	0.135
F(000)	196
θ range (º)	2.59 - 26.36
No. reflections collected	1564
No. reflections observed I>2σ(I)	618
No. parameters refined	150
R_1 (obs. data)	0.0428
wR2 (obs. data)	0.1039
Goodness-of-fit, S	0.756
Residual ρ_{max}, ρ_{min} (e $Å^{-3}$)	0.138, -0.136

Table A-3: *Crystallographic data for compound **3**.*

Compound	[9-MeAH](PF_6) · H_2O
Formula	C_6 H_{10} F_3 N_5 O $P_{0.5}$
Formula weight (g mol^{-1})	240.68
Crystal color and habit	colorless blocks
Crystal system	triclinic
Space group	P $\bar{1}$
a (Å)	6.2750(13)
b (Å)	8.2360(16)
c (Å)	10.059(2)
α (º)	76.52(3)
β (º)	88.96(3)
γ (º)	74.72(3)
Z	2
V ($Å^3$)	487.16(17)
ρ_{calc} (g cm^{-1})	1.641
μ(Mo Kα) (mm^{-1})	0.232
F(000)	247
θ range (º)	2.08 - 28.35
No. reflections collected	2239
No. reflections observed I>2σ(I)	1174
No. parameters refined	182
R_1 (obs. data)	0.0439
wR2 (obs. data)	0.1127
Goodness-of-fit, S	0.871
Residual ρ_{max}, ρ_{min} (e $Å^{-3}$)	0.23, -0.41

Table A-4: *Crystallographic data for compound **4**.*

Compound	[(9-EtAH)](NO$_3$)
Formula	C_7 H_{10} N_6 O_3
Formula weight (g mol^{-1})	226.21
Crystal color and habit	colorless needles
Crystal system	triclinic
Space group	P $\bar{1}$
a (Å)	7.3630(15)
b (Å)	7.5750(15)
c (Å)	9.2060(18)
α (º)	93.04(3)
β (º)	99.06(3)
γ (º)	107.55(3)
Z	2
V (Å^3)	480.68(17)
ρ_{calc} (g cm^{-1})	1.563
μ(Mo Kα) (mm^{-1})	0.126
F(000)	236
θ range (º)	3.37 - 27.92
No. reflections collected	2142
No. reflections observed I>2σ(I)	708
No. parameters refined	185
R1 (obs. data)	0.0356
wR2 (obs. data)	0.0783
Goodness-of-fit, S	0.619
Residual ρ_{max}, ρ_{min} (e Å^{-3})	0.135, -0.168

Table A-5: *Crystallographic data for compound **5**.*

Compound	[9-MeAH](NO$_3$) · H_2O
Formula	C_5 H_8 N_4 O_4
Formula weight (g mol^{-1})	188.15
Crystal color and habit	colorless prisms
Crystal system	triclinic
Space group	P $\bar{1}$
a (Å)	6.8730(14)
b (Å)	7.4110(15)
c (Å)	8.2880(17)
α (º)	107.32(3)
β (º)	94.99(3)
γ (º)	6.8730(14)
Z	2
V (Å^3)	400.32(14)
ρ_{calc} (g cm^{-1})	1.561
μ(Mo Kα) (mm^{-1})	0.135
F(000)	196
θ range (º)	2.59 - 26.36
No. reflections collected	1564
No. reflections observed I>2σ(I)	618
No. parameters refined	150
R_1 (obs. data)	0.0428
wR2 (obs. data)	0.1039
Goodness-of-fit, S	0.756
Residual ρ_{max}, ρ_{min} (e Å^{-3})	0.138, -0.136

Table A-6: *Crystallographic data for compound* ***6***.

Compound	$[(9\text{-EtGH})_2] \cdot 4H_2O$
Formula	$C_{28}\ H_{52}\ N_{20}\ O_{12}$
Formula weight (g mol^{-1})	860.9
Crystal color and habit	colorless prisms
Crystal system	triclinic
Space group	$P\ \overline{1}$
a (Å)	6.7490(15)
b (Å)	11.534(4)
c (Å)	12.982(4)
α (º)	99.49(5)
β (º)	98.34(3)
γ (º)	95.47(3)
Z	1
V ($Å^3$)	978.8(5)
ρ_{calc} (g cm^{-1})	1.461
μ (Mo Kα) (mm^{-1})	0.116
F(000)	456
θ range (º)	2.63 - 26.38
No. reflections collected	3919
No. reflections observed I>2σ(I)	1377
No. parameters refined	375
R_1 (obs. data)	0.0337
wR2 (obs. data)	0.0578
Goodness-of-fit, S	0.548
Residual ρ_{max}, ρ_{min} (e $Å^{-3}$)	0.198, -0.203

Table A-7: *Crystallographic data for compound 7*.

Compound	$[(9\text{-EtGH})_2] \cdot 7H_2O$
Formula	$C_7\ H_{16}\ N_5\ O_{4.5}$
Formula weight (g mol^{-1})	860.90
Crystal color and habit	colorless prisms
Crystal system	monoclinic
Space group	$P2_1/c$
a (Å)	14.879(3)
b (Å)	11.187(2)
c (Å)	14.990(3)
α (º)	90
β (º)	111.08(3)
γ (º)	90
Z	8
V ($Å^3$)	2328.2(8)
ρ_{calc} (g cm^{-1})	1.382
μ (Mo Kα) (mm^{-1})	0.115
F(000)	1032
θ range (º)	2.33 - 23.38
No. reflections collected	3326
No. reflections observed I>2σ(I)	760
No. parameters refined	349
R_1 (obs. data)	0.0502
wR2 (obs. data)	0.1061
Goodness-of-fit, S	0.667
Residual ρ_{max}, ρ_{min} (e $Å^{-3}$)	0.266, -0.225

Table A-8: *Crystallographic data for compound **8**.*

Compound	[(9-MeAH)(9-MeHxH)](ClO$_4$)
Formula	C_{48} H_{56} Cl_4 N_{36} O_{20}
Formula weight (g mol^{-1})	1599.09
Crystal color and habit	colorless prisms
Crystal system	monoclinic
Space group	$P2_1/c$
a (Å)	8.8040(18)
b (Å)	8.1930(16)
c (Å)	24.008(6)
β (º)	102.85(3)
Z	1
V (Å^3)	1688.4(6)
ρ_{calc} (g cm^{-1})	1.573
μ (Mo Kα) (mm^{-1})	0.276
F(000)	824
θ range (º)	2.37 - 26.41
No. reflections collected	2946
No. reflections observed I>2σ(I)	891
No. parameters refined	300
R_1 (obs. data)	0.0536
wR2 (obs. data)	0.1269
Goodness-of-fit, S	0.734
Residual ρ_{max}, ρ_{min} (e Å^{-3})	0.341, -0.22

Table A-9: *Crystallographic data for compound **9**.*

Compound	[(dien)Pt(1-MeC-*N3*)](ClO$_4$)$_2$
Formula	C_9 H_{20} Cl_2 N_6 O_9 Pt
Formula weight (g mol^{-1})	622.3
Crystal color and habit	colorless blocks
Crystal system	orthorhombic
Space group	Pbca
a (Å)	15.088(3)
b (Å)	12.195(2)
c (Å)	19.506(4)
Z	8
V (Å^3)	3589.1(12)
ρ_{calc} (g cm^{-1})	2.303
μ (Mo Kα) (mm^{-1})	8.176
F(000)	2400
θ range (º)	2.39 - 27.5
No. reflections collected	4116
No. reflections observed I>2σ(I)	3279
No. parameters refined	244
R_1 (obs. data)	0.0606
wR2 (obs. data)	0.1647
Goodness-of-fit, S	1.106
Residual ρ_{max}, ρ_{min} (e Å^{-3})	4.487, -5.855

Table A-12: *Crystallographic data for compound **12**.*

	12
Compound	$[(NH)_3Pt(1\text{-}MeC\text{-}N3)](ClO_4)_2 \cdot ½\ KClO_4$
Formula	$C_5\ H_{16}\ Cl_{2.5}\ K_{0.5}\ N_6\ O_{11}\ Pt$
Formula weight (g mol^{-1})	639.5
Crystal color and habit	colorless cubes
Crystal system	monoclinic
Space group	C2/c
a (Å)	26.837(5)
b (Å)	7.0420(14)
c (Å)	22.738(5)
α (º)	90
β (º)	125.37(3)
γ (º)	90
Z	8
V ($Å^3$)	3504.1(12)
ρ_{calc} (g cm^{-1})	2.424
μ (Mo Kα) (mm^{-1})	8.576
F(000)	2448
θ range (º)	1.86 - 27.5
No. reflections collected	3966
No. reflections observed I>2σ(I)	3017
No. parameters refined	237
R1 (obs. data)	0.034
wR2 (obs. data)	0.083
Goodness-of-fit, S	0.959
Residual ρ_{max}, ρ_{min} (e $Å^{-3}$)	1.031, -1.28

Table A-14: *Crystallographic data for compound **14**.*

Compound	$[(dien)Pd(1\text{-}MeC\text{-}N3)](ClO_4)_2$
Formula	$C_9\ H_{20}\ Cl_2\ N_6\ O_9\ Pd$
Formula weight (g mol^{-1})	1067.22
Crystal color and habit	yellow blocks
Crystal system	orthorhombic
Space group	Pbca
a (Å)	15.186(3)
b (Å)	12.235(2)
c (Å)	19.697(4)
Z	4
V ($Å^3$)	3659.7(13)
ρ_{calc} (g cm^{-1})	1.937
μ (Mo Kα) (mm^{-1})	1.364
F(000)	2144
θ range (º)	2.37 - 26.77
No. reflections collected	3603
No. reflections observed I>2σ(I)	1872
No. parameters refined	244
R_1 (obs. data)	0.0308
wR2 (obs. data)	0.0565
Goodness-of-fit, S	0.815
Residual ρ_{max}, ρ_{min} (e $Å^{-3}$)	0.585, -0.635

Table A-20: *Crystallographic data for compound **20**.*

Compound	[Pt(1-MeC)$_3$I]I
Formula	$C_{15}H_{21}N_9O_3I_2Pt$
Formula weight (g mol^{-1})	824.30
Crystal color and habit	dark yellow cubes
Crystal system	monoclinic
Space group	$P2_1/n$
a (Å)	12.199
b (Å)	14.184
c (Å)	13.565
β(º)	107.831
Z	4
V (Å^3)	2234.4
ρ_{calc} (g cm^{-1})	2.450
μ(Mo Kα) (mm^{-1})	9.080
F(000)	1528
θ range (º)	2.87 – 27.90
No. reflections collected	5293
No. reflections observed I>2σ(I)	3157
No. parameters refined	271
R_1 (obs. data)	0.0629
wR2 (obs. data)	0.1833
Goodness-of-fit, S	1.037
Residual ρ_{max}, ρ_{min} (e Å^{-3})	1.688, -2.955

Table A-23: *Crystallographic data for compound **23**.*

Compound	*trans*-[Pt(1-MeC-*N3*)(1-MeC-*N4*)I$_2$]·2H$_2$O
Formula	$C_{10}H_{18}N_3O_4I_2Pt$
Formula weight (g mol^{-1})	693.16
Crystal color and habit	dark yellow sticks
Crystal system	triclinic
Space group	$P\bar{1}$
a (Å)	9.209
b (Å)	9.675
c (Å)	12.073
α (º)	100.22
β (º)	107.32
γ (º)	103.87
Z	2
V (Å^3)	960.4
ρ_{calc} (g cm^{-1})	2.542
μ(Mo Kα) (mm^{-1})	10.545
F(000)	672
θ range (º)	3.16 – 25.12
No. reflections collected	3124
No. reflections observed I>2σ(I)	1074
No. parameters refined	208
R_1 (obs. data)	0.0302
wR2 (obs. data)	0.0647
Goodness-of-fit, S	0.548
Residual ρ_{max}, ρ_{min} (e Å^{-3})	0.581, -0.867

Table A-24: *Crystallographic data for compound **24**.*

Compound	*trans*-[Pt(1-MeC-*N3*)(1-MeC-*N4*)Cl_2]
Formula	$C_{10}H_{14}N_3O_2Cl_2Pt$
Formula weight (g mol^{-1})	474.23
Crystal color and habit	yellow sticks
Crystal system	triclinic
Space group	$P\bar{1}$
a (Å)	7.1250(14)
b (Å)	10.073(2)
c (Å)	10.771(2)
α (º)	101.05(3)
β (º)	94.01(3)
γ (º)	101.70(3)
Z	2
V ($Å^3$)	738.2(3)
ρ_{calc} (g cm^{-1})	2.323
μ(Mo Kα) (mm^{-1})	9.879
F(000)	488
θ range (º)	3.33 - 32.01
No. reflections collected	4493
No. reflections observed I>2σ(I)	2123
No. parameters refined	246
R_1 (obs. data)	0.0266
wR2 (obs. data)	0.0382
Goodness-of-fit, S	0.495
Residual ρ_{max}, ρ_{min} (e $Å^{-3}$)	0.879, -0.792

Table A-22: *Crystallographic data for compound **22**.*

Compound	*trans*-[Pt(1-MeC-*N3*)$_2Cl_2$]
Formula	C_{10} H_{14} Cl_2 N_6 O_2 Pt
Formula weight (g mol^{-1})	516.26
Crystal color and habit	yellow prisms
Crystal system	triclinic
Space group	$P\bar{1}$
a (Å)	6.8480(14)
b (Å)	7.3470(15)
c (Å)	8.4700(17)
α (º)	67.43(3)
β (º)	73.35(3)
γ (º)	89.23(3)
Z	1
V ($Å^3$)	374.75(13)
ρ_{calc} (g cm^{-1})	2.288
μ(Mo Kα) (mm^{-1})	9.73
F(000)	244
θ range (º)	2.73 - 28.05
No. reflections collected	1511
No. reflections observed I>2σ(I)	1131
No. parameters refined	125
R_1 (obs. data)	0.0662
wR2 (obs. data)	0.1759
Goodness-of-fit, S	1.003
Residual ρ_{max}, ρ_{min} (e $Å^{-3}$)	5.928, -1.132

Table A-25: *Crystallographic data for compound **25**.*

Compound	(4,4'-BipyH)I · H_2O
Formula	C_{10} H_{11} N_2 O_1 I
Formula weight (g mol^{-1})	302.11
Crystal color and habit	colorless blocks
Crystal system	orthorhombic
Space group	$P2_12_12_1$
a (Å)	7.142(1)
b (Å)	9.715(2)
c (Å)	15.913(3)
Z	4
V ($Å^3$)	1104.1(4)
ρ_{calc} (g cm^{-1})	1.817
μ (Mo Kα) (mm^{-1})	2.871
F(000)	584
θ range (º)	2.46 - 27.49
No. reflections collected	2525
No. reflections observed I>2σ(I)	1130
No. parameters refined	171
R_1 (obs. data)	0.0273
wR2 (obs. data)	0.0432
Goodness-of-fit, S	0.591
Residual ρ_{max}, ρ_{min} (e $Å^{-3}$)	0.308, -0.464
Flack x parameter	0.56(3)

Table A-26: *Crystallographic data for compound **26**.*

Compound	[Ag(pyz)](NO_3)
Formula	C_8 H_8 N_6 O_6 Ag_2
Formula weight (g mol^{-1})	499.94
Crystal color and habit	colorless prisms
Crystal system	triclinic
Space group	$P\bar{1}$
a (Å)	3.4990(7)
b (Å)	6.4250(13)
c (Å)	14.193(3)
α (º)	90.81(3)
β (º)	95.76(3)
γ (º)	91.65(3)
Z	1
V ($Å^3$)	317.28(11)
ρ_{calc} (g cm^{-1})	2.617
μ (Mo Kα) (mm^{-1})	3.13
F(000)	240
θ range (º)	1.44 - 26.78
No. reflections collected	1341
No. reflections observed I>2σ(I)	1047
No. parameters refined	100
R_1 (obs. data)	0.079
wR2 (obs. data)	0.2278
Goodness-of-fit, S	1.161
Residual ρ_{max}, ρ_{min} (e $Å^{-3}$)	5.159, -1.389

Table A-27: *Crystallographic data for compound **27**.*

Compound	$[Pt(1\text{-}MeC\text{-}N3)_3(pyz)](NO_3)_2 \cdot H_2O$
Formula	$C_{19}\ H_{27}\ N_{13}\ O_{10}\ Pt$
Formula weight (g mol^{-1})	792.63
Crystal color and habit	colorless prisms
Crystal system	orthorhombic
Space group	Pbca
a (Å)	11.781(2)
b (Å)	14.109(3)
c (Å)	34.284(7)
Z	8
V (Å^3)	5699(2)
ρ_{calc} (g cm^{-1})	1.848
μ (Mo Kα) (mm^{-1})	5
F(000)	3120
θ range (º)	1.19 - 26.37
No. reflections collected	5732
No. reflections observed I>2σ(I)	2591
No. parameters refined	368
R_1 (obs. data)	0.0437
wR2 (obs. data)	0.0984
Goodness-of-fit, S	0.846
Residual ρ_{max}, ρ_{min} (e Å^{-3})	1.551, -1.111

Table A-28: *Crystallographic data for compound **28**.*

Compound	$[Pt(1\text{-}MeC\text{-}N3)_3(pyz)Ag](NO_3)_3 \cdot H_2O$
Formula	$C_{19}\ H_{27}\ N_{14}\ O_{13}\ Ag\ Pt$
Formula weight (g mol^{-1})	962.51
Crystal color and habit	colorless prisms
Crystal system	monoclinic
Space group	$P2_1/c$
a (Å)	9.2260(18)
b (Å)	18.004(4)
c (Å)	18.724(4)
β (º)	99.66(3)
Z	4
V (Å^3)	3066.0(10)
ρ_{calc} (g cm^{-1})	2.085
μ (Mo Kα) (mm^{-1})	5.283
F(000)	1872
θ range (º)	2.24 - 27.50
No. reflections collected	7020
No. reflections observed I>2σ(I)	4484
No. parameters refined	433
R_1 (obs. data)	0.0413
wR2 (obs. data)	0.0941
Goodness-of-fit, S	0.906
Residual ρ_{max}, ρ_{min} (e Å^{-3})	1.245, -1.425

Table A-29: Crystallographic data for compound **29**.

Compound	$[Pt(9\text{-}MeHxH\text{-}N7)_4]\ (NO_3)_2 \cdot H_2O$
Formula	$C_{24}\ H_{26}\ N_{18}\ O_{11}\ Pt$
Formula weight (g mmol^{-1})	937.72
Crystal color and habit	white cubes
Crystal system	triclinic
Space group	P-1
a (Å)	9.4960(19)
b (Å)	9.5420(19)
c (Å)	18.721(4)
α (º)	87.88(3)
β (º)	81.98(3)
γ (º)	85.42(3)
Z	2
V (Å^3)	1673.8(6)
ρ_{calc} (g cm^{-1})	1.861
μ (Mo Kα) (mm^{-1})	4.278
F(000)	924
θ range (º)	2.38 - 27.5
No. reflections collected	7621
No. reflections observed I>2σ(I)	5446
No. parameters refined	487
R1 (obs. data)	0.0403
wR2 (obs. data)	0.0806
Goodness-of-fit, S	0.989
Residual ρ_{max}, ρ_{min} (e Å^{-3})	2.043, -1.246

Table A-32: Crystallographic data for compound **32**.

Compound	$\{[(H_2O)Cu(9\text{-}MeHxH)_4Pt]_2\ Cu(ClO_4)_4\}\ (ClO_4)_2(NO_3)_4 \cdot 6H_2O$
Formula	$C_{24}\ H_{38}\ Cl_3\ Cu_{1.5}\ N_{18}\ O_{29}\ Pt$
Formula weight (g mmol^{-1})	1439.47
Crystal color and habit	yellow prisms
Crystal system	triclinic
Space group	P-1
a (Å)	11.211(2)
b (Å)	11.605(2)
c (Å)	18.442(4)
α (º)	89.50(3)
β (º)	75.92(3)
γ (º)	87.81(3)
Z	2
V (Å^3)	2325.5(8)
ρ_{calc} (g cm^{-1})	2.056
μ (Mo Kα) (mm^{-1})	3.973
F(000)	1425
θ range (º)	2.28 - 27.5
No. reflections collected	9909
No. reflections observed I>2σ(I)	5780
No. parameters refined	681
R1 (obs. data)	0.0534
wR2 (obs. data)	0.1354
Goodness-of-fit, S	0.926
Residual ρ_{max}, ρ_{min} (e Å^{-3})	1.968, -1.058

6.- References.

[1] J. Müller, E. Freisinger, P. J. Sanz Miguel, B. Lippert, *Inorg. Chem.,* 2003, 42, 5117.

[2] P. J. Sanz Miguel, P. Lax, M. Willermann, B. Lippert, *Inorg. Chim. Acta,* 2003, 42, 5117.

[3] J. E. Šponer, P. J. Sanz Miguel, L. Rodriguez-Santiago, A. Erxleben, M. Krumm, M. Sodupe, J. Šponer, B. Lippert, *Angew. Chem., Int. Ed.,* 2004, 43, 5396.

[4] P. J. Sanz Miguel, Bernhard Lippert, *Dalton Trans.,* 2005, 1679.

[5] P. Amo-Ochoa, P. J. Sanz Miguel, P. Lax, I. Alonso, M. Roitzsch, F. Zamora, B. Lippert, *Angew. Chem., in press*.

[6] Wolfram Saenger, Principles of Nucleic Acid Structure, Springer-Verlag, New York (1984).

[7] T. J. Kistenmacher, M. Rossi, J. P. Caradonna, L. G. Marzilli, *Adv. Mol. Relax. Int. Proc.*, 1979, 15, 119.

[8] M. Rossi, L. G. Marzilli, T. J. Kistenmacher, *Acta Crystallogr., Sect. B*, 1978, 34, 2030.

[9] F. van Bolhuis, P. B. Koster, Z. Migchelsen, *Acta Crystallogr.,* 1967, 23, 90.

[10] J. Runsink, S. Swen-Walstra, Z. Migchelsen, *Acta Crystallogr., Sect. B*, 1972, 28, 1331.

[11] T. J. Kistenmacher, M. Rossi, L. G. Marzilli, *Biopolymers,* 1975, 17, 2581.

[12] T. J. Kistenmacher, M. Rossi, C. C. Chiang, J. P. Caradonna, L. G. Marzilli, *Adv. Mol. Relax. Interact. Proc.,* 1980, 17, 113.

[13] A. Schimanski, E. Freisinger, A. Erxleben, B. Lippert, *Inorg. Chim. Acta,* 1998, 283, 223.

[14] J. Müller, E. Freisinger, *Acta Crystallogr., Sect. E*, 2005, E61, o320.

[15] H. Teitelbaum, S.W. Englander, *J. Mol. Biol.*, 1975, 92, 55.

[16] T. Krüger, C. Bruhn, D. Steinborn, *Org. Biomol. Chem.*, 2004, 2, 2513.

[17] R. F. Bryan, K.-I. Tomita, *Acta Crystallogr.,* 1962, 15, 1174.

[18] B. L. Trus, K. E. Marsh, *Acta Crystallogr., Sect. B*, 1972, 28, 1834.

[19] M. Rossi, J. P. Caradonna, L. G. Marzilli, T. J. Kistenmacher, *Adv. Mol. Relax. Interact. Proc.*, 1979, 15, 103.

[20] M. Rossi, T. J. Kistenmacher, *Acta Cryst., Sect. B.*, 1977, B33, 3962.

[21] R. F. Bryan, K.-I. Tomita, *Acta Crystallogr.*, 1951, 4, 81.

[22] G. Bandoli, A. Dolmella, S. Gatto, *J. Chem. Cryst.*, 1995, 25, 143.

[23] A. Kettani, A. Gorin, A. Majumdar, T. Hermann, E. Skripkin, H. Zhao, R. Jones, D. J. Patel, *J. Mol. Biol.*, 2000, 297, 627.

[24] R. J. Walker, P. Tollin, J. N. Low, *Cryst. Struct. Commun.*, 1987, B37, 140.

[25] V. Lager, K. Huml, *Acta Crystallogr.*, 1978, B34, 1881.

[26] R. Destro, T. J. Kistenmacher, R. E. Marsh, *Acta Cryst., Sect. B,* 1974, B30, 79.

[27] S. J. Sowerby, M. Edelwirth, W. M. Heckl, *J. Phys. Chem. B,* 1998, 102, 5914.

[28] K. Kanie, T. Yasuda, S. Ujiie, T. Kato, *Chem. Commun.,* 2000, 1899.

[29] T. Giorgi, S. Lena, P. Mariani, M. A. Cremonini, S. Masiero, S. Pieraccini, J. P. Rabe, P. Samori, G. P. Spada, G. Gottarelli, *J. Am. Chem. Soc.,* 2003, 125, 14741.

[30] J. Pranata, S. G. Wierschke, W. L. Jorgensen, *J. Am. Chem. Soc.*, 1991, 113, 2810.

[31] J. Sartorius, H.-J. Schneider, *Chem. Eur. J.*, 1996, 2, 1446.

[32] G. Gottarelli, S. Masiero, E. Mezzina, S. Pieraccini, J. P. Rabe, P. Samorí, G. P. Spada, *Chem. Eur. J.*, 2000, 6, 3242.

[33] C. Kang, X. Zhang, R. Ratliff, R. Moyzis, A. Rich, *Nature*, 1992, 356, 126.

[34] G. Laughlan, A. I. H. Murchie, D. G. Norman, M. H. Moore, P. C. E. Moody, D. M. Lilley, B. Luisi, *Science*, 1994, 265, 520.

[35] I. B. Rother, M. Willermann, B. Lippert, *Supramolecular Chemistry,* 2002, 14, 189.

[36] R. Ludwig, Angew. Chem. Int. Ed., 2001, 40, 1808.

[37] R. Custelcean, C. Afloroaei, M. Vlassa, M. Polverejan, *Angew. Chem. Int. Ed.,* 2000, 39, 3094.

[38] L. Randaccio, E. Zangrando, A. Cesàro, D. Holthenrich, B. Lippert, *J. Mol. Struct.,* 1998, 440, 221.

[39] K. Liu, M. G. Brown, C. Carter, R. J. Saykally, J. K. Gregory, D. C. Clary, *Nature*, 1996, 381, 501.

[40] K. Nauta, R. E. Miller, *Science*, 2000, 287, 293.

[41] F. Weinhold, *J. Chem. Phys.*, 1998, 109, 367.

[42] J. M. Ugalde, I. Alkorta, J. Elguero, *Angew. Chem., Int. Ed.*, 2000, 39, 717.

[43] J. Kim, D. Majumdar, H. M. Lee, K. S. Kim, *J. Chem. Phys.*, 1999, 110, 9128.

[44] K. Liu, J. D. Cruzan, R. J. Saykally, *Science*, 1996, 271, 929.

[45] S. Supriya, S. Manikumari, P. Raghavaiah, S. K. Das, *New J. Chem.*, 2003, 27, 218.

[46] L.-S. Long, Y. R. Wu, R. B. Huang, L. S. Zheng, *Inorg. Chem.*, 2004, 43, 3798.

[47] B. Q. Ma, H.L. Sun, S. Gao, *Chem. Commun.,* 2004, 2220.

[48] C. Foces-Foces, F. H. Cano, M. Martinez-Ripoll, R. Faure, C. Roussel, R. M. Claramunt, C. Lopez, D. Sanz, *Tetrahedron: Asymmetry*, 1990, 1, 65.

[49] R. J. Doedens, E. Yphannes, M. I. Khan, *Chem. Commun.*, 2002, 62.

[50] J. N. Moorthy, R. Natarajan, P. Venugopalan, *Angew. Chem., Int. Ed.*, 2002, 41, 3417.

[51] S. K. Ghosh, P. K. Bharadwaj, *Inorg. Chem.*, 2004, 43, 6887.

[52] J. L. Atwood, L. J. Barbour, T. J. Ness, C. L. Raston, P. L. Raston, *J. Am. Chem. Soc.*, 2001, 123, 7192.

[53] W. B. Blanton, S. W. Gordon-Wylie, G. R. Clark, K. D. Jordan, J. T. Wood, U. Geiserand, T. J. Collins, *J. Am. Chem. Soc.*, 1999, 121, 3551.

[54] L. J. Barbour, G. W. Orr, J. L. Atwood, *Chem. Commun.*, 2000, 859.

[55] S. Pal, N. B. Sankaran, A. Samanta, *Angew. Chem., Int. Ed.*, 2003, 42, 1741.

[56] B. H. Ye, B. B. Ding, Y. Q. Weng, X. M. Chen, *Inorg. Chem.*, 2004, 43, 6866.

[57] B. Sreenivalusu, J. J. Vittal, *Angew. Chem., Int. Ed.*, 2004, 116, 5893.

[58] K. M. Park, R. Kuroda, T. Iwamoto, *Angew. Chem., Int. Ed.*, 1993, 32, 884.

[59] K. Raghuraman, K. K. Katti, L. J. Barbour, N. Pillarsetty, C. L. Barnes, K. V. Katti, *J. Am. Chem. Soc.*, 2003, 125, 6955.

[60] C. Janiak, T. G. Scharman, *J. Am. Chem. Soc.*, 2002, 124, 14010.

[61] B. Q. Ma, H. L. Sun, S. Gao, *Angew. Chem., Int. Ed.*, 2004, 43, 1374.

[62] P. K. Patel, A. S. R. Koti, R. V. Hosur, *Nucl. Acids Res.*, 1999, 27, 3836.

[63] B. Pan, Y. Xiong, K. Shi, M. Sundaralingam, *Structure*, 2003, 11, 825.

[64] B. Pan, Y. Xiong, K. Shi, J. Deng, M. Sundaralingam, *Structure*, 2003, 11, 815.

[65] J. T. Davis, *Angew. Chem., Int. Ed.*, 2004, 43, 668.

[66] D. J. Patel, S. Bouaziz, A. Kettani, Y. Wang, in (Ed.) S. Neidle, *Oxford Handbook of Nucleic Acid Structure*, Oxford University Press, Oxford, 1999, 389.

[67] G. N. Parkinson, M. P. H. Lee, S. Neidle, *Nature*, 2002, 417, 876.

[68] N. Escaja, J. L. Gelpi, M. Orozco, M. Rico, E. Pedroso, C. Gonzalez, *J. Am. Chem. Soc.*, 2003, 125, 5654.

[69] A. I. H. Murchie, D. M. J. Lilley, *EMBO J.*, 1994, 13, 993.

[70] D. Mohanty, M. Bansal, *Biophys. J.*, 1995, 69, 1046.

[71] M. C. Shiber, E. H. Braswell, H. Klump, J. R. Fresco, *Nucl. Acids Res.*, 1996, 24, 5004.

[72] J. Gu, J. Leszczynski, *J. Phys. Chem. A.*, 2000, 104, 1898.

[73] W. N. Hunter, T. Brown, in (Ed.) S. Neidle, *Oxford Handbook of Nucleic Acid Structure*, Oxford University Press, Oxford, 1999, 313.

[74] 9-Methylhypoxanthine: A. L. Spek, W. J. J. Smeets, Cambridge Crystallographic Data Centre, CCDC No. 140800. http://www.ccdc.cam.ac.uk.

[75] R. K. O. Sigel, E. Freisinger, S. Metzger, B. Lippert, *J. Am. Chem. Soc.*, 1998, 120, 12000.

[76] E. Freisinger, I. B. Rother, M. S. Lüth, B. Lippert, *Proc. Natl. Acad. Sci. USA*, 2003, 100, 3748.

[77] X. Gao, D. J. Patel, *J. Am. Chem. Soc.*, 1988, 110, 5178

[78] B. Lippert, *Coord. Chem. Rev.*, 2000, 200-202, 487.

[79] J. Müller, E. Zangrando, N. Pahlke, E. Freisinger, L. Randaccio, B. Lippert, *Chem. Eur. J.*, 1998, 4, 397.

[80] T. Lindahl, *Nature*, 1993, 362, 709.

[81] T. Lindahl, B. Nyberg, *Biochemistry*, 1974, 13, 3405.

[82] B. K. Duncan, J. H. Miller, *Nature*, 1980, 287, 560.

[83] W. M. III Rideout, G. A. Coetzee, A. F. Olumi, P. A. Jones, *Science*, 1990, 249, 1288.

[84] D. N. Cooper, H. Youssoufian, *Hum. Genet.*, 1988, 78, 151.

[85] A. Viswanathan, H. J. You, P. W. Doetsch, *Science*, 1999, 284, 159.

[86] R. Y.-H. Wang, K. C. Kuo, C. W. Gehrke, L.-H. Huang, M. Ehrlich, *Biochim. Biophys. Acta*, 1982, 697, 371.

[87] L. A. Frederico, T. A. Kunkel, B. Ramsay Shaw, *Biochemistry*, 1990, 29, 2532.

[88] B. Ramsay Shaw, *In Structural Biology: The State of the Art.* (Eds. R. H. Sarma, M. H. Sarma), Adenine Press, Shenectady, N.Y., 1994, 367.

[89] G. C. Ireton, G. McDermott, M. E. Black, B. L. Stoddard, *J. Mol. Biol.*, 2002, 315, 687.

[90] J. Arpalahti, K. D. Klika, *Eur. J. Inorg. Chem.*, 2003, 4195.

[91] K. D. Klika, J. Arpalahti, *Chem. Commun.*, 2004, 666.

[92] E. Zangrando, F. Picherri, L. Randaccio, B. Lippert, *Coord. Chem. Rev.,* 1996, 156, 275.

[93] W. Brüning, I. Ascaso, E. Freisinger, M. Sabat, B. Lippert, *Inorg. Chim. Acta,* 2002, 339, 400.

[94] R. B. Martin, *Science*, 1963, 139, 1198.

[95] R. Stewart, M. G. Harris, *Can. J. Chem.,* 1977, 55, 3807.

[96] M. Garijo Añorbe, M. S. Lüth, M. Roitzsch, M. Morell Cerdà, P. Lax, G. Kampf, H. Sigel, B. Lippert, *Chem. Eur. J.,* 2004, 10, 1046.

[97] H. Friebolin, “Ein- und zweidimensionale NMR-Spektroskopie”, Wiley-VCH, Weinheim (1988).

[98] M. J. Clarke, *J. Am. Chem. Soc.*, 1978, *100*, 5068.

[99] J. Arpalahti, K. D. Klika, *Eur. J. Inorg. Chem.*, 1999, 1199.

[100] J. Viljanen, K. D. Klika, R. Sillanpää, J. Arpalahti, *Inorg. Chem.*, 1999, 38, 4924.

[101] J. Arpalahti, K. D. Klika, S. Molander, *Eur. J. Inorg. Chem.*, 2000, 1007.

[102] F. Pichierri, D. Holthenrich, E. Zangrando, B. Lippert, L. Randaccio, *J. Biol. Inorg. Chem.*, 1996, 1, 439.

[103] B. Lippert, H. Schöllhorn, U. Thewalt, *J. Am. Chem. Soc.*, 1986, 108, 6616.

[104] H. Schöllhorn, R. Beyerle-Pfnür, U. Thewalt, B. Lippert, *J. Am. Chem. Soc.*, 1986, 108, 3680.

[105] V. Swaminathan, M. Sundaralingam, *CRC Crit. Rev. Biochem.,* 1979, 6, 245.

[106] R. W. Gellert, R. Bau, Met. Ions Biol. Syst., 1979, 8, 57; (c) D. J. Hodgson, *Prog. Inorg. Chem.*, 1977, 23, 211.

[107] H. Schöllhorn, U. Thewalt, B. Lippert, *J. Am. Chem. Soc.*, 1989, 111, 7213.

[108] J. Müller, Doktorarbeit (Universität Dortmund), Logos Verlag Berlin (1999).

[109] R. Ménard, M. T. Phan Viet, M. Zador, *Inorg. Chim. Acta*, 1987, 136, 25.

[110] A. Hegmans, E. Freisinger, E. Zangrando, A. Ashfar, E. Hübener, T. G. Appleton, B. Lippert, *Inorg. Chim. Acta*, 1998, 279, 152.

[111] J. Müller, F. Glahé, E. Freisinger, B. Lippert, *Inorg. Chem.*, 1999, 38, 3160.

[112] R. Beyerle-Pfnür, H. Schöllhorn, U. Thewalt, B. Lippert, *J. Chem. Soc., Chem. Commun.*, 1985, 1510.

[113] T. Steiner, *Acta Crystallogr., Sect. B*, 1998, 54, 456.

[114] J. M. Casas, J. Fornies, A. Martín, *J. Chem. Soc., Dalton Trans.*, 1997, 1559.

[115] B. Lippert, C. J. L. Lock, R. A. Speranzini, *Inorg. Chem.*, 1981, 20, 808.

[116] B. E. Brown, C. J. L. Lock, Acta Crystallogr., Sect. C, 1988, 44, 611.

[117] E. Sinn, C. M. Flynn, R. B. Martin, *Inorg. Chem.*, 1977, 16, 2403.

[118] R. Faggiani, B. Lippert, C. J. L. Lock, *Inorg. Chem.*, 1982, 21, 3210.

[119] R. Faggiani, C. J. L. Lock, B. Lippert, *Inorg. Chim. Acta*, 1985, 106, 75.

[120] M. J. Clarke, *Inorg. Chem.*, 1980, 19, 1103.

[121] J. Müller, R. K. O. Sigel, B. Lippert, *J. Inorg. Biochem.,* 2000, 79, 261.

[122] See, e.g. Various articles in P.N.A.S. special issue “Supramolecular Chemistry and Self-Assembly Special Feature”, 2002, 99:8, 4763-5188.

[123] S. Leininger, B. Olenyuk, P.J. Stang, *Chem. Rev.*, 2000, 100, 853.

[124] H. D. Flack, *Acta Crystallogr., Sect. A*, 1983, 39, 876.

[125] M. Yu Subbotin, L. A. Aslanov, *Zh. Neorg. Khim.*, 1986, 31, 901.

[126] D. J. Baker, J. S. Buckleton, G. R. Clark, R. P. Cooney, C. E. F. Rickard, *J. Mol. Struct.*, 1990, 239.

[127] V. P. Fedin, M. N. Sokolov, A. V. Virovets, N. V. Podberezskaya, V. Ye. Fedorov, *Polyhedron*, 1992, 11, 853.

[128] N. W. Alcock, A. Samotus, J. Szklarzewicz, *J. Chem. Soc., Dalton Trans.*, 1993, 885.

[129] A. Z. Lipka, *Z. Naturforsch*., *Teil B*, 1983, 38, 1615.

[130] R. D. Shannon, *Acta Crystallogr., Sect. A*, 1976, 32, 751.

[131] B. Mestvedt, *Acta Crystallogr.*, 1960, 13, 1043.

[132] P. A. Iyere, W. Y. Boadi, D. Atwood, S. Parkin, *Acta Crystallogr., Sect. B*, 2003, 59, 664.

[133] K. F. Bowes, G. Ferguson, A. J. Lough, C. Glidewell, *Acta Crystallogr., Sect. B*, 2003, 59, 100.

[134] P. A. Iyere, L. J. Kairen, A. W. Cordes, C. T. Eagle, T. A. Nile, G. L. Schimek, W. T. Pennington, *Cryst. Eng.*, 1998, 2, 159.

[135] T. J. R. Weakley, *Acta Crystallogr., Sect. C*, 1987, 43, 2144.

[136] S. Weng, *Acta Crystallogr., Sect. C*, 1999, 55, 2105.

[137] B. Dolling, A. L. Gillon, A. G. Orpen, J. Starbuck, X.-M. Wang, *Chem. Commun.*, 2001, 567.

[138] A. D. Bond, N. Feeder, J. E. Redman, J. K. M. Sanders, *Acta Crystallogr., Sect. E*, 2001, 57, o869.

[139] P. A. Iyere, W. Y. Boadi, R. S. Brooks, D. Atwood, S. Parkin, *Acta Crystallogr., Sect. E*, 2002, 58, o825.

[140] R. G. Vranka, E. L. Amma, *Inorg. Chem.,*1966, 5, 1021.

[141] C. R. Bondy, P. A. Gale, S. J. Loeb, *Chem Commun.*, 2001, 729.

[142] C. R. Bondy, P. A. Gale, S. J. Loeb, *J. Am. Chem. Soc.*, 2004, 126, 530.

[143] D. K. Chand, K. Biradha, M. Fujita, *Chem. Commun.*, 2001, 1652.

[144] L. C. Tabares, J. A. R. Navarro, J. M. Salas, *J. Am. Chem. Soc.*, 2001, 123, 383.

[145] M. J. Zaworotko, *Angew. Chem., Int. Ed.*, 2000, 39, 3052.

[146] S.-K. Yoo, J. Y. Ryu, J. Y. Lee, C. Kim, J.-J. Kim, Y. Kim, *Dalton Trans.*, 2003, 1454.

[147] D. M. L. Goodgame, S. Menzer, A. T. Ross, D. J. Williams, *J. Chem. Soc.*, *Chem. Commun.*, 1994, 2605.

[148] N. Hadjiliadis, T. Theophanides, *Inorg. Chim. Acta*, 1976, 16, 77.

[149] H.-J. Korte, R. Bau, *Inorg. Chim. Acta*, 1983, 79, 251.

[150] M. Krumm, I. Mutikainen, B. Lippert, *Inorg. Chem.*, 1991, 30, 884.

[151] P. T. Selvi, M. Murali, M. Palaniandavar, M. Köckerling, G. Henkel, *Inorg. Chim. Acta*, 2002, 340,139.

[152] M. Mizutani, S. Miwa, N. Fukushima, Y. Funahashi, T. Ozawa, K. Jitsukuwa, H. Masuda, *Inorg. Chim. Acta*, 2002, 339, 543.

[153] A. Panfil, A. Terron, J.J. Fiol, M. Quiros, *Polyhedron*, 1994, 13, 2513.

[154] M. Palaniandavar, I. Somasundaram, M. Lakshiminarayanan, H. Manohar, *J. Chem. Soc., Dalton Trans*., 1996, 1333.

[155] E. Freisinger, A. Schneider, M. Drumm, A. Hegmans, S. Meier, B. Lippert, *J. Chem. Soc.*, *Dalton Trans.*, 2000, 3281.

[156] H. Rauter, I. Mutikainen, M. Blomberg, C. J. L. Lock, P. Amo-Ochoa, E. Freisinger, L. Randaccio, E. Zangrando, E. Chiarparin, B. Lippert, *Angew. Chem. Int. Ed. Engl.*, 1997, 36, 1296.

[157] B. Lippert, D. Neugebauer, *Inorg. Chem.*, 1982, 21, 451.

[158] B. Lippert, U. Thewalt, H. Schöllhorn, D. M. L. Goodgame, R. W. Rollins, *Inorg. Chem.*, 1984, 23, 2807.

[159] E. Freisinger, S. Meier, B. Lippert, *J. Chem. Soc.*, *Dalton Trans.*, 2000, 3274.

[160] J. A. R. Navarro, M. B. L. Janik, E. Freisinger, B. Lippert, *Inorg. Chem.*, 1999, 38, 426.

[161] J. Kozelka, H.-P. Lüthi, E. Dubler, R. W. Kunz, *Inorg. Chim. Acta*, 1984, 86, 155, 235.

[162] B. Lippert, *Prog. Inorg. Chem.*, 1989, 37, 1.

[163] D. Neugebauer, B. Lippert, *J. Am. Chem. Soc.*, 1982, 104, 6596.

[164] I. Mutikainen, O. Orama, A. Pajunen, B. Lippert, *Inorg. Chim. Acta*, 1987, 137, 189.

[165] A. Hegmans, E. Freisinger, E. Zangrando, A Pichierri, L. Randaccio, C. Mealli, M. Gerdan, A. X. Trautwein, B. Lippert, *Chem. Eur. J.*, 1999, 5, 3010.

[166] G. Fusch, E. C. Fusch, A. Erxleben, J. Hüttermann, H.-J. Scholl, B. Lippert, *Inorg. Chim. Acta*, 1996, 252, 167.

[167] C. Meiser, E. Freisinger, B. Lippert, *J. Chem. Soc.*, *Dalton Trans.*, 1998, 2059.

[168] A. Schreiber, E. C. Hillgeris, B. Lippert, *Z. Naturforsch.*, 1993, 48b, 1603.

[169] M. S. Lüth, E. Freisinger, B. Lippert, *Chem. Eur. J.*, 2001, 7, 2104.

[170] G. Raudaschl-Sieber, H. Schöllhorn, U. Thewalt, B. Lippert, *J. Am. Chem. Soc.*, 1985, 107, 3591.

[171] C. Meiser, B. Song, E. Freisinger, M. Peilert, H. Sigel, B. Lippert, *Chem. Eur. J.*, 1997, 3, 388.

[172] M. Krumm, E. Zangrando, L. Randaccio, S. Menzer, A. Danzmann, D. Holthenrich, B. Lippert, *Inorg. Chem.*, 1993, 32, 2183.

[173] I. Dieter-Wurm, M. Sabat, B. Lippert, *J. Am. Chem. Soc.*, 1992, 114, 357.

[174] R. K. O. Sigel, B. Lippert, *Chem. Commun.*, 1999, 2167.

[175] R. K. O. Sigel, E. Freisinger, B. Lippert, *J. Biol. Inorg. Chem.*, 2000, 5, 287.

[176] J. F. Berry, F. A. Cotton, P. Lei, T. Lu, C. A. Murillo, *Inorg. Chem.*, 2003, 42, 3534.

[177] C. Y. Yeh, Y.-L. Chiang, G. H. Lee, S.-M. Peng, *Inorg. Chem.*, 2002, 41, 4096.

[178] B. Knobloch, R. K. O. Sigel, B. Lippert, H. Sigel, *Angew. Chem., Int. Ed.*, 2004, 43, 3793.

[179] H. T. Chifotides, K. M. Koshlap, L. M. Pérez, K. R. Dunbar, *J. Am. Chem. Soc.*, 2003, 125, 10703.

[180] H. T. Chifotides, K. M. Koshlap, L. M. Pérez, K. R. Dunbar, *J. Am. Chem. Soc.*, 2003, 125, 10714.

[181] C. A. Crawford, E. F. Day, V. P. Saharan, K. Folting, J. C. Huffman, K. R. Dunbar, G. Christou, *Chem. Commun.*, 1996, 1113.

[182] KappaCCD package, Nonius, Delft, The Netherlands, 1997.

[183] Z. Otwinowsky, W. Minor, DENZO and SCALEPACK. *Methods Enzymol*, 1997, 276, 307.

[184] G. M. Sheldrick, *Acta Crystallogr., Sect. A 46*, 1990, 467.

[185] G. M. Sheldrick, SHELXTL-PLUS (VMS), Siemens Analytical X-Ray Instruments, Madison, WI, 1990.

[186] G. M. Sheldrick, SHELXL-97, program for crystal structure refinement, University of Göttingen, Germany, 1993.

[187] L. J. Farrugia, *J. Appl. Cryst., 1999, 32, 837*. Windows programs for the solution, refinement and analysis of single crystal X-ray diffraction data. http://www.chem.gla.ac.uk/~louis/wingx.

[188] R. Lumry, E. L. Smitz, R. Glantz, *J. Am. Chem. Soc.*,1951, 73, 4336.

[189] R. Tribolet, H. Sigel, *Eur. J. Biochem.*, 1987, 163, 353.

[190] Gaussian 98, Revision A.7, M. J. Frisch, G. W. Trucks, H. B. Schlegel, G. E. Scuseria, M. A. Robb, J. R. Cheeseman, V. G. Zakrzewski, J. A. Montgomery, Jr., R. E. Stratmann, J. C. Burant, S. Dapprich, J. M. Millam, A. D. Daniels, K. N. Kudin, M. C. Strain, O. Farkas, J. Tomasi, V. Barone, M. Cossi, R. Cammi, B. Mennucci, C. Pomelli, C. Adamo, S. Clifford, J. Ochterski, G. A. Petersson, P. Y. Ayala, Q. Cui, K. Morokuma, D. K. Malick, A. D. Rabuck, K. Raghavachari, J. B. Foresman, J. Cioslowski, J. V. Ortiz, A. G. Baboul, B. B. Stefanov, G. Liu, A. Liashenko, P. Piskorz, I. Komaromi, R. Gomperts, R. L. Martin, D. J. Fox, T. Keith, M. A. Al-Laham, C. Y. Peng, A. Nanayakkara, C. Gonzalez, M. Challacombe, P. M. W. Gill, B. Johnson, W. Chen, M. W. Wong, J. L. Andres, C. Gonzalez, M. Head-Gordon, E. S. Replogle, J. A. Pople, Gaussian, Inc., Pittsburgh PA, 1998.

[191] Gaussian 03, Revision C.02, M. J. Frisch, G. W. Trucks, H. B. Schlegel, G. E. Scuseria, M. A. Robb, J. R. Cheeseman, J. A. Montgomery, Jr., T. Vreven, K. N. Kudin, J. C. Burant, J. M. Millam, S. S. Iyengar, J. Tomasi, V. Barone, B. Mennucci, M. Cossi, G. Scalmani, N. Rega, G. A. Petersson, H. Nakatsuji, M. Hada, M. Ehara, K. Toyota, R. Fukuda, J. Hasegawa, M. Ishida, T. Nakajima, Y. Honda, O. Kitao, H. Nakai, M. Klene, X. Li, J. E. Knox, H. P. Hratchian, J. B. Cross, C. Adamo, J. Jaramillo, R. Gomperts, R. E. Stratmann, O. Yazyev, A. J. Austin, R. Cammi, C. Pomelli, J. W. Ochterski, P. Y. Ayala, K. Morokuma, G. A. Voth, P. Salvador, J. J. Dannenberg, V. G. Zakrzewski, S. Dapprich, A. D. Daniels, M. C. Strain, O. Farkas, D. K. Malick, A. D. Rabuck, K. Raghavachari, J. B. Foresman, J. V. Ortiz, Q. Cui, A. G. Baboul, S. Clifford, J. Cioslowski, B. B. Stefanov, G. Liu, A. Liashenko, P. Piskorz, I. Komaromi, R. L. Martin, D. J. Fox, T. Keith, M. A. Al-Laham, C. Y. Peng, A. Nanayakkara, M. Challacombe, P. M. W. Gill, B. Johnson, W. Chen, M. W. Wong, C. Gonzalez, J. A. Pople, Gaussian, Inc., Wallingford CT, 2004.

[192] A. D. Becke, J. Chem. Phys., 1993, 98, 5648.

[193] C. Lee, W. Yang, R.G. Parr, *Phys. Rev. B37*, 1998, 785.

[194] W. Micklitz, B. Lippert, H. Schöllhorn, U. Thewalt, *J. Heterocyclic Chem.*, 1989, 26, 1499.

[195] G. Krüger, *Hoppe-Seyler's Z. Physiol. Chem.*, 1894, 18, 434.

[196] J. S. Nowick, J. S. Chem, G. Noronha, *J. Am. Chem. Soc.*, 1993, 115, 7636.

[197] E. G. Talman, W. Brüning, J. Reedijk, A. L. Spek, N. Veldman, *Inorg. Chem.*, 1997, 36, 854.

[198] *Inorganic Syntheses, 1983, Volume 22, p. 124*.

[199] G. W. Watt, W. A. Clude, *Inorg. Chem.*, 1968, 7, 335.

[200] D. Gupta, M. Hueselkopf, M. Morell Cerdà, Ralf Ludwig, B. Lippert, *Inorg. Chem.*, 2004, 43, 3386.

1 # [(1-MeCH)(1-MeC)]$I_3 \cdot 2H_2O$

2 # [(1-MeCH)](NO_3)

3 # [(9-MeAH)](PF_6)

4 # [(9-EtAH)](NO_3)

5 # [(9-MeAH)]$(NO_3) \cdot H_2O$

6 # $[(9\text{-EtGH})_2] \cdot 4H_2O$

7 # $[(9\text{-EtGH})_2] \cdot 7H_2O$

8 # [(9-MeAH)(9-MeHxH)](ClO_4)

9 # [(dien)Pt(1-MeC-*N3*)]$(ClO_4)_2$

10 [(dien)Pt(1-MeU-*N3*)]$^+$

11a *syn*-[(dien)Pt(1-MeC$^-$-*N4*)]$^+$

11b *anti*-[(dien)Pt(1-MeC-*N4*)]$^+$

12 # $[(NH)_3$Pt(1-MeC-*N3*)$](ClO_4)_2 \cdot$ ½ $KClO_4$

13 $[(NH)_3$Pt(1-MeU-*N3*)]$^+$

14 # [(dien)Pd(1-MeC-*N3*)]$(ClO_4)_2$

15 [(dien)Pt(*N3*-1-MeC-*N4*)Pt(dien)]$^{3+}$

16 $[(NH_3)$Pt(*N3*-1-MeC-*N4*)Pt(dien)]$^{3+}$

17 [(dien)Pd(*N3*-1-MeC-*N4*)Pd(dien)]$^{3+}$

18 [(dien)Pd(*N3*-1-MeC-*N4*)Pt(dien)]$^{3+}$

19 {[(dien)Pt]$_3$(1-MeC-*N3,N4,N4*)}$^{3+}$

20 # [Pt(1-MeC-*N3*)$_3$I]I

21 # *trans*-[Pt(1-MeC-*N3*)$_2I_2$]

22 # *trans*-[Pt(1-MeC-*N3*)$_2Cl_2$]

23 # *trans*-[Pt(1-MeC-*N3*)(1-MeC-*N4*)$I_2] \cdot 2H_2O$

24 # *trans*-[Pt(1-MeC-*N3*)(1-MeC-*N4*)Cl_2]

25 # [(4,4'-bipy)H]$I \cdot H_2O$

26 # [Ag(pyz)](NO_3)

27 # [Pt(1-MeC-*N3*)$_3$(pyz)]$(NO_3)_2 \cdot H_2O$

28 # [Pt(1-MeC-*N3*)$_3$(pyz)Ag]$(NO_3)_3 \cdot H_2O$

29 # [Pt(9-MeHxH-*N7*)$_4$]$(NO_3)_2 \cdot H_2O$

30 [Pt(9-EtGH-*N7*)$_4$]$(NO_3)_2$

31 *trans*-[Pt(1-MeC-*N3*)$_2$(9-EtGH-*N7*)$_2$]$(NO_3)_2$

32 # {[(H_2O)Cu(*O6*-9-MeHxH-*N7*)$_4$Pt]$_2$Cu$(ClO_4)_4$}$(ClO_4)_2(NO_3)_4 \cdot 6H_2O$

1-MeC	1-methylcytosine
1-MeC$^+$	1-methylcytosinium
1-MeC$^-$	1-methylcytosine anion (deprotonated at N4)
1-MeUH	1-methyluracile
1-MeU$^-$	1-methyluracilate
9-MeA	9-methyladenine
9-MeAH$^+$	9-methyladeninium
9-EtA	9-ethyladenine
9-EtAH$^+$	9-ethyladeninium
9-EtG$^-$	9-ethylguanine anion
9-EtGH	9-ethylguanine
9-MeHxH	9-methylhypoxanthine
pyz	pyrazine
bipy	4,4'-bipyridyl
dien	diethylenetriamine
[(dien)Pt^{II}]	[(dien)Pt(H_2O)]$^{2+}$ or [(dien)Pt(D_2O)]$^{2+}$
δ	chemical shift
ppm	parts per million
s	singlet
d	doublet
t	triplet
q	quadruplet
v	reaction rate
k	rate constant
$t_{½}$	half-life
r.m.s.	root mean square
TSP	sodium 3-trimethylsilyl-propanesulfonate
TMA	tetramethylammonium bromide
DSS	sodium 2,2-dimethyl-2-silapentane-5-sulfonate
h	hour
d	day
EDX	Energy Dispersive X-ray Analysis